POLITECNICO DI TORINO
Repository ISTITUZIONALE

Fully bio-based polymer blends: optimization of processing aspects and influence of compatibilizers. Development of strategies to properties improvement

Original
Fully bio-based polymer blends: optimization of processing aspects and influence of compatibilizers. Development of strategies to properties improvement / D'Anna, Alessandra. - (2022 Mar 21), pp. 1-214.

Availability:
This version is available at: 11583/2959949 since: 2022-03-29T16:58:06Z

Publisher:
Politecnico di Torino

Published
DOI:

Terms of use:
Altro tipo di accesso

This article is made available under terms and conditions as specified in the corresponding bibliographic description in the repository

Publisher copyright

(Article begins on next page)

16 July 2022

Doctoral Dissertation
Doctoral Program in Materials Science and Technology (34th Cycle)

Fully bio-based polymer blends: optimization of processing aspects and influence of compatibilizers. Development of strategies to properties improvement

Alessandra D'Anna

******

Supervisors
Prof. Alberto Frache, Supervisor
Prof. Rossella Arrigo, Co-Supervisor

Doctoral Examination Commitee
Prof. Luigi Botta, Università degli Studi di Palermo
Prof. Orietta Monticelli, Università degli Studi di Genova
Prof. Barbara Di Credico, Università degli Studi di Milano Bicocca
Prof. Massimo Messori, Politecnico di Torino
Prof. Claudio Badini, Politecnico di Torino

Politecnico di Torino
21 Marzo 2022

This thesis is licensed under a Creative Commons License, Attribution - Non-commercial - No Derivative Works 4.0 International: see www.creativecommons.org. The text may be reproduced for non-commercial purposes, provided that credit is given to the original author.

I hereby declare that, the contents and organisation of this dissertation constitute my own original work and does not compromise in any way the rights of third parties, including those relating to the security of personal data.

Alessandra D'Anna
Turin, 2022

To my Father

Summary

In the recent years, the concerns related to the environmental issues stimulated an increasing interest towards the application of biodegradable polymers. However, the use of these renewable resources, in alternative to the conventional petrochemical derived products, has some disadvantages such as limited thermo-mechanical properties. A possible and effective method to overcome some biopolymers limitations is the development of bio-based polymer blends.

Particularly, the purpose of this PhD dissertation is the study of compatibilized biopolymer blends: different strategies of compatibilization derived from a detailed state of the art were discussed. The aim is to develop fully bio-based materials with advanced thermo-mechanical and mechanical properties overcoming the limitations related to the immiscibility of the biopolymer phases. Concerning the experimental trials, the use of natural surfactants, the use of nanoparticles connected to an accurate study of the influence of process parameters during melt compounding and, finally, the use of a third biopolymer phase were employed as methods in order to obtain materials with improved interfacial adhesion between the immiscible phases. In particular, the study was focused on blends composed by poly(lactic-acid) (PLA) as continuous phase and different biopolymers as dispersed phases. The choice of using PLA is correlated to the well-known biocompatibility and biodegradability of this biopolymer but, especially, to its easy processability that allows the use of existing polymer-processing equipment and techniques for petrochemical-derived products.

Morphological investigation and detailed studies of thermal, thermo-mechanical and rheological properties are reported.

Particularly, an innovative use of non-ionic surfactants has been tested in a model system based on poly(lactic-acid) (PLA) and low-density polyethylene (LDPE). Subsequently, the effectiveness of the proposed strategy was evaluated for fully bio-based PLA/ poly-hydroxy butyrate (PHB) blends. In addition, for the bio-based blends a further compatibilization system based on solid non-ionic surfactants, named Synperonic (Syn), was used. Morphological analyses of the compatibilized blends indicated that in both compatibilized systems a certain grade of compatibility and improved interfacial adhesion between phases, as compared to the non-compatibilized blend, were achieved. Finally, a remarkable increase of the elastic modulus values was obtained for the compatibilized blends as compared to the pure counterparts, with a consequent significant enhancement of the heat distortion temperature values which allows to obtain a wider application working range of these materials.

A very important aspect, broadly studied in this PhD dissertation, is the influence of the process parameters on the final properties of the blends by knowing

that their microstructure is closely related to the melt blending process and the conditions under which the process takes place. The results of the characterizations of PLA/PHB blends processed with different screw configurations of a co-rotating twin screw extruder, flow rate and screw speed are reported. In addition, nanofilled PLA/PHB blends with nanoclays were processed by varying the screw configuration and the screw speed. In this case, XRD analyses, SEM observations and rheological characterization were exploited to infer the coupled effect of the process parameters and nanoclay presence on the microstructure of the filled blend. Preliminary thermodynamic calculations allowed predicting the preferential localization of the nanoclay in the interfacial region between the polymeric phases. The relaxation mechanism of the particles of the dispersed phase in nanofilled blend processed, by rheological measurements, is not fully completed due to an interaction between polymer ad filler in the interfacial region with a consequent modification of the blend morphology and, specifically, a development of an enhanced microstructure. Therefore, by varying the screw configuration, particularly the presence of backflow and distribution elements, high shear stresses are induced during the processing able to allow a better interaction between polymers and clay.

Finally, another compatibilization strategy reported in the work thesis was the introduction of a further biopolymer phase in a binary immiscible blend. In particular, poly-butylene succinate (PBS) was used as ductile phase in order to enhance the elongation at break of the PLA/PHB brittle blend. The ternary systems reported ductile behaviour with elongation at break increased up to 297% overcoming the brittleness typical of PLA and PHB polymers.

Contents

List of Figures

List of Tables

List of Abbreviations

The main abbreviations used in the thesis are classified alphabetically.

ATR-FTIR	Attenuated total reflection – Fourier Transform Infrared Spectroscopy
Ca	Capillary number
Ca_{crit}	Critical Capillary number
CL	Bentonite organo-modified with bis(hydrogenated tallow alkyl)dimethyl salt (Cloisite 5)
CLTE	Coefficient of Linear Thermal Expansions
d_{av}	Average diameter [μm]
DC	Direct Compounding
DMTA	Dynamic Mechanic Thermal Analysis
DBTT	Ductile-to-brittle transition temperature
DSC	Differential Scanning Calorimetry
E’	Dynamic storage modulus [MPa]
E_a	Flow activation energy
e.g.	For example
EDX	Energy Dispersive X-Ray Analysis
FDA	Food and Drug Administration
G’	Rheological storage modulus [Pa]
G’’	Rheological loss modulus [Pa]
G*	Rheological complex modulus [Pa]
HDT	Heat Distortion temperature [°C]
HLB	Hydrophile-lipophile balance
i.e.	That is
LDPE	Low-density polyethylene
MB	Masterbatch
Mg	Magnesium
M_w	Molecular weights
p or η	Viscosity ratio
PBAT	Poly-butylene adipate terephthalate
PBS	Poly-butylene succinate
PDLLA	Poly(DL-lactide)
PHA	Poly-hydroxy alkenoate
PHB	Poly-hydroxy butyrate
PHBt	Filled Poly-hydroxy butyrate

PHBV	Poly(3-hydroxybutyrate-co-3-hydroxyvalerate)
PLA	Poly-lactic acid
SEM	Scanning Electron Microscopy
Syn	Synperonic
Span80	Span TM 80-LQ-(RB)
Si	Silica
SP	Screw configurations
SSE	Single-screw extruder
Tanδ	Loss factor (E''/E') (DMTA analysis)
TGA	Thermogravimetric analysis
TSE	Twin-screw extruder
Tween80	Tween TM 80-LQ-(CQ)
T_c	Crystallization temperature [°C]
T_{cc}	Cold crystallization temperature [°C]
T_g	Glass transition temperature [°C]
T_m	Melting Temperature [°C]
std. dev	Standard deviation
wt%	Weight percentage [%]
X_c	Crystallinity degree [%]
XRD	X-ray diffraction
ΔH	Enthalpy [J/g]
ΔH_{cc}	Cold crystallization enthalpy [J/g]
ΔH_m	Melting enthalpy [J/g]
$\Delta H_{100\%}$	Melting enthalpy for a 100% crystalline [J/g]
α (ω)	Slope of storage modulus (Rheology)
Ɛ	Elongation at break [%]
λH(λ)	Weighted relaxation spectra
η*	Complex viscosity [Pa*s]
ρ	Density [g/cm^3]
σ_{max}	Maximum tensile strength [MPa]
ω	Angular frequency [rad/s]
ω_a	Wetting coefficient
χ_{12}	Flory-Huggins interaction parameter
γ	Interfacial tension [mN/m]
γ^d	Dispersive component of interfacial tension [mN/m]
γ^p	Polar component of interfacial tension [mN/m]
λ_{ikj}	Spreading coefficient

Chapter 1

Introduction

1.1 Environmental issues and the use of biopolymers

In the recent years, the socio-economic and environmental impact of polymeric materials have played a fundamental role in our society. Although the conventional polymers have considerably improved our lives, they now threaten the environment and the human health since the associated carbon emission and persistency of polymers destabilize the fragile balance of many ecosystems.

The socio-economic impact of polymers is very extensive; during 2019, the global polymers production almost reached 370 million tonnes, of which 58 million tonnes were produced in Europe. This result shows that, globally, only 17% of plastics production is attributed to Europe, preceded by Asia and Oceania (51%) and North America (18%). Worldwide, China is the biggest player, with 30% of total polymeric waste [1].

The socio-economic influence is directly reflected in the environmental impact, since the excessive consumption of conventional polymers inevitably affects our ecosystem. Therefore, it is necessary to implement an alternative economic model to the linear one; a possible solution has been found in the circular bio-economy which has been adopted, in recent years, by the European Union. In order to manage resources, the circular bio-economy proposes an efficient use of biomasses, including waste and side streams, for the sustainable production of high value-added products. In particular, in February 2021, the European Parliament approved a new plan to achieve a zero-carbon, ecologically sustainable, toxic-free and fully circular economy by 2050, where the main adopted rules are related to the plastics sector.

One of the fundamental features in the development of a sustainable global economic approach is played by the use of biodegradable and/or bio-based polymers directly acquired from the natural environment, in alternative to the conventional not biodegradable fossil fuel-based polymers. The concept of

biopolymer has been established as a material that fulfils at least one of the two following conditions: partially or completely ‘’bio-based’’ or biodegradable under controlled environmental influences.

Partially or completely bio-based means that the polymers and/or the monomers are derived from biomasses[2]; these polymers could be biodegradable or not.

On the other hand, a polymer can be considered biodegradable when it is converted to natural substances within a defined period of time. For example, the European standard UNI EN 13432 establishes that biopolymers must biodegrade by 90% within 3 months and after 6 months they must be digested by microorganisms by 90%. Particularly, according to the American Society for Testing Materials (ASTM), a biodegradable plastic is defined as “a plastic in which degradation results from the action of naturally occurring microorganisms, such as bacteria, fungi, and algae.” According to the European standard for biodegradable products, the scientific definition of biodegradable material is “materials that are part of the earth’s innate cycles like the carbon cycle and capable of decomposing back into natural elements.” [3]. The concept of biodegradability is directly correlated to the chemical structure of the polymer and not from its origin.

Figure 1 shows the classification of polymeric materials and it is possible to distinguish four types of polymers of which three classes can be classified under the term of biopolymer.

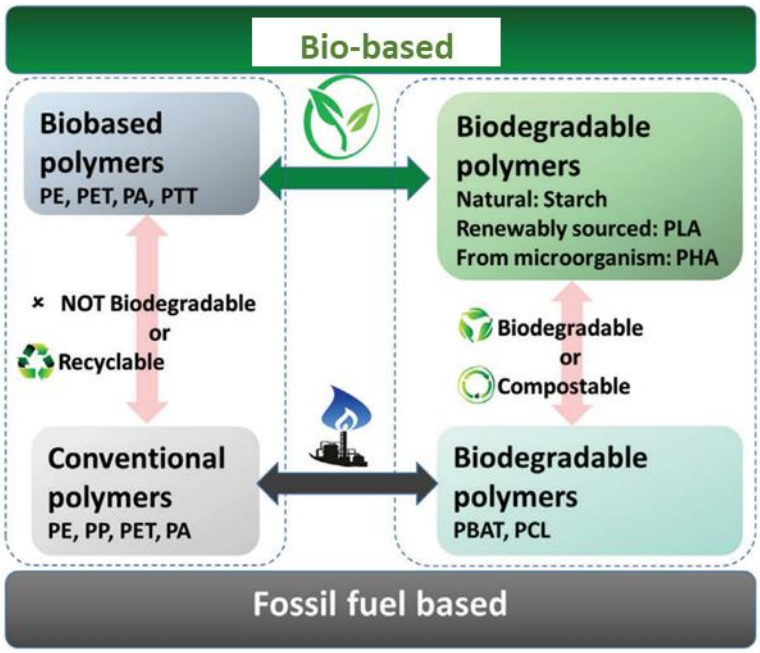

Figure 1. System of polymers classification. Adapted from [4].

- Conventional polymers are obtained from not-biodegradable petrochemical raw; this group is represented by polymers such as polyethylene PE, polyethylene terephthalate PET, polypropylene PP and polyamides PA.
- Not biodegradable bio-based polymers have similar characteristics to those of conventional polymers; the difference between these two is the source of

the monomer. Recently, new synthesis developments have attempted to replace the fossil raw materials used in the traditional synthesis of conventional polymers with renewable feedstock. The aim is to produce bio-based conventional polymers such as bio-PE, bio-PET and bio-PP. These polymers are equivalent, from a performance point of view, to the fossil fuel-based polymers but they minimise the environmental impact.

- Bio-based and biodegradable polymers are obtained from different sources such for example natural and renewable sources and from microorganisms. Due to their low environmental impact, this category of biopolymers has attracted a growing interest in the last years. The most popular exploited, in term of production volumes, is the polylactide or polylactic acid (PLA).
- Fossil fuel-based biodegradable polymers include all biodegradable polymers derived from petrochemical feedstocks. These biopolymers are 100% biodegradable and they include, for example, poly(ϵ-caprolactone) (PCL) and poly (butylene-adipate-co-terephthalate) (PBAT).

The total global production of biopolymers in 2019 was only 2.1 million tonnes, as showed in Figure 2. Particularly, starch, followed by PLA and PBAT, are the most produced biopolymers, while PE, PA, PET, and poly (trimethylene terephthalate) (PTT) are the most commonly produced bio-based non-biodegradable polymers. Bio-based non-biodegradable polymers, which include bio-based PE, PET, and PA, represent 44.5% of biopolymers produced annually, while biodegradable polymers account for 55.5% of the global production of biopolymers. The estimated production growth is a remarkable 14% over 4 years. Specifically, this means that if plastic production remained constant in the next 10 years, biopolymers would rise to about 2% of the total plastic market [5].

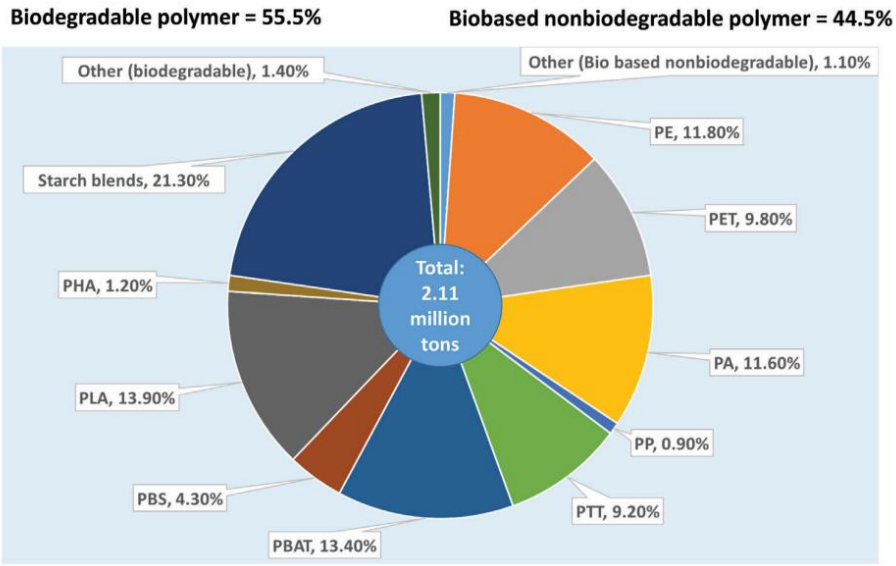

Figure 2. Global annual production of biopolymers in 2019, reprinted with the permission from European Bioplastics [5].

The use of biopolymers allows reducing the environmental impact without compromising the level of safety in the management of consumer goods, up today guaranteed by the fossil fuel-based polymeric materials [6]. In fact, due to their properties which are very close to those of petrochemical-derived products, biopolymers represent a sustainable alternative for a wide variety of applications, ranging from industrial to biomedical fields. In particular, the main markets for these materials include the automotive industry, electrical components, aerospace, construction, agriculture, biomedical and packaging. Figure 3(a) and Figure 3 (b) report the typical applications of biopolymers and the information on global biopolymers production collected by the European Bioplastics Association, respectively. It is worthy to note that the main field of application of these sustainable materials is the packaging sector; in general, polymers are widely exploited in this sector considering that the 40% of the total plastic production in Europe, each year, is occupied by this category. The biopolymer packaging market is set to grow from 484.7 kilotons in 2017 to 1147.9 kilotons in 2023 with an annual growth rate (CAGR) of 15.9% [7].

Biopolymers are also found in biomedical applications such as tissue engineering, wound healing, and drug delivery. This is due to their excellent properties, such as biocompatibility, non-toxicity, and non-immunogenicity and comparable mechanical properties with respect to the conventional fossil fuel-based polymers. For instance, PLA has received the approval from the Food and Drug Administration (FDA) for use in biomedical applications owing to its biodegradability and biocompatibility [8].

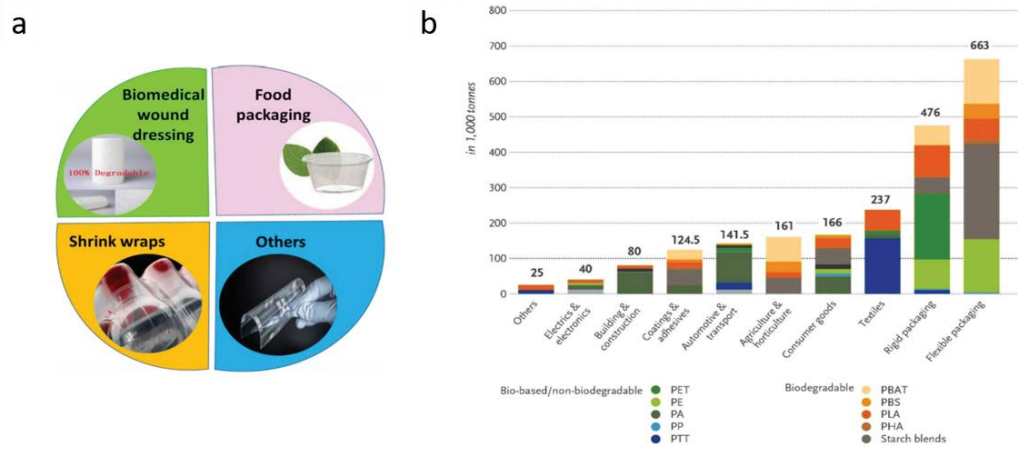

Figure 3. Typical application of biopolymers. Reprinted from [4] (a) and Global biopolymer production capacity by market segment. Collected from the European Bioplastics [5] (b).

However, the use of biodegradable polymers alone has some limitations, such hydrophilicity, heat sealing difficulties, high water vapor and oxygen permeability, and brittleness that limits their use to larger volumes. Therefore, since the growing demand for new sustainable sources and materials has encouraged the necessity to obtain biopolymers with tailored properties, in order to further widen their fields of application, blending of different biopolymer types has been used. In addition, as compared to the complex and highly costly synthesis of new biopolymers, biopolymers blends constitute a very versatile and economically convenient route to produce materials with enhanced properties.

1.2 PhD Framework and objectives

The aim of the PhD thesis is to produce sustainable materials with advanced properties from biopolymers.

Biopolymers are, often, used in combination with other bio-based polymeric phases because of the possibility of profitably combining the main properties of the phases constituting the blend. However, biopolymers have some disadvantages: they are often immiscible with each other and therefore mixtures of two of more biopolymers exhibit poor mechanical and thermo-mechanical properties. In this scenario, the scientific research has moved towards new alternative based on the development of biopolymer blends with superior properties.

In this regard, during the PhD thesis project several strategies have been pursued, such as the use of natural compatibilizers systems in the blend and the optimization of the process parameters.

In both cases, the thermal, thermo-mechanical, mechanical and rheological properties were evaluated, including a detailed study of the morphology characterising the obtained materials.

1.3 Thesis structure

The thesis is structured in the following chapters:

- Chapter 2 will focus on thermodynamics issues and related theoretical correlations on the mixing of high molecular species. Particular attention will be devoted to the morphology development of the polymer mixtures and the rheological considerations needed to examine polymer blends.
- In the Chapter 3, the state of the art of biopolymer blends has been discussed. Particular attention is reserved to the morphology, mechanical and thermal properties of PLA-based blends.
- In Chapter 4, a general point of view of different compatibilization strategies was analysed, i.e. the use of compatibilizers and the study of the influence of process parameters on the optimization of morphological structure of biopolymer blends.

- From Chapter 5 to Chapter 7 the results of the experimental trials of the thesis have been reported. In particular Chapter 5 is focused on the use of natural surfactants in PLA-based blends. The influence of different compatibilizers on the final microstructures and thermo-mechanical properties of the studied biopolymer blends was investigated and peculiar attention was paid to the study of rheological properties.
- In the Chapter 6, the studies of the influence of process parameters in term of variation of flow rate, screw configuration and screw speed on the final morphological structure of the studied mixtures, were reported. The results concern the thermal, thermo-mechanical and rheological properties and, also, the morphological development of the final materials.
- Chapter 7 is focused on the study of ternary biopolymer blends. The influence of third polymeric phase on the mechanical properties were evaluated.

The materials, the instruments for the experimental trials and the characterization techniques used for the discussion of the results are reported in separated sections in the Appendices.

Chapter 2

Theoretical aspects of polymer blends

A polymer blend is a mixture of two or more different species of polymers, containing at least 2 wt% of the dispersed phase [9]. The aim of the development of polymer blends is to exploit certain properties of single polymer components to the advantage of the final properties of the mixtures, generating materials with enhanced chemical, structural and mechanical properties. It is possible to classify polymer blends as miscible or immiscible.

Miscible blends are homogenous single-phase systems, which combine the properties of the components by displaying unique characteristics. In fact, the strong specific interactions established between polymers allow the components to interpenetrate into each other, resulting in the achievement of materials with superior properties and good cohesion between phases [10].

On the contrary, immiscible (or partially miscible) polymer blends are multiphase systems whose properties are generally of minor significance than those of the individual components due to the lack of interaction between the polymers.

Therefore, for a polymer blend one of the most important characteristics is the phase behaviour. In fact, a miscible polymer mixture is characterized by a single phase, while an immiscible blend shows a phase separation or, if it is a partially miscible blend will present various levels of mixing between the components.

Furthermore, in order to accurately study polymer blends, it is important to highlight the differences between the concepts of compatibility and miscibility, which are often misunderstood. A compatible blend is a system consisting of two or more immiscible polymeric phases displaying macroscopically uniform physical properties, caused by sufficiently strong interactions between the constituents of the blend [11]. The compatibility depends on temperature and regimes of mixing; in addition, incompatible systems may become partially or totally compatible due to

the modification of the chemical structure of macromolecules leading to an increase in the interaction between the immiscible polymers constituent the mixtures with a consequent change on the final performance of the systems.

2.1 Thermodynamic issues of polymer blends

2.1.1 Flory-Huggins Theory

The basic thermodynamic relationship for studying the miscibility of polymer blends is defined by the contribution of the Gibbs free mixing energy ΔG_m. The most important correlation governing mixtures of dissimilar components is expressed as follow:

Equation 1. $$\boldsymbol{\Delta G_m = \Delta H_m - T\Delta S_m}$$

where ΔG_m is Gibbs free energy of mixing, ΔH_m is the free enthalpy of mixing, ΔS_m is the entropy of mixing and T is the specific temperature.

At constant temperature and pressure, the necessary condition for the miscibility of the system is $\Delta G_m \leq 0$ which is fulfilled when $\Delta H_m \leq 0$ and $\Delta S_m > 0$ or $|T\Delta S_m| > |\Delta H_m|$ if $\Delta H_m > 0$; the negative value of the Gibbs free energy of mixing is a necessary criterion but it is not a sufficient requirement. In order to achieve miscibility between the phases the equation below must also be satisfied:

Equation 2. $$\boldsymbol{\frac{\partial^2 \Delta G_m}{\partial \phi^2} > 0}$$

with ϕ as volume fraction.

The basic theory for assessing the miscibility of polymer blends was developed by Flory [12] [13] and Huggins [14] [15]. For binary system containing two components denoted by i, where i= 1 and i=2 indicate polymer 1 and polymer 2 respectively, the Flory-Huggins relation can be expressed as follow:

Equation 3. $$\boldsymbol{\frac{\Delta G_m}{RT} = \frac{\phi_1}{V_1} ln\phi_1 + \frac{\phi_2}{V_2} ln\phi_2 + \chi'_{12}\phi_1\phi_2 \ \ with \ \ \chi'_{12} = \frac{\chi_{12}}{V_{ref}}}$$

$$\boldsymbol{\Delta G_m = RTV \left[\frac{\phi_1}{V_1} \ln \phi_1 + \frac{\phi_2}{V_2} \ln \phi_2 \right] + B\phi_1\phi_2 \ with \ \ B = \chi_{12} RT \left(\frac{V}{V_{ref}}\right)}$$

where R = gas constant, T= temperature, ϕ_i = volume fraction, V = total volume, V_i = molar volume of component i, χ'_{12} = Flory-Huggins interaction parameter and V_{ref}= reference volume. The latter term, V_{ref}, is often calculated as the square root of the product of the molecular or molar volumes of the individual segment units of

the polymeric components ($V_{ref} = \sqrt{V_1 V_2}$). χ'_{12}, the interaction parameter, is further simplified to χ_{12} and, often, as a binary density parameter, B. The first two logarithmic terms of Equation 3 indicate the combinatory entropy of mixing, whereas the third term is the enthalpy of mixing. Since for polymeric species V_i assume large values, the miscibility or immiscibility of a polymer blend is determined by the product of Flory-Huggins interaction parameter and volume fraction $\chi'_{12}\,\phi_1\,\phi_2$ [16].

The critical Flory-Huggins interaction parameter can be defined from the Equation 2. Indeed, by setting the second derivative of the Gibbs free energy mixing with respect to the volume fraction to zero ($\frac{\partial^2 \Delta G_m}{\partial \phi^2} = 0$), the critical conditions of phase separation can be expressed as:

Equation 4. $$\chi'_{12,cr} = \frac{1}{2}\left(\frac{1}{\sqrt{V_1}} + \frac{1}{\sqrt{V_2}}\right)^2$$

Equation 5. $$B_{cr} = \frac{RTV}{2}\left(\frac{1}{\sqrt{V_1}} + \frac{1}{\sqrt{V_2}}\right)^2$$

From the Equation 4 and Equation 5 it is possible to determine the miscibility conditions for systems with species of different molecular weights. Particularly, polymer blends (where V_1 and $V_2 >> 1$) are miscible when $\chi_{12} < 0$ and $\chi_{12,cr} \approx 0$.

2.1.2 Solubility parameter concept

Using the Flory-Huggins equation (Equation 3), Coleman derived the following relationship [17]:

Equation 6. $$\frac{\Delta G_m}{RT} = \frac{V}{V_{ref}}\left[\frac{\phi_1}{N_1} ln\phi_1 + \frac{\phi_2}{N_2} ln\phi_2 + \chi'_{12}\phi_1\phi_2\right] + \frac{\Delta G_H}{RT}$$

where N_1 and N_2 are the polymerization degree of the two blend components and ΔG_H is the free energy related to specific interactions between polymers.

Equation 6 distinguishes three contributions to the free energy of mixing: the configurational entropy given by the two logarithmic terms, the dispersive or Van der Waals interactions represented by the interaction parameter $\chi'_{12}\phi_1\phi_2$ and the strong interaction term ΔG_H which is equal to zero in systems with no specific interaction. The Flory-Huggins interaction parameter, according to Coleman studies, can be related to the concept of solubility [17].

The basic concept involves the match of the solubility parameter for the two components of the blend to achieve miscibility. For solvent-solvent mixtures, the difference of the solubility parameter can be rather large to achieve miscibility; in solvent-polymer mixtures, the difference of the solubility parameter is much lower

to achieve miscibility, while in polymer-polymer mixtures the solubility parameters must be almost identical to achieve miscibility in the absence of strong polar or hydrogen bonding interactions.

Therefore, as a result of these considerations, the Flory-Huggins interaction parameter χ can be defined by following the equation:

Equation 7. $$\chi' = \frac{V_{ref}}{RT}(\delta_1 - \delta_2)^2$$

with δ_1 and δ_2 solubility parameters of polymer 1 and 2, respectively.

The interaction parameter from Equation 7 can be equal to zero when the $\delta_1 = \delta_2$ predicting miscibility between the polymers of the blend. Notwithstanding, the biggest drawback of the solubility parameter approach, is the omission of the effects of specific interactions that could allow to have a negative value of χ'.

2.1.3 Thermodynamics of Phase Separation

In polymer blends it is unusual to fulfil the condition for miscibility ($\Delta G_m \leq 0$ and $\frac{\partial^2 \Delta G_m}{\partial \phi^2} > 0$), since a phase separation is usually present. The thermodynamic conditions for phase separation are illustrated by the phase diagrams of a polymer mixture. Some preliminary remarks must be made before establishing a phase diagram of a binary system. In particular, several definitions are included in the following equation:

Equation 8.

$$\textbf{Binodal: } \Delta\mu_i^{phase\,1} = \Delta\mu_i^{phase\,2}$$

$$\textbf{Spinodal: } \left(\frac{\partial^2 \Delta G_m}{\partial \phi^2}\right)_{P,T} = 0$$

$$\textbf{Critical point: } \left(\frac{\partial^3 \Delta G_m}{\partial \phi^3}\right)_{P,T} = 0$$

$$\textbf{Stability condition: } \left(\frac{\partial^4 \Delta G_m}{\partial \phi^4}\right)_{P,T} > 0$$

Figure 4(a) shows two different graphs with the variation of Gibbs free energy of mixing of a blend consisting of polymer A and polymer B as a function of volume fraction (upper part of the figure) and the liquid-liquid phase diagram for a polymer mixture (lower part of the figure). A generic graph relative to the phase diagram is reported also in Figure 4(b).

If, at a defined temperature, the free energy curve exhibits a region in which the Gibbs free energy of mixing is not at a minimum, a phase separation occurs with the formation of two different composition phases b_1 and b_2 located at the tangent

of the curve. At these peculiar points, the compositions lie on the binodal curve of the corresponding phase diagram. Specifically, the binodal curve is related to the equilibrium phase boundary between the single-phase and the phase-separated region (Figure 4(b)). In a binary system this behaviour is associated to the chemical potentials μ_i^{phase} that are equal in both phases as expressed in the Equation 8; by definition μ_i^{phase} is defined as the rate of change of the Gibbs function of the system with respect to the change in the number of moles of a specific component.

Considering the intermediate compositions between the inflection points, a_1 and a_2 (in Figure 4(a)), phase separation proceeds spontaneously from the composition fluctuations and these points are located on the spinodal curves which correspond to the position where the second derivative of Gibbs free energy mixing with respect to the volume fraction is equal to zero, as reported in Equation 8.

Binodal and spinodal curves coincide at a critical point, at a defined temperature value, which corresponds to the third derivative of ΔG_m equal to zero. The temperatures at the critical point are defined as LCST (lower critical solution temperature) at higher temperature and UCST (upper critical solution temperature) at lower. In particular, the LCST is the critical temperature below which the components of a mixture are miscible for all compositions; whereas the UCST is the critical temperature above which the components of the polymer blend are miscible. The phase diagram with two critical points is fundamental to define the morphological structure characteristic of mixtures with low molecular weight components; while for polymer blends usually one critical point is accessible, typically the lower critical solution temperature LCST.

In particular, the origin to the critical point can be traced to the temperature effects on miscibility. Since it is well-known that the miscibility depends on the value of the Flory-Huggins interaction parameter χ_{12}, it is important distinguish the main contributions affecting χ_{12}. The interaction parameter is a complex function of many independent variables such as concentration, temperature, pressure and molecular weight. In a first approach, three main contributions to the interaction parameter can be distinguished with rather distinct dependencies on T: the contributions of dispersive forces in χ_{12}, with a $1/T$ dependence; the contributions of free volume increasing with T and the specific interaction contribution in χ_{12}, typically increasing with T [18]. Thus, the different temperature dependencies of these contributions affect the interaction parameter differently. Whereas for low molecular weight systems the dispersion interactions and free volume effects dominate the final value of χ_{12} and two critical points UCST and LCST are visible, the miscibility of polymer systems is influenced by the presence of specific interactions that contribute a negative value of the interaction parameter but increase with T until it is balanced by the free volume contribution leading to a single critical temperature value, usually LCST.

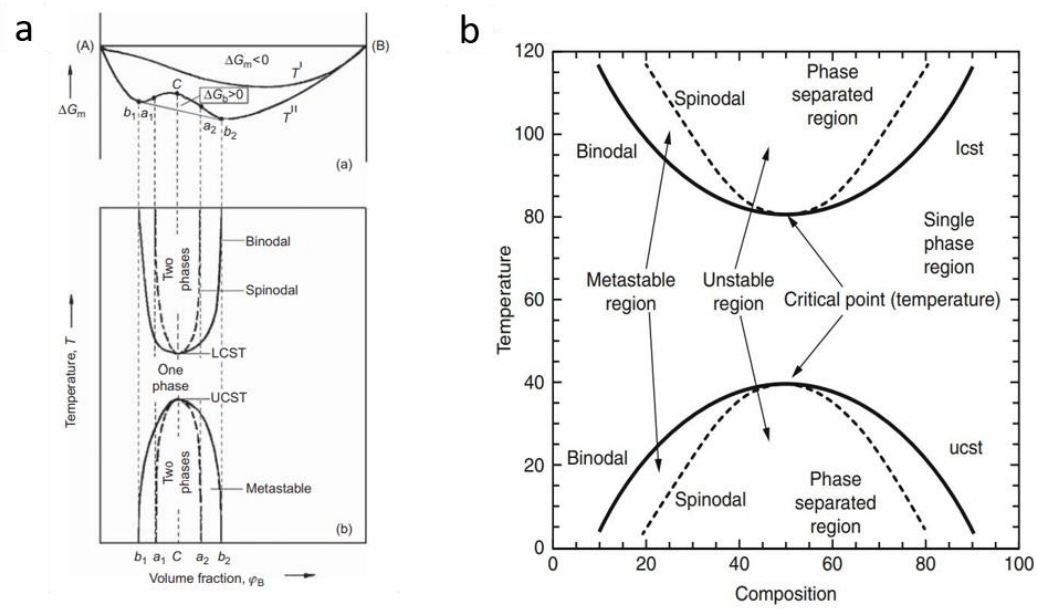

Figure 4. Variation of Gibbs free energy of mixing of a polymer A - polymer B blend as a function of volume fraction and the corresponding phase diagram (a); schematic phase diagram showing LCST and UCST behaviour for a polymer mixture (b).

To better understand the different regions corresponding to the degrees of miscibility of a generic polymer blend, it is necessary to examine the phase diagram in Figure 1b, which can be divided into three different regions:

1. The single-phase miscible region between the two binodal curves;
2. The four fragmented metastable regions between the binodal and spinodal curves;
3. The two-phase separated regions of immiscibility bounded by the spinodal curves.

The mechanism of phase separation occurs when a single-phase system undergoes either a change in composition or a change in T or P values to move from the single-phase region into the metastable region or the two-phase region via the spinodal curves; however, a substantial difference in the incidence of these two just mentioned cases is found. When the system moves from the single-phase region into the metastable region the mechanism of phase separation typically occurs by crystallization and slow nucleation is follow by growth of the phase-separated domains; this peculiar case is called ‘’nucleation and growth’’ or NG. Conversely, when the system jumps from a single-phase region into the two-phase immiscible region, bypassing the spinodal curves, the phases separate spontaneously and the latter case is known as the ‘’spinodal decomposition’’ or SD. A schematic representation of these two different phase separation developments is reported in Figure 5[19].

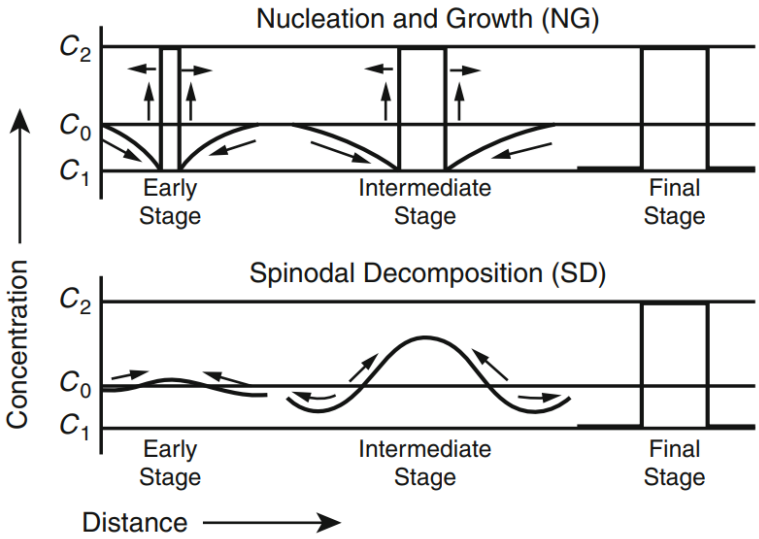

Figure 5. Schematic representation of the density fluctuations during the Nucleation and growth NG and the Spinodal decomposition SD. Reprinted under CC BY 4.0 license from [19].

Looking at the schematic representation above, three different stages of phase separation process can be clearly distinguished: namely an initial, an intermediate and a final stage. The upper and the lower concentration values (C_1 and C_2) are provided by the tie-line limits intersecting the binodal curves at constant temperature.

For the NG process, the evolution of the dispersion pattern follows a linear time dependence. When the concentration of the dispersed phase is above 10-15% the nucleation and growth mechanism is slower than the rapid growth of regularly spaced concentration waves that characterise the spinodal process. In contrast, at lower phase concentrations, the two phase-separation processes are very similar.

The spinodal decomposition mechanism SD follows a semilogarithmic time dependence and it starts with a segmental density fluctuation that increases in amplitude and wavelength. This peculiar mechanism is spontaneous because in the spinodal region the concentration fluctuations are delocalized.

A representation of the blend morphology obtained with NG and SD is shown in Figure 6.

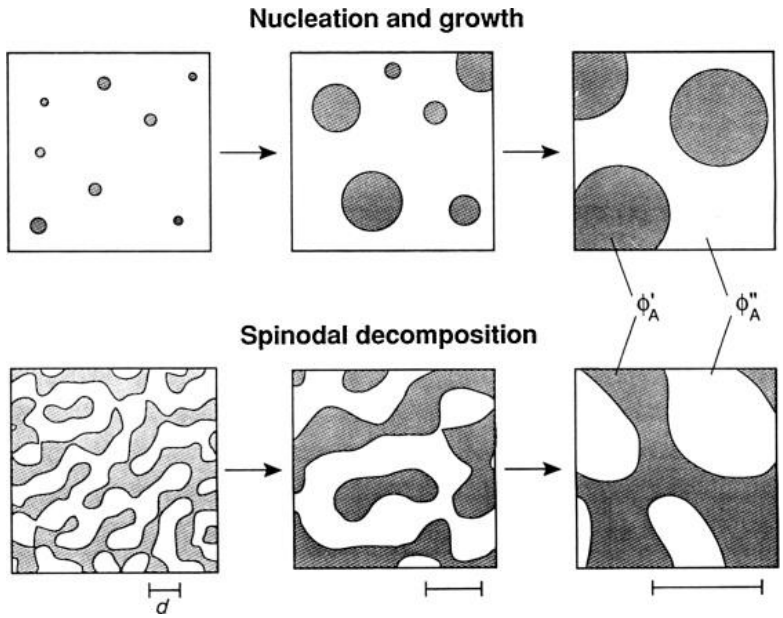

Figure 6. Nucleation and growth NG and spinodal decomposition SD patterns in a binary polymer blend. Reprinted with the permission of [20].

As is visible in Figure 6, in NG mechanism, a small particle (nucleus) with near equilibrium concentration from the uniform solution is generated and grows gradually with time; some domains having different sizes and positions are observed. In contrast, in the SD process, a periodic fluctuation of the concentration in the system spontaneously maintains the regularity of the morphology, allowing equilibrium to be reached so that a co-continuous morphological structure is obtained.

2.2 Morphology development of polymer blends

An important element to define the final properties of a polymer mixture is the control of morphology. [21] [22] [23]. The final morphology of a polymer blend depends on intrinsic parameters such as rheological behaviour and interfacial tension. A very decisive index to study the development of microstructure of the systems is the concentration of each polymeric phase and the adhesion between them. Figure 7 shows a schematic example of the morphology developments in an immiscible blend of a polymer A (black) and a polymer B (white). Polymer A at low volume fraction values ϕ_2 represents the dispersed phase and achieves the shape of the spheres at equilibrium due to the effect of the interfacial tension. As ϕ_2 increase, the morphology changes from a discontinuous dispersion of spherical drops to a morphological structure characterized by the coexistence of the two continuous phases of A and B; at this concentration value, $\phi_2 = \phi_{PI}$, where ϕ_{PI} is the phase inversion volume fraction and the distinction between dispersed phase A and matrix B falls away resulting in a co-continuous morphological structure [24]. A further increase of ϕ_2 of polymer A leads to a phase inversion and the component A becomes the matrix with the polymer B as dispersed phase.

In order to better understand the development of the final morphology of a mixture, it is necessary to analyse in detail each of possible microstructures.

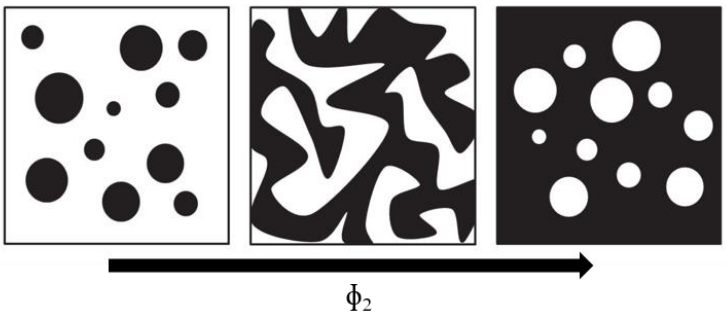

Figure 7. Schematic representation of the morphology development of a binary blend with two component A (black) and B (white). The volume fraction ϕ_2, relative to the polymer A, increases from left to right.

2.2.1 Droplet deformation: breakup and coalescence

Regarding the formation of a droplet structure, it is appropriate to define the interfacial tension and the adhesion between the polymeric phases since they are the most important features of the development of this typical microstructure.

The interface corresponds to the boundary region between two polymeric phases; in particular, an immiscible blend is characterised by a high interfacial tension and a low adhesion between the mixture components. Good and Girifalco combined interfacial tension with surface tension and solubility parameters [25]:

$$\Gamma_{AB} = \Gamma_A + \Gamma_B - 2\varphi\sqrt{\Gamma_A\Gamma_B} \qquad \textbf{Equation 9.}$$

where Γ_{AB} is the interfacial tension between polymers, Γ_A and Γ_B are the surface tension of polymer A and B, respectively and φ is the interaction parameter of Good and Girifalco which varies between 0.79 and 0.98, according to the values reported by Wu [26].

The surface tension Γ_i can be correlated to the solubility parameter δ_i and the density ρ_i using the Equation 10.

$$\Gamma_i = 0.2575\frac{\delta_i}{\sqrt[3]{\rho_i}} \qquad \textbf{Equation 10.}$$

Considering φ and ρ equal to 1 and by combining the previous equations the following correlation can be obtain:

$$\Gamma_{AB} \cong 0.26(\delta_A - \delta_B)^2 \qquad \textbf{Equation 11.}$$

This relationship leads to conclude that low values of interfacial tension are obtained when the solubility parameters of the polymeric phases in a polymer blend are similar.

It is fundamental to consider that the droplets are subjected to the Drag force, deriving from the applied stress field, which tends to break up them. This force can be defined as:

Equation 12. $$F_{Drag} \sim \eta_c \dot{\gamma} a^2$$

where η_c is the viscosity of the continuous phase,$\dot{\gamma}$ the shear rate and a the area of the droplet.

The morphology of mixtures depends on the interplay between interfacial tension and Drag force; thus, it is possible to define a dimensionless capillary number, Ca as the ratio between these two quantities:

Equation 13. $$C_a = \frac{F_{Drag}}{F_{interfacial}} = \frac{\eta_c \dot{\gamma} D_d}{2\Gamma_{AB}}$$

where D_d is the diameter of the droplet. The Equation 13 is valid only for creeping flow, so the Reynolds number of the deformation is much smaller than the critical value for turbulence [27].

Considering that in many processing operations the melt is subjected not only to shear but also to elongational deformations, it is important to consider the morphological changes caused by the elongation stress. Thus, it is possible to define the capillary number under elongational deformations:

Equation 14. $$C_{aE} = \frac{\eta_{Em} \varepsilon D_d}{2\Gamma_{AB}}$$

where η_{Em} and ε are the elongational viscosity of the matrix and the elongational rate, respectively.

The capillary number becomes important when changes in morphology occur during the deformation. In fact, at sufficiently high stresses the droplet shape of the disperse phase is unstable; the droplet can be further elongated and breaks with the formation of new particles. The process of the breakup is described by the critical capillary number Ca_{crit}, which is found to be dependent on the viscosity ratio (*p)* between the viscosity of the dispersed phase (η_d) and the viscosity of the matrix or continuous phase (η_m). For $Ca<Ca_{crit}$ the shape of the deformed droplets is stable and can be predicted theoretically as a function of deformation.

A comprehensive experimental work on the determination of the critical capillarity number for Newtonian liquid can be found in a study by Grace [27].

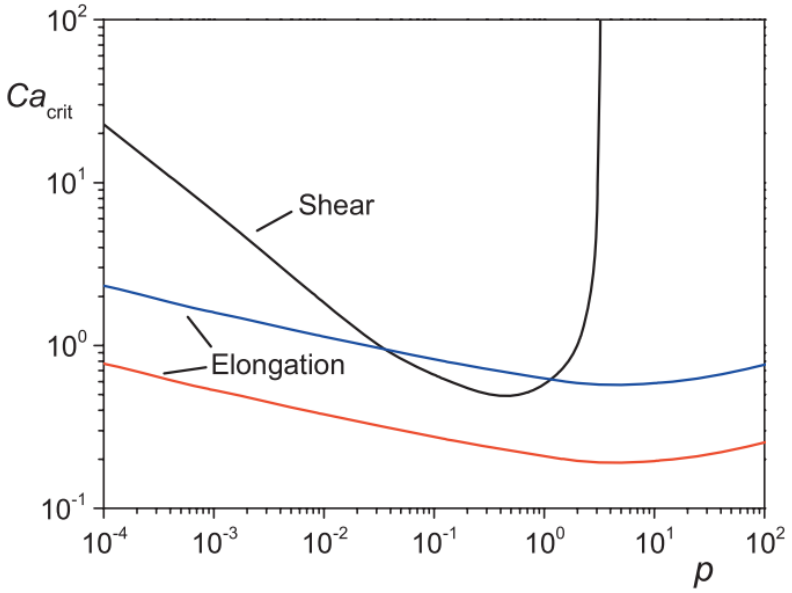

Figure 8. Critical capillary number Ca_{crit} in shear and elongation as a function of the viscosity ratio $p=\eta_d/\eta_m$ Reprinted with the permission from [27].

The trend curves of the critical capillary number as a function of the viscosity ratio are significantly different in shear and elongation flow and the curves are reported in Figure 8. In particular, in shear the Ca_{crit} decreases earlier as a function of viscosity ratio, and for $p>4$ droplet breakup was no longer found. The critical capillary numbers determined during the elongational flow are smaller than those in shear for the whole viscosity ratio range reported in Figure 8. This result means that the elongation flow is more effective with respect to the shear one in promoting the droplet breakage.

However, the curves reported in Figure 8 have to be only qualitatively considered for polymer blends since the measurements were performed on Newtonian fluids in both shear and elongational flow regimes [27]. Therefore, the use of the curves for polymeric materials that usually show non-Newtonian behaviour is not straightforward. The polymer constituting the blends have viscoelastic properties that influence the deformation and breakage of droplets and, consequently, the critical capillary number. In fact, while the behaviour of Newtonian fluids is well known, the behaviour of polymers is certainly more difficult to understand and to model than that of a Newtonian fluid.

Despite the several differences, the Newtonian case gives some guidelines such as the theory of Taylor on instability and droplet breakup in polymer mixtures [28]. According to whom:

- for $Ca<<Ca_{crit}$ the droplet shape is in equilibrium;
- for $Ca>>Ca_{crit}$ deformation of the droplet shape occurs neglecting the effect of interfacial tension.

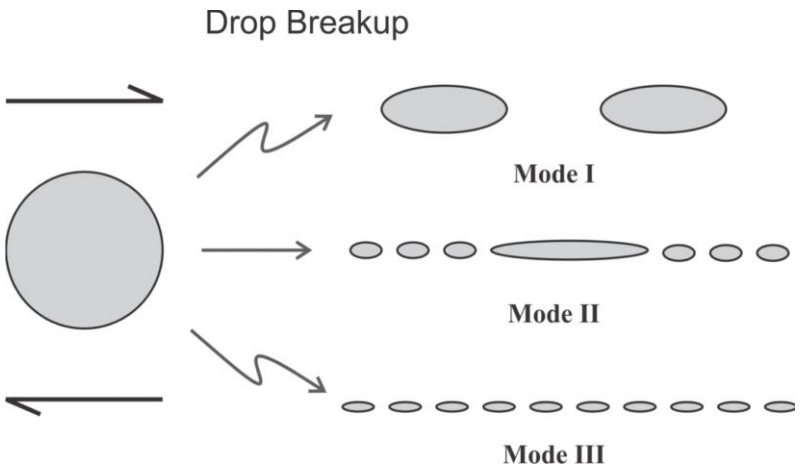

Figure 9. Breakup mechanisms of a non-Newtonian droplet in a fluid. Reprinted with the permission from [29].

As shown in Figure 9, the instability generated by the flow causes the droplets to break up into smaller particles in different ways. The Mode I called mid-point pinching, allows that the drop undergoes breakup through mid-point pinching, producing two droplets of nearly equal size. In the edge breakup or Mode II, the drop becomes unstable preferentially at their edges, leading to detachment of smaller droplets from the intact central segment; finally, the droplets in the Mode III homogeneous breakup break apart into a large number of drops with equal dimensions and sizes [29].

The deformation of the droplets of the dispersed phase can be characterized not only by the breakup phenomenon, but also by the coalescence mechanism which occurs at small concentration of the dispersed phase. During flow, the droplets can get close enough to each other so that the dispersed structures combine into a larger particle. Two types of coalescence can be identified: the first is determined by equilibrium thermodynamics (liquid-liquid miscibility, interfacial tension coefficient and rheological condition of the interphase) and the second one is defined by dynamics and flow conditions. However, due to the great number of parameters affecting the coalescence mechanism, existing theories are rather restrictive; a state of art relative to this mechanism is discussed by Fortelny in his work ‘’Coalescence in polymer blends: solved and open problems’’[30]. The coalescence involves four consecutive stages: the collision between droplets, the drainage of the thin film trapped between the droplets, the rupture of the thin film and the merging of the drops. The collision is considered as the critical event, without which there is obviously no coalescence but, it is essential to emphasise that a collision of two drops does not always result in a single larger drop. In fact, the hydrodynamic forces can push the colliding drops together or the thin film developed between the drops may resist.

The coalescence does not occur if the flow reverses and separates the two droplets or if the film resists; a schematic representation of the coalescence mechanism is reported in Figure 10.

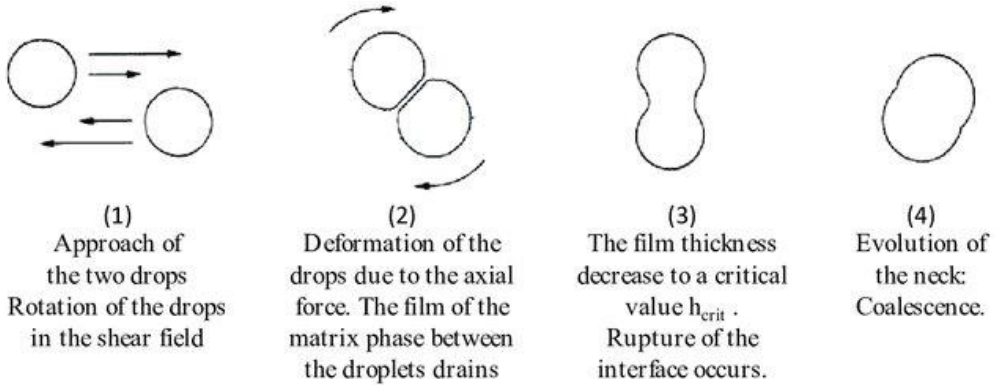

Figure 10. Schematic representation of the coalescence process. Reprinted under CC BY 4.0 license from [31].

The coalescence is considered as a dynamic phenomenon and it will be promoted by low shear rate and low resistance films between the drops. The resistance of the film is governed by the time required for the matrix to be drained between the contacting droplets; two different limitations for drained film have been considered in literature. One model considers the hypothesis of a fully mobile interface: at small and intermediate values of viscosity ratio. The other model assumes immobile interface, applicable when the viscosity ratio is well above unity. Both models describe the evolution of the droplet size as a function of the time. The frequency of collision, contact time and hydrodynamic forces are combined with the film drainage model to give the probability that the collision between the drops results in a coalescence event.

2.2.2 Phase co-continuity

In a binary system of two polymers, consisting of a matrix and a dispersed phase, the increase of the minor phase can allow obtaining a morphology different from the droplet one. In particular, as reported in Figure 11, the dispersed phase is a discontinuous dispersion of droplets (a) progressively interconnect until a fibril structure is obtained (b). At a certain concentration called phase inversion volume fraction ϕ_{PI}, the discrimination between continuous and dispersed phase disappears and the morphology of the system becomes co-continuous (c).

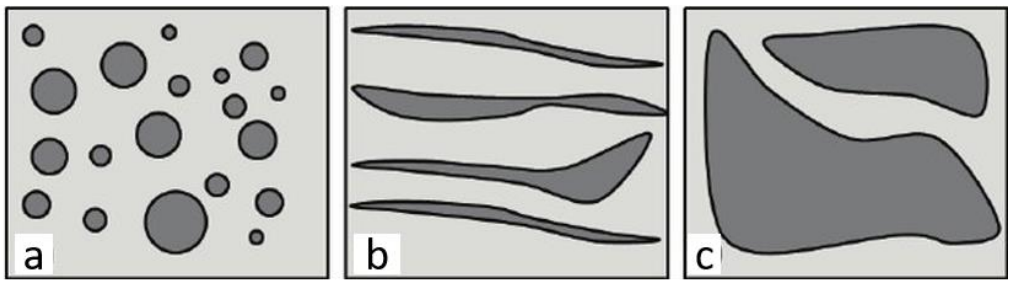

Figure 11. Different morphologies of immiscible polymer blends (a) dilute droplet blends; (b) elongated fibrils; (c) co-continuous structure. Reprinted under CC BY 4.0 license from [32].

Phase-continuity is one of the most important aspects of blend morphology because the co-continuity could allow to improve the final properties of the blend. Therefore, it is of interest to determine the composition at which co-continuity morphology can be formed.

Two definitions for co-continuous structures have been proposed and the differences are graphically reported in Figure 12. The first one considers the blend as a system in which the two polymers form two different and complementary reversed networks without interruptions; the range of relative composition in which it occurs is called the phase inversion point ϕ_{PI} [33]. The second definition was proposed by Utracki and it is based on the concept of percolation threshold; a co-continuous structure occurs if the two components of the mixture form two structures, one for each polymer, extended over the whole volume. The range of volume fractions is between the critical volume fractions ϕ_{cr} of the polymers constituting the mixture, also called percolation threshold volume fractions, ϕ_{perc} [24].

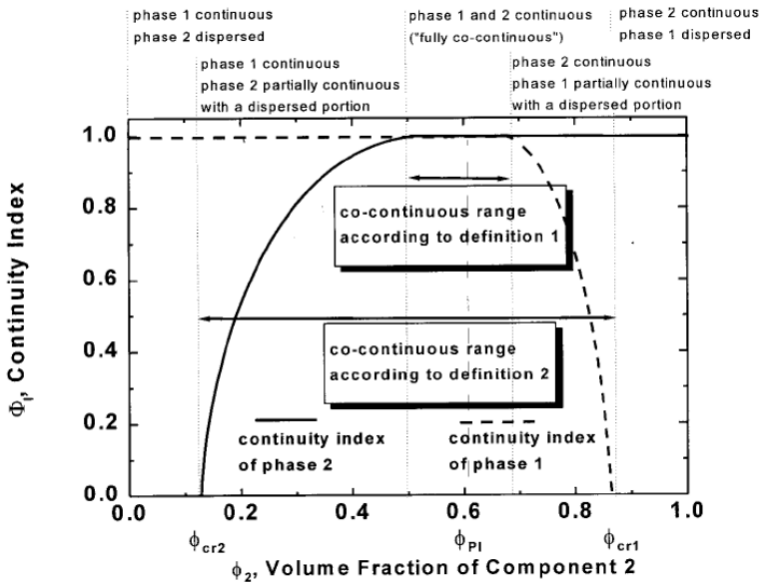

Figure 12. Difference between the two definitions of the co-continuous structure in a polymer blend. Reprinted with the permission from [33].

In particular, the first definition is the most used in literature, but it can be considered a special case of the second one, with both the components having ϕ_{PI} equal to 1.

The threshold percolation theory, proposed by Utracki [24], is based on an average volume fraction ϕ_{onset} equal to 0.19± 0.09 for which the onset of co-continuity occurs; as an example, Figure 13 reports the variation of phase co-continuity in high-density polyethylene/polystyrene (HDPE/PS) blends.

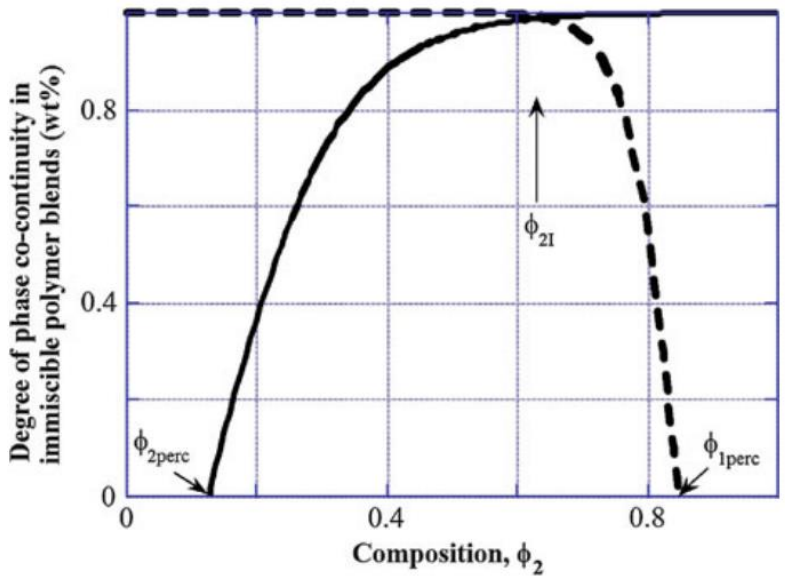

Figure 13. Co-continuous range and phase inversion point ϕ_{PI} in HDPE/PS immiscible blends, defined by the percolation threshold theory of Lyngaae-Jorgensen and Utracki; reprinted with the permission from [24].

Lyngaae-Jorgensen and Utracki [24] in their work demonstrated that for immiscible blends the onset of phase co-continuity coincides with the percolation threshold. In fact, the data obtained for HDPE/PS mixtures by selective extraction of the matrix phase, indicate that the onset of phase co-continuity occurred at ϕ_{1perc} = 0.16 and ϕ_{2perc} = 0.15, whereas ϕ_{PI} = 0.64. Thus, at equilibrium and within the region of low volume fraction of the dispersed phase, if $\phi_2 < \phi_{2perc}$ the morphology is characterized by droplet-like morphology, whereas at $\phi_2 > \phi_{2perc}$ a co-continuous structure is generally observed. The breadth of the range of co-continuity composition depends on the size of the experimental concentration step used during the selective extraction tests. The main condition proposed to relate the phase inversion composition ϕ_{PI} of both components (matrix and dispersed phase) and viscosity ratio p is expressed by the following equation [34]:

Equation 15. $$\frac{\phi_{PI1}}{\phi_{PI2}} = \frac{\eta_1}{\eta_2} = p \qquad \text{or} \qquad \phi_{PI2} = \frac{1}{(1+p)}$$

with ϕ_{PI1} =1- ϕ_{PI2} where ϕ_{PI1} and ϕ_{PI2} are the volume fractions 1 and 2, respectively, at the phase inversion. The Equation 15 is defined as the co-continuity condition and it is proposed by Paul and Barlow [35] as a generalization of the experimental observations reported by Avgeropoulos *et al* [36].

The relationship is applicable to systems prepared at low stresses; therefore, the viscosity ratio p should correspond not to viscosity ratio at zero-stress but to its value at the shear stress used to prepare the blends. Furthermore, the Equation 15 was found to describe the phase inversion for systems with nearly equal polymer viscosities where $p \rightarrow 1$; with an increase of the viscosity ratio, a more rapid change of ϕ_{PI2} can be found.

2.3 Rheological considerations

Fundamental aspects in the study of polymeric mixtures are the rheological investigations of the blends; in particular, it is important to consider an extension of the general rheological dependencies observed for single polymeric component. Obviously, the basic definitions of rheological functions are identical for both single-phase and multiphase polymer systems. However, any constitutive equation to describe the flow in polymer blends, especially in immiscible mixtures, should combine three different elements: the stress-induced effects on the concentration gradient, an orientation function and a description of the stress-strain behaviour of the systems considering that the final morphology is influenced by the flow.

For immiscible blends, the flow is affected by three different phases: the polymeric components and the interphase. The morphological structure of a blend determines the rheological behaviour in the molten state and the final properties of the polymer mixture.

In this section, two fundamental aspects of the rheological behaviour of polymer blends will be examined: first, the study of viscosity with the aim of defining the mixing rules, i.e. the relationships that predict the viscosity of a blend as a function of the properties of the individual components, the composition and the interfacial properties; second, the study of the elastic behaviour of polymer mixture as a result of the presence of the interphase and the viscoelastic properties of the polymers.

2.3.1 Viscosity of polymer blends

It is very difficult to define a complete theory describing how the viscosity of a blend varies with the viscosities of the individual polymer components. Therefore, a simple approach that correlates the viscosity of the mixture with those of its components A and B is required; this relationship is expressed through the mixing rules:

Equation 16. $$\eta = f(\eta_A, \eta_B, \phi)$$

Equation 17. $$\eta^n = \eta_A^n \phi + \eta_B^n (1 - \phi)$$

where η_A and η_B are the viscosities of each component of polymer blend and ϕ is the volumetric fraction of polymer A. In Equation 17, used to predict the physical properties of heterogeneous system [37], three cases can occur:

- n=1 corresponds to a linear mixing rule where the viscosity of the blend is the linear average of those of components A and B:

Equation 18. $$\eta = \eta_A\phi + \eta_B(1-\phi)$$

- $n \rightarrow 0$ gives a logarithmic relationship:

Equation 19. $$\log\eta = \log\eta_A\phi + \log\eta_B(1-\phi)$$

- $n = -1$ corresponds to a linear mixing rule with the reciprocals of the viscosities:

Equation 20. $$\frac{1}{\eta} = \frac{1}{\eta_A}\phi + \frac{1}{\eta_B}(1-\phi)$$

Among the three possible cases, the most reasonable is the linear law (n=1) providing that the graph of viscosity as a function of volume fraction is linear and that the extremes correspond to the viscosity values of the pure components. However, taking into consideration an immiscible polymer blend, Figure 14 shows that a positive or negative deviation from the expected linear trend can be obtained; nevertheless, Ablazova et al. [38] have demonstrated in several studies that it is difficult predict the frequently observed change from a positive to a negative deviation behaviour when moving from low to high shear rates.

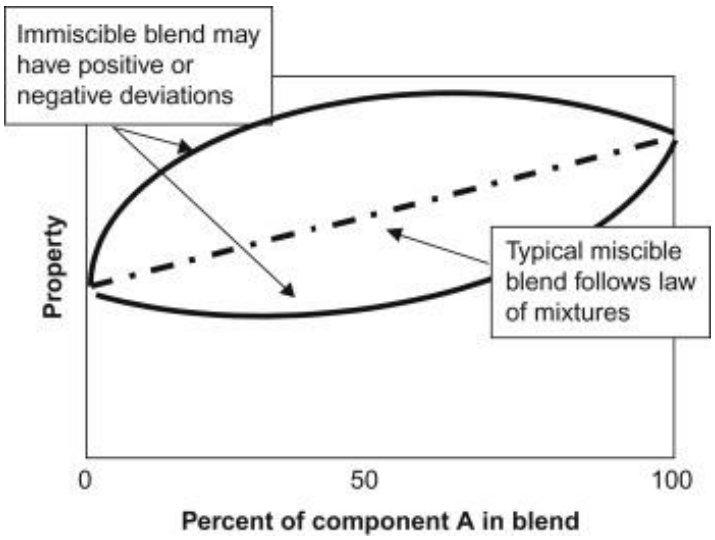

Figure 14. Variation of a certain property in a blend depending on the percentage of the A component. The behaviour of miscible and immiscible blends is plotted with dashed and continuous lines, respectively. Reprinted with the permission from [39].

More complex empirical relationships can be found in literature; as an example Utracki [40] proposed the following mixing rule:

Equation 21. $$\log\eta = \log\eta_L + \Delta\log\eta^E$$

where $log\eta_L$ represents a negative deviation contribution:

Equation 22. $$log\eta_L = -\log\left\{1 + \beta[\phi_A(1-\phi_A]^{\frac{1}{2}}\right\} - \log\left(\frac{\phi_A}{\eta_A} + \frac{1-\phi_A}{\eta_B}\right)$$

The Equation 22 describes the telescopic, multi-layered flow of two liquids. Slip between layers is controlled by the interlayer parameter β. In Equation 21 $\Delta log\eta^E$ is an ''excess'' viscosity term which produces a positive deviation contribution and it is described by the following relationship:

Equation 23. $$\Delta\log\eta^E = \eta_{max}\left[1 - \frac{(\phi-\phi_1)^2}{\phi(1-\phi_1)^2 + \phi_1^2(1-\phi)}\right]$$

where ϕ_1 is the phase inversion volume fraction and η_{max} is an empirical constant.

The relationship (Equation 21) formulated by Utracki is a perfect example of mixing rule because it is capable to consider any deviation (negative or positive) from linear behaviour, but it is a descriptive relationship and not at all predictive.

Mixing laws, based on physical models, can include some information on the blend morphology. As mentioned in paragraph 2.2, an immiscible mixture can be characterized by different basic microstructures including the droplet morphology. In this particular case, the influence of the dispersed phase on the viscosity is considered as a correction to the viscosity of the continuous phase.

The following relationship of the viscosity of a mixture of two Newtonian fluids was derived by Taylor in 1934 [41] and it represents a mixing law for an emulsion of noninteracting Newtonian droplets in a Newtonian matrix in shear flow:

Equation 24. $$\eta = \eta_m(1 + \frac{5p+2}{2p+2}\phi)$$

where η_m, p and ϕ are matrix viscosity, viscosity ratio and volume fraction of the droplets, respectively.

The Equation 24 allows to conclude that the viscosity of the blend is always higher than the viscosity of the matrix ad it gives a confirmation of the viscosity behaviour that results in a positive deviation, at low shear rate; thus, the blend is characterized by a droplet-like morphology where the disperse phase has a higher viscosity than the viscosity of the matrix. However, a possible change of the microstructure, from a droplet-like to a co-continuous morphology, cannot be predicted by the Equation 24.

By increasing the concentrations of the dispersed phase, the dilution hypothesis of Taylor (Equation 24) was modified by Choi and Schowalter [42]:

Equation 25. $$\eta = \eta_m\left[1 + \frac{5p+2}{2p+2}\phi + \frac{5(5p+2)}{8(p+1)^2}\phi^2\right]$$

These relationships, represented by Equation 24 and Equation 25, cannot predict viscosity behaviour at intermediate concentrations approaching the phase inversion phenomenon [34].

In shear flow, the size of the dispersed phase will depend upon the competition between the break-up and coalescence phenomena. Droplet radius and rheological parameters can be correlated. Particularly, the breakup only occurs for particles with a radius above a critical value R_{break} [27] [41], which is inversely proportional to shear rate; coalescence, on the other hand, takes place only for droplets with a radius below a critical size R_{coal} [43] depending by the exponent υ relative to the amount of surface mobility:

Equation 26. $$R_{break} = K\dot{\gamma}^{-1} \quad and \quad R_{coal} = K\dot{\gamma}^{-\nu}\ ;\ \nu < 1$$

Elmendrop [44] predicted that at low shear rates steady-state drop size is controlled by coalescence; in this case $R_{coal} < R_{break}$ and the droplets will never reach a size large enough for breakup to set in. Conversely, at high values of shear rates $R_{break} < R_{coal}$ and the particles will always breakup before reaching the limiting size for coalescence.

2.3.2 Viscoelastic behaviour of polymer blends

The presence of elastic effects in immiscible blends is generated by two distinct causes: the elasticity of the interface caused by interfacial tension and the intrinsic viscoelastic behaviour of the polymer components.

In Figure 15 the trends of the elastic modulus G' of an immiscible polymer blend and those of each component are reported. The effect of the interface elasticity is visible in the shoulder of the G' curve of the mixture, appearing at intermediate frequencies. At high frequencies, where the predominant contribution is given by the elasticity of the polymer, the value of G' is similar to that of the matrix; at low frequencies, instead, the elasticity of the blend is higher than that of the more elastic component constituting the mixture.

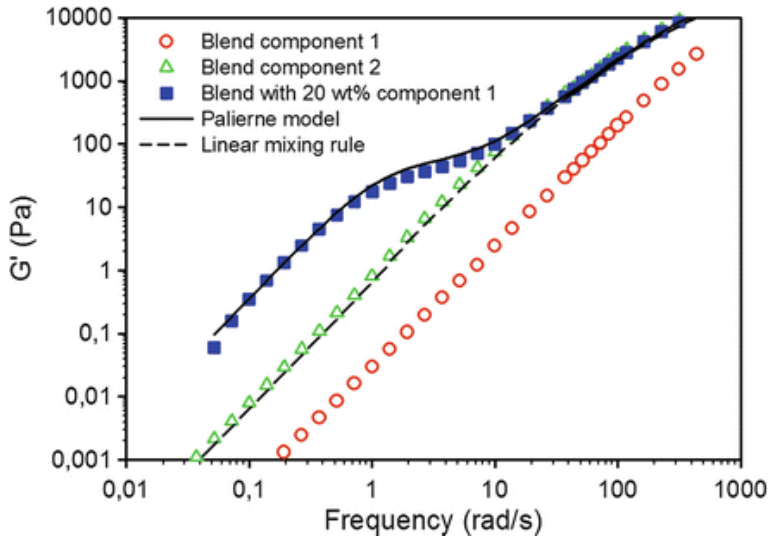

Figure 15. Trend of G' modulus as a function of the frequency of immiscible polymer blend and neat components. Reprinted with the permission from [45].

Palierne [46] proposed a generalized approach to predict the elastic and dissipative moduli of an immiscible blend, by correlating the viscoelastic properties of the components, the composition of the mixture and the influence of particles sizes and interfacial tension:

Equation 27.

$$G^*(\omega) = G_m^* \frac{1+3\phi H(\omega)}{1-2\phi H(\omega)} \quad with$$

$$H(\omega) = \frac{8\frac{\alpha}{D}(2G_m^*+5G_d^*)+(G_d^*+G_m^*)(16G_m^*+19G_d^*)}{80\frac{\alpha}{D}(G_m^*+G_d^*)+(3G_m^*+2G_d^*)(16G_m^*+19G_d^*)}$$

where G_d^* and G_m^* are, the complex moduli of the dispersed phase and the matrix, respectively, ϕ_i is the volume fraction of droplets with radius R_i and α is the interfacial tension. The validity of the model is limited to a dilute emulsion; thus, it is not applicable to concentrated blends. In Figure 16 an example of the good agreement between model prediction and experimental behaviour is shown.

The model of Palierne can be simplified in order to determine the average size of the disperse phase, assuming that the two phases show Newtonian behaviour and that the droplets of the dispersed phase are equal in size and shape. Therefore, an explicit correlation for the characteristic relaxation time of the interface τ_{int} can be calculated as follow:

Equation 28.

$$\tau_{int} = \frac{D\eta_m}{8\alpha} \cdot \frac{(19p+16)\cdot[2p+3-2\phi(p-1)]}{10(p+1)-2\phi(5p+2)}$$

τ_{int} can be easily derived from the time relaxation spectra of the blend; the weighted relaxation spectrum ($\tau H(\tau)$) can be calculated with data coming from small amplitude oscillatory shear measurements, using the method proposed by

Honerkamp and Weese [47] which is based on the response of an infinite number of Maxwell models placed on parallel:

Equation 29. $$G'(\omega) = \int_{-\infty}^{+\infty} H(\tau) \frac{\omega^2\tau^2}{1+\omega^2\tau^2}\, d\ln\tau$$

Equation 30. $$G''(\omega) = \int_{-\infty}^{+\infty} H(\tau) \frac{\omega\tau}{1+\omega^2\tau^2}\, d\ln\tau$$

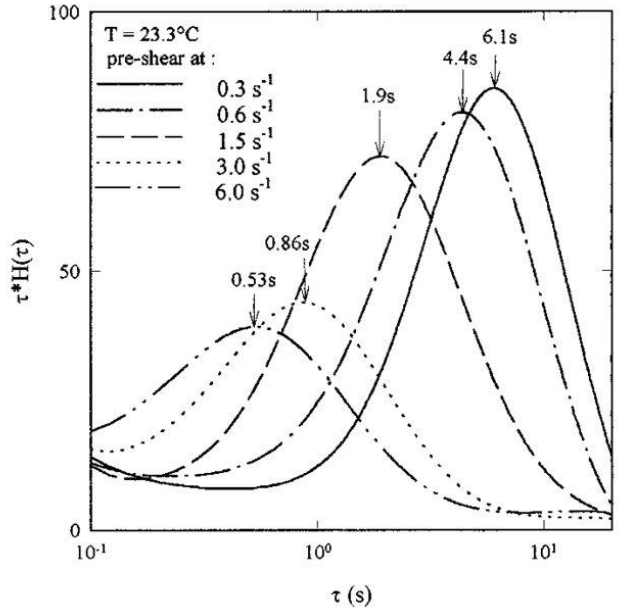

Figure 16. Example of interfacial relaxation spectra for immiscible polydimethyilsiloxane PDMS/poly-isobutene PIB blend with 30 wt% of PIB dispersed phase after different shear rate. Reprinted with the permission from [48].

In the example shown in Figure 16 the blend was exposed to a stationary shear flow at different shear rates in order to produce droplets of decreasing diameter as the shear rate increases. The relaxation time is visible as the local maximum of the spectrum; it is evident that the relaxation time shifts to lower values as the shear rate increases, resulting in a clear sign of decreasing inclusion size.

Therefore, by knowing the value of the relaxation time and the other physical parameters, through the Palierne method it is possible to calculate the size of the droplets from Equation 28.

However, some limitations are present: the independent measurement of the interfacial tension is essential but also complex to derive and, additionally, the Palierne model is valid in the hypothesis of dilute emulsion and not for concentrated mixtures.

Chapter 3

Biopolymers and development of biopolymer blends

3.1 Biopolymers

Biopolymers received wide attention in the early 1970s and have been extensively investigated in academia and industry because their use reduces carbon dioxide emissions, municipal solid waste and dependency on fossil fuel-based resources. An exhaustive classification of biopolymers is given in the Chapter 1, but a schematic representation is also reported here in Figure 17.

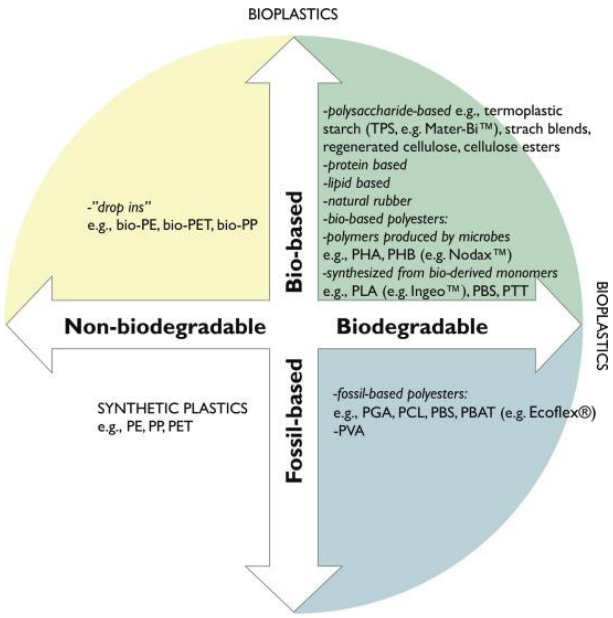

Figure 17. Schematic representation of the classification of biopolymers. Reprinted with the permission from [49].

Biodegradable polymers derived from renewable resources include polylactic acid PLA which is the most widely used at industrial level since its properties are similar to those of fossil-fuel polymers; and the polyhydroxyalkanoates PHAs which are interestingly biodegradable polymers as they are extremely adaptable in numerous application fields and generate minimal environmental impact.

PLA is a polyester derived from LA lactic acid monomer, which can be recovered from the renewable sources. (bacterial fermentation of carbohydrates such as corn, potatoes and several biomasses). This biopolymer is well known for its biocompatibility and biodegradability, and can be easily processed using existing polymer-processing equipment and techniques. The properties of the PLA can be different due to the presence of the pendent methyl group on the alpha carbon atom by generating L-, D- and DL-lactide isomers. In particular, L-lactide is produced by microorganisms, while DL-lactide is a synthetic mixture of L- and D- forms.

L-lactide homopolymer (PLLA) is a semi-crystalline polymer with a melting point (T_m) of 160-180°C and a glass transition temperature (T_g) of 55-65°C [50] . It is characterized by a slow crystallization rate and its crystallinity depends on processing condition such as cooling rate and annealing status. PLLA is characterized by high tensile strength and modulus and low elongation ad break; in fact, it exhibits much higher tensile strength (≈60 MPa) and elastic modulus (≈3 GPa) than many fossil fuel-based polymers [51] . For instance, high-density polyethylene (HDPE) has typical strength and modulus of 20 MPa and 1 GPa, respectively, whereas polypropylene (PP) shows typical strength and modulus of 30 MPa and 1.5 GPa [52]. One of the main disadvantages of PLA is its brittleness which significantly limits the applications of this material; in fact, the typical tensile strain at break of PLA is less than 6%. Several methods have been used to increase the elongation at break of PLA, such as the copolymerization of lactides with other monomers, the addition of miscible plasticizers and the blending with ductile polymers by maintaining its biodegradability. The above-mentioned methods can significantly increase the elongation of PLA; however, the strength and the modulus decrease at the same time [53] [54].

PHAs are biodegradable polymers synthetized and accumulated by bacteria as carbon and energy storage materials; more than 250 species of bacteria have been reported to produce PHAs. The most studied PHAs are the poly(3-hydroxybutyrate) (PHB) and its copolymer poly(3-hydroxybutyrate-co-3-hydroxyvalerate) (PHBV). The former is a crystalline thermoplastic polymer with a T_m of 175°C, T_g equal to 9°C, a crystallinity content of 80% and most of these properties are similar to those of PP. With the introduction of the hydroxyvalerate units (HV), the regular structure that characterized the PHB is transformed and the crystallinity, crystallization rate, glass transition temperature and melt temperature decrease as the content of HV increases [55]; however PHBV becomes more flexible at higher percentage of HV. Table 1 shows the thermal and mechanical properties of PHB and PHBV with different mole ratios of HV [56].

Table 1. Thermal and mechanical properties of PHB and PHBV.

	T_g (°C)	T_m (°C)	Modulus (GPa)	Strength (MPa)	Strain at break (%)
PHB	9	175	3.8	45	4
PHBV (11%HV)	2	157	3.7	38	5
PHBV (20%HV)	-5	114	1.9	26	27
PHBV (28% HV)	-8	102	1.5	21	700
PHBV (34%HV)	-9	97	1.2	18	970

PHAs have been mixed with many biodegradable and non-biodegradable polymers to improve their properties. In particular, PHB was found to be miscible with poly(ethylene oxide) (PEO), poly(vinyl acetate) (PVAc), poly(p-vinyl phenol), poly(vinylidene fluoride), and poly(methyl methacrylate) (PMMA). Conversely, PHB is not miscible or it is only partially miscible with poly(vinyl acetate-covinyl alcohol), PCL, PLA and poly(oxymethylene) [57].

Biodegradable polymers can be derived not only from natural resources but also from petroleum; this category includes poly(butylene succinate) (PBS).

PBS is one of the most important biodegradable polyesters synthesized by polycondensation between succinic acid and butanediol. This material exhibits a melting temperature >100°C, a thermal degradation temperature T_{onset} >300°C and other properties similar to lower-density polyethylene (LDPE), HDPE and PP [58]. The physical and mechanical properties of PBS are summarized in Table 2.

Table 2. Comparison of the properties of PBS and LDPE, HDPE and PP.

	PBS	LDPE	HDPE	PP
T_g (°C)	-32	-120	-120	5
T_m (°C)	114	110	129	163
HDT (°C)	97	88	110	145
Tensile strength (MPa)	57	35	39	44
Yield strength (MPa)	32	12	27	31
Flexural modulus (MPa)	656	276	1070	1370
Strain at break (%)	700	400	650	800

PBS can be processed for injection moulding, extrusion, and film blowing using conventional equipment; in fact, it is considered a potential alternative to petrochemical polyolefins also at industrial level.

3.2 Applications of biopolymers

The applications of biopolymers are numerous and include many industrial fields due to their excellent properties such as biocompatibility, biodegradability, non-toxicity and comparable mechanical properties with respect to conventional fossil fuel-based polymers.

Although the biopolymers have received attention in the last years because they are considered a good solution to reduce the environmental pollution, it is important to define the areas where these materials may be suitable according to their characteristics. For instance, it is impossible to use a compostable polymer as PLA in water pipes, but a bio-based non-biodegradable PP or PE are perfect solutions for this application.

The wide range of applicability of biopolymers includes food packaging, biomedicine, agriculture, automotive industries and others. However, the food packaging is the most relevant field of application at industrial level for these materials; while the other fields of application are still under development. An overview of the applications of biopolymers is reported in Figure 18.

Figure 18. Summary representation of the numerous fields of application of biopolymers. Reprinted with the permission from European Bioplastics Association [5].

In order to have a defined understanding of the use of biopolymers, the main fields of application will be analysed below.

The main purpose of the use of polymers in *food packaging* is to protect food from physical and chemical damage during distribution and to maintain the shelf-life. In recent years, the characteristic non-toxicity of bio-based polymers allowed to concentrate the almost exclusive use of biopolymers in this field of application, replacing fossil-fuel based polymers. The materials selected for the packaging

applications must have optimized mechanical properties and, in addition, they should maintain certain requirements such as protection of food quality from contamination and formation of a good barrier. The most common biopolymers used for this application are PLA, PHAs, thermoplastic starch (TPS), cellulose and proteins due to their non-toxicity and odour-lessness. For example, the gas barrier properties of a PLA-cellulose blend of a multi-layer package have been investigated and the results show that this mixture has sufficient gas barrier properties [59]. In another work, Cinelli *et al.* applied a whey protein layer to a commercial compostable packaging film and evaluated its oxygen barrier properties without compromising the biodegradability, obtaining an improvement in oxygen barrier properties [60].

Nevertheless, some limitations exist for the full exploitation of biopolymers in this field, because of their high cost, poor processability and high hydrophobicity compared to the fossil fuel-based polymers. A potential solution to mitigate these disadvantages is the formulation of blends with other biopolymers that do not compromise their biodegradability characteristics or by using reinforcing elements such as nanoclays. These nanoparticles have attracted considerable interests in food packaging because their introduction into polymer-based systems is easy and they have low cost [61]. The incorporation of these nanofillers into biopolymers or in blend of two different biodegradable components, can improve not only gas barrier properties but, also, thermo-mechanical performance, flexural properties and impact strength. As an example, nanoclays can significantly improve the heat distortion temperature (HDT) of PLA, thereby expanding its field of application [62]. Bathia *et al.* [63] studied a blend between PLA and PBS with a weight ratio of 80/20; however, due to the poor interfacial interaction between these biopolymers, the authors do not achieve the desired improvements in properties. A good increase in oxygen barrier performance (increased by ≈28%) is obtained by incorporating 5 wt% Cloisite30B nanoclay into a PLA/PBS mixture.

As shown in Figure 18, biopolymers are also used in *biomedical industry* especially in drug delivery, tissue engineering and implants and scaffolds. The growing interest in biomedical applications of biopolymers is due to their biocompatibility, non- toxicity and non-immunogenicity.

For example, PLA has recently received approval from the Food and Drug Administration (FDA) for the use in biomedical application owing to its biodegradability and biocompatibility [8]. Some studies have investigated the potential application of PLA containing chitin and lignin for implantation and healing application. The results show that with the introduction of lignin, a decrease in tensile strength and elongation at break is achieved; however, the cell metabolic activity is not altered [64]. On the contrary, the mechanical performances of PLA enhance with the addition of chitin and the final materials have antimicrobial activity against E. coli bacteria [65].

A marked improvement in HDT value, tensile modulus, flexural strength and impact strength is found for a PBS-based composite containing biocarbon and graphene [66]. Figure 19 reports the results of this study and it can be noticed that the mechanical properties of PBS composites exceed those of the pure biopolymer.

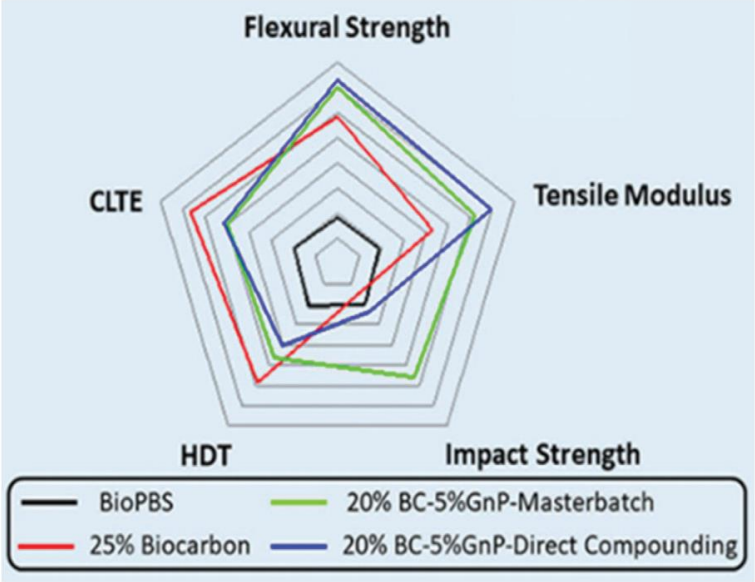

Figure 19. Effect of biocarbon and graphene on the mechanical properties of PBS. Reprinted under CC BY 4.0 license from [66].

The Bio-composite loaded with 25 wt % biocarbon, in red line, shows improvements of 57, 13, and 32% in tensile modulus, heat distortion temperature HDT, and coefficient of linear thermal expansions CLTE, respectively. CLTE is a measure of dimensional expansion in response to changes in heat and a low CLTE and a high HDT are indicative of greater thermo-dimensional stability. Further improvements are found when graphene is added to the bio-composite. As to concern the development of composites with graphene, two processing methods are used direct compounding DC and masterbatch MB processing techniques. Composites processed using the DC technique show the greatest increase in tensile strength and modulus: 17 and 120%, respectively. Composites processed using the MB technique have slightly lower strength and modulus but almost twice the impact strength compared with DC blends [66].

Biodegradable polymers offer specific advantages in *agriculture and horticulture*. Mulching films are the most important example of the application of biopolymers in these industries. They can be used to modify soil temperature, limit weed growth, prevent moisture loss, and improve crop yield as well as precocity [67] [68].

For example, La Mantia *et al.* [68] studied different systems of biodegradable polymers to prepare nets for fruits and vegetables in order to replace traditional PE-based nets. In this context, the used blend of PLA and PBAT is a good alternative to fossil-fuel based polymers. Tensile strength and modulus from are dependent to the orientation of the filaments. Furthermore, the mechanical properties of the studied systems are good despite the decrease of the elongation at break and, thus, deformability which is not of primary importance for this application [68].

Rapisarda et al. [69] studied the soil degradation of irrigation tubes based on biodegradable polymers. PLA/PBAT blends are characterized from rheological and mechanical points of view. Irrigation pipes are subjected to photoaging with

continued exposure to UV radiation up to 22 days. The authors investigate the influence of temperature and UV irradiation on soil burial degradation. In the studied biopolymers the degradation in soil occurred faster at 50 °C. Additionally, for all of the samples, soil degradation appeared to be encouraged by UV exposure. By comparing the changes in the CO groups measured by the ATR-FTIR spectra to the data of the soil degradation, an increase of the CO groups was highlighted for the samples, which showed low soil degradation kinetic [69].

Biopolymers have also application in the *electrical, electronic and automotive sectors*. In particular, electrical and electronic industries could benefit from specialized bioplastic films for such applications. For instance, Nakatsuka compared PLA with PE and polyvinyl chloride (PVC). The results show that the resistivity of PLA (order of 10^{17} Ωcm) is higher than PE (order of 10^{16} Ωcm) and PVC (order of 10^{11}-10^{14} Ωcm). The dielectric dissipation factor of the three polymers is: PLA=0.01%, PE=0.01% and PVC=0.10%. In general, PLA has as good electrical properties as other basic polymers used in the electrical and electronic industries [70].

In the *automotive industry*, manufacturers have turned to durable bio-based or partly bio-based bioplastics to produce robust dashboard components and solid interior and exterior features [71]. Components made entirely or partially from bioplastics can provide a safety standard that is of ultimate importance in the transport sector. Products include seat covers and airbags, as well as steering wheels. PLA is an environmentally friendly material used for automotive applications, the rigidity of this biopolymer is an advantage for these applications [72].

3.3 Biopolymer blends

3.3.1 Development of biopolymer blends

Biopolymer blending has attracted much attention as an easy and cost-effective method to develop polymeric materials that have versatility for commercial applications. In other words, the properties of the blends can be manipulated according to their end use through the correct selection of the polymeric components. Today, the market pressure is so high that producers of plastics need to provide better and more economic materials with superior combinations of properties to replace traditional fossil-fuel based polymers [73].

The most exploited methods used for the preparation of biopolymer blends are solution blending and melt blending. However, the selection of a specific method relies on different factors such as the miscibility of the blend components, the physical structure and the properties of the final product [52].

The *solution blending* method, typically, involves three different steps: dissolution of the polymer constituents in a solvent able to solubilize both polymers, mechanical mixing of the blend components and the evaporation of the used

solvent. Because of this last step, and in particular due to the difficult of the evaporation of the solvents and their high cost, this method is rarely used on an industrial level, commonly in biomedical industry. Several solvents are used during the preparation of the biopolymer mixtures via solution blending, including chloroform, dichloromethane, dimethylformamide, tetrahydrofuran and 1,4-dioxan. Furthermore, the presence of the solvent plays a crucial role in determining the final microstructure of the mixture. For example, considering PLA/chitosan blends prepared using different solvents such as chloroform, dichloromethane and tetrahydrofuran, it has been demonstrated that the final morphology is significantly affected by the type of the solvent used [74].

In contrast to the solution blending, no solvents are needed in *melt blending* process. In this method, the components of the blend are mixed together at a temperature above the melting temperature of crystalline polymer or the critical flow temperature of amorphous polymer that is, according to Han *et al*. [75], the temperature at which an amorphous polymer may be regarded as 'liquid' from a rheological point of view. The aim of melt blending is to ensure a homogeneous distribution of the dispersed phase of the mixture in order to increase the extent of the interfacial surface. Within an extruder, the actual deformation results from the superposition of shear and elongation stresses. Among the various types of devices, a co-rotating and intermeshing twin-screw extruder is one of the most used at industrial level, since the complex flow and the high mechanical stresses developed during the process allow to mix polymer-based systems containing high contents (> 20 wt%) of the dispersed phase, such as polymer blend. In fact, this configuration is able to provide the highest possible elongational deformation and to multiply the shear stresses undergone by the polymers thanks to the combination of two parallel screws.

The most important advantage in the use of the melt blending is the greater possibility, compared to the solution blending method, of having final materials with desired and improved properties with a better mixing between the biopolymers. For instance, it has been investigated that a more defined morphology can be obtained in PLA/PHB blends prepared using the melt blending method compared to the solution method (with chloroform as solvent) [76]. Furthermore, the processing parameters, such as the screw profile and speed, flow rate, temperature profile, possible presence of side feeder and the sequence of introduction of different components should be optimized during the extrusion process. The process is the result of a closely correlated relationship between extrusion conditions, material structure and properties.

The correlations between the extrusion conditions and the final microstructure are schematized in Figure 20. The final product structure is a function of the process but also a function of the independent variables such as screw speed, screw configuration, barrel temperature and all extrusion parameters. For example, the mechanical stresses generated during extrusion are a direct function of the rheological properties of the material which in turn depend on the changes in material structure along the extruder [77].

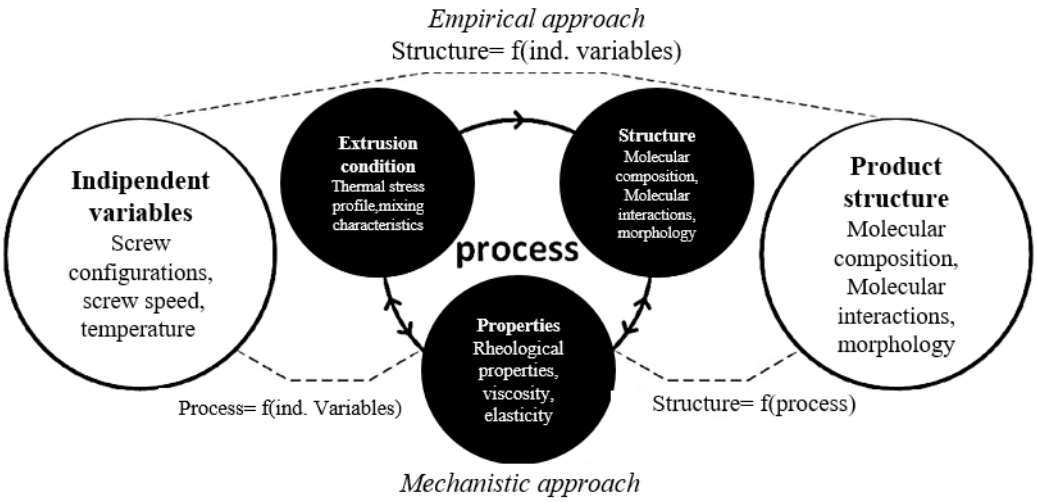

Figure 20. Mechanistic interrelation between independent variables, extrusion condition, material properties, and structure in extrusion processing (Mw: molecular weight). Modified from [77].

In order to understand structural changes in extrusion, the processing conditions have to be characterized on a local level by in-depth analysis of the thermal and mechanical stress profile together with the mixing characteristics in extrusion process [78] [79]. The morphology, and consequently, the final characteristics of the resulting materials are highly affected by the extrusion process [80] [81] [82] as previously discussed in the paragraph 2.2.1 (Chapter 2).

Different devices can be used to perform a melt-blending process, such as single-screw extruder (SSE) and twin-screw extruder (TSE). It is claimed that the SSE, in standard configuration is inadequate fort the preparation of blends with controlled morphology. Furthermore, due to the presence of ‘’dead spaces’’ the reproducibility of the extrusions of the SSE extruded blends may be poor. More expensive but easier to control are the TSE extruders. In addition, the modular design of TSE makes it possible to adjust the relative magnitude of the distributive and dispersive mixing depending on the desired effect [83]. As far as the production of polymer blend is considered, the screw design in TSEs can be properly tailored by changing the sequence and type of screw elements along the screw in order to achieve good dispersion and miscibility between polymers. In this way, almost an infinite number of screw configurations can put together to have the best final performances of the processed polymer blends adjusting the ratio of the dispersive-to-distributive mixing and obtaining products with peculiar characteristics and functional properties.

In this thesis, all biopolymer blends were obtained through melt blending using TSEs; an exhaustive and more detailed investigation of melt extrusion and the influence of the process parameters on the final properties of the materials will be presented in the Chapter 4.

3.3.2 PLA-based polymer blends

In this paragraph, the main achievements related to the development of PLA-based blends will be reviewed. Polymer blending has been used to overcome the limitations of PLA; in fact, the resulting materials allow to extend its range of applicability. Before discussing the final properties of PLA-based blends, the thermodynamic aspects and the miscibility between PLA and other polymers must be considered. As mentioned in Chapter 2, the poor properties of a mixture compared to those of neat polymers can be attributed to the phase separation resulting from the full immiscibility between the polymers. It has been defined that the miscibility of a system composed by two different phases is governed by the value of the Flory-Huggins interaction parameter χ_{12} which can be calculated using the solubility parameters of the two polymers. A limitation of the relationship between the χ_{12} and solubility is that the interaction parameter always has a positive value, which implies the positive value of the mixing entropy (in the absence of specific interactions), and thus, it describes immiscible blends. Therefore, the closer the interaction parameter is to zero, the more miscible the mixture is considered to be; in this regard, as an example the values of interaction parameters of different PLA-based systems (with PC, PS and PMMA) and the morphologies of PLA/PMMA, PLA/PC and PLA/PS blends are reported in Figure 21 [52].

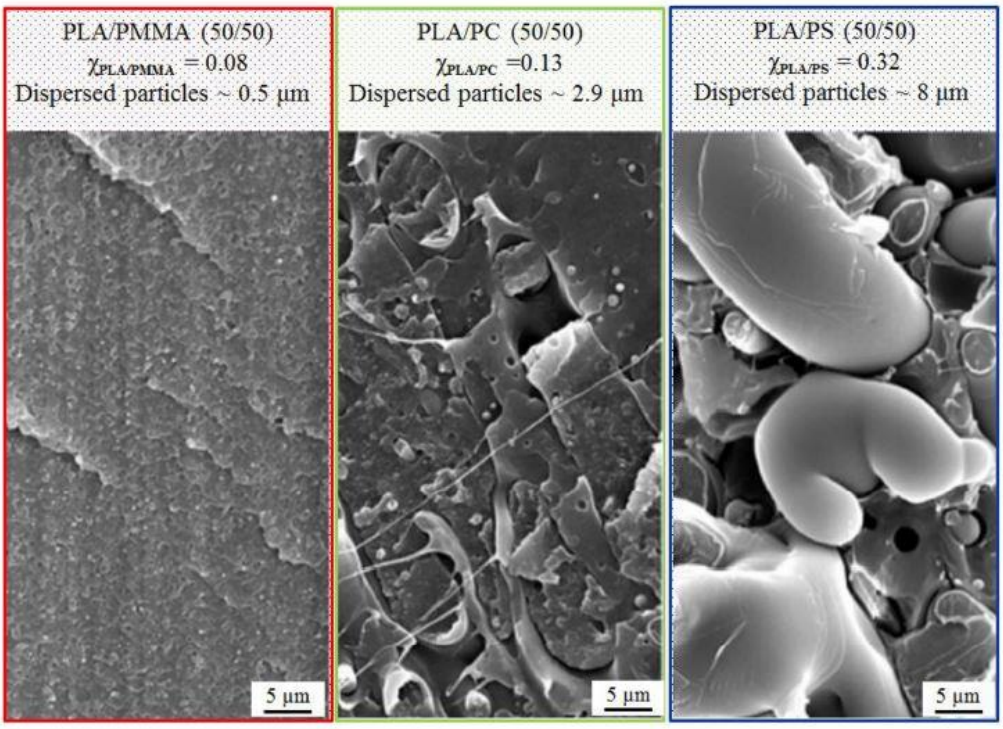

Figure 21. Interaction parameter and morphologies of PLA/PMMA, PLA/PC and PLA/PS. All the formulations are at 50wt%/50 wt%. The interaction parameters were calculated using the solubility parameters of the components. Reprinted with the permission from [52].

In this recent review of Hamad, K., et al [21], PLA/PMMA blend shows a high degree of miscibility compared to the other systems, in fact, the relative interaction parameter is $\chi_{PLA/PMMA}$ =0.08 and it is lower with respect to the other values ($\chi_{PLA/PC}$ = 0.13 and $\chi_{PLA/PS}$ = 0.32). In addition, the interaction parameters are consistent with the morphologies of the polymer blends; this can be seen by comparing the size of the dispersed particles in the three polymer blends considered, prepared under the same processing conditions using an internal mixer at 190°C for 12 minutes [84].

In the following paragraphs, several studies involving rheological, thermal and mechanical properties on PLA-based blends characterized by a specific microstructure will be presented. The dispersed phases considered are those of greatest interest for the purposes of this thesis: PBS and PHB.

3.3.2.1 Morphological analysis and rheological properties for studying the microstructure of PLA-based biopolymer blends

The evaluation of the rheological behaviour of polymer-based blends represents an effective tool to investigate the established polymer/polymer interactions, allowing achieving important information about the morphology of the blend. For this reason, this section is devoted to the main achievements concerning the rheological behaviour of PLA-based blend and the rheology/morphology correlations. related microstructures developed, through SEM observation, have been reported in this section.

Gui *et al.* [85] investigated the rheological properties and the microstructure of of PLA/PBSA blends. The behaviours of the G' of the PLA/PBSA blends at medium- and low-frequency regions are very complicated. The slope of log G' as a function of the frequency decreases with increasing amounts of PBSA at the terminal region, indicating that blends show much larger elasticities than the pure matrix. The enhancement of elasticity at low frequencies is attributed to larger stored energies through the interface tension between the two separate phases. In fact, dispersed droplets require energy to deform from equilibrium spherical shapes to the transition state, such as ellipsoids, and the energy required is temporarily stored.

Figure 22 shows SEM micrographs, at 5–30 wt% of PBSA content.

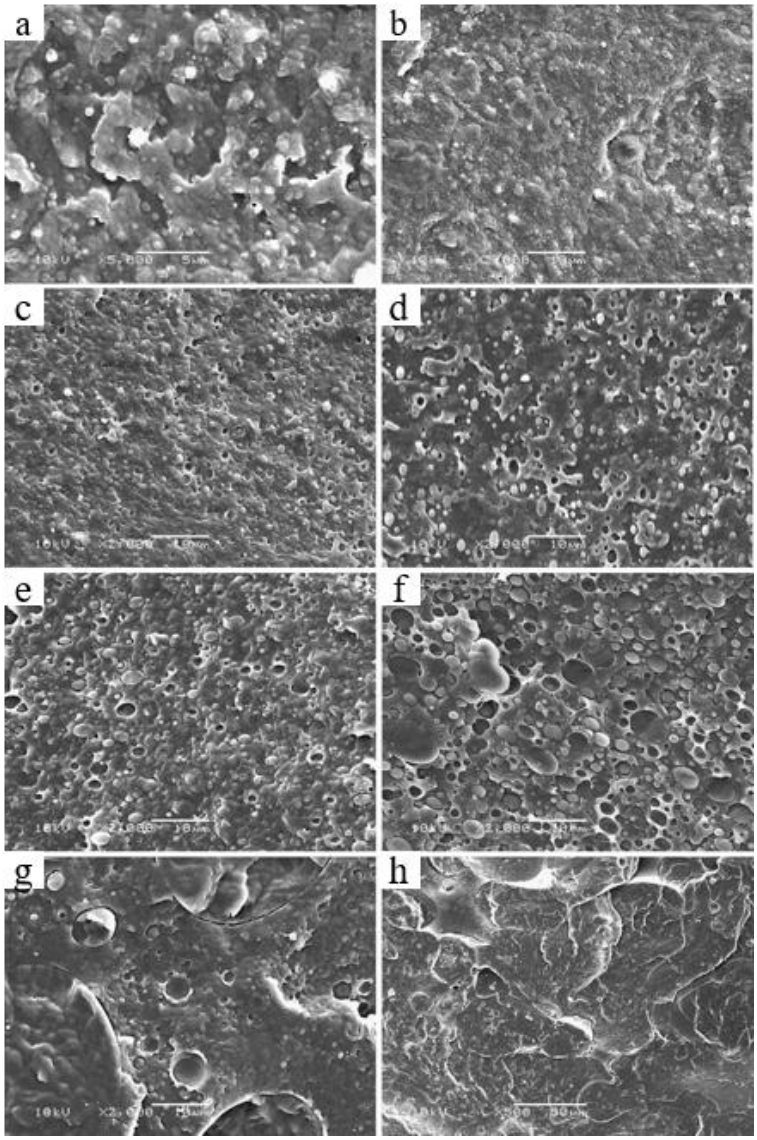

Figure 22. SEM micrographs of morphology phase development: a 95/5 PLA/PBSA (×5,000), b 95/5 PLA/PBSA (×2,000), c 90/10 PLA/PBSA (×2,000), d 85/15 PLA/PBSA (×2,000), e 80/20 PLA/PBSA (×2,000), f 70/30 PLA/PBSA (×2,000), g 60/40 PLA/PBSA (×2,000), h 60/40 PLA/PBSA (×500). Reprinted under CC BY 4.0 license from [85].

The interfacial tension values calculated through Palierne model of PLA/PBS immiscible blends are widely documented in literature. In a work, Nofar *et al.* [86] report an interfacial tension of ~1.5 mN/m. Wu *et al.* [87] determine an interfacial tension at 190 °C of ~1.1 mN/m. Conversely, Yakohara *et al.* [88] reveal that the interfacial tension between PLA and PBS is ~3.5 mN/m. Under similar condition, a value of 3.7 mN/m was also reported by Xu *et al.* [89]. The different values of interfacial tension of PLA/PBS systems, calculated with Palierne model are probably caused by the process conditions. In fact, different stresses applied to the material during melt blending can lead to different interactions between the components of the mixture by changing the interface between the polymers.

The rheological and morphological properties of PLA/PBS blends produced using a twin-screw extruder were studied also by Bhatia *et al.* [90]. The blend

containing 50 wt% PLA and 50 wt% PBS shows an onset of the shear thinning region at lower frequencies with respect to the neat components. Furthermore, the viscosity measurements reveal that the blends containing 10 and 20 wt% PBS are characterized by viscosity values between those of the neat polymers by suggesting a high degree of compatibility for a content of PBS below 20 wt%. SEM micrographs show a very fine distribution of the PBS phase in the PLA matrix for the blends containing small amounts of PBS (< 20 wt%).

In another work, Ojijo *et al.* [91] investigated the correlation between the interfacial area and properties of incompatible PLA/PBSA blends. PLA/PBSA blends with various compositions, from 0 to 100 wt% of PLA, were prepared using an internal mixer at 185 °C. The phase morphologies of the prepared blends are dependent on their respective composition and are reported in Figure 23. Furthermore, the viscosity of PBSA (80 Pa*s) is much lower than that of PLA (1180 Pa*s). Therefore, better mixing should then be realized in the PLA-dominated compositions than in the opposite, but corresponding, PBSA-dominated compositions. In fact, when PBSA polymer is the matrix, it fails to deform PLA, and in fact PLA droplet size, for instance the 30/70 sample (Figure 23 (g)), is larger than PBSA droplets in 70/30 sample (Figure 23(b)). In addition, a co-continuous morphology was achieved for the blend containing 40 wt% PLA.

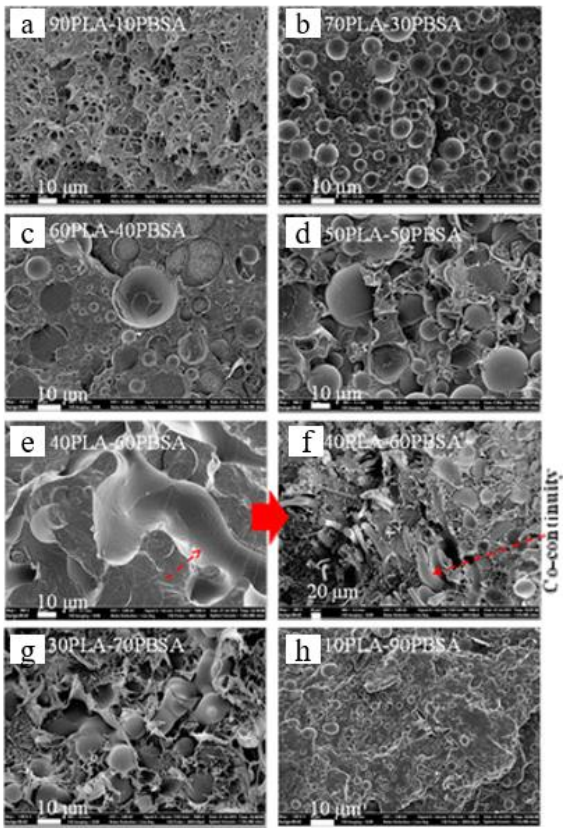

Figure 23. SEM micrographs of PLA/PBSA blends at different compositions; low-magnification SEM image of 40/60 sample at a different location from illustrating co-continuous morphology (f). Reprinted under CC BY 4.0 license [91] Copyright 2012 American Chemical Society.

Guan *et al.* [92] studied PLA/PHBV blends containing 0, 10, 20 and 30 wt% of dispersed PHBV phase. The immiscibility nature of the two biopolymers is evident from morphological observations, since as the minor phase is present as clearly defined spheres with an increasing average diameter as the PHBV content increases.

In general, for obtaining a peculiar morphology in a polymer blend, the processing condition such as mixing technology, time and temperature should be selected based on the characteristics of the single components. For instance, considering the mixing between PLA and PHBV and in particular their thermal stabilities and related viscosity ratio, the processing conditions were thoroughly selected to obtain PLA/PHBV 50/50 blend with a co-continuous morphology [93]. Thus, Gerard *et al*. [93] defined the mixing temperature and mixing time of 165°C and 6 minutes, respectively, to obtain the optimal viscosity ratio required in order to have a co-continuous morphology in PLA/PHBV 50/50 mixture; the trend of complex viscosity and the microstructures are reported in Figure 24.

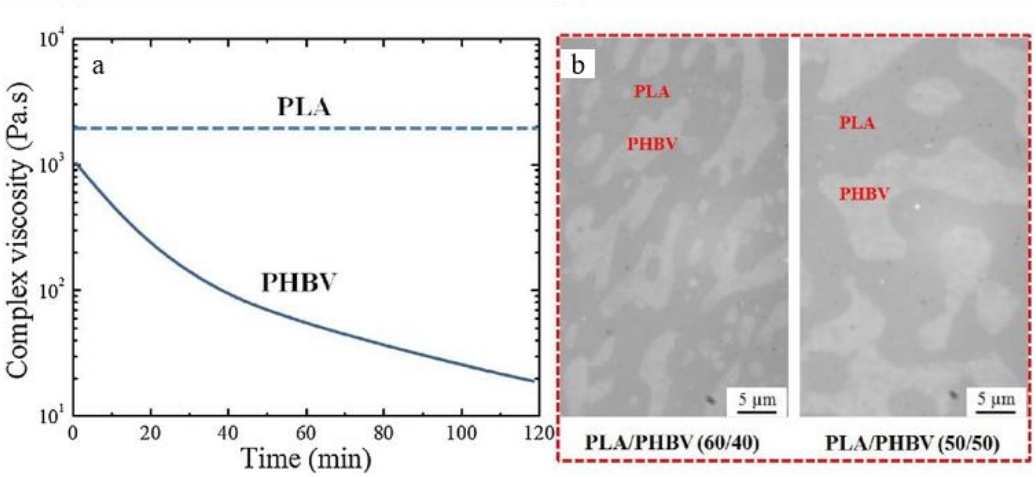

Figure 24. Complex viscosity of PLA and PHBV as a function to time (a). Morphology of PLA/PHBV blends prepared by an internal mixer at 165 ◦C for 6 min (b). Under the mixing conditions used in this work, PLA/PHBV (50/50) blend exhibited a co-continuous morphology. Modified from [93].

3.3.2.2 Thermal analysis method to define the dispersion state of two polymers in PLA-based biopolymer blends

Thermal characteristics of the system such as thermal degradation rate, stability, glass transition temperature, melting temperature, crystallization temperature, degree of crystallinity and heat of fusion play an important role in polymer-based systems. These properties can be determined using analytical techniques and the Differential Scanning Calorimetry DSC is the most widely used.

In addition, knowing the crystallinity degree of a polymer is important since crystallinity affects many physical and mechanical properties of the final blend such as storage modulus, density and permeability.

In mixtures of immiscible polymers, crystallization occurs within the domains of the almost neat component. However, even though the two phases are physically separate, they can exert a profound influence on each other [94]. The presence of the second component can disturb the normal crystallization process, thus influencing crystallization kinetics, semi-crystalline morphology, etc. Important factors are the composition of the blend, the molecular structure of the components, the phase interaction and the crystallization conditions. These factors influence the development of the crystal morphology, the degree of crystallinity (X_c), the glass transition temperature (T_g) and shape and size of the dispersed phase [94].
Park and Im studied PLA/PBS blends with various compositions and, in particular, the influence of PBS dispersed phase was tested. The results show that PBS effectively increase the crystallization rate of PLA; in addition, the blends show a single T_g over the total composition range suggesting the miscibility only in the amorphous phase (Figure 25) [95] [96]. Furthermore, two distinct melting peaks of PLA and PBS exist without any co-crystallization between the two polymers. Similar results were found in PLA/PBS blends by Yokohara and Yamaguchi, although rheological measurements were used to evaluate the degree of compatibility between the components [88].

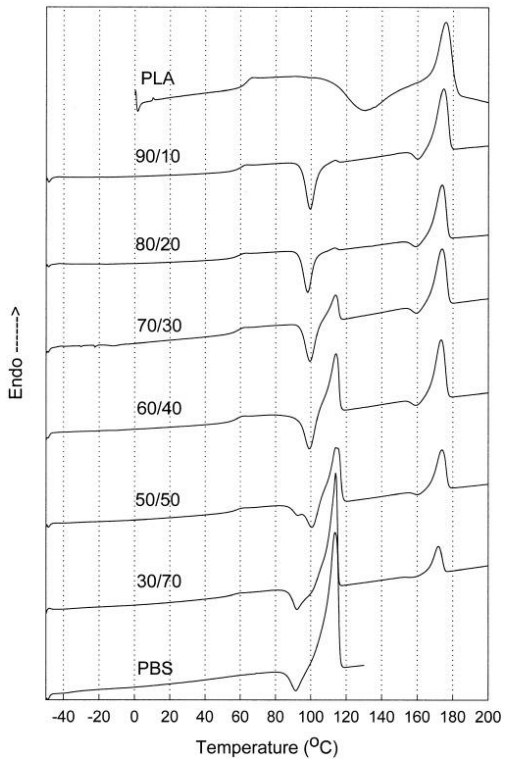

Figure 25. DSC thermograms of PLA/PBS blends: single glass transition temperature in the mixture. Reprinted with the permission from [96].

In their studies, Wang [97] and Deng [98] found that the crystallization of PLA improves in the presence of PBS due to the lubrication effect of the molten phase of PBS during melt crystallization or the nucleation ability of PBS during cold

crystallization of PLA. The increase of the crystallization kinetics was also found in the PLA/PHB blend studied by Bartczack *et al.* [99] and Musiol *et al.* [100]. Similar results are present in PLA/PHBV polymer mixtures where the crystallization of PLA could be increase due to the role of PHBV dispersed phase acting as a nucleating agent [101] [102].

3.3.2.3 Mechanical properties of PLA-based biopolymer blends

There are several simultaneous and synergic phenomena that contribute to the mechanical properties of polymer blends. Important factors are the recovery of mobility of macromolecular chains at interfaces linked to the change in the morphology of the interfacial layers and the shift of the possible brittle-to-ductile transition to a lower temperature. In particular, temperature dependencies, strain rate, concentration of components, molecular characteristics of the components and other factors influence the change on mechanical behaviour of polymer-based systems, morphology, and phase structure which are the most important factors contributing to the final mechanical properties of the blends.

The main objective of using PLA-based blends is to improve its strength and toughness. Figure 26 shows the toughness as a function of strength or modulus of the most studied PLA-based systems.

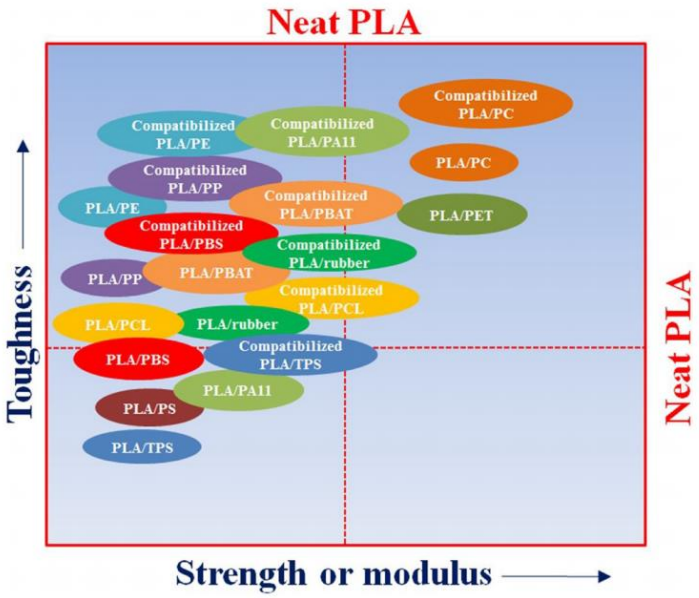

Figure 26. Toughness vs. strength and modulus of PLA polymer blends compared with those of neat PLA. Reprinted with the permission from [52].

Lee *et al.* [103] studied the influence of PBSA as dispersed phase with different weight ratios in PLA-based blends processed by twin-screw extruder at 180°C. Interestingly, with the presence of PBSA phase at 10-20 wt% the impact strength of the blends improves of about two and half times of PLA, resulting in a value of

5 kJ/m^2 compared to the impact strength of 2.5 kJ/m^2 of the matrix. Nevertheless, the tensile modulus decreases at 300 MPa in the blend with 80 wt% of PBS compared to 1200 MPa of modulus in PLA neat polymer. In addition, the presence of PBSA has no effect on the value of the elongation at break, demonstrating poor compatibility in the range of compositions investigated [103].

In the study of Pivsa-Art *et al.* [104] the elongation at break, in the same system as above, improved by only 6%, as reported in Figure 27. However, Nofar *et al.* [105] showed that the strain of a blend with 25 wt% of PBSA could be improved by 150% when prepared in an internal mixer with a mixing time of 10 min under a nitrogen atmosphere. In another work, the improvement of elongation at break was up to 250% with only 10 wt% of PBS presents in fibril phase morphology (Figure 28) [98]. Hassan *et al.* in a study of PLA/PBS blend reported that the improvement in ductility is achieved at the expense of tensile strength, which decreases markedly [106]. Conversely, Bathia *et al.* [90] found no improvement in the elongation at break of PLA/PBS blends.

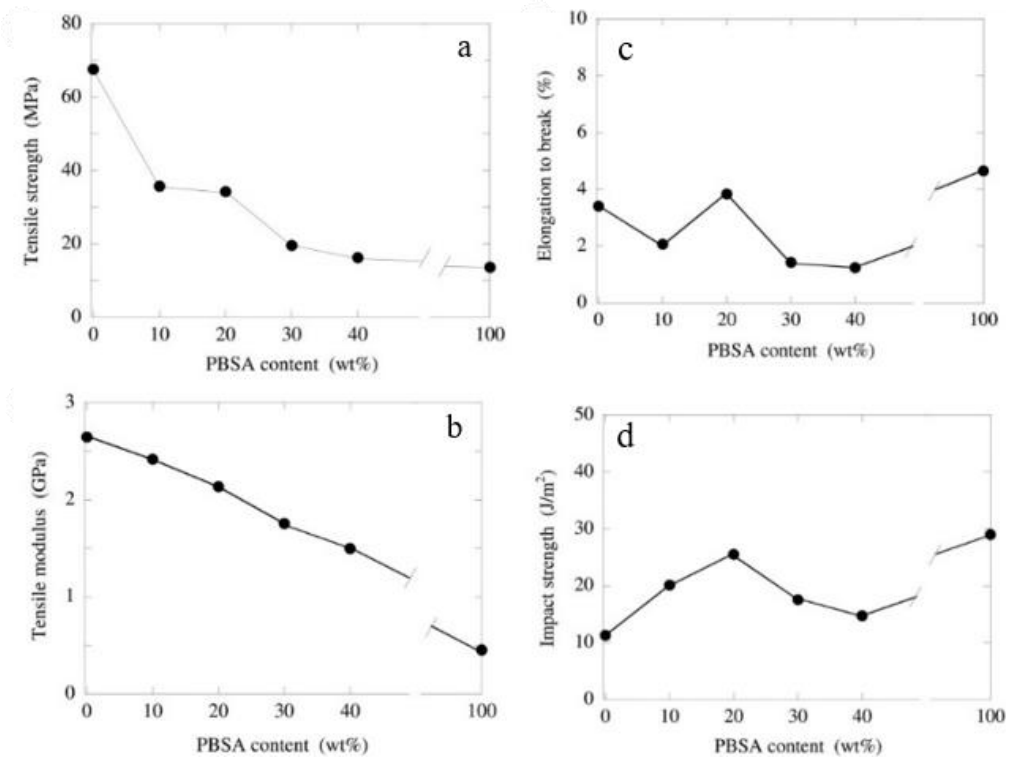

Figure 27. Mechanical properties of PLA/PBSA blends. Reprinted with the permission from [104].

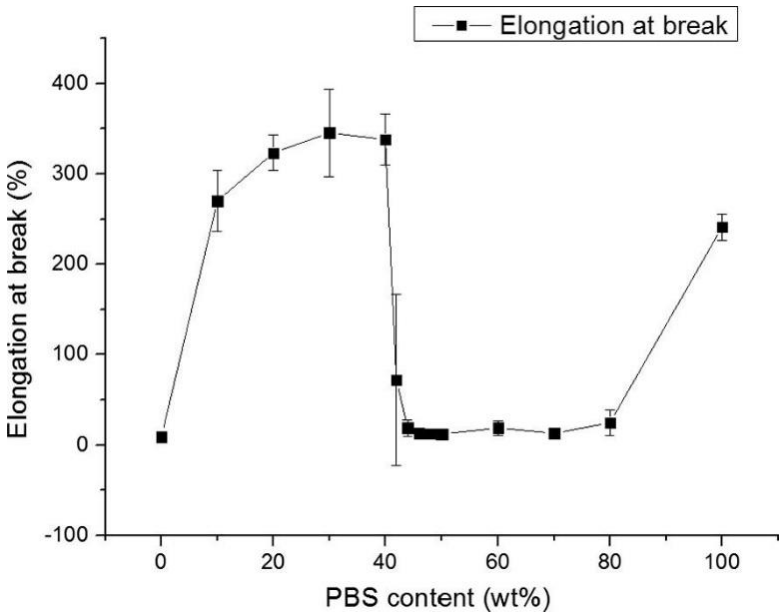

Figure 28. Improved elongation at break in PLA/PBS polymer blends with small amount of dispersed phase. Reprinted with the permission from [98].

By analyzing the mechanical properties, different behaviour can be found in PLA/PHB blends. Bartczak *et al.* demonstated that the elongation at break and the impact strength can be improved in the system when 20 wt% of PHB was used as dispersed phase [99].

Conversely, in another study, tensile strength of PLA/PHB with 25 wt% of PHB polymer is lower than those of PLA and PHB, with no change in the elongation at break (~7%). The modulus of the studied blend results lower than those of the components. In particular, in blend system is 1270 MPa compared to 1400 and 1950 MPa of PBS and PLA, respectively [107].

Arrieta *et al*. [108] studied the mechanical performance of PLA/PHB films for packaging application with different weight ratios of PLA and PHB. In particular, PLA/PHB films showed Young modulus significant higher than neat PHB and neat PLA. The tensile strength and the elongation at break of PLA/PHB blends decrease with PHB content. In fact, the values of tensile strength pass from 31 MPa in the blend with 15 wt% of PHB to 2.5 MPa with 75 wt% of PHB. Concerning the elongation at break, this is 100% and 6% in the blends with 15 wt% and 75 wt% of PHB phase, respectively. In addition, for higher contents of PHB, in those blends in which it is the continuous phase both, tensile stress and elongation at break, result lower than those of neat PLA . Nevertheless, the PLA/PHB 75:25 blend shows better mechanical performance than neat PLA confirming that the finely dispersed PHB crystals acts as a filler for PLA matrix. Similarly, the impact resistance of PLA/PHB 75/25 results higher than that of homopolymers [108].

Chapter 4

Compatibilization strategies for biopolymer-based blends

A polymer blend composed of two partially miscible or immiscible polymers can be characterized by a fine morphology. The microstructure in this case allows obtaining a resulting material with superior performances resulting from the combination of the advantageous properties of the blend components which have a good interfacial adhesion. On the contrary, if the polymers constituent the system present high interfacial tension and insufficient interaction with each other, the blends are incompatible and exhibit an uneven morphological structure leading to poor final properties of blends. In the latter case, compatibility can be improved through an appropriate method called compatibilization. The most important roles of the compatibilization strategies are: reducing the size of the domains of dispersed phase by reducing the interfacial tension with the consequent increase of the interfacial adhesion, and preventing the coalescence of the particles of the dispersed phase, thus stabilizing the formed fine phase morphology.

The methods of compatibilization of polymer blends are based on similar techniques both in fossil-fuel and bio-based polymer systems. However, it is important to emphasize that, with the use of biopolymers, it is more appropriate to use natural compatibilizers that have a low environmental impact in order to obtain a fully bio-based material.

The different strategies for the compatibilization of immiscible blends will be extensively discussed in this Chapter. First, the influence of different types of compatibilizer species will be described, then a detailed analysis of the influence of process variables on the development of the microstructure mixtures will be addressed. Although the study of process aspects is not included in the typical definition of compatibilization methods, it is fundamental to notice that the variation of process conditions during the extrusion, e.g. the flow rate, the

temperature profile, the screw rotation speed and also the configuration of the screw, causes a change in the shear applied on the materials by affecting the final morphology of the mixture.

4.1 Typologies of compatibilizers in blending processes

Compatibilizers are specific species that have a significant influence on the interfacial adhesion of the polymeric components of immiscible mixtures. These structures can be generated *in situ* during the processing or can also be pre-made and added into the blend; these two different methods of compatibilization are reactive and non-reactive strategies, respectively.

In the case of reactive method, the compatibilizers are formed *in situ* during the melt blending process. This might involve the addition of polymers with reactive groups, the addition of small molecular weight chemicals or the creation of reactive groups on the polymers constituting the blends.

In contrast, non-reactive methods include the addition of pre-made block-copolymers in the mixture, the incorporation of amphiphilic low molecular weight compounds and ionomers and the use of nanoparticles or, sometimes, the addition of a third polymeric phase in the blend.

In the following paragraphs, a detailed study of both methods will be provided, referring exclusively to biopolymer-based blends. It is important emphasise that only non-reactive methods have been used in this thesis.

4.1.1 Reactive compatibilization methods

4.1.1.1 Addition of polymers with reactive groups or chemical modification of one of the blend components

The addition of a reactive polymer could improve the compatibility of the mixture if the reactive polymer is miscible with one component and reactive towards the functional groups of the other component. The compatibilizers block or graft polymers are formed *in situ* through reaction of the reactive polymer with the mixture components during the process. Mechanisms of copolymer formation with different reactive polymers in an immiscible A/B blend are demonstrated by Koning *et al*. [109] and Zeng *et al*. [110] and are shown in Figure 29.

The reactive polymers (A*) can be polymer A functionalized with X which can be present in both pendent or terminal positions or it can be a polymer with reactive groups different from the components of the blend. Concerning polymer B, it can have reactive functionality Y in both pendent or terminal positions as showed in Figure 1. Thus, there is a possibility of formation of copolymer such as (B)-*graft*-(A*), (A*)-*graft*-(B) and (A*)-*block*-(B).

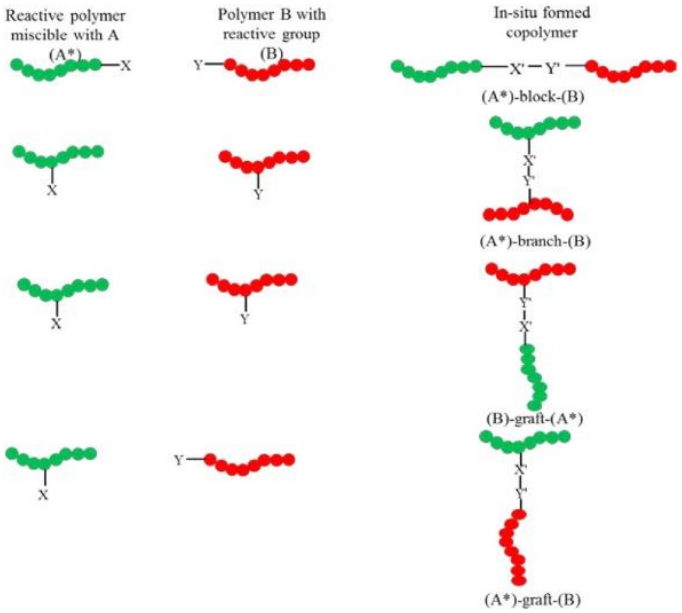

Figure 29. Mechanism of formation of different types copolymer during processing. Reprinted with the permission from [111].

For example, Hassouna *et al*. [112] synthetized block-copolymers in situ using maleic anhydride (MA) grafted PLA and hydroxyl terminated poly(ethylene glycol) (PEG) in order to improve compatibility of PEG/PLA blends.

Figure 30 reports the mechanism of PEG grafting MAG-PLA by reactive extrusion. Once the radical is formed, hydrogen abstraction can occur producing a PLA which may react with MA. The resulting polymer radical may then combine with another radical (MA, peroxide, or polymer radicals or hydrogen) and further undergo a β-scission. In order to react easily with the anhydride functions grafted in the resulting PLA chains, to improve the compatibility with PLA and to slow down the plasticizer from migrating from the bulk, PEG chains terminated with hydroxyl groups were selected.

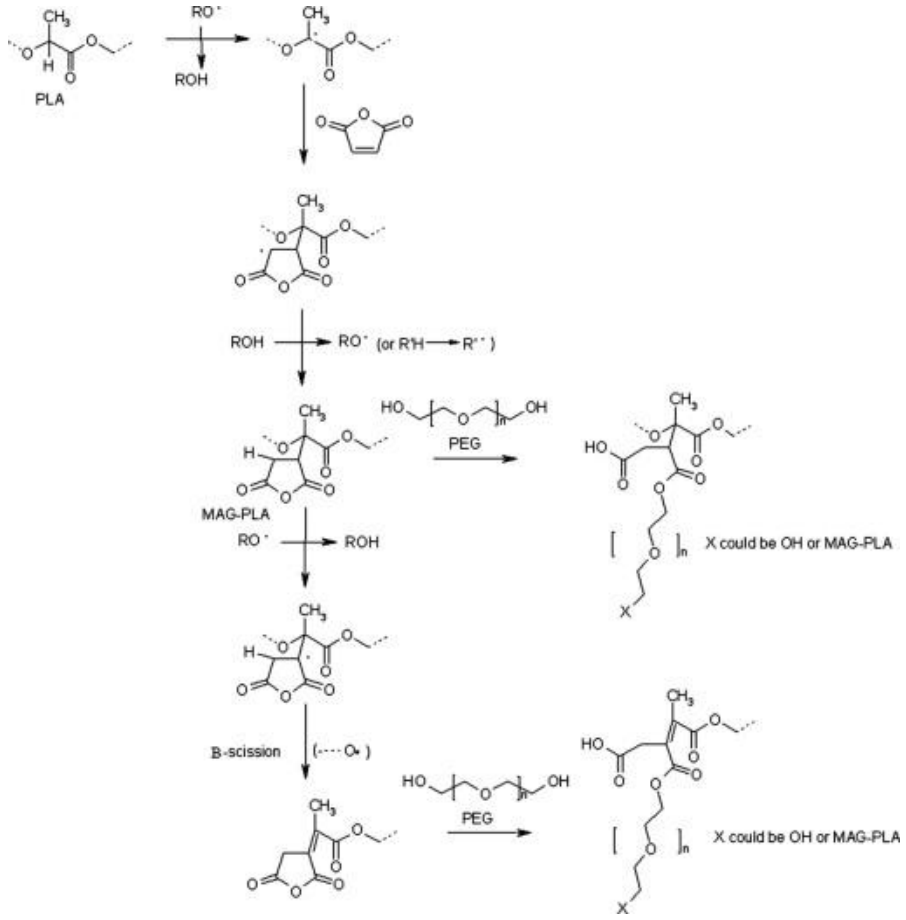

Figure 30. Mechanism of PEG grafting MAG-PLA by reactive extrusion. Reprinted with the permission from [112].

Blends containing anhydride-grafted PCL [113] [114], PHB [115] and PLA [116] [117] have been prepared in this way. Particularly, unsaturated anhydrides and maleic anhydride are often attached to biopolymers via radical reaction using different peroxide initiator. In a study of Gardella *et. al* [118], the toughness of PLA/PCL systems (70/30 wt%) is improved by the presence of the MA-*g*-PLA compatibilizer. The improved toughness of this mixture was attributed to the formation of covalent bonds between the hydroxyl groups of PCL polymer and the MA groups of the grafted polymer. Specifically, the process of PLA maleation creates anhydride functional groups on the polymer which are able to react with the PCL hydroxyl end groups during melt blending, thus providing interfacial bonding that enhances the compatibility between the two polymers (Figure 31). As a result, the domain size of the dispersed PCL phase in PLA matrix decreases in the presence of MA-g-PLA as observable form SEM micrographs reported in Figure 32 [118].

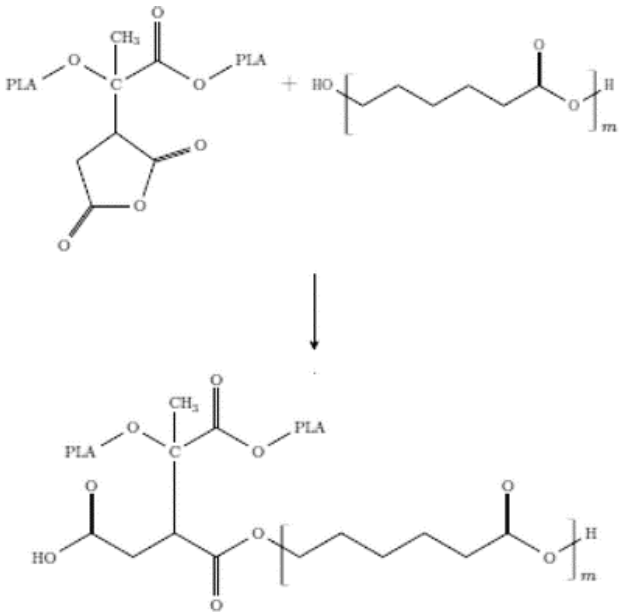

Figure 31. Reaction scheme between PLA-*g*-MA and PCL. Reprinted with the permission from [118].

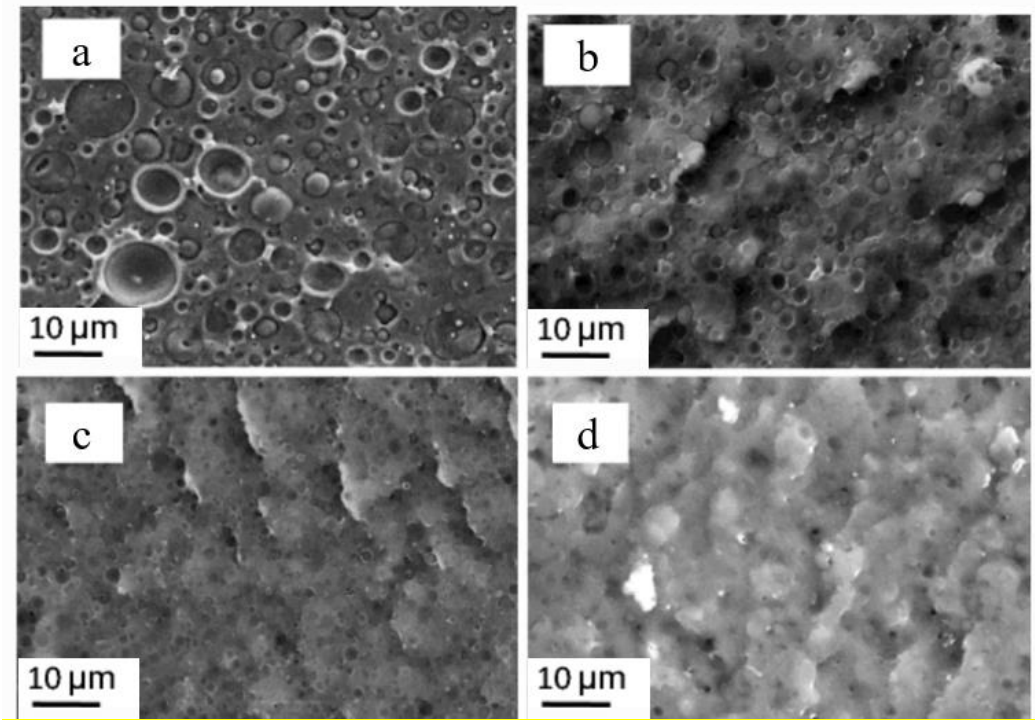

Figure 32. SEM micrographs of the blends: PLAPCL (a), PLA(PLA-*g*-MA)$_{10}$PCL (b), PLA(PLA-*g*-MA)$_{50}$PCL (c), and PLA-*g*-MAPCL (d). Modified from [118].

4.1.1.2 Addition of low molecular weight chemicals

This strategy involves a one-step process and is cost-effective due to the relatively low concentration of compatibilizers, usually 0.1-3 wt% of reactive low molecular weight chemicals added to compatibilize the system [119]. Low-molecular-weight reactive species are added into the molten blends to form *in situ* copolymers by reaction with the blend components. This method of compatibilization allows the use of different components such as isocyanates, peroxides, chain extenders and glycidyl methacrylate; examples of low molecular weight chemicals and their chemical structures are reported in Figure 33.

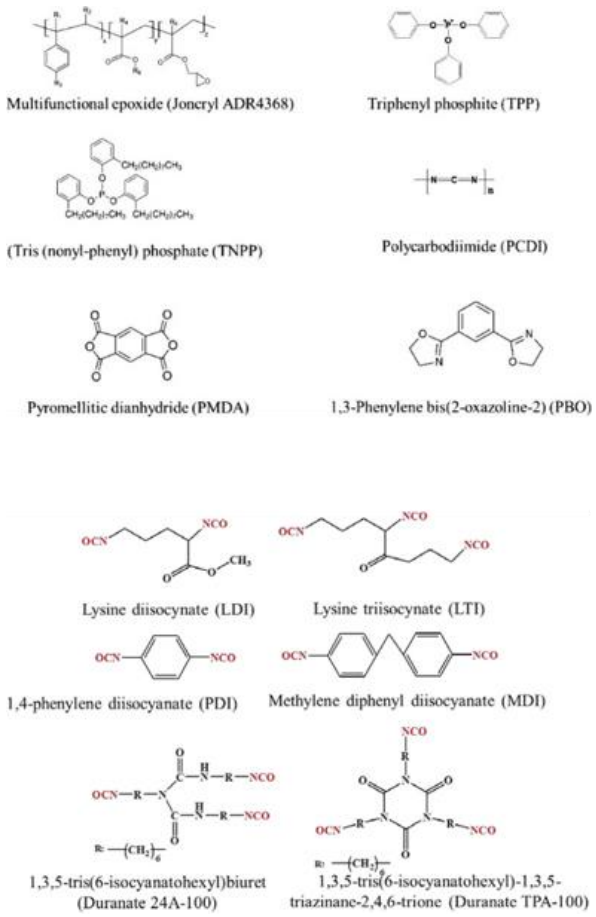

Figure 33. Chemical structures of low molecular weight chemicals. Modified from [120] [121] and [122].

In polyester blend systems, Joncryl can form non-linear copolymers through hydrogen extraction from the carboxyl group of blended polymers. The compatibility of PLA/PBSA blend (with 60 wt% of PLA and 40wt% of PBSA) is improved with Joncryl chain extender in the system studied by Ojijo *et al*. [123]. It was hypothesized that at the interphase of the two polymers, there are *in situ* generated co-polymers, which are non-linear due to the multi-functionality of the Joncryl. The reaction between the polymers constituting the blend and the

compatibilizing species is confirmed by Fourier transform infrared spectroscopy FTIR. In particular, the absorption bands at 843 and 907 cm^{-1} assigned to the asymmetric and symmetric ring deformation vibrations of the Joncryl epoxy groups disappear in the compatibilized sample, suggesting the ring opening of the epoxide function in reaction with the carboxyl and/or hydroxyl end groups of PLA and PBSA (Figure 34)[123].

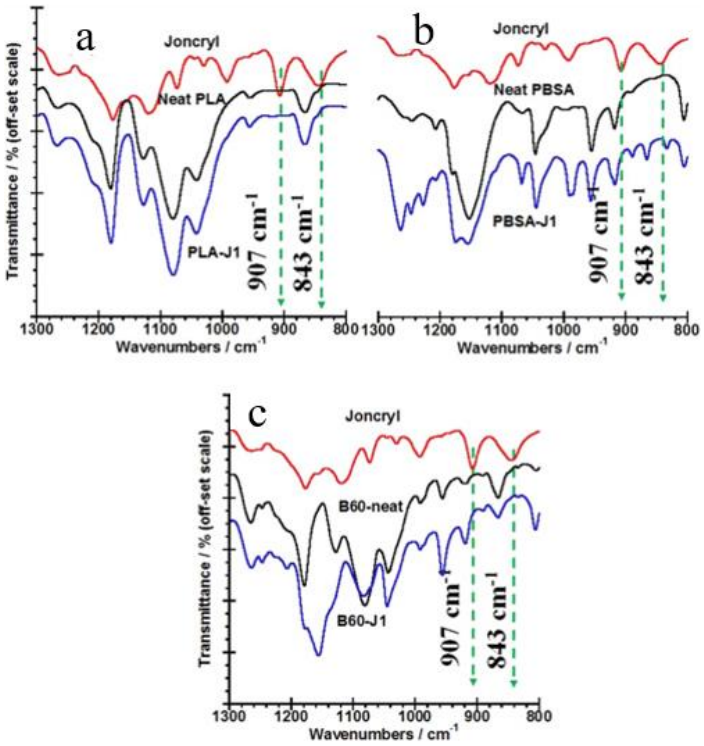

Figure 34. FTIR spectra for Joncryl and neat PLA and PLA with 1wt% Joncryl (PLA-J1) (a), neat PBSA and PBSA with 1 wt% Joncryl (PBSA-J1) (b) and neat PLA/PBSA blend containing 40 wt% PBSA (B60) and B60 blend containing 1 wt% Joncryl (c). Modified from [123].

The improved compatibility of PLA/PBSA blends is also encountered in the mechanical properties of the system. In fact, in the blend containing 1 wt% of Joncryl the impact strength increases from 9.8 to 34.7 kJ/m^2 and the elongation at break increases up to ≈200% compared to the neat blend.

In addition, the morphology of the PLA/PBSA systems with a Joncryl content of 0, 0.5, 0.6 and 1 wt%, was analysed through SEM micrographs. A co-continuous morphology is found as a result of the stabilization of coalescence through the non-linear PLA-PBSA copolymer formed *in situ*. The generalized reaction mechanism and the schematic mechanism of morphology modification during the reactive process are reported in Figure 35[123].

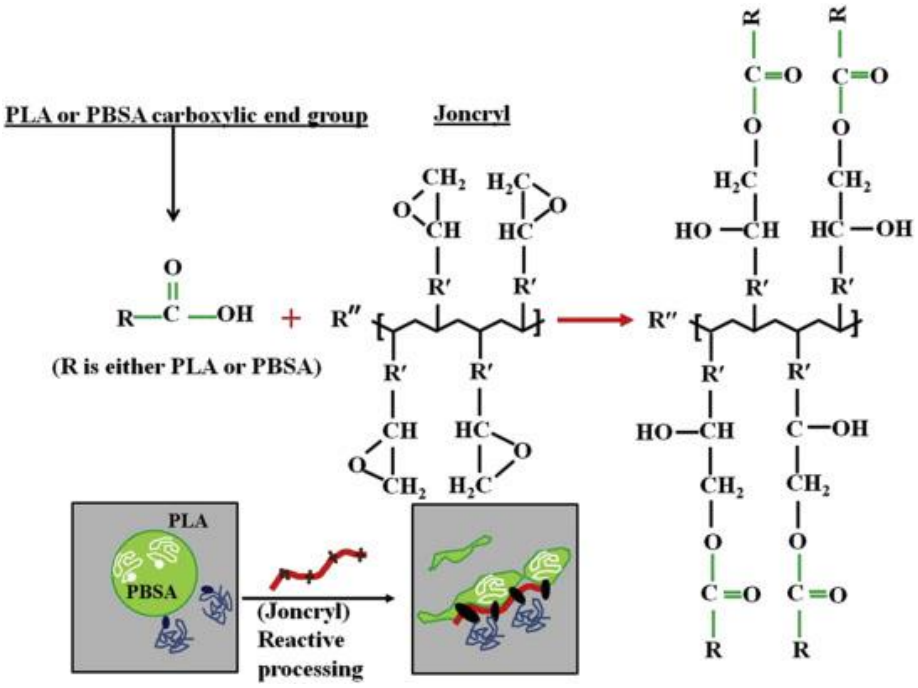

Figure 35. Generalized reaction mechanism of Joncryl-PLA and/or PBSA carboxyl end groups. The inset 'cartoon' depicts the modification of the PLA/PBSA blend interface by Joncryl through the formation of non-linear copolymer. The cartoon depicts only the interphase reactions, intra-phase chain linkages are not shown. Reprinted with the permission from [123].

In several studies, Dicumyl peroxide (DCP) has been used as initiator to compatibilize biopolymer-based blends. In particular, in a PHB/PDLLA blends, using DCP as a crosslinking agent, Dong *et al*. found the enhancement in the impact strength and flexibility of the systems [124]. Free radicals on both of the PHB and PDLLA chains can be initiated by DCP via a hydrogen absorption mechanism, consequently grafting occurs at the interface of the PHB/PDLLA blends via a combination of the free radicals. The PHB/PDLLA blend with 0.5 wt% of DCP shows higher impact toughness, tensile and flexural properties compared to the non-reactive PHB/PDLLA blend [124]. It was found that the tensile strength of the blends increases of 5 MPa after incorporation of 0.5 wt% of DCP, while the impact toughness increases of around 30% in the blend with 30 wt% of PDLLA. In Figure 36 the trend of the mechanical properties of the compatibilized blend with 0.5 wt% of DCP (X-blends) and the neat blend PHB/PDLLA (Physical blends) as a function of the content of PDLLA are reported.

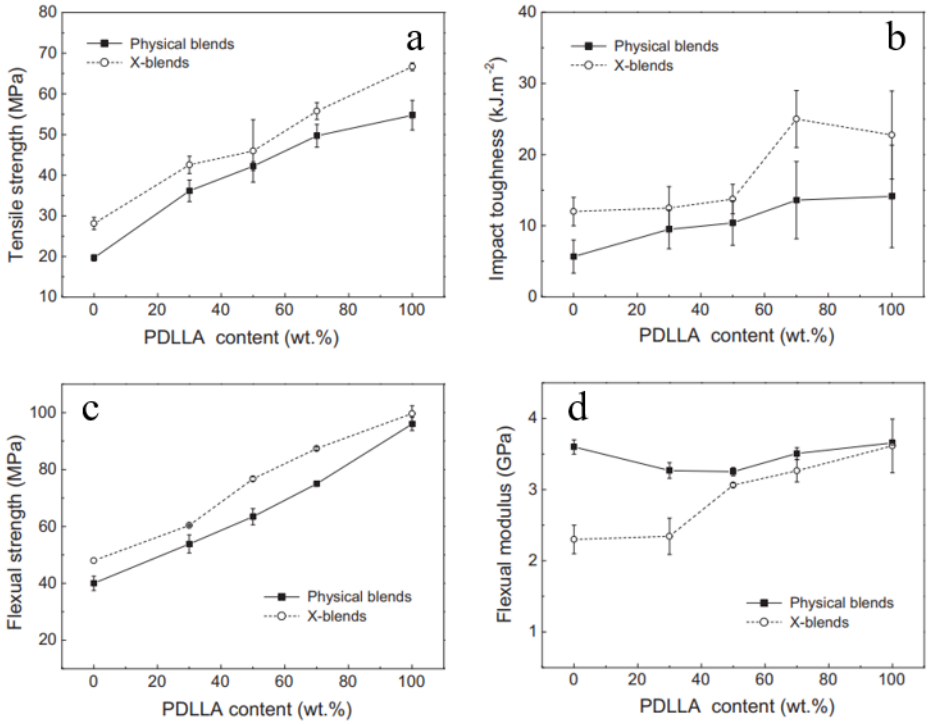

Figure 36. Effect of PDLLA content on the mechanical properties of the PHB/PDLLA blends before and after partial crosslinking by using 0.5 wt% DCP: tensile strength (a), notched Izod impact toughness (b), flexural strength (c) and flexural modulus (d). Modified from [124].

Wang *et al*. [97] used DCP initiator in PLLA/PBS (80/20) immiscible blends. The compatibilized blend shows a significant improvement of the impact strength; in particular, the blend compatibilized with 0.1 phr of DCP presents a value of impact strength 12 times higher than that of neat PLLA and 7 times higher than that of non-compatibilized PLLA/PBS (80/20) blend. Furthermore, the compatibilization does not influence the values of elongation at break, notwithstanding a decrease of tensile strength and flexural properties [97].

Ojijo *et al.* [121] performed *in situ* compatibilization of PLA/PBS blends with triphenyl phosphite (TPP). The blend with 70 wt% of PLA and 30 wt% of PBS is selected to study the effect of varying TPP concentration. In particular, the mixture with 2 wt% of TPP shows a higher elongation at break (19.7 % vs. 6% for the neat blend), without significant modifications of tensile modulus and strength compared to the neat blend. Regarding morphology, with the incorporation of TPP into the PLA/PBS blend, the size of the domains of dispersed phase decreases due to the improved compatibility between the biopolymers; this finding is attributed to the formation of PLA-*g*-PBS copolymer by a heterogeneous coupling reaction. As the TPP content was increased, there was a reduction in the PBSA domain size from an average of approximately 8 μm to a size of ~2.7 μm, below which no further reduction is observed. The minimum dimension is defined by the authors as critical size and it is obtained in the blend with approximately 2% TPP, further underscoring the fact that it is the optimal concentration. The micrographs of the compatibilized blends and the dependence of the size of dispersed phase from the amount of TPP are reported in Figure 37 [121].

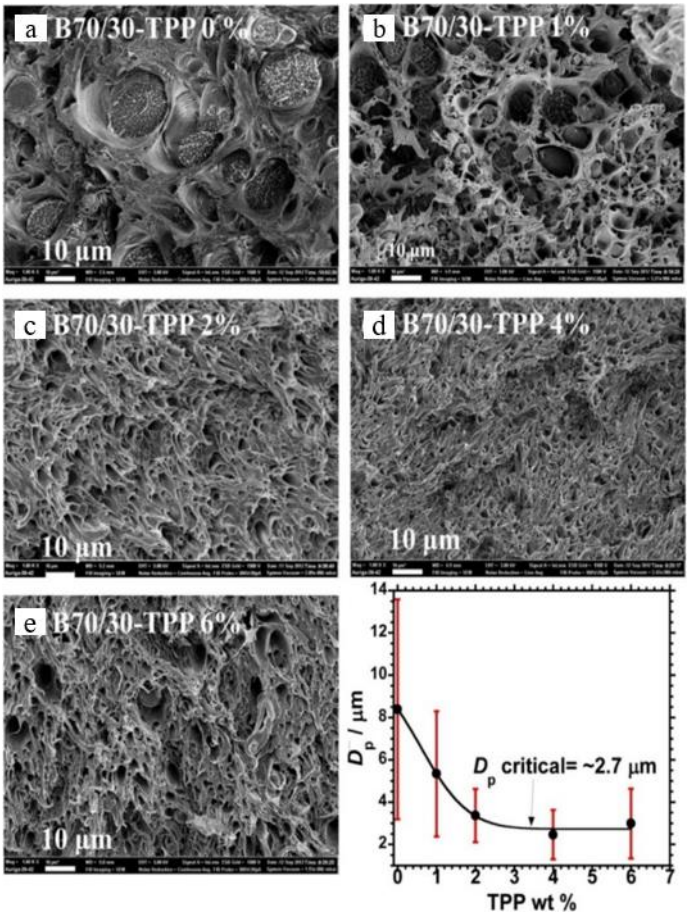

Figure 37. SEM images of the neat B70/30 blend and blends compatibilized with different quantities of TPP (a-e). The graph shows the average diameter of the dispersed phase as a function of TPP. All of the samples were annealed at 80 °C for 15 h before imaging the tensile-fractured surfaces. Reprinted under CC BY 4.0 license from [121].

4.1.2 Non-reactive compatibilization methods

4.1.2.1 Addition of pre-made copolymers

Ex situ compatibilization of immiscible biopolymer blends is a strategy to improve the compatibility of components of immiscible blends through the addition of pre-made copolymers. The method of operation of using a pre-made block copolymer as a compatibilizer is that one block can be miscible with one component of the mixture, while the second block can be miscible with other blend component [109]. To use this strategy, the first step is the synthesis of copolymers with suitable functionality [125] [126] which, subsequently, was mixed with the polymer constituent the blend; the compatibilizer can be a block or a graft copolymer as showed in Figure 38.

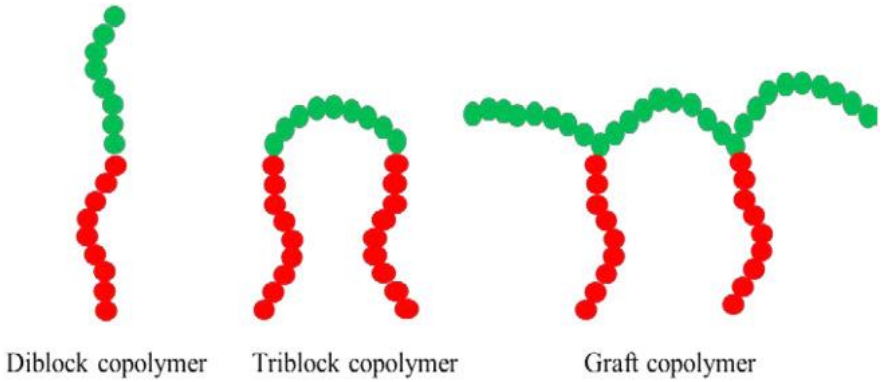

Figure 38. Different types of copolymers. Reprinted with the permission from [111].

An immiscible polymer blend, constituted by a polymer A and a polymer B, can be compatibilized with copolymer of di-block (C-*b*-D), tri-block (C-*b*-D-*b*-C or D-*b*-C-*b*-D) and multi graft or single graft (C-*g*-D or D-*g*-C) copolymers. The block or graft copolymer C and D can be combined with the polymer of A and the polymer of B, respectively [110]. Thus, the block or graft of C is miscible with polymer A and the block or graft of D is miscible with polymer B. There are several studies in literature, some of which are shown in the Table 3.

Table 3. Different pre-made copolymers compatibilizers used in compatibilization of immiscible bio-based polymer blends.

	Compatibilizer	Ref.
PLLA/PBS	PLLA-PBS block copolymer	[127]
PLA/PBS	Poly(butylene succinate-co-lactic acid) copolymer	[128]
PLA/PBAT	PLA-PBAT-PLA triblock copolymer	[129]
PLLA/PBS	Tri-arm PLLA block poly(glycidyl methacrylates) copolymer	[127]
PLA/Starch	PLA grafted starch copolymer	[130]
PLA/PCL	PLA-PCL diblock copolymer	[131] [132]

The use of these compatibilizers is essential to stabilize the morphology of immiscible blends by adjusting the interfacial adhesion between the polymers.

Figure 39 shows the mechanism of morphology development of a compatibilized system during the melt blending [133]. In particular, in immiscible non-compatibilized blends the droplet size of the dispersed phase is larger than that of the compatibilized blend due to the rapid coalescence and low compatibility between the phases. In compatibilized blend with copolymer, the diameter of the dispersed phase reduces to < 1μm by diffusion of the compatibilizer which generates a new interface between the components of the blend and prevents the coalescence phenomenon; in addition, usually after the process of compatibilization with copolymers, the interfacial thickness of the blend increases by 4-6 nm [133].

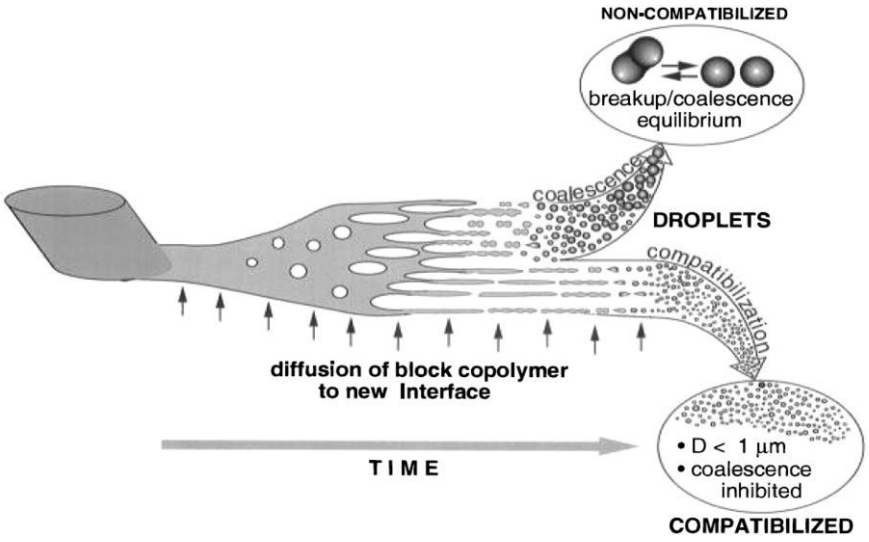

Figure 39. Schematic of morphology development during melt blending. As pellets or powder of the minor phase soften, layers peel off. These stretch out into sheets which break up into fibers and then droplets. Unless block copolymer can rapidly cover the new interface these droplets will coalesce to larger particles. Reprinted under CC BY 4.0 license from [133].

The good interfacial adhesion developed in immiscible blends compatibilized with pre-made copolymers can improve the mechanical performances as compared to the corresponding non-compatibilized system.

As an example, Supthanyakul *et al*. studied PLA/PBS blend compatibilized with random copolymer of poly(butylene succinate-co-lactic acid) rPBSL [128], showing an improvement in toughness for the compatibilized blend. The increase of toughness can be attributed to the good adhesion between the polymer phases in the presence of rPBSL. In addition, the elongation at break of the blend with 5 phr of copolymer increases to 34% in contrast the that of the neat blend which presents an elongation equal to 8% [128]. The results of the mechanical properties are supported by the study of morphology through SEM and AFM (Figure 40). The improved compatibility between PLA and PBS is evident in the reported SEM micrograph, where a disappearance of the voids of the dispersed phase particles in the compatibilized mixture can be noticed. Non-contact mode atomic force microscopy AFM revealed that the roughness of compatibilized blend with 5 phr of rPBSL decreases from 25 to 5 nm supporting the result that the system with copolymer presented a less phase separation compared to the non-compatibilized PLA/PBS blend [128].

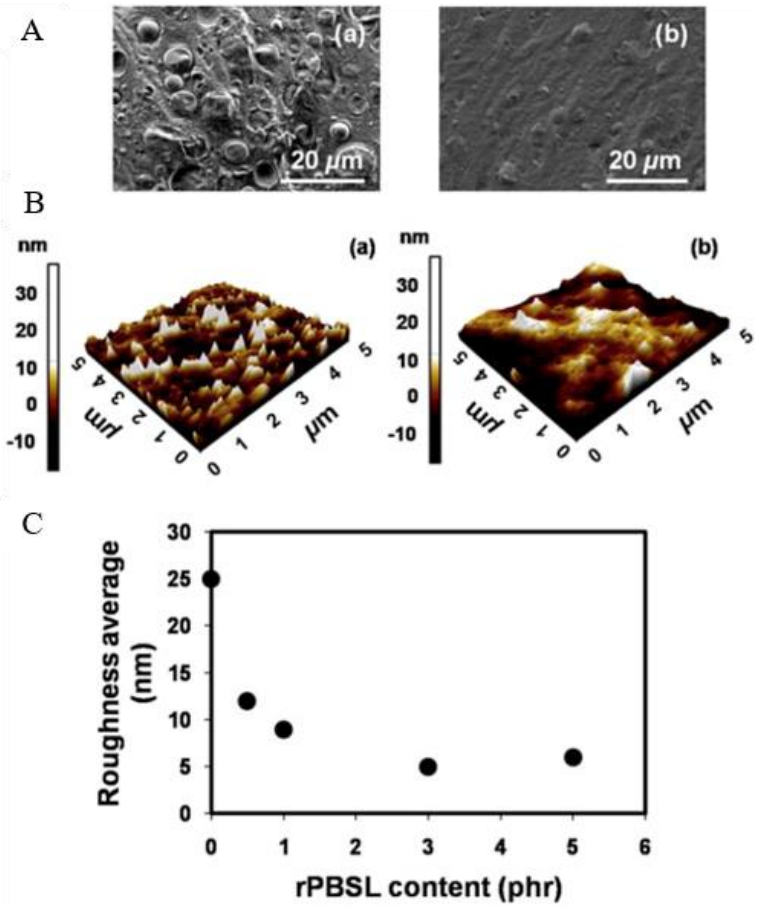

Figure 40. SEM micrographs (A), AFM micrographs (B) of PLA/PBS (80/20) film (a), PLA/PBS (80/20) film containing rPBSL at 5 phr (b), and roughness average of PLA/PBS (80/20) film under rPBSL content variation (C). Reprinted with the permission from [128].

PLA/PBAT blend with 80 wt% of PLA and 20 wt% oh PBAT was compatibilized using simultaneously two different molecular weight tri-block PLA-PBAT-PLA copolymers as compatibilizers [129]. The average molecular weights of the copolymers were of 17 kg/mol and 29 kg/mol for compatibilizer 1 (CP1) and compatibilizer 2 (CP2), respectively. Due to the compatibilization effect, an increase of the elongation at break of the compatibilized PLA/PBAT blend is observed; in fact, PLA/PBAT blend with 0.5 wt% of CP1 and CP2 shows elongation at break (~226%) over 8 times higher than that of neat PLA/PBAT (~27%).

This result is attributed to the migration of CP2 at the interface with the help of high mobility of low-molecular weight compatibilizer CP1. Consequently, the high-molecular weight compatibilizer CP2 contributed to promote good adhesion between PLA and PBAT in the blend [129].

From the above reported studies, it is evident that the pre-made copolymers act as effective compatibilizers in bio-based immiscible polymer blends. However, this strategy is not industrially favourable due to the additional step required to synthesise the copolymer [134]. Thus, this compatibilization method is only suitable for polymer blends with economically favourable production costs.

4.1.2.2 Incorporation of amphiphilic low molecular weight compounds and ionomers

Amphiphilic molecules are compound consisting of two different parts of hydrophobic and hydrophilic polar groups such as carboxylates (CO_2^-), sulphates (SO_4^-), sulfonates (SO_3^-), and amines (NH_3^+) [135]. These compounds have interfacial activity and give rise to a wide range of surface chemistry functions including wetting, emulsifying, softening, solubilizing and compatibilizing [136] and are widely used in food [137], agricultural [138] and plastic industries [139] [140] [141].

Yokesahachart and Yoksan [142] used three different amphiphilic compounds to compatibilize a TPS/PLA immiscible blend. The exploited compatibilizers were Tween 60, linoleic acid and zein and they were added at 1.55 wt%. At first, the authors studied the influence of the amphiphilic compound in TPS phase and later the resulting materials were blended with PLA. Thus, blends containing amphiphiles TPSTW/PLA, TPSLA/PLA and TPSZE/PLA were prepared [142]. The presence of amphiphiles facilitates processability of the TPS/PLA blends, especially when PLA content is ≤50 wt%. The elongation at break of the compatibilized blends varies from 1% to 16% and the values are significantly lower than that of the TPS materials containing amphiphilic compound. This result might be due to the rigidity and brittleness of PLA. Considering the effect of the different amphiphiles, zein allows obtaining a stronger and more rigid TPS/PLA material (PLA content blend ≤50 wt%) as compared to the Tween 60 and linoleic acid. On the contrary, Tween 60 and linoleic acid provide more extensible blends than zein [142].

Ionomers are commercially available materials with either hydrogen or a metal cation as the neutralizing agent for the acid group [143]. Ionomers contain both anionic repeating units and a small fraction of repeating units containing ionic species, where the ionic groups make up less than 15% of the polymer. For example, an ionomer is the ethylene-methacrylic acid copolymer, which is a zinc or sodium salt of copolymers derived from ethylene and methacrylic acid.

The introduction of ion sites improves the number and intensity of the interaction points between the two polymers constituting the mixture, allowing the obtainment of a good compatibility [144] [145].

Lim *et al.* [144] studied two different blends: poly(3-hydroxybutyrate-co-3-hydroxyhexanoate) (PHB-HHx)/PBS and PHB-HHX/PBS-based ionomers (PBSi) with a content of 1.0 and 3.0 mol% of sodium sulfonate ionic group: succinic acid SA, 1,4-butanediol BD and titanium tetra-butoxide are used without further purification to produce PBSi. Sulfonated dimethyl fumarate (SDMF) containing sodium sulfonate ionic group is synthesized by using dimethyl fumarate (DMF) and sodium hydrogen sulphite ($NaHSO_4$) [146]. Pure poly(butylene succinate) PBS and PBS ionomer with SDMF content of 1.0 and 3.0 mol% are synthesized [147]; the structure of PHB-HHX and PBSi are shown in Figure 41.

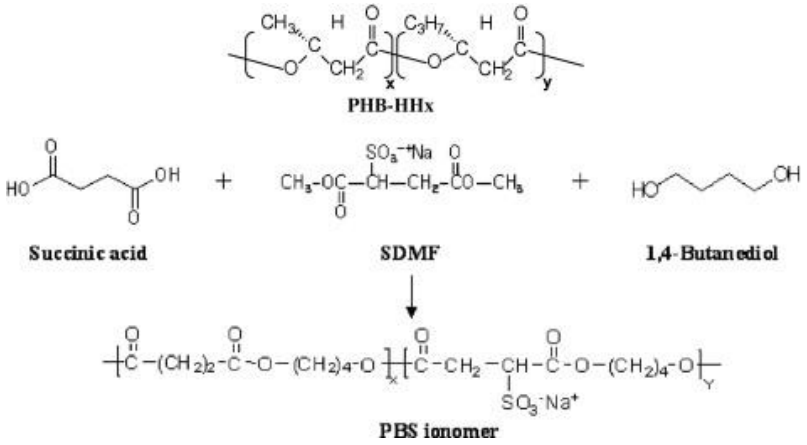

Figure 41. Structure of PHB-HHX and PBS ionomer. Reprinted with the permission from [144].

PHB-HHx/PBS and PHB-HHX/PBSi are prepared by melt compounding and characterized. DMTA analyses show that PBSi reduces the crystallinity of PHB-HHx and this behaviour increases in proportion to the ionic group content because the sodium metal carbonyl interaction between the PHB polymer and PBS ionomer became much stronger, resulting in the improvement of the compatibility of the blends [144].

Figure 42 shows the values of storage moduli versus temperature for PHB-HHx/PBS and PHB-HHx/PBSi blends. At same composition (1 wt%), an increase in the concentration of ionic group causes the decrease in modulus confirming that the ionic group allows to decrease the crystallization rate in the blends [144]. Because the presence of specific interactions for the presence of the ionomer, the calculated interaction parameter is negative for all blend systems.

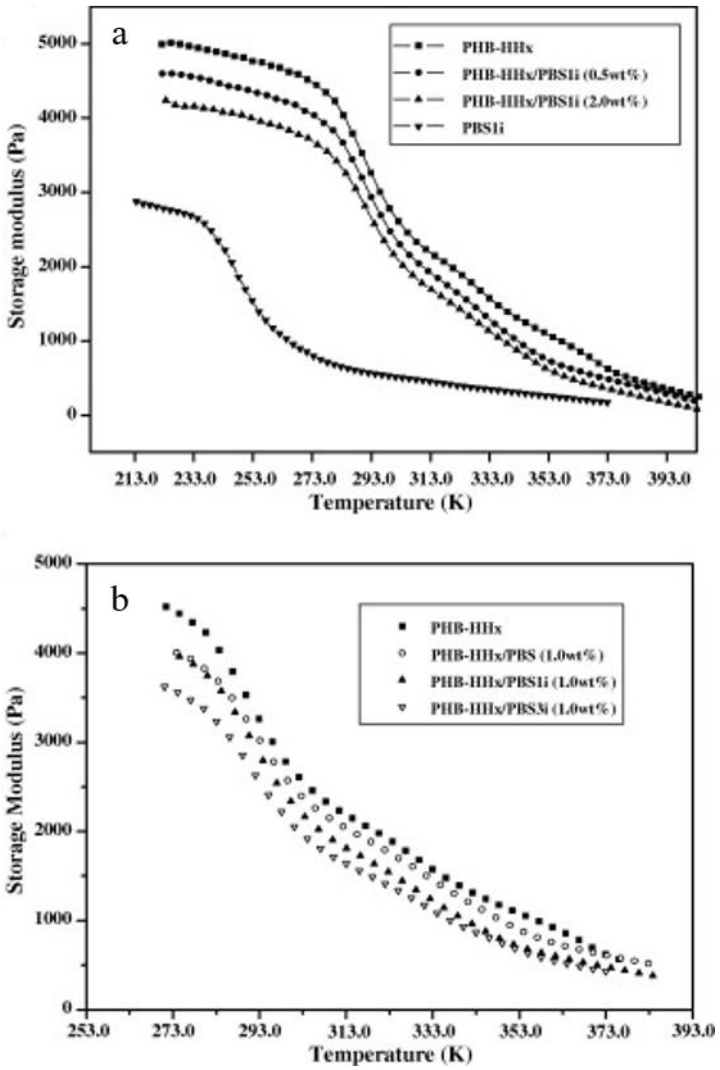

Figure 42. Temperature dependence of the storage modulus for the PHB-HHx/PBS ionomer blends; PHB-HHx/PBS1i blends (a) and PHB-HHx/PBS and PHB-HHx/PBSi (1 wt%) (b). Reprinted with the permission from [144].

In another work, Park *et al.* [148] studied the influence of PBS ionomer in a blend of PLA/PBSi. In this case, the interaction parameters of the blend PLA/PBS and PLA/PBSi are 0.007 and 0.011, respectively. Although both blends show positive values, which correspond to thermodynamically immiscible blends, being the interaction parameter value of PLA/PBSi lower than the other blend, the PLA and PBSi phases result more compatible among them [148]. In addition, the results of tensile tests report an improvement in mechanical properties in PLA/PBSi blends. In fact, the elongation of the PLA is 8% and increases drastically in PLA blends when the content of PBS or PBSi is above 10 wt%. In particular, the PLA/PBSi blend with 20 wt% of PBSi shows an elongation of almost 150%. On the other hand, the elongation of PLA/PBS blends with 20 wt% of PBS increases up to about 87%. Consequently, the elongation of PLA improves significantly by adding PBSi. The effect of ionomer in the blend system was shown to be better than that of pure PBS [148].

4.1.2.3 Addition of a third polymer in the blend

A third polymeric phase can act as a compatibilizer in immiscible binary blends. Before discussing the numerous studies that have confirmed the improvement in compatibility between two polymers, it is important to describe the mechanism of dispersion of each phase into the other that defines the final morphology of the system.

The tendency of a liquid droplet to spontaneously spread on a solid or on a liquid surface of another component is a phenomenon of the wetting physics. Harkins [149] [150] presented a thermodynamic explanation of this effect by demonstrating that a liquid spreads on a surface or wets it completely if the interfacial free energy of the resulting system decreases. From several experiments conducted by Harkins, it was possible to define the spreading coefficient λ_{ikj} with a simple and useful mathematical expression that can predict the wetting characteristic of ternary systems:

Equation 31. $$\lambda_{ikj} = \gamma_{ij} - (\gamma_{ik} + \gamma_{jk})$$

where γ are the interfacial tensions between the different pairs of materials. The spreading coefficient provides the tendency of component *k* to spontaneously spreads at the interface of components *i* and *j*. If the spreading coefficient is negative, the component *k* does not wet the *ij* interface.

Torza and Mason [151] used the approach of Harkins and generalized it for a blend of three immiscible components. In ternary immiscible mixtures with constituents A, B, and C, the three spreading coefficients are calculated by successively designating components A, B, and C as the component *k* that diffuses at the interface of the other two components *i* and *j*. Depending on the values of the three spreading coefficients, four different morphologies can result in blends consisting of two major phases and one minor phase [152].

Figure 43 (a), (b) and (c) correspond to complete wetting; two are complete segregation of disperse phase into the matrix and the third corresponds to spreading of the minor phase at the interface of two major ones. Conversely, Figure 43(d) shows the typical morphology in the case of partial wetting [152].

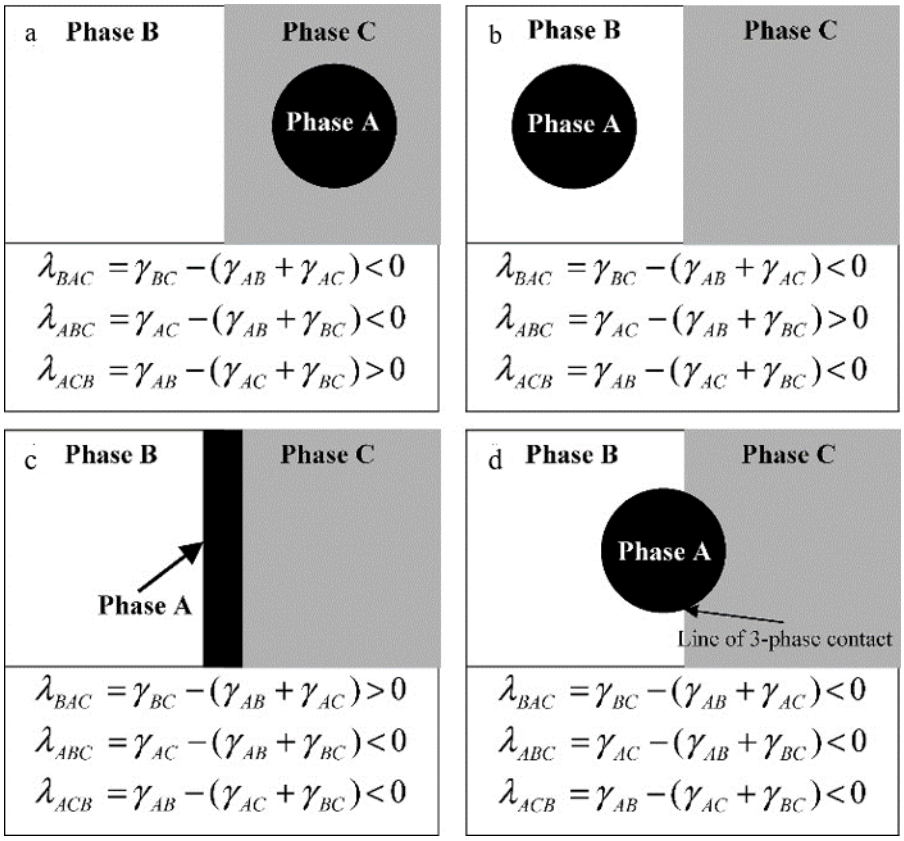

Figure 43. Possible morphologies in a ternary system composed of two major phases B and C (in white and grey) and one minor phase A (black), as predicted by the spreading coefficients. From part (a) to part (c), morphologies displaying complete wetting, in which phases C, B and A respectively wet the AB, AC and BC interfaces. The morphology in part (d) displays partial wetting, in which none of the phases locates between the other two, resulting in a line of contact along which the three phases meet. Reprinted under CC BY 4.0 license from [152].

As an alternative to the mathematical approach, the surface characteristics of a system are widely evaluated experimentally through measurements of the contact angle. Recently, Bulatovic *et al.* [153] used different test liquids (water, formamide and diiodomethane) with specific surface energy values to calculate the surface energy of PLA, PCL and TPS in order to examine the potential miscibility of PCL/PLA/TPS blends. The comparison of the average contact angle values with water confirms that the PCL is the most hydrophobic; in fact, the contact angle of PCL results 99.7° as compared to 68° and 55.6° of PLA and TPS, respectively. In the latter case, TPS presents a lower contact angle value as a consequence of polarity and pronounced hydrophilic nature. Therefore, it is expected that the presence of TPS in the PLA/PCL binary blends may change the wettability of the surface.

Figure 44 reports the possible phase morphology for PLA/PCL/TPS polymer blend after calculation of the spreading coefficient (Equation 31).

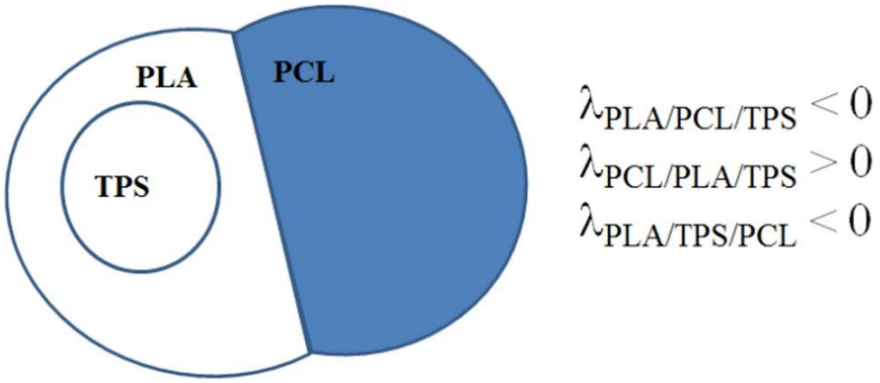

Figure 44. Possible phase morphologies for a PLA/PCL/TPS polymer blend, and their relations of the spreading coefficients. Reprinted with the permission from [153].

Furthermore, the authors reported a detailed study of ternary PCL/PLA/TPS blends morphology. SEM micrographs reported in Figure 45 show that the addition of TPS results in poor adhesion at the phase interface and the presence of micropores in the polymer matrix is observed. Thus, with the addition of TPS in binary PCL/PLA blends, the compatibility of the system does not improve. However, a refinement of morphology is achieved with a PLA content of 70 wt% (Figure 45 (f)) [153].

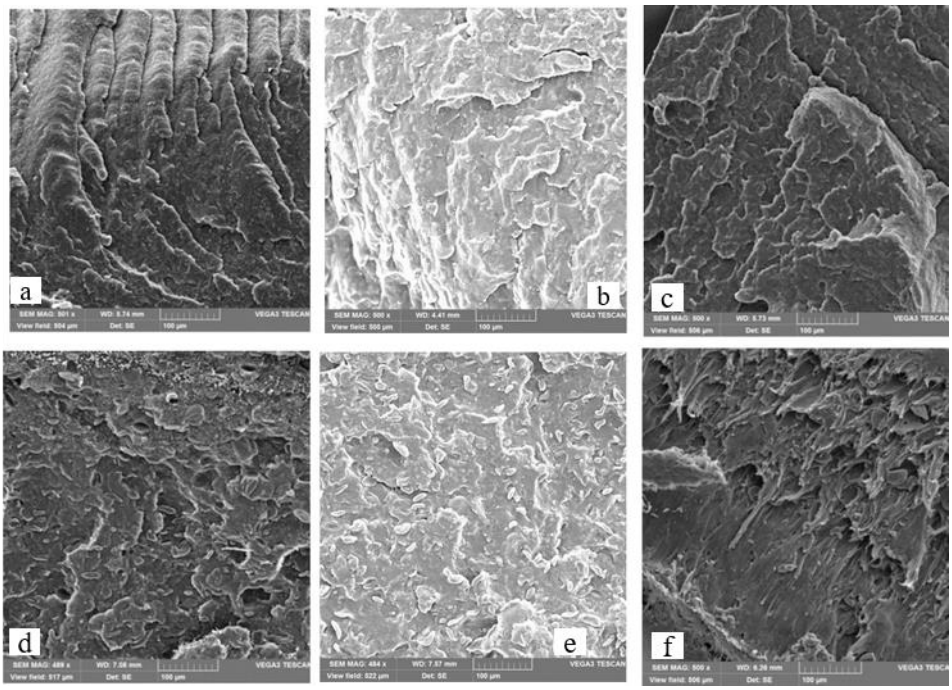

Figure 45. SEM micrographs of binary PCL70/PLA30 (a), PCL50/PLA50 (b), PCL30/PLA70 (c), and ternary PCL70/PLA30/TPS (d), PCL50/PLA50/TPS (d), and PCL30/PLA70/TPS (f) blends. Reprinted with the permission from [153].

Fenni et al. [154] studied PLA/PCL/PBS, PLA/PBS/PCL and PCL/PLA/PBS blends with weight ratio of 40/10/45. The prepared ternary blend exhibits a partial wetting morphology in which droplets of the minor phase self-assemble at the interface of the other components (Figure 46).

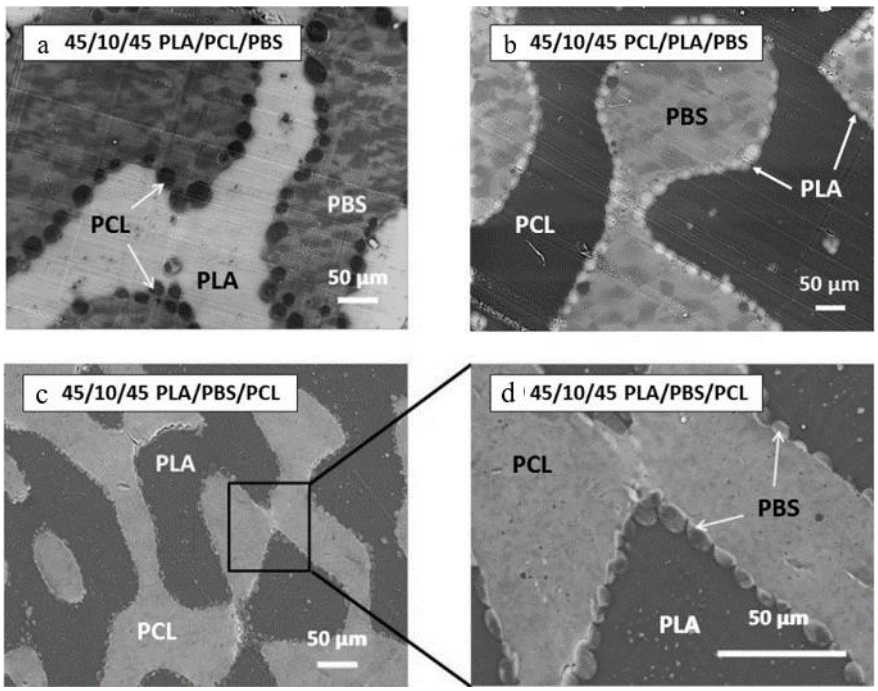

Figure 46. Scanning electron microscope (SEM) micrographs of PLA/PCL/PBS, PCL/PLA/PBS and PLA/PBS/PCL ternary blends with weight composition of 45/10/45 after annealing for 20 min at 185°C; (a) and (b) were directly imaged after cryo-microtoming; (c) and (d) were stained by tungstic acid followed by gold coating (~1 nm thickness) before SEM analysis. Reprinted with the permission from [154].

The formation of co-continuous structures in ternary blends are reported by Hedrick *et al*. [155]. In their work the authors studied PLA/PHBV/polypropylene carbonate (PPC) ternary polymer blends with increasing PPC content from 20 to 40 wt%. From the SEM images it can be observed that the morphology of the ternary blends changes from droplet structure (at low content of PPC 20 wt%) to co-continuous structure (at high PPC content 30 and 40 wt%). The Figure 47 shows a schematic illustration of the change in the morphology of ternary blends.

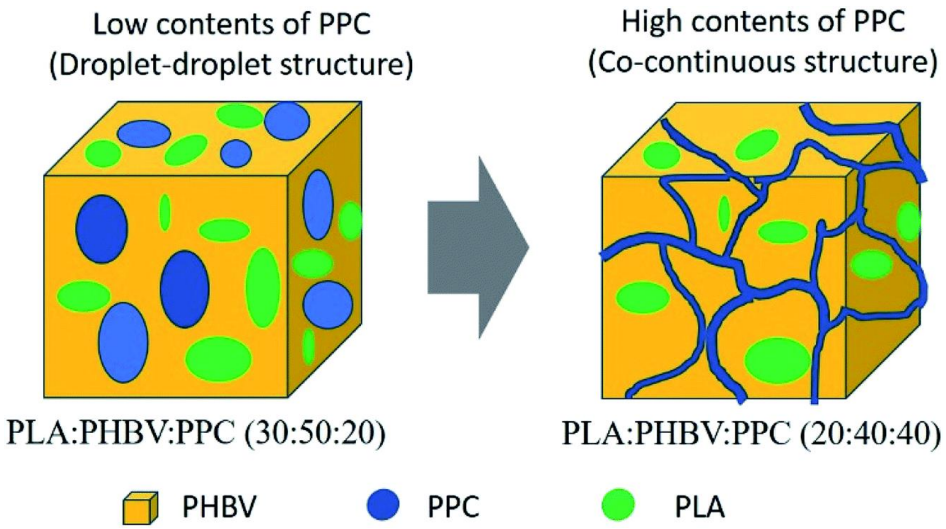

Figure 47. Schematic illustration detailing the transition from droplet–droplet to co-continuous morphology for biopolymer phases of ternary blends. Reprinted under CC BY 4.0 license from [155].

Although a reduction in particle size of minor phase is not reported, the three polymers are not completely immiscible. In fact, the presence of the third polymeric phase PPC (at 40 wt%), allows obtaining a fundamental improvement of the elongation at break from 5.2% for neat PLA polymer to 215% for ternary blend [155], as reported in Figure 48.

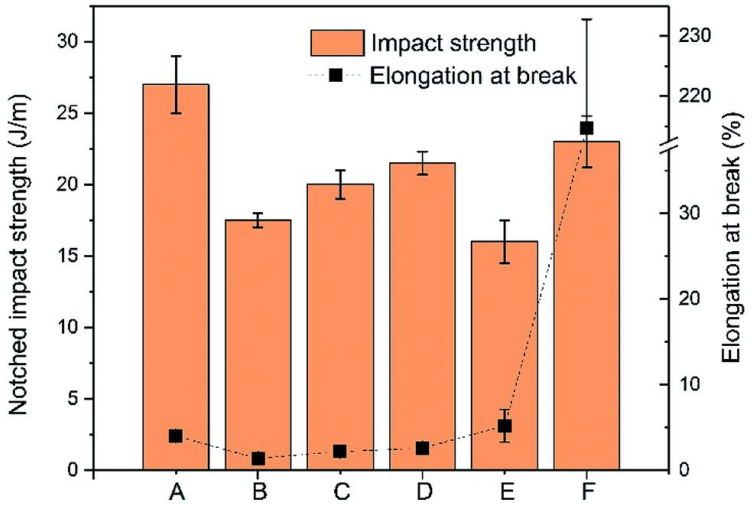

Figure 48. Impact strength and elongation at break of samples where A: 100% PLA, B: 100% PHBV, C: PLA : PHBV (35 : 65), D: PLA : PHBV : PPC (30 : 50 : 20), E: PLA : PHBV : PPC (25 : 45 : 30), and F: PLA : PHBV : PPC (20 : 40 : 40). Reprinted under CC BY 4.0 license from [155].

The optimization of mechanical properties was found also in the study of PHBV/PLA/PBS ternary blend by Zhang *et al.* [156]. Ternary blends show an excellent balance in tensile properties compared to the neat polymers. Modulus and tensile strength values indicate that, blending PLA with small amount of PHBV and PBS, an improvement of flexibility of PLA by slightly reducing its tensile strength can be found. The elongation at break of PLA/PHBV/PBS 60/30/10 blend increases above 5 times over that of the neat PLA; in PLA/PHBV/PBS 60/10/30 this value

further increases by more than 10 times over that of neat PLA. Thus, a transition from brittle to ductile fracture in ternary blend specimens was reported and the results are showed in Figure 49.

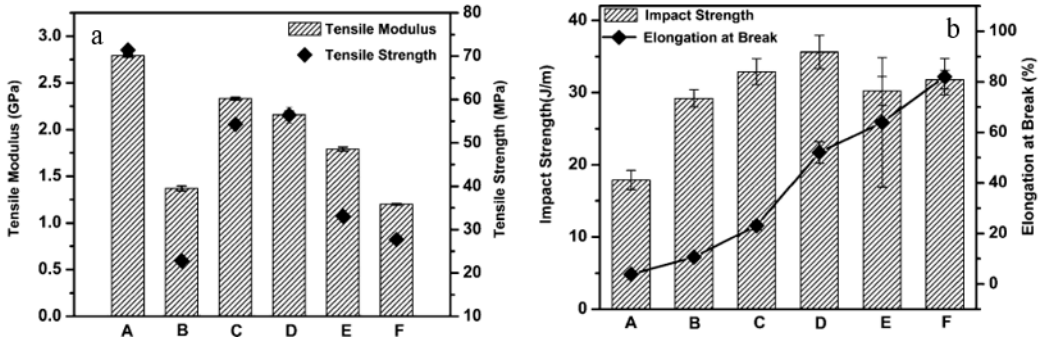

Figure 49. Tensile modulus and strength of PLA/PHBV/PBS ternary blends as function of the weight fraction (a) and Notched Izod impact strength and percent elongation at break of PLA/PHBV/PBS ternary blends as function of the weight fraction (b): (A) neat PLA; (B) neat PHBV; (C) PLA/PHBV/PBS 60/30/10; (D) PLA/PHBV/PBS 60/10/30; (E) PHBV/PLA/PBS 60/30/10; (F) PHBV/PLA/PBS 60/10/30. Reprinted under CC BY 4.0 license from [156].

4.1.2.4 Use of nanoparticles as compatibilizer agents

The addition of nanoparticles to an immiscible biopolymer blend is an alternative method of improving compatibility between the polymers constituting the mixture. When the additives are located at the interface between the components, they act as interfacial modifiers by enhancing interfacial adhesion of the polymers. At microscopical level, the presence of nanoparticles can promote the achievement of a fine morphology with a reduced size of the dispersed phase by preventing the phenomenon of coalescence. Therefore, the microstructure is stabilized, resulting in an improvement of the properties of the blends.

Figure 50 shows the distribution of the studies regarding PLA-based blend nanocomposites until 2018; the graph is focused on the different types of nanoparticles [157].

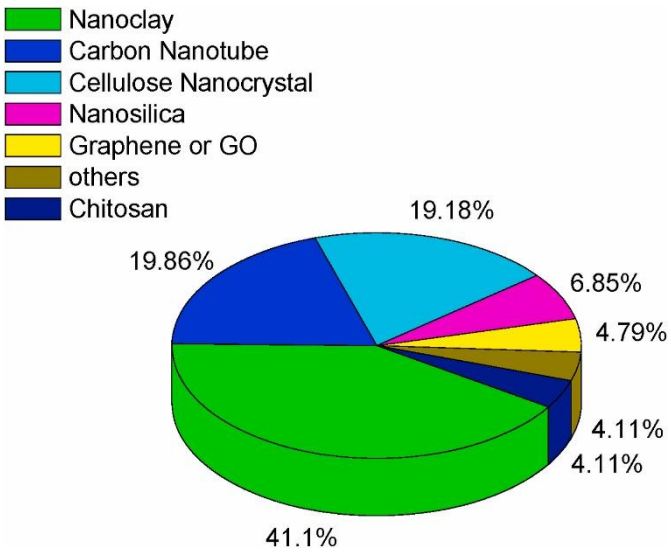

Figure 50. Distribution of studies on PLA-based blend nanocomposites with various nanoparticles. Reprinted under CC BY 4.0 license from [157].

The easy incorporation of nanoparticles during melting allows them to be located at the interface between the components of the blend or in one of the two polymer phases. The selective localization of the various nanoparticles such as nanoclays, nanosilica, carbon nanotubes (CNTs), graphene and cellulose nanocrystals (CNCs) is one of the most important factors to achieve a nanocomposite blend with improved performances [158] [159] [160].

In a condition of thermodynamically equilibrium, the specific interaction between the two polymeric components determines the final localization of the nanoparticles. Therefore, the nanoparticles can be expected to be localized within polymer A or B, or at the interface between them. The thermodynamic localization of the filler can be predicted through the determination of the wetting coefficient ω_a, in a thermodynamic equilibrium state. It depends on the interfacial energies γ_{xy} where x or y is polymer A, polymer B or clay according to the Young's Equation [161]:

Equation 32. $$\omega_a \frac{\gamma_{clay-polymerB} - \gamma_{clay-polymerA}}{\gamma_{polymerA-polymerB}}$$

If $\omega_a > 1$, the clay will be preferentially dispersed in polymer A, if $\omega_a < -1$ the clay be located in polymer B and for $-1 < \omega_a < 1$ the nanoparticle will be located at interfaces between polymers A and B. Since the determination of the interfacial energies between nanoparticle and polymers is difficult, these were estimated using surface energies, which consist of dispersive γ^d and polar γ^p components [162]:

Equation 33. $$\gamma_x = \gamma_x^d + \gamma_x^p$$

Equation 34. $\gamma_y = \gamma_y^d + \gamma_y^p$

These two components of surface energy can be used to calculate interface energy using the harmonic- mean equation [163]:

Equation 35. $\gamma_{xy} = \gamma_x + \gamma_y - 4\left(\frac{\gamma_x^d \gamma_y^d}{\gamma_x^d + \gamma_y^d} + \frac{\gamma_x^p \gamma_y^p}{\gamma_x^p + \gamma_y^p}\right)$

and the geometric-mean equation [164]:

Equation 36. $\gamma_{xy} = \gamma_x + \gamma_y - 2\left(\sqrt{\gamma_x^d \gamma_y^d} + \sqrt{\gamma_x^p \gamma_y^p}\right)$

The surface tension levels reported in the literature have been measured at room temperature and need to be corrected for the processing temperature. To this aim, the Guggenheim equation developed for small molecule liquids can be applied to polymers to calculate surface tension levels at the desired temperatures [165]:

Equation 37. $-\frac{\partial \gamma}{\partial T} = \frac{11}{9}\frac{\gamma_0}{T_c}\left(1 - \frac{T}{T_c}\right)$

where γ_0 is the surface tension at T = 0 and Tc represents the critical temperature.

The value of – dγ/dT relative to the polymers and the filler are usually taken from the literature [165].

The localization of the nanoparticles in one of the phases allows the reduction of the interfacial energy and, in most studies, it has become very clear that the filler tends to locate in the phase with high affinity during the process [166] [167]. Furthermore, beside the thermodynamic effect on the preferential localization of the filler in a polymer blend, kinetic effects such as the compounding sequence, melt viscosity, melt compounding time and shear rate are fundamental to determine the final localization of nanoparticles [168] [167] [169]. In particular, in blend composites, the melt viscosity plays a significant role on the final localization of the nanoparticles and, thus, on the final morphology of the systems. In addition, if the processing conditions, e.g. different mixing times, are controlled, the nanoparticles can be selectively localized at the interface between the phases or within one of the polymers. Huang *et al.* [170] showed that different mixing times resulted in different localization of CNTs in PLA/PCL blend. The mixing time is defined, by the authors, as the time after incorporation of PCL into the premixed PLA/nanofillers composite. The authors observed a migration of the nanofiller mainly in the PLA phase after 1 minute of mixing. However, with the increase of the mixing time from 1 to 4 minutes, an accumulation of the nanofillers at the

interface is observed. A further increase of the mixing time up to 20 minutes involves a dispersion of nanofillers into the PCL phase [170]. It is worthy to note that with a careful control of process parameters a specific localization of the filler can be attained by kinetic aspects.

It is well documented in literature that the nanofillers can stabilize the morphology of an immiscible blend in order to enhance the compatibility of polymers constituting the blend [158] [171] [172]. However, the reduction of the size of dispersed phase and the complete stabilization of the microstructure of polymer blends is achieved when the compatibilizers are located in the continuous phase or at interface [157].

As an example, Shahlari and Lee [173] reported that when organo-modified clay (Cloisite 30B (C30B)) particles is located at the interface of PBAT/PLA blend, with 80 wt% of PLA and 20 wt% of PHB, a significant reduction in the size of the PLA domain is obtained. The result from morphological analysis is attributed to the physical barrier effect of the clays at the interface against coalescence phenomenon.

A good degree of dispersion of C30B and Sepiolite SP in a blend PHBV/PLA blend is obtained [174]. In particular, the presence of nanoparticles leads to favourable interfacial interactions between the two polymers. SEM micrographs of fractured surface of the blends with the combination of nanofillers are reported in Figure 51. Figure 51 (d) and Figure 51 (e) show the more homogeneous morphology obtained with the presence of both Sepiolite and C30B nanocalys, which reduce the interfacial tension between the polymer phases [174].

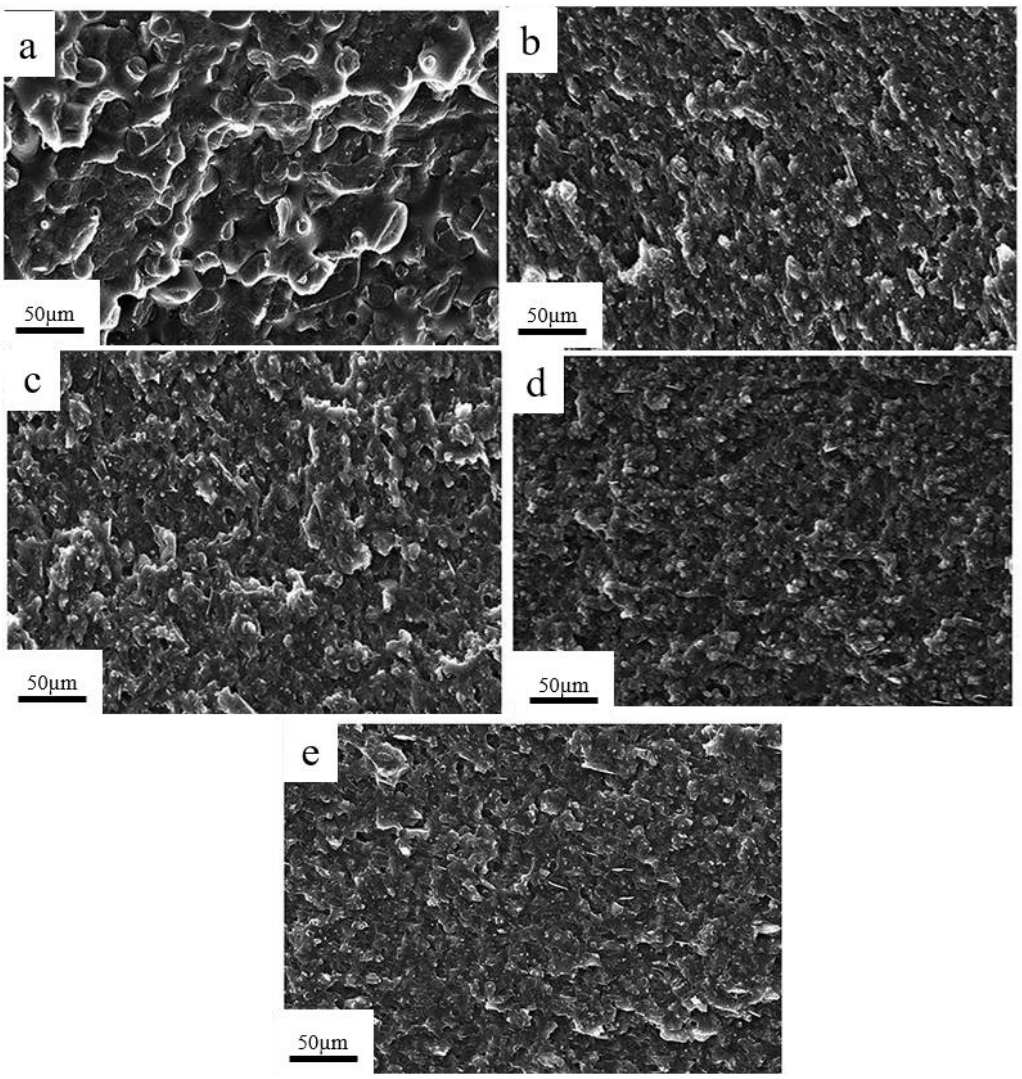

Figure 51. **SEM micrographs of fractured surface of PHBV/PLA blend (a), PHBV/PLA/3C30B (b), PHBV/PLA/3SP (c), PHBV/PLA/1.5SP/1.5C30B (d) and PHBV/PLA/2.5SP/2.5C30B (e). Modified from [174].**

The incorporation of Sepiolite and C30B causes an increase in the modulus of PHBV/PLA blend. In particular, the increase in storage modulus is higher when C30B and Sepiolite are combined and the enhancement in modulus and hardness of PHBV/PLA blend is more pronounced when 2.5% of Sepiolite and 2.5% of C30B are added, resulting in the increase of 32% of modulus in PHBV/PLA blend. A synergistic effect of Sepiolite and C30B is highlighted, leading to clear reinforcement effect and improvement of mechanical behaviour of PHBV/PLA blend [174].

Chen *et al.* [175] evaluated the effect of two twice-functionalized organoclays TFCs on the compatibility between PLLA and PBS. The nanofiller is almost exclusively located in the PLLA phase and the domain size of the dispersed PBS particles did not change when the content of the TFC was less than 0.5 wt%. However, when the amount of TFC increased, the clay was found to be located in both PLLA and PBS phases and the size of the disperse PBS phase decreases gradually with a further increase of the compatibilizer content. SEM images of the

PLLA/PBS blends containing various amounts of the TFC are reported in Figure 52.

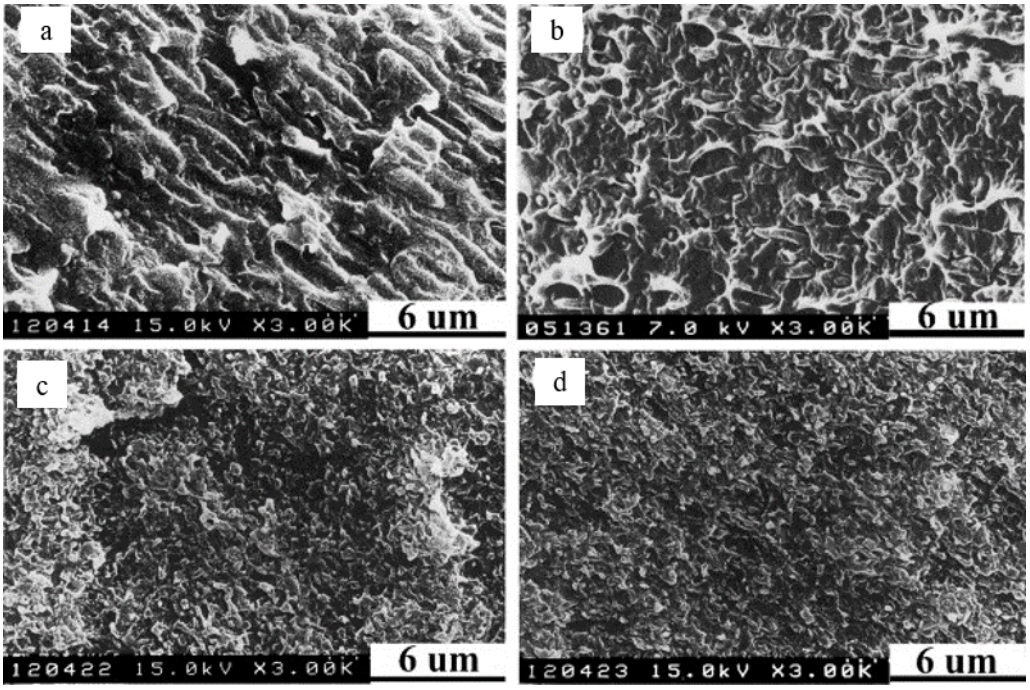

Figure 52. SEM micrographs of the PLLA/PBS blends with various amounts of TFC 0 (a), 0.5 (b), 2, 5 wt%(c) and 5 wt% (d). Modified from [175].

In addition, the introduction of TFC to the PLLA/PBS blend significantly increases the tensile modulus and the elongation at break. This demonstrated that TFC acts as a reinforcing filler, due to its high aspect ratio and lamellar structure. The elastic modulus passes from 1075 MPa for PLLA/PBS non-compatibilized blend to 1626 MPa and 1990 MPa for PLLA/PBS containing 5 and 10 wt% of TFC, respectively. The elongation at break of the PLLA/PBS blend increases up to 118% in compatibilized blend with 10 wt% of TFC compared to the 71% of the non-compatibilized blend [175].

Hoidy *et al.* [176] studied a PLA/PCL blend with organo-modified clay OMMT. The presence of the nanoclay not only enhances the compatibility between the immiscible polymer phases, but also improves mechanical properties of the final blends.

Cloisite 30B was used to compatibilize PLA/PBS blend [177]. The content of nanoclay was important to determine the final microstructure and properties of the system. In fact, a co-continuous morphology is achieved in the blend with 50 wt% of PLA, 50 wt% of PBS and 3 wt% of filler. A further increase in Cl30B content allows to have a lamellar morphology accompanied by low value of elongation at break [177]. The results of mechanical properties as a function of the Cl30B content are reported in Figure 53.

The Young's modulus increases continuously with the clay content; an improvement of about 15% is observed with an addition of 4.5 wt % of Cl30B, whereas a maximum of 41% of improvement is noted with an addition of 7 wt %

od Cl30B. The elongation at break remains almost constant up to about 3 wt % of Cl30B and then dramatically decreases in the nanocomposite with 7 wt% of nanoclay up to 85% less, compared to the pure matrix [177].

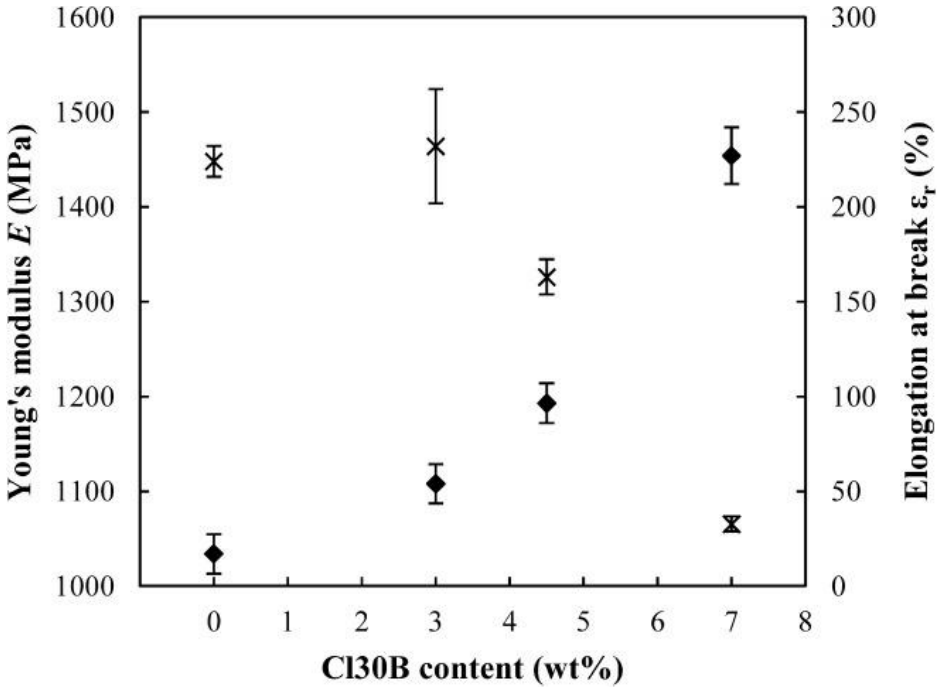

Figure 53. Young's modulus (♦) and elongation at break (×) as function of Cl30B content. Reprinted with the permission from [177].

In some studies, the toughness increases when nanoparticles are located inside the matrix, while in some others when they are in droplets or the interface. Such discrepancies can induce the issue that solid-state mechanical testing is less sensitive to localization and instead rely on the overall bulk dispersion/distribution of nanoparticles [157]. However, most studies with nanoparticles at the interface, as above-mentioned, claimed significant enhancement in mechanical properties.

4.2 Influence of process parameters in extrusion through melt blending

In Chapter 2, particularly in the Paragraphs 2.2.1, the capillary number Ca_{crit} which is dependent on the viscosity ratio (*p)* was defined. The curves of the critical capillary number as a function of the viscosity ratio, in the experimental work of Grace [27], are significantly different in shear and elongation flow. Thus, the morphology developed in polymer blends is strictly related to the Ca_{crit} which describes the process of breakup of the droplets and the flow parameters during the process.

In fact, in order to determine the behaviour of polymer blends during the melt-blending (o compounding) process, it is possible, through a systematic and detailed study, verify the evolution of the morphology along the extruder. The first step is the description of the flow mechanics and the fundamental assumption in twin-screw extruder (TSE) is that there are 'strong' and 'weak' zones. Within the former, the screw elements are completely filled; there is a positive pressure, large deforming stresses, and usually a circulation of material that offers a potential for changes the morphology of the mixtures. The "weak" zones are partially filled, and mainly consisted of conveying elements. Here the material is transported at ambient pressure or under vacuum and the stresses are minimal.

In the literature, the study of the development of the morphology of a polymer blend and the influence of the process parameters on the final material performance is mainly focused on fossil-fuel based polymer blends, while the study of bio-based and biodegradable polymers is yet underdeveloped [178]. For this reason, in this paragraph, the literature references reported are based on blends of polymers obtained from petrochemical-derived products.

Utracki and Shi [178] in 1992 proposed the first model of development of morphology of polymer blends in a TSE. The model considered the mechanism of micro-rheological dispersion but the phenomenon of coalescence was neglected. Its validity was assessed by comparing the predictions with the droplet diameter measured experimentally at different axial positions in the twin-screw extruder. In the assumed absence of coalescence, the model predicted a continuous decrease of the dimensions of the droplets, while the experiment indicated their stabilization. Subsequently, another model refined these calculations and introduced coalescence between droplets [179]. The model is fully predictive and good agreement with experimental data was found.

Nevertheless, it is impossible to have a clear overview of the evolution of morphology in immiscible polymer blends during compounding in a twin-screw extruder, since morphology is influenced by the rheological properties of the constituent components, blend composition and processing variables. Considering the compound in a TSE of two semi-crystalline polymers A and B, a schematic representation of the trend of the temperature along the extruder is reported in Figure 54.

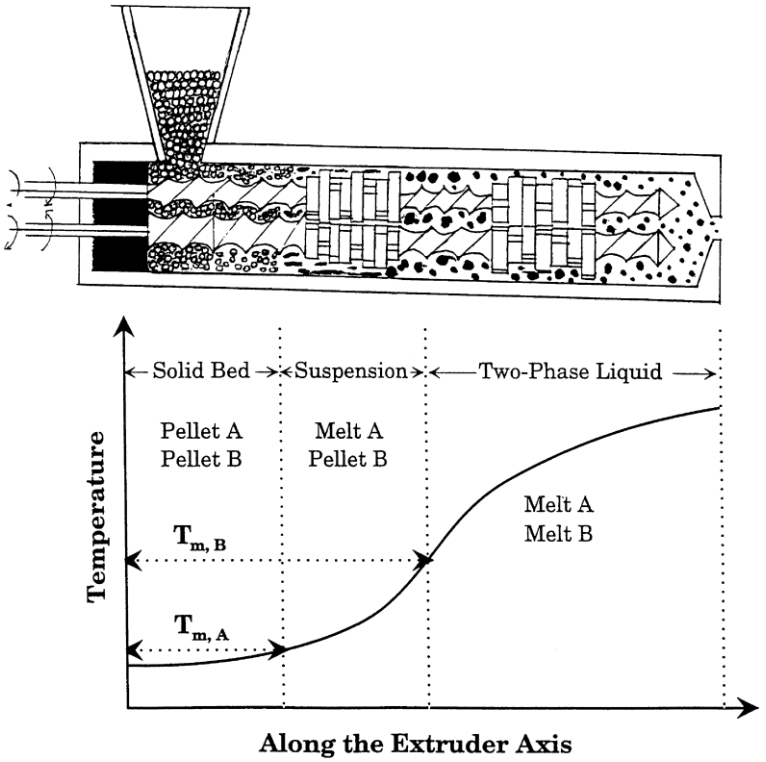

Figure 54. Schematic diagram describing a twin-screw extruder, in which a pair of immiscible crystalline polymers are extruded under a pre-set temperature profile along the extruder axis. Reprinted with the permission from [180].

Assuming that the melting point of polymer A ($T_{m,A}$) is lower than the melting point of polymer B ($T_{m,B}$), at the front end of the extruder where polymer A melts first, the mixture is a suspension consisting of molten polymer A forming the continuous phase and solid polymer B. As the suspension moves along the axis of the extruder and reaches a temperature at which polymer B begins to melt, the liquid mixture will form a dispersed morphology, where droplets of polymer B are dispersed in the matrix of polymer A. There are two possibilities: the same mode of dispersion pattern persists throughout the rest of the extruder or a phase-inversion may occur, where polymer B now becomes the continuous phase and polymer A becomes the dispersed phase.

Lee *at al*. [180] investigated the evolution of the morphology of immiscible blends based on fossil-fuel derived polymer. They used different polymers PMMA, PS, PC, PP and HDPE and studied four pairs of polymer blends in order to evaluate the morphology developed in systems constituted by amorphous/crystalline polymers and amorphous/amorphous polymers, considering the critical flow temperature T_{cf} and the melting point T_m in the case of amorphous and crystalline polymers, respectively. The authors reported in a schematic diagram the expected morphology developed during melt blending in TSE by considering the volume fraction and the viscosity of each polymer (Figure 55). The results obtained are the same in the case of a system of two crystalline polymers and two amorphous polymers.

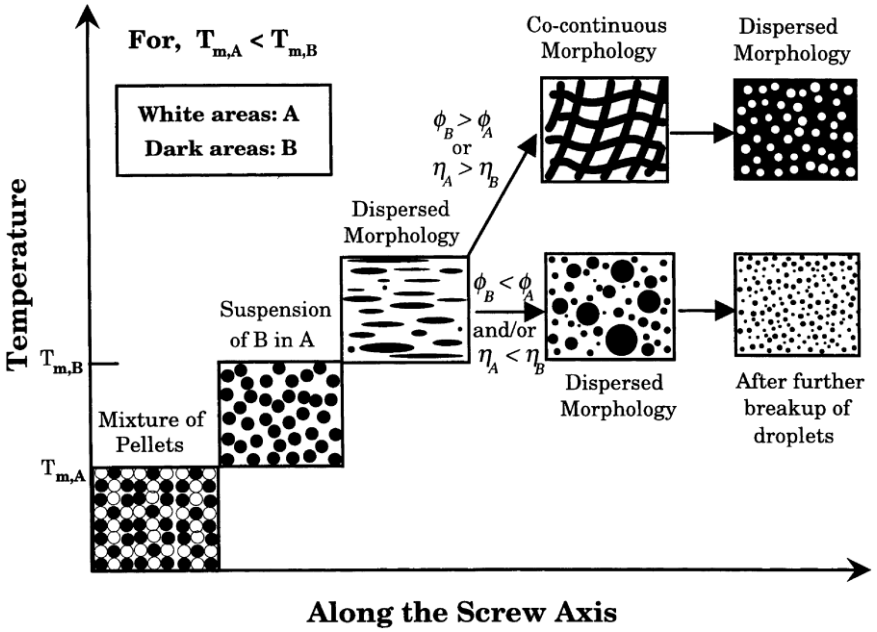

Figure 55. Schematic diagram describing the evolution of blend morphology of a pair of immiscible polymers, A and B, along the axis of a twin-screw extruder, where the melting point of polymer A is assumed to be lower than that of polymer B. in the Figure ϕ_i and η_i are the volume fraction and the viscosity, respectively. Reprinted with the permission from [180].

In the studied system PS/PMMA, being the T_{cf} of PS lower than that of PMMA, in the first part of the extruder, particularly before the kneading block presents in the screw configuration reported in Figure 56, PS is the continuous phase with particles of PMMA dispersed in the matrix. Beyond that position, the evolution of the blend morphology depends on blend composition ϕ_i or viscosity ratio η_i, as reported in Figure 55. Specifically, when the PMMA is the minor and more viscous component it will form the dispersed phase and the PS will be the continuous phase [180]. On the other hand, when the PMMA is the major and more viscous component it was found to be the continuous phase with PS as dispersed phase. The evolution of morphology of these two cases is reported in Figure 56 and Figure 57 where the light and dark areas represent PMMA and PS phases, respectively. It is worthy to underline that the above observations are applied in all systems investigated in the study [180].

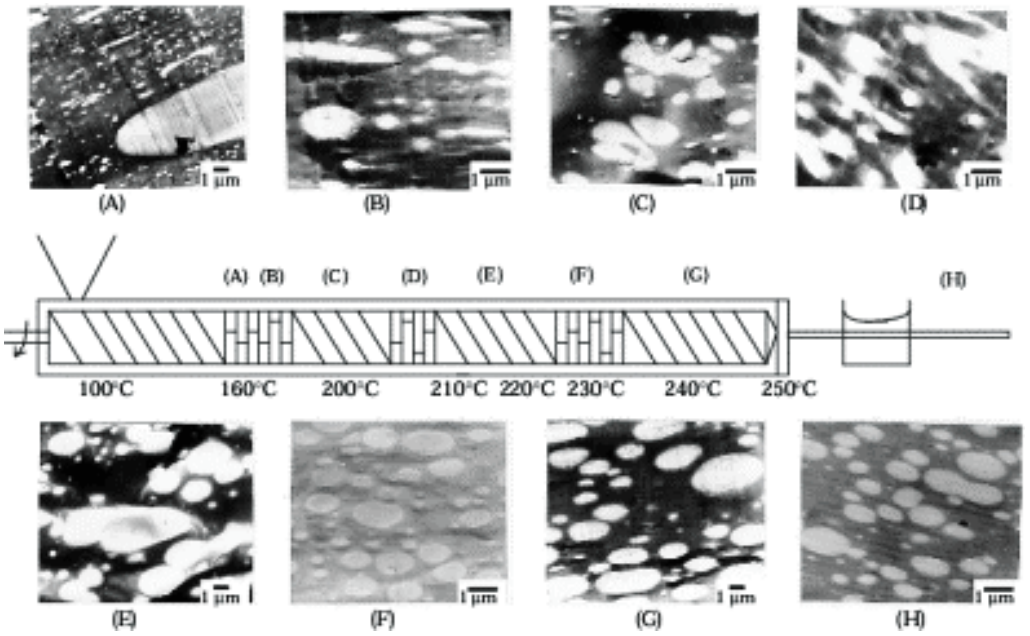

Figure 56. The evolution of morphology in 30/70 PMMA/PS blend during compounding in a twin-screw extruder: at the front end of the first kneading block (160°C) (A); at the exit of the first kneading block (160°C) (B); between the first and second kneading blocks (200°C) (C); at the front end of the second kneading block (200°C) (D); between the second and third kneading blocks (220°C) (E); at exit of the third kneading block (230°C) (F); between the third kneading block and the die (240°C) (G); extrudate (H). Reprinted with the permission from [180].

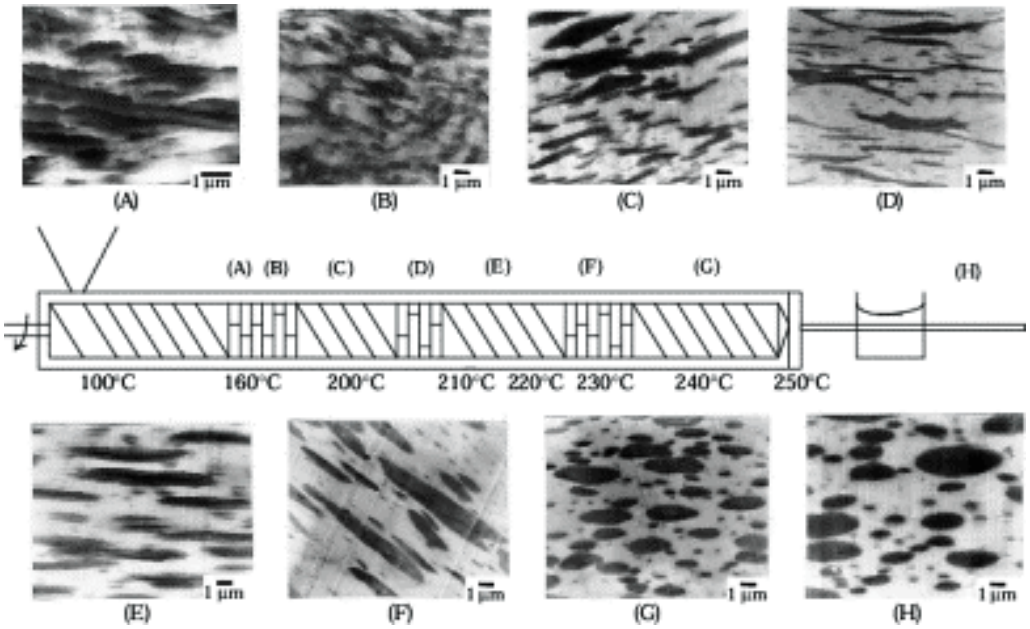

Figure 57. The evolution of morphology in 70/30 PMMA/PS blend during compounding in a twin-screw extruder: at the front end of the first kneading block (160°C) (A); at the exit of the first kneading block (160°C) (B); between the first and second kneading blocks (200°C) (C); at the front end of the second kneading block (200°C) (D); between the second and third kneading blocks (220°C) (E); at exit of the third kneading block (230°C) (F); between the third kneading block and the die (240°C) (G); extrudate (H).. Reprinted with the permission from [180].

However, the above results, are not consistent with the principle of minimum energy dissipation, which provides that in a flow of two immiscible components,

the liquid having lower viscosity is expected to form the continuous phase [180]. There is a delicate relationship, which controls the state of dispersion in a mixture of immiscible polymers, between blend ratio and viscosity ratio. From the above results, it is possible concluding that the blend ratio played a predominant role in determining the state of dispersion of the studied systems.

In addition to the viscosity ratio and blend composition, the final morphology is influenced by the screw profile. The final product obtained with a TSE depend mainly on the dispersive and distribution mixing generated by the kneading blocks [181]. Different experimental and numerical investigations are presented in several contributions in the literature on the importance of the best selection of kneading blocks, particularly their staggering angle and their position along the axis of the extruder, during the process [182] [183] [184] [185]. A blend processed in a TSE is sensible to extrusion parameters such as for example the width and angle of the kneading blocks of the screw [186]. Despite this, the influence of the different elements of the screw profile during the production process of a polymer blend is not reported in detail in literature.

Ambrosio *et al.* [187] studied the influence of process parameters in an extrusion process performed in a TSE on the morphology and mechanical properties of a PBT/ABS compatibilized with methyl methacrylate-ethyl methacrylate-glycidyl methacrylate (MMA-GMA-EA) terpolymer (88 wt% MMA, 10 wt% GA and wt2% EA). Two different configuration of screw profiles were used and are reported in Figure 58.

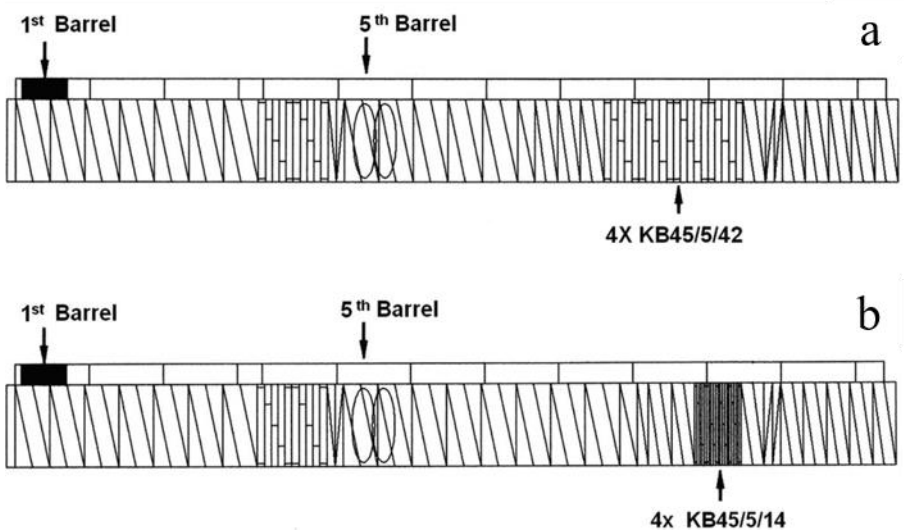

Figure 58. Type screw 4KB45/5/42 with four KB45/5/42 kneading blocks in the mixing region (a). Type screw 4KB/45/5/14 with four KB45/5/14 kneading blocks in the mixing region (b). Both screws have two kneading blocks type KB45/5/42 before the side feeder in the 5th barrel. Reprinted with the permission from [187].

The difference among these screw profiles is the width of the kneading discs in the mixing region of the screw. Four kneading discs orientated at 45° from each other with a total width of the discs of 42 mm and 14 mm for the first screw (Figure 58(a)) and the second screw (Figure 58(b)) respectively, were used in this region.

The larger kneading discs in the first screw profile produce high shear intensity, that is beneficial for the dispersion mixing. The shorter kneading discs in the second screw profile generate lower shear intensity and are more suitable for the distribution mixing [186]. Furthermore, the authors evaluated the influence of feed rate and screw rotation speed on the impact strength of the resulting materials. The impact strength tests were performed at different temperatures to determine the ductile-to-brittle transition temperature (DBTT) of the samples. Figure 59 reports the influence of feed ratio on the impact strength of PBT/ABS/MGE blends processed at 120 rpm.

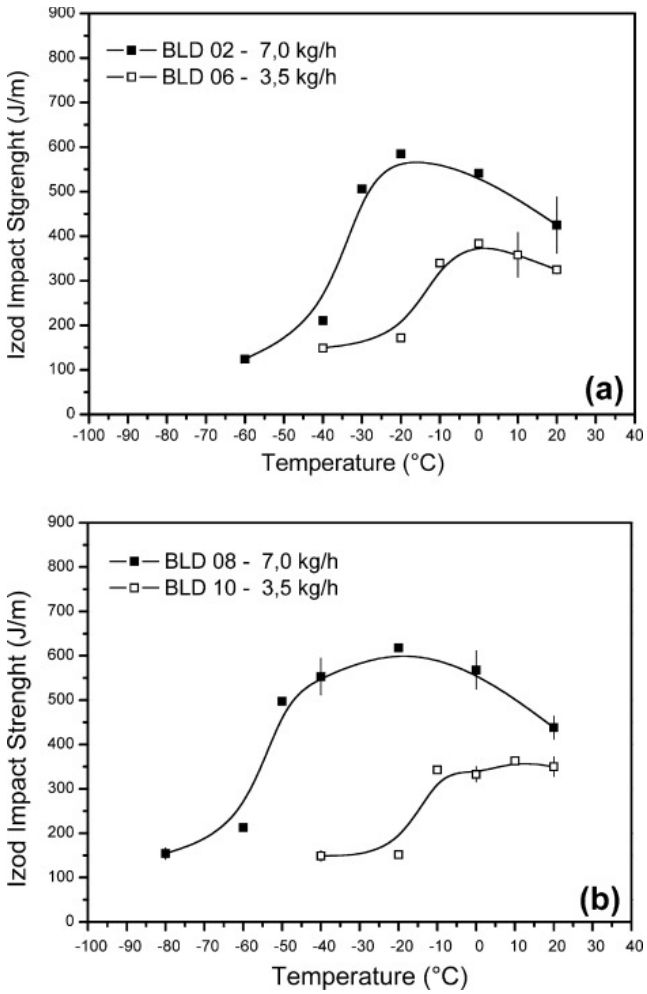

Figure 59. Influence of feed rate into the intermeshing co-rotating twin screw extruder on the impact strength of PBT/ABS/MGE blends processed at 120 rpm. Screw profile 1 4KB45/5/42 (a); Screw profile 2 4KB45/5/14 (b). Modified from [187]

The important consequence of the decrease of the feed rate for both screw profiles is the increase of the residence time of the melt in the extruder; this occurs because the screw channels would not have been completely loaded, giving them insufficient pressure to transport the material forward [187]. In addition, an increase of the impact strength was observed for the blend processed with high feed ratio (7 kg/h).

Regarding the influence of screw rotation speed, the blends processed at 120 rpm for both screw profiles show higher value of impact strength as compared to those processed at 240 rpm, as shown in Figure 60. This finding, according to the authors, is due to the influence of the screw speed on the rate of MGE crosslinking reaction. Probably, the incorporation of MGE in the 5th barrel allows occurring undesirable reactions which are intensified by the higher screw rotation speed (240 rpm) leading to the formation of more brittle phase and a decrease of the Izod impact strength value of the compatibilized systems as compared to those obtained at 120 rpm [187].

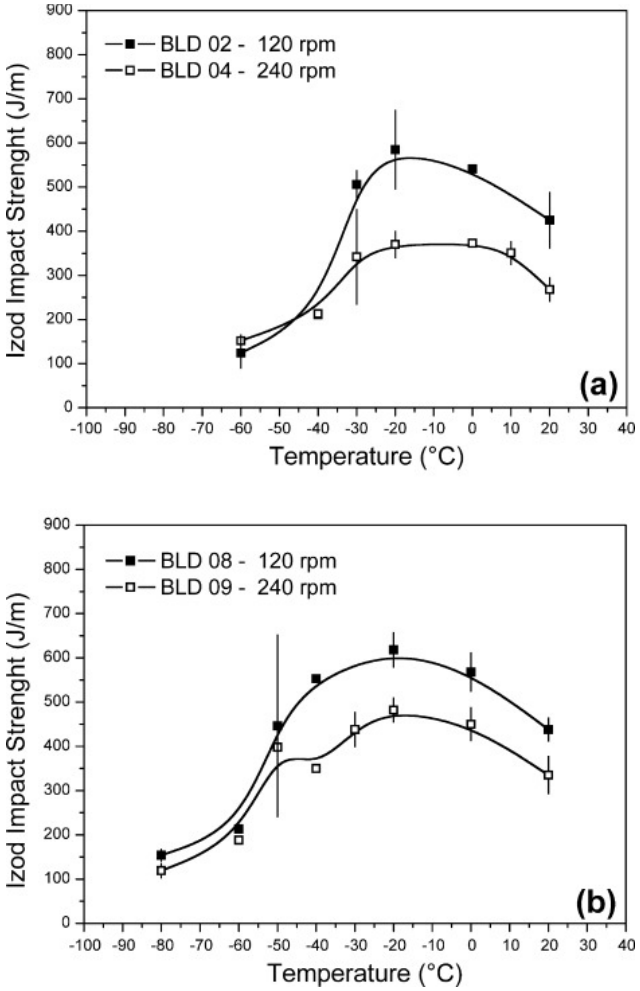

Figure 60. Influence of screw rotation speed in the intermeshing co-rotating twin screw extruder on the notched Izod impact strength of samples of the PBT/ABS/MGE blends, processed at 7.0 kg/h. Screw 4KB45/5/42 (a); Screw 4KB45/5/14 (b). Modified from [187].

The influence of feed rate and of screw rotation speed on mechanical properties of a compatibilized blend was also studied by Hu *et al.* [188]. The study is focused on the effect of process parameters on the *in situ* compatibilization of PP/PBAT blends with the functional monomer of glycidyl methacrylate (GMA) into PP polymer. The results report a linear decrease of the elongation at break and impact strength with the increase of the feed rate (Figure 61(a) and Figure 61(b)). In addition, an increase in screw rotation speed generates a decrease of the

residence time by enhancing the mixing intensity. These two opposing effects influence the elongation at break and the impact strength of the compatibilized blend; in fact, a decrease of the mechanical properties is found with increasing of the rotation screw speed, as reported in Figure 61(c) and Figure 61(d)[188].

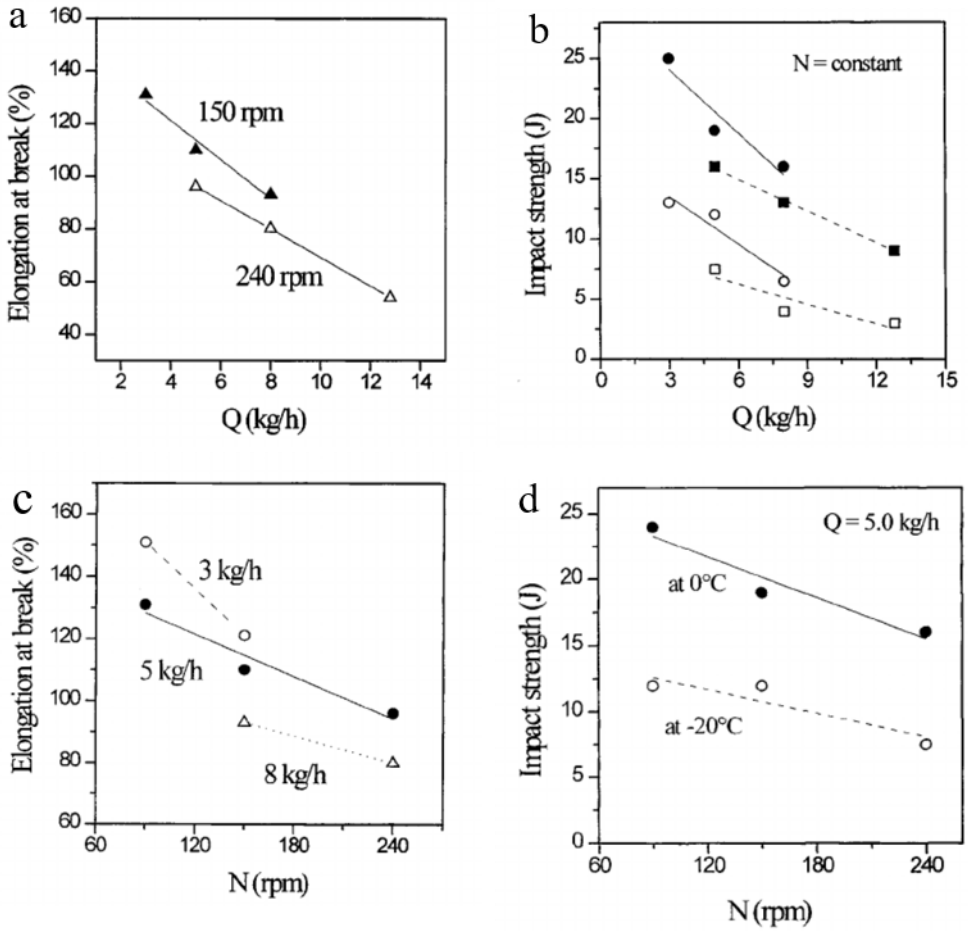

Figure 61. Variation of the elongation at break on the compatibilized PP/PBAT blends as a function of feed rate at 150 and 240 rpm (a) and the variation of impact strength at constant screw rotation speed N (b) Variation of the elongation at break on the compatibilized PP/PBAT blends as a function of screw rotation speed N for three different feed rates Q (c) and the variation of impact strength at a particular feed rate Q (d) Reprinted with the permission from [188].

Chapter 5

Use of natural surfactants in PLA-based blends

Part of the work described in the Chapter 5 has been previously published in:

''Casamento F, D'Anna A, Arrigo R, Frache A. Rheological behaviour and morphology of poly (lactic acid)/low-density polyethylene blends based on virgin and recycled polymers: Compatibilization with natural surfactants. Journal of Applied Polymer Science. 2021'' [189]

''D'Anna A, Arrigo R, Frache A. PLA/PHB Blends: Biocompatibilizer Effect. Polymers. 2019'' [190]

5.1 Introduction

In the previous chapters, it has already been extensively discussed that immiscible polymer blends require the presence of a third phase, known as compatibilizer, which can increase the interfacial adhesion between the polymers in order to obtain a morphological refinement and an improvement of the final properties of the systems.

Non-ionic surfactants have traditionally been used as emulsifiers with the ability to stabilise an emulsion of oil-in-water (O/W) or water-in-oil (W/O) by acting on the reduction of interfacial tension [191] [192] [193].

In this respect, this chapter will report the results of the innovative use of various non-ionic surfactants to improve the compatibility of polymer blends although non-ionic surfactants are not widely used as compatibilizers in immiscible polymer blends. The surfactants present the ability to lower the surface tension of

the system and, therefore, their use in immiscible blends is strongly recommended in order to increase the interfacial adhesion between the phases that constitute the blend. Moreover, the surfactants used in this section of the experimentation are defined biocompatible and renewable by the FDA. Initially, the compatibilization system was tested on a PLA/LDPE model system in order to define the optimal amount of surfactants to be used. Subsequently, their use has been tested on bio-based PLA/PHB polymer blends with the aim of obtaining fully bio-based polymer systems.

5.2 Compatibilization systems

Several papers have indicated that surfactants could also be used as compatibilizers in polymer blends and composite systems specifically for polar and non-polar polymers [194] [195]. This is due to the fact that surfactants have an amphiphilic character that contains non-polar and polar parts (hydrophobic and hydrophilic groups) [196] that are able to increase interfacial adhesion between non-polar and polar polymers by ensuring compatibility between phases in the blend system [197].

The amphiphilic character of non-ionic surfactants is controlled by the value of the hydrophilic-lipophilic index (HLB) whose method of definition was introduced in the late 1940s by Imperial Chemical Industries (ICI) [198]. In particular, the HLB index of a non-ionic surfactant is an expression of its Hydrophile-Lipophile balance, thus the balance of size and strength of the hydrophilic (polar) and the lipophilic (non-polar) groups of the surfactant. For example, a surfactant with high lipophilic character is characterized by a low HLB number (below 9) and, conversely, high HLB values (above 11) are typical in surfactant with strong hydrophilic character; those in the range of 9-11 are intermediate or neutral. Among the several non-ionic surfactants, ethoxylated sorbitan ester (Tween) and sorbitan ester (Span), whose chemical structures are reported in Figure 62, are the most used. Figure 63 shows the arbitrary scale, from 0 to 20, of the HLB values of non-ionic liquid surfactants Tween and Span.

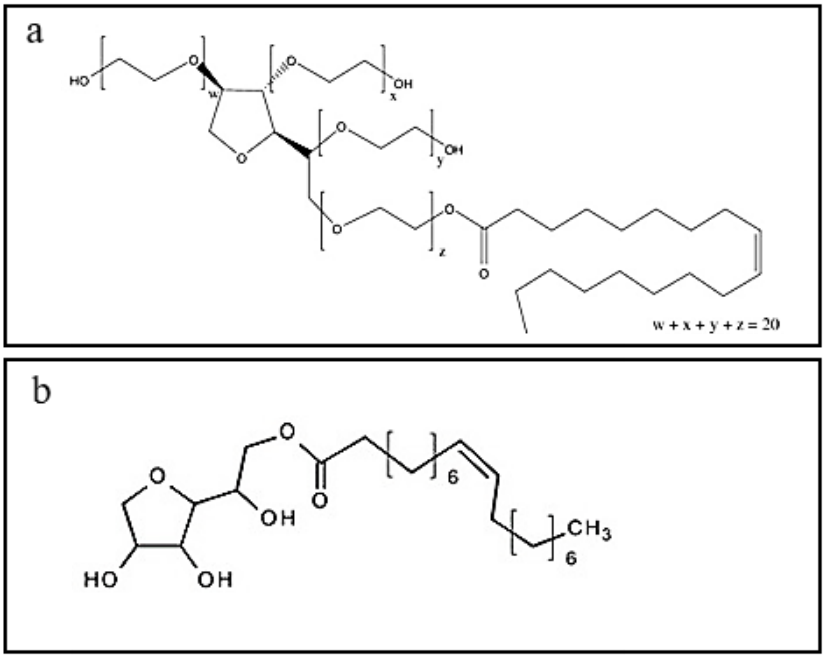

Figure 62. Chemical structures of Tween (a) and Span (b) non-ionic liquid surfactants.

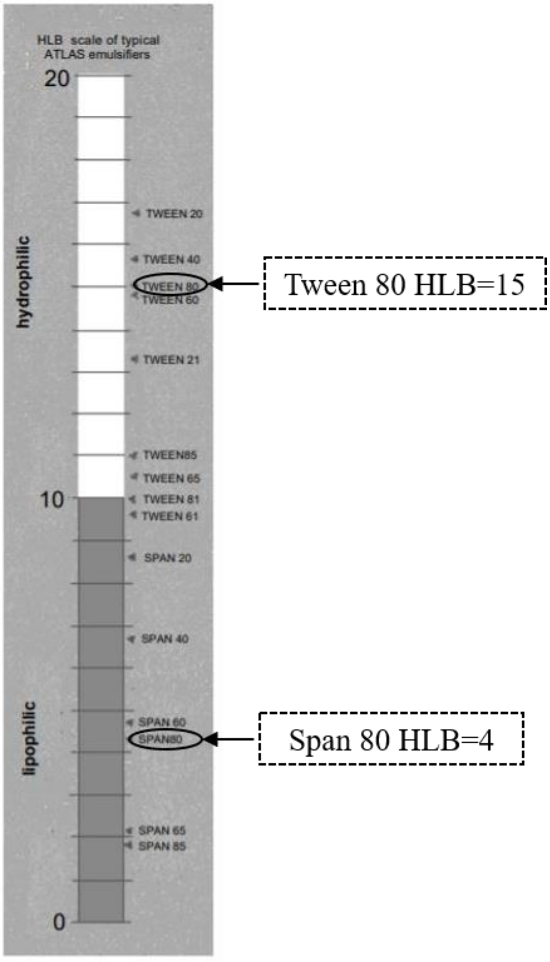

Figure 63. HLB scale of typical non-ionic surfactants with a defined lipophilic-hydrophilic character. Modified from [198]

It is also possible, to obtain a specific HLB index, by combining two or more emulsifiers. In this thesis, Tween 80 and Span 80, whose chemical structure are

reported in Figure 62 were mixed at different weight ratios. The resulting mixture is characterized by a specific hydrophile–lipophile index (HLB) having Tween 80 and Span 80 hydrophilic and hydrophobic character, respectively. When two or more emulsifiers are blended, the resulting HLB of the mixture is calculated using the mixing rule [198]. In fact, knowing that HLB = 15 for Tween 80 (highest hydrophilicity) and HLB = 4 for Span 80 (highest lipophilicity), it is possible to calculate the HLB index for each composition of the two emulsifiers with the following Equation:

Equation 38. $$\%(\boldsymbol{A}) = \frac{\boldsymbol{X - HLB_B}}{\boldsymbol{HLB_A - HLB_B}} * \mathbf{100} \quad \textbf{and} \quad \%(\boldsymbol{B}) = \mathbf{100} - \%\,(\boldsymbol{A})$$

where %(A) and %(B) are the percentage of emulsifier A and B, respectively, to achieve a defined HLB number represented by X value.

Furthermore, a further solid non-ionic surfactant, named Synperonic PE/F 87 (Syn) (Figure 64) is possible to use. The Synperonic PE series are groups of non-ionic, tri-block copolymer surfactants composed of polyethylene oxide and polypropylene oxide (PEO/PPO). The products in this range differ only in their molecular weight, hydrophobic/hydrophilic character and their physical state i.e. solid or liquid. This substance/mixture contains no components considered to be either persistent, bioaccumulative and toxic (PBT), or very persistent and very bioaccumulative (vPvB) at levels of 0.1% or higher.

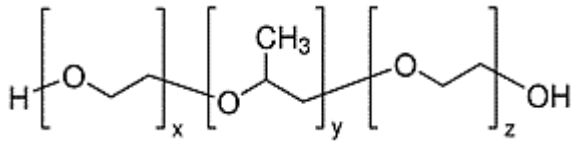

Figure 64. Chemical structure of Synperonic PE/F 87, Syn.

In this work, different mixtures of Tween 80 and Span were used to compatibilize PLA-based blends. For each case, the value of HLB index was selected in order to match the polarity of the resulting polymer blends.

Firstly, PLA/LDPE blend was studied as a model system; in fact, since PLA and LDPE present polar and apolar characteristics, respectively, the introduction of emulsifier mixtures having different HLB allowed gaining fundamental insights into the provided mechanism of compatibilization. Subsequently, the effectiveness of the proposed strategy was evaluated for fully bio-based PLA/PHB blends.

In addition, in PLA/PHB blends the compatibilization system based on solid non-ionic surfactants Synperonic was used.

5.3 Preparation of the blends

PLA and PHB pellets were first dried overnight at 70 °C in a vacuum oven. PLA-based blends were prepared using a DSM Explore twin screw mini-extruder with protective Nitrogen atmosphere; details about the used device are reported in the Appendix A.2. The extrusion processing condition for PLA/LDPE and PLA/PHB blends are summarized in Table 4.

Table 4. Processing conditions of PLA/LDPE and PLA/PHB blends.

	T [°C]	Screw speed [rpm]	Processing time [min]
PLA/LDPE	190	70	2
PLA/PHB	180	100	3

PLA/LDPE model blends

Non-compatibilized PLA/LDPE blends at different weight ratios were prepared. Obtained blends were designed as PLA/LDPE X/Y, where X and Y indicate PLA and LDPE content (wt%), respectively; blends with composition 10/90, 30/70, 50/50, 70/30 and 90/10 were prepared. The two surfactants were first manually mixed and then dissolved in about 5 ml acetone, to be added easily in the mini extruder chamber. The weight ratios of non-ionic surfactants with a specific hydrophilic-lipophilic content calculated by Equation 38 are reported in Table 5 and the resulting mixture was added in the blend at 1 wt%.

Table 5. HLB and composition of the used surfactant mixtures.

HLB	Tween 80 (wt%)	Span 80 (wt%)
12	72	28
10	54	46
9	44	56

PLA/PHB blends

PLA/PHB blends with a weight content of 70 wt% of PLA and 30 wt% of PHB were compatibilized using mixtures of Tween 80 and Span 80 with an HLB index of 12 varying the mixture additive content in a range from 0.1 to 5 wt%. Furthermore, the solid surfactant Syn was introduced in the blend with the same weight content range (from 0.1 to 5 wt%) in order to compare both compatibilization systems. The formulations of studied blends are reported in Table 6.

Table 6. Composition and code of the studied blends (all percentages are referred to as wt%).

Composition	Code
PLA: 70% and PHB: 30%	PLA/PHB
PLA: 70% and PHB: 30% and HLB12: 0.1%	PLA/PHB/0.1HLB12
PLA: 70% and PHB: 30% and HLB12: 0.5%	PLA/PHB/0.5HLB12
PLA: 70% and PHB: 30% and HLB12: 1%	PLA/PHB/1HLB12
PLA: 70% and PHB: 30% and HLB12: 2%	PLA/PHB/2HLB12
PLA: 70% and PHB: 30% and HLB12: 5%	PLA/PHB/5HLB12
PLA: 70% and PHB: 30% and Syn: 0.1%	PLA/PHB/0.1Syn
PLA: 70% and PHB: 30% and Syn: 0.5%	PLA/PHB/0.5Syn
PLA: 70% and PHB: 30% and Syn: 1%	PLA/PHB/1Syn
PLA: 70% and PHB: 30% and Syn: 2%	PLA/PHB/2Syn
PLA: 70% and PHB: 30% and Syn: 5%	PLA/PHB/5Syn

Thermal stability of non-ionic surfactants

TGA analyses were performed on Tween80 and Span80 liquid surfactants, the mixture with HLB index equal to 12 and the solid surfactant Synperonic. As shown in Figure 65, the compatibilizers are thermally stable at the processing temperature selected for the preparation of the blends (180°C and 190°C). The results of the weight loss at 190°C of non-ionic surfactants recorded during TGA analyses are reported in Table 7.

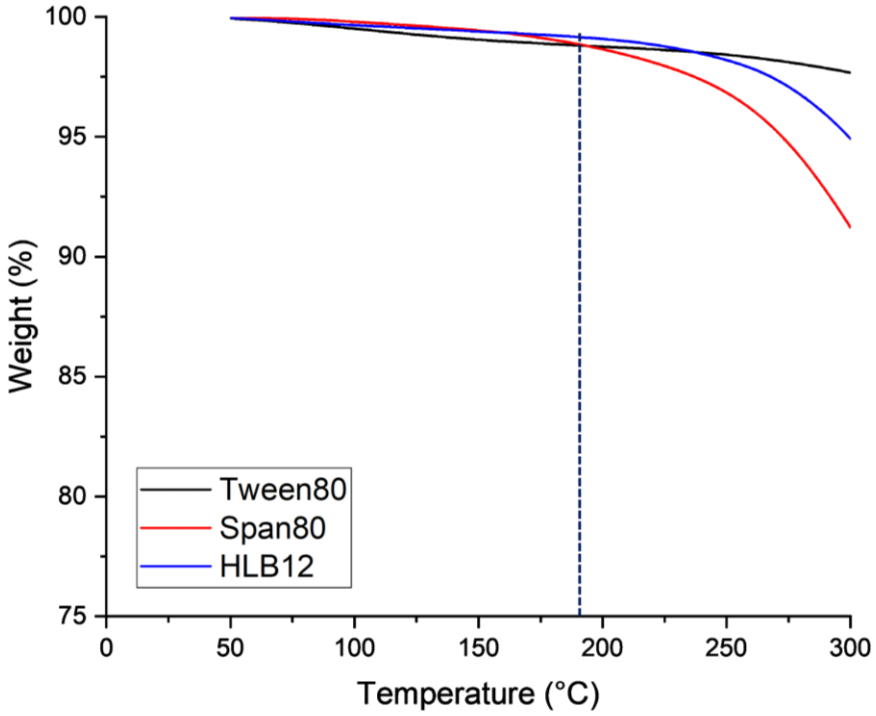

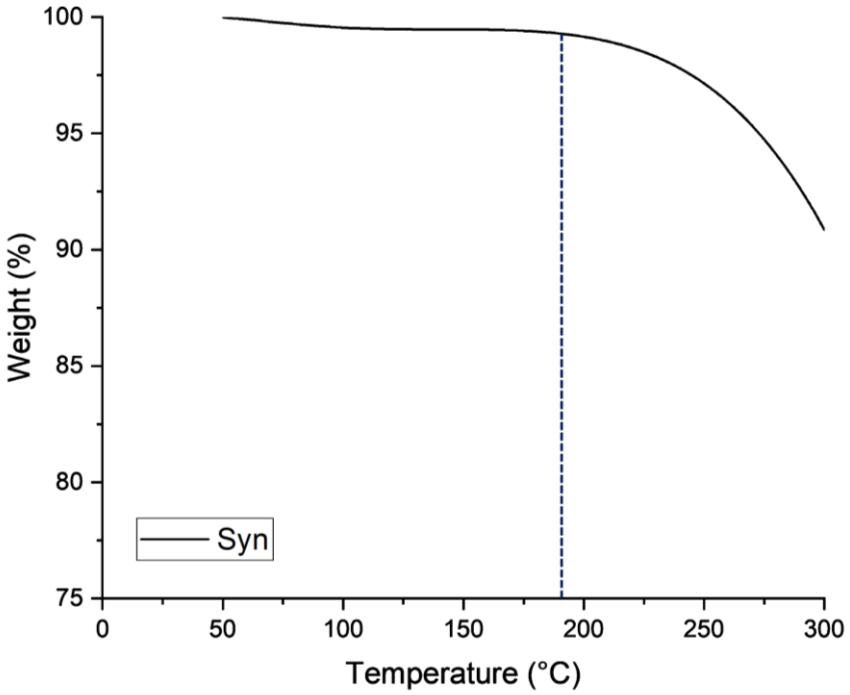

Figure 65. TGA curves of Tween80, Span80, mixture of liquid surfactants with HLB12 and solid surfactant Syn.

Table 7. Weight loss at 190°C of non-ionic surfactants from TGA analyses.

Sample	Weight loss @ 190 °C [%]
Tween80	1.19
Span80	1.13
Mixture having HLB=12	0.84
Syn	0.71

The characterizations of all tested PLA-based blends involved thermal and thermomechanical and rheological analyses, and morphological observations. Details about the performed characterizations are provided in Appendix A.3.

5.4 PLA/LDPE blends

5.4.1 Non-compatibilized PLA/LDPE blends

The study on non-compatibilized blends is performed on formulations with different weight ratios of PLA and LDPE. The analysis of the thermal behaviour of the formulated blends is carried out to assess the thermal characteristics of the blend, which may be relevant for obtaining indirect information regarding miscibility between PLA and LDPE phases.

Figure 66 reports the thermograms of all developed blends, including those of the two neat polymers, recorded during the second heating scan. PLA shows the glass transition temperature (T_g) at 61 °C, while the observed exothermic peak at about 100°C and the endothermic peak at about 170°C can be related to the cold crystallization and melting, respectively [199]. On the other hand, the thermogram of LDPE shows an endothermic peak at 105°C, related to the melting of the polymer [200].

In the blends the glass transition (T_g) and cold crystallization (T_{cc}) temperatures of PLA, and the melting temperature (T_m) for both PLA and LDPE are almost unchanged with respect to those of the neat polymers. Interestingly, the cold crystallisation of PLA is not visible in the mixture with 10 wt% PLA. This result can probably be attributed to the overlapping of T_{cc} of PLA and T_m of LDPE. In contrast, in the formulation with the opposite weight content, i.e. PLA/LDPE 90/10 the melting of LPDE is not visible in the thermogram.

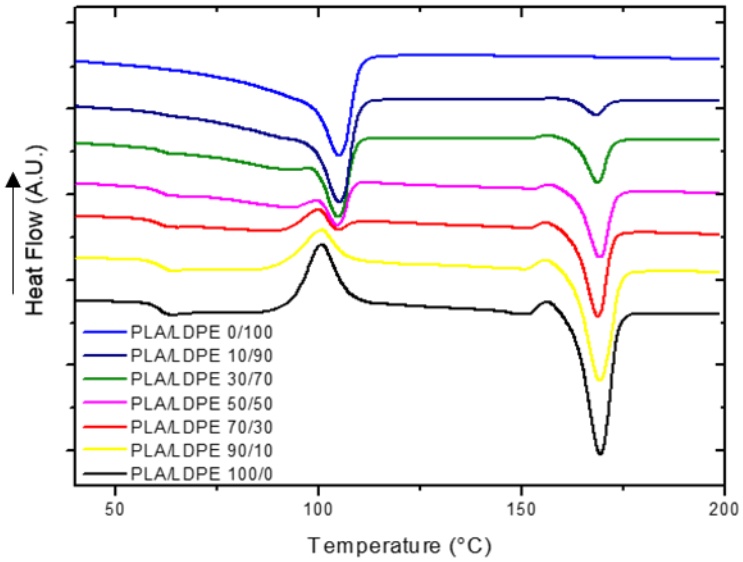

Figure 66. DSC thermograms of non-compatibilized PLA/LDPE blends, recorded during the second heating scan. Reprinted with the permission from [189].

As widely reported in the literature, the invariance of the glass transition temperature is a proof of the immiscibility between two polymers [19]; therefore, DSC results confirm the immiscibility between PLA and LDPE for each selected composition.

As none of the studied compositions show significant variations of characteristic temperatures compared to the pure polymers, the system PLA/LDPE 70/30 was selected for further investigations, in order to focus the attention of the study on a system having PLA as the primary phase. Figure 67 and Figure 68 show the variation of the complex viscosity and storage modulus G', respectively, as a function of the frequency for the blend and the neat polymers.

PLA shows a well-pronounced Newtonian behaviour with an extended plateau at low-intermediate frequency values. On the contrary, the rheological behaviour of

LDPE is remarkably non-Newtonian; in fact, the shear-thinning region extends over all the investigated frequency range. The curve of blend is intermediate between those of neat polymers at high frequencies, but higher values of complex viscosity are recorded in the low frequency region.

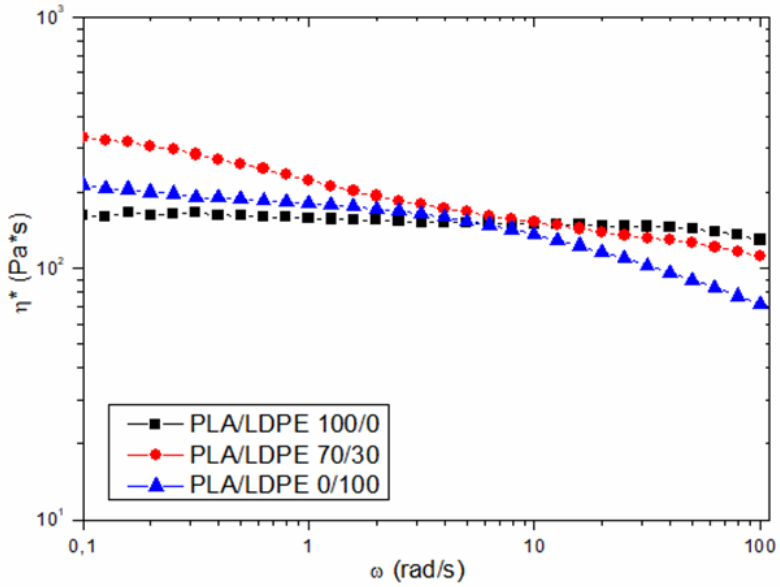

Figure 67. Complex viscosity η* as a function of the frequency for PLA/LDPE 70/30 blend and neat polymers. Reprinted with the permission from [189].

A similar trend is observed for the storage modulus; in fact, as observable in Figure 68; the G' values of the blend are intermediate between those of the polymers at high frequencies and higher at low and intermediate frequencies. The rheological response of the blend is attributable to a separate phase droplet-like morphology. In particular, the creation of interfaces between the two polymers and the occurrence of phenomena of shape relaxation of the dispersed particles of LDPE during oscillatory shear flow, result in an excess elasticity, which induces the increase of both viscosity and storage modulus as compared to the neat polymers. This feature is more pronounced in the low frequency region, where the response of large portions of macromolecules is recorded; conversely, at higher frequencies the effect is less remarkable, since the curves reflect the response of small fraction of polymer chains, associated with a dynamic population that relax faster; as a result, the rheological response of the blend is governed by that of the single polymers [201].

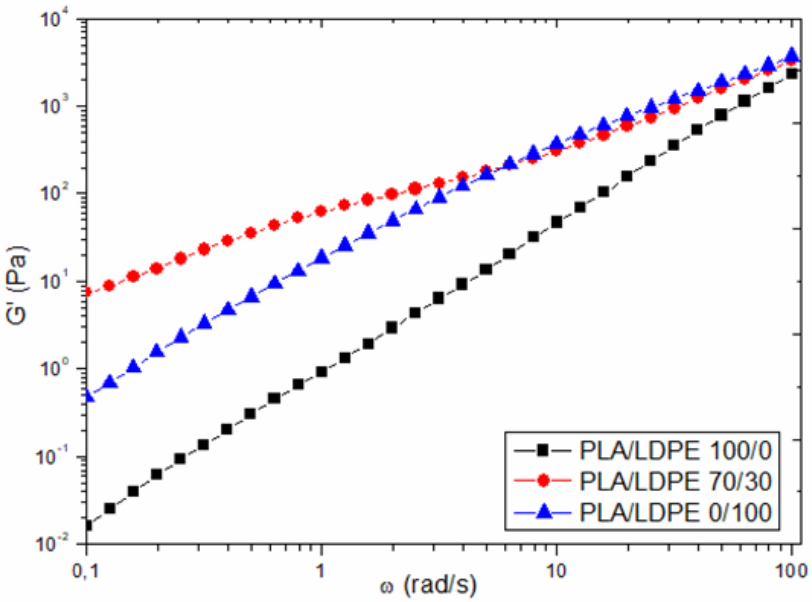

Figure 68. Storage modulus G' as a function of the frequency for PLA/LDPE 70/30 blend and neat polymers. Reprinted with the permission from [189].

The morphology of the formulated blend was evaluated through SEM observations. In Figure 69(a-b), the SEM micrographs of the fracture surface of the blend at two different magnifications are reported.

The blend shows a droplet-like morphology, typical of an immiscible blend, with the spherical LDPE domains dispersed in the PLA matrix [202]. In addition, empty cavities on the surface are present, indicating a weak interfacial adhesion between the polymers.

To gain further insights into the blend morphology, an evaluation of the size of the dispersed LDPE domains was performed through the image processing software ImageJ (Figure 69(c)). The average dimensions of the droplets of the minor phase were fitted with a Gauss-like distribution curve. The appearance of three main peaks, centred at about 45, 65 and 85 μm is noticeable, highlighting the achievement of a heterogeneous morphology; the main size of the droplets was 88.14 μm.

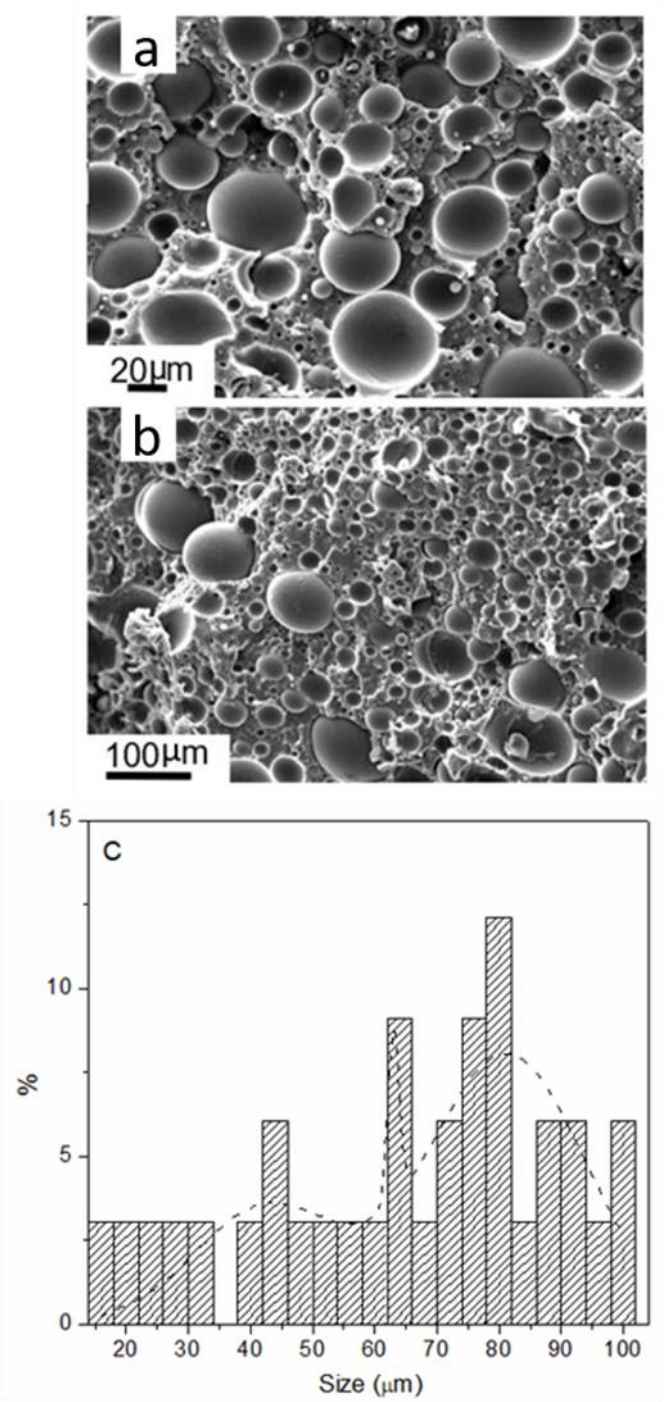

Figure 69. SEM micrographs of PLA/LDPE 70/30 blend at different magnifications (a-b); size distribution of dispersed LDPE particles (c). Reprinted with the permission from [189].

5.4.2 Compatibilized PLA/LDPE blends

Figure 70 shows the results of the thermal analysis recorded during the second heating scan and performed on PLA/LDPE 70/30 compatibilized blends.

The addition of Tween80 and Span80 mixtures causes a reduction of about 2°C of the glass transition temperature (T_g) which passes from 61°C in non-compatibilized blend to 59°C in compatibilized PLA/LDPE 70/30 systems (see the values reported in Table 8). The observed reduction in the glass transition temperature indicates an improvement of the compatibility between the two polymers [203].

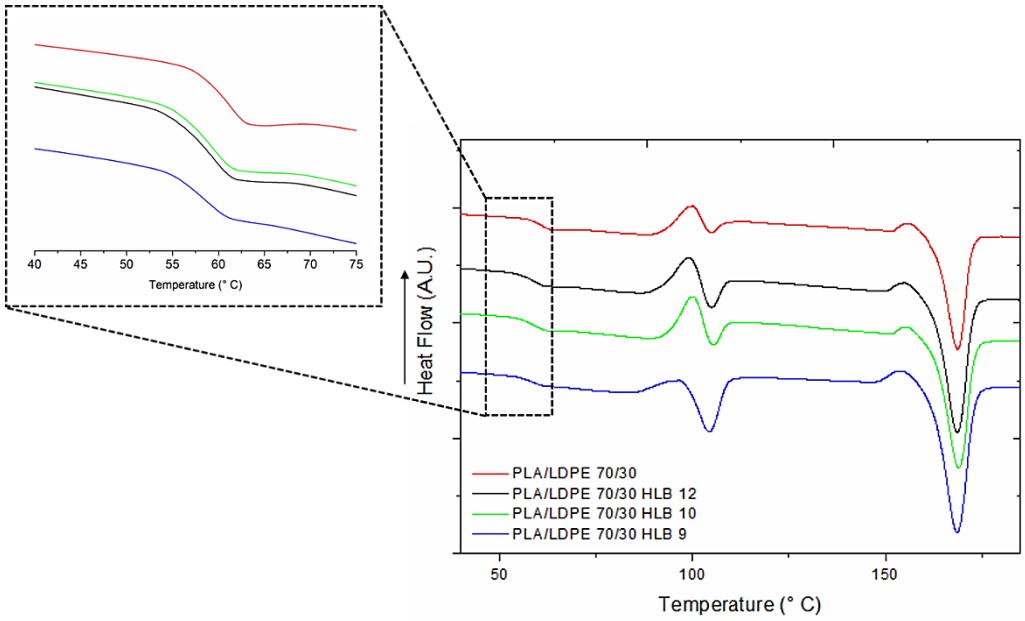

Figure 70. DSC thermograms of non-compatibilized and compatibilized PLA/LDPE 70/30 blends with different HLB index recorded during second heating scan. Modified from [189].

Table 8. Glass transition temperatures of non-compatibilized and compatibilized PLA/LDPE 70/30 blends.

Material	T_g (°C)
PLA/LDPE 70/30	61.1
PLA/LDPE 70/30 HLB 12	59.6
PLA/LDPE 70/30 HLB 10	59.4
PLA/LDPE 70/30 HLB 9	58.3

Nevertheless, the decrease of 2°C of glass transitions temperature cannot be considered as unique demonstration of the increased compatibility between the two polymers. In fact, rheological, thermo-mechanical and morphological analyses are performed to confirm the beneficial effect of the exploited compatibilizer systems on the compatibility between PLA and LDPE phases. Figure 71 and Figure 72

report the variation of the complex viscosity and G' as a function of the frequency, respectively, for all studied systems. Both non-compatibilized and compatibilized blends show a similar rheological response and, thus, the presence of the compatibilizers with different HLB indices has no significant effects on the rheological response of the blends.

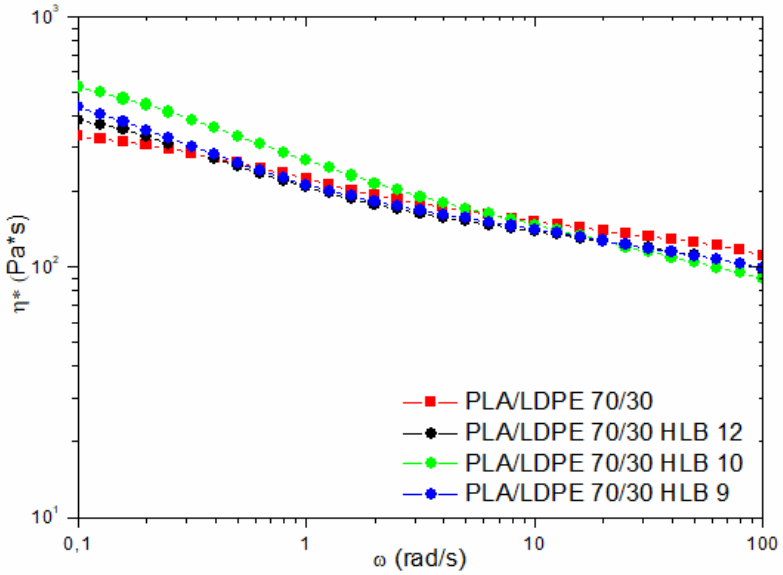

Figure 71. Complex viscosity η* as a function of the frequency for PLA/LDPE 70/30 blend and compatibilized PLA/LDPE 70/30 with different HLB indices. Reprinted with the permission from [189].

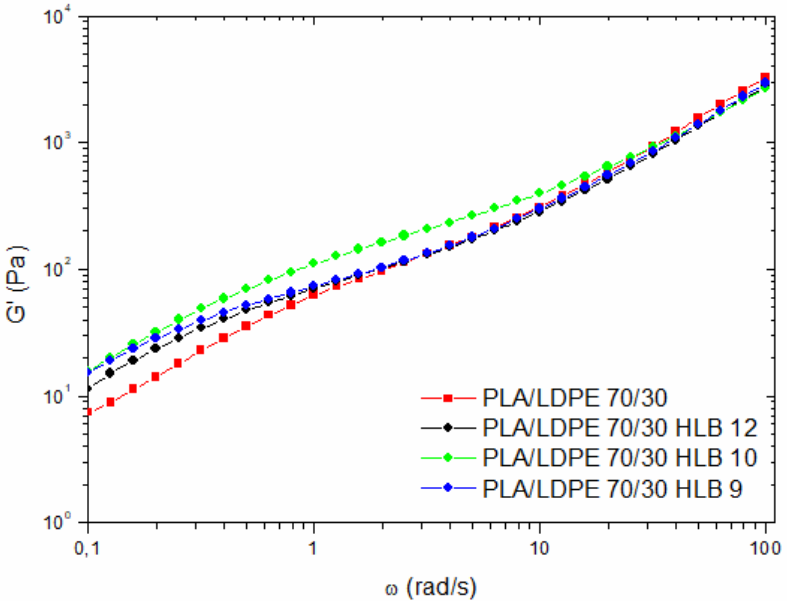

Figure 72. Storage modulus G' as a function of the frequency for PLA/LDPE 70/30 blend and compatibilized PLA/LDPE 70/30 with different HLB indices. Reprinted with the permission from [189].

Figure 73 shows the results of the thermo-mechanical analyses of all evaluated blends; in particular, the dynamic storage modulus E' and the trend of tanδ as a function of the temperature are reported.

The presence of compatibilizers causes an increase of the E' value at 35°C: particularly, E' value in the blend with HLB 12 results 19% higher than the non-compatibilized blend, while the compatibilized blends with a mixture of surfactants corresponding to an index HLB 9 and 10 present an increase of dynamic storage modulus of 5% with respect to that of the PLA/LDPE blend (Figure 73 (a)).

The variation of tanδ (i.e. the ratio between the dynamic loss modulus, E", and E') as a function of the temperature is reported in Figure 73(b). The peak of the damping curves occurs for the compatibilized blends at slightly lower temperatures, 84°C, as compared to non-compatibilized material (85°C). In addition, broader peaks are obtained for compatibilized systems, indicating the achievement of a partial miscibility between the polymeric components and an improved dispersion on LDPE phase [204] [106].

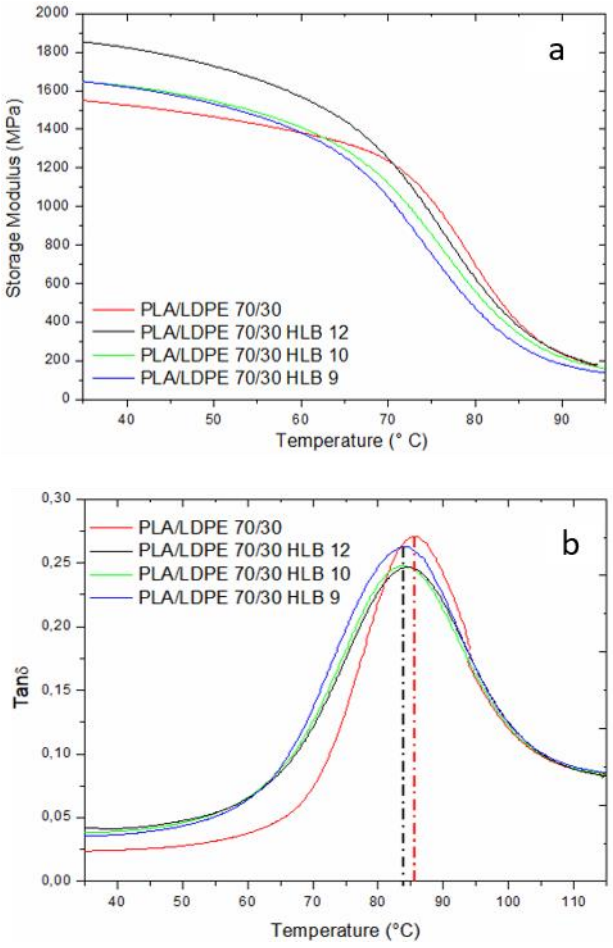

Figure 73. DMA traces: dynamic storage modulus E' (a) and tanδ (b) for PLA/LDPE 70/30 blend and compatibilized PLA/LDPE 70/30 with different HLB indices. Modified from [189].

Since the improved properties were exhibited by the compatibilizer system with HLB12, we decided to evaluate its morphology through SEM analysis and the resulting micrograph is reported in Figure 74(a). A significant reduction in the average particles size of the dispersed phase was observed compared to non-compatibilized blend, previously reported in Figure 69 (a). In fact, the measured mean size of the dispersed particles is 40.19 μm, meaning a reduction of 54%.

In Figure 74(b), the size distribution of the droplets constituting the LDPE dispersed phase for the PLA/LDPE 70/30 HLB 12 system is reported (red curve), along with the distribution curve of the non-compatibilized blend (dashed line). A significant beneficial effect of the HLB 12 presence on the morphology homogeneity can be clearly observed since, in the case of compatibilized system, the distribution curve exhibits two sharp peaks centred at about 12 and 38 μm, with a remarkable decrease of the maximum droplet size as compared to the non-compatibilized blend.

Figure 74(c) shows the supposed mechanism of compatibilization, involving the preferential localization of the surfactant molecules in the interfacial region between the two polymeric phases. More specifically, the hydrophilic group of the surfactant mixture, interacting with the polar PLA matrix, and the lipophilic parts, directed towards the non-polar dispersed droplets of LDPE, are able to induce a refinement of the blend morphology. Nevertheless, the presence of many holes in the surface of fracture, as well as the pronounced interfaces between continuous and dispersed phases, indicating that the adhesion between the two phases remained rather weak.

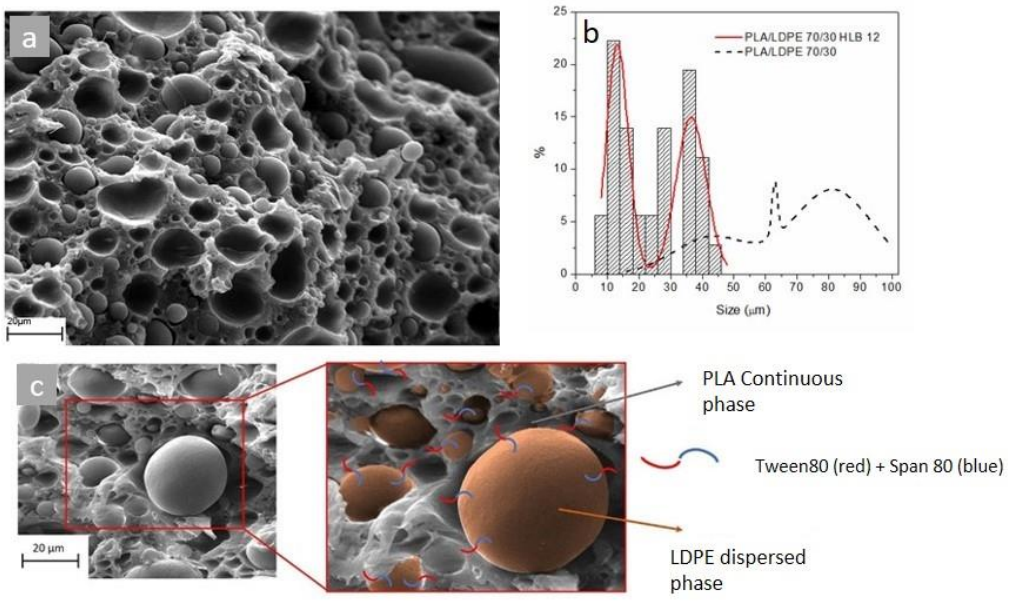

Figure 74. SEM micrograph (a) and size distribution of the dispersed particles (b) for the blends PLA/LDPE 70/30 HLB 12 and schematism of the compatibilization mechanism (c). Modified from [189].

5.4.3 PLA/LDPE 70/30 blends based on re-processed polymers

The blends PLA/LDPE 70/30, both non-compatibilized and compatibilized with the mixture having HLB 12, were also prepared using re-processed polymers, i.e. PLA and LDPE underwent two extrusion cycles.

The aim was to evaluate the influence of the proposed strategy of compatibilization on blend of the same composition but consisting of re-processed polymers. Particularly, the compatibilized mixture exploited in this second part of the study was the one having HLB 12 since this combination of Span 80 and Tween 80 content brought to the higher improvements over the non-compatibilized blend based on virgin polymers.

These blends made of re-processed polymers are:

- Blend r-PLA/r-LDPE 70/30: polymers were first extruded alone and finally blended together in a second extrusion.
- Blend r-PLA/r-LDPE 70/30 HLB 12: polymers were first extruded alone and then mixed together with the addition of the compatibilizer at 1 wt% in the second extrusion.

Figure 75 shows the DSC thermograms of non-compatibilized and compatibilized r-PLA/r-LDPE 70/30 blends and the values of T_g of the materials are reported in Table 9. Similarly to what observed for virgin polymers-based blends, the introduction of the compatibilizer mixture causes the decrease of the value of the glass transition temperature.

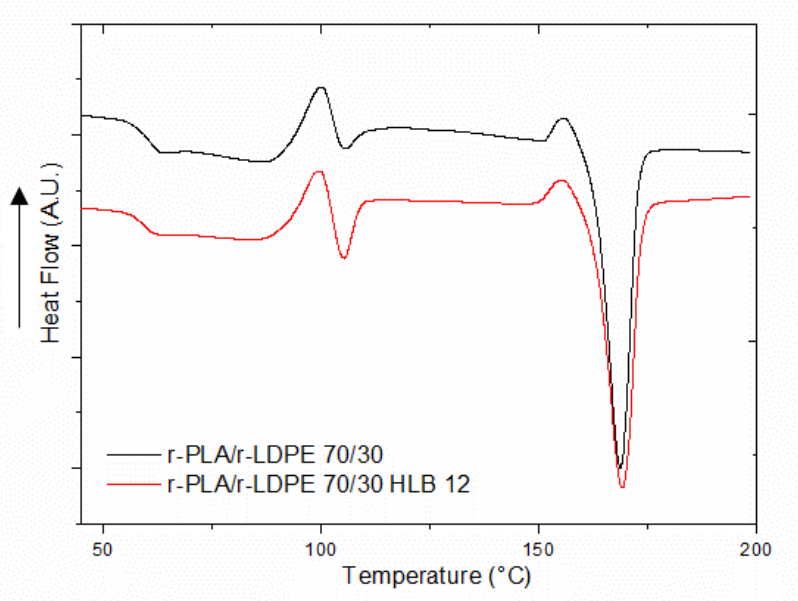

Figure 75. DSC thermograms of non-compatibilized and compatibilized r-PLA/r-LDPE 70/30 blends; recorded during second heating ramp. Reprinted with the permission from [189].

Table 9. Glass transition temperature of re-processed PLA/LDPE 70/30 blends.

Material	T_g (°C)
r-PLA/r-LDPE 70/30	61.1
r-PLA/r-LDPE 70/30 HLB 12	59.7

Nevertheless, thermal characterization of the blend with re-processed polymers is not enough to predict the change in the microstructure of the systems.

Figure 76 reports the trend of the dynamic storage modulus E' as a function of temperature for re-processed polymers-based blends, along with the curve of non-compatibilized PLA/LDPE 70/30 system. The non-compatibilized blend obtained through re-processed polymers presents higher values of E' as compared to the blend based on virgin polymers; in particular r-PLA/r-LDPE 70/30 reaches the value of E' of 1690 MPa, evaluated at 35°C, with respect to the PLA/LDPE 70/30 blend based on virgin polymers which exhibits a modulus of 1570 MPa.

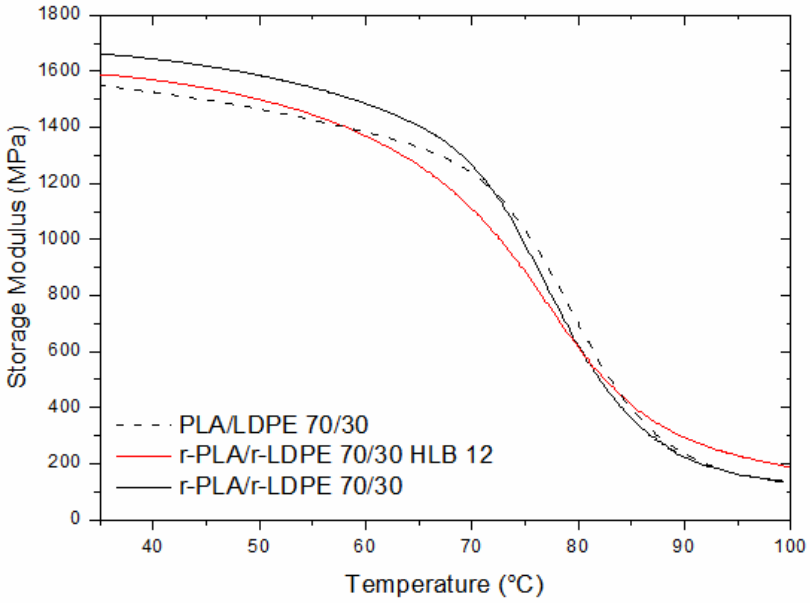

Figure 76. Dynamic storage modulus E' as a function of temperature both for PLA/LDPE 70/30 blend and re-processed polymers-based blend, compatibilized and non-compatibilized. Reprinted with the permission from [189].

This finding can be related to the improved compatibility between the polymers, whose molecular weights (M_W) could have been decreased due to the reprocessing [205]. As reported in literature, the decrease of M_W can generate a reduction of the interfacial tension between the phases of an immiscible polymer blend [206]. This prediction can be confirmed through the results of the rheological characterization. In fact, as observable in Figure 77, re-processed polymers-based blends, both compatibilized and non-compatibilized, show lower values of viscosity as compared to the blends based on virgin polymers, indicating that the re-processing caused a decrease of polymer molecular weight. Furthermore, it is evident that the non-compatibilized r-PLA/r-LDPE 70/30 exhibits a well-pronounced Newtonian behaviour compared to the virgin polymers-based blends,

while the trend of the compatibilized blend based on re-processed polymers is very similar to that of PLA/LDPE 70/30 HLB 12.

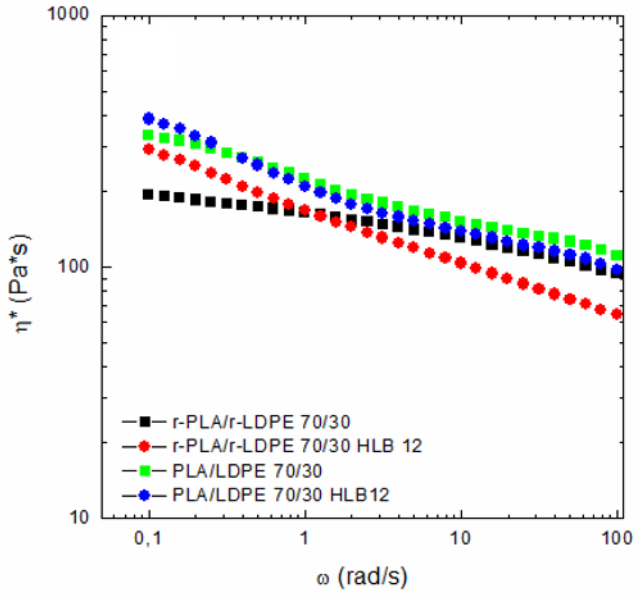

Figure 77. Complex viscosity η* as a function of the frequency of compatibilized and non-compatibilized blends based on virgin and re-processed PLA and LDPE polymers.

The differences between the viscoelastic behaviour of the two materials based on re-processed polymers is more evident looking at the curves of G', reported in Figure 78(a). It is evident that the compatibilized r-PLA/r-LDPE 70/30 HLB 12 blend shows the typical trend of an immiscible blend, already observed for blends based on virgin polymers. In particular, the curve of G' presents a shoulder at low and intermediate frequencies, associable with the relaxation phenomena of dispersed particles of a characteristic droplet structure. Differently, for the blend r-PLA/r-LDPE 70/30 the shoulder in the storage modulus trend is not present, and a significant decrease of the slope of G' in the low frequency region can be observed. As widely documented in literature, this finding can be explained considering the existence of complex morphologies showing slow relaxation dynamics [207]. To further investigate this finding, the value of the G' slope (α (ω)) was calculated, following the Equation 39 and the results are reported in Figure 78(b).

Equation 39. $$\alpha\,(\omega) = \frac{d \log G'}{d \log \omega}$$

r-PLA/r-LDPE 70/30 HLB 12 blend shows a progressive decrease of the G' slope as a function of the frequency, reflecting the relaxation of a single dynamic population, associable to the droplets constituting the dispersed phase. Conversely, the curve of the non-compatibilized blend remains almost constant over the frequency range, indicating the relaxation of r-LDPE particles of different shapes and dimensions that, relaxing continuously over a long-time interval, generate a continuous spectrum of relaxation times.

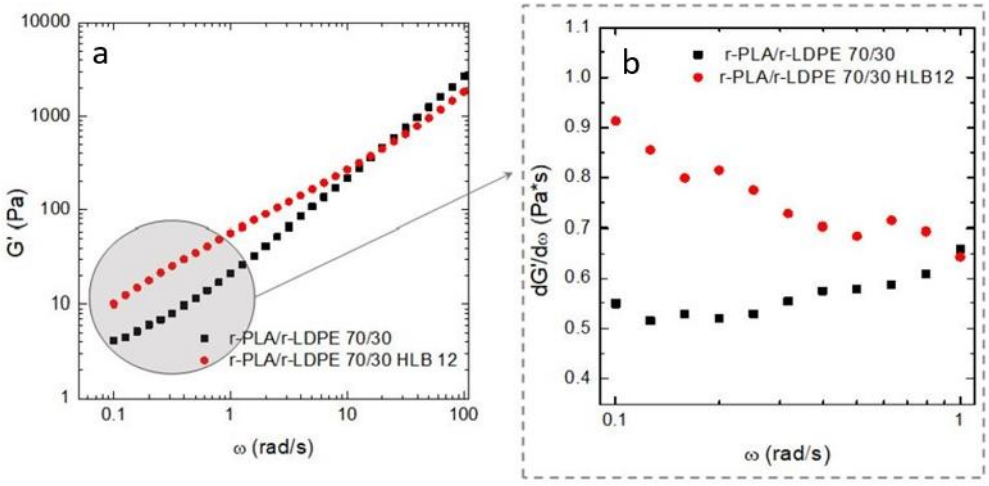

Figure 78. Storage modulus G' (a) and dG'/dω curves (b) as a function of frequency for re-processed polymers-based blends.

To complete the study of these materials, the morphology of the re-processed polymers-based blends was investigated through SEM analysis and representative micrographs are reported in Figure 79(a) and Figure 79(b). Both the non-compatibilized and compatibilized r-PLA/r-LDPE 70/30 blends showed a biphasic morphology but the fracture surface did not exhibit a large number of holes, suggesting higher interfacial adhesion as compared to the blends obtained with virgin polymers; this is consistent with the hypothesis of a decrease of molecular weight, which would bring to a reduction of interfacial tension between the two phases [206].

The addition of the compatibilizer causes the formation of many small particles, showing lower size compared to the non-compatibilized blend, notwithstanding the presence of coarse-elongated particles of much higher size. The morphological observations suggest that the compatibilization effectively induces the reduction of the dimension of the dispersed particles, similarly to the compatibilized blend obtained from virgin polymers, but this morphological refinement is not uniform in the material and the dispersed phase is present in different shape and size.

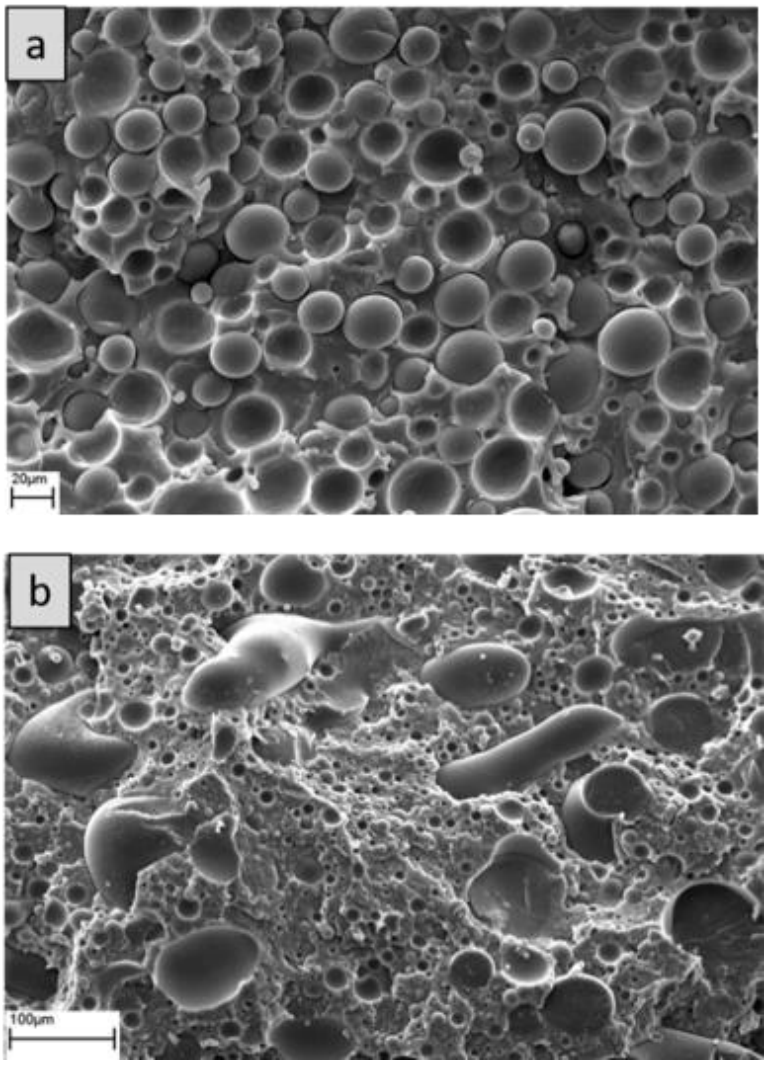

Figure 79. SEM micrographs for non-compatibilized (a) and compatibilized (b) r-PLA/r-LDPE 70/30 blends. Reprinted with the permission from [189].

A more detailed analysis of the microstructure of materials can be obtained from the analysis of the weighted relaxation spectra. The weighted relaxation spectrum ($\lambda H(\lambda)$), showed in Figure 80(a) and Figure 80(b), can be calculated with data coming from small amplitude oscillatory shear measurements, using the method proposed by Honerkamp and Weese [47].

Generally, for a polymer blend, peaks appearing at short relaxation times were attributed to the relaxation processes of the blend constituents, while on the right side of the spectrum, signals observed at longer times are related with the relaxation of the blend interface [208].

As observable in the spectra reported in Figure 80 (a), PLA/LDPE blend exhibit three different peaks: the first one related to the relaxation of blend components, the second one attributable to the shape-relaxation of the LDPE dispersed droplets, and a peak not completely formed at longer times, associable with the presence of a population of droplets having larger size, which were not able to fully relax in the tested time interval. In the compatibilized blend, the presence of HLB 12 caused the disappearance of the peak at long relaxation times, indicating a beneficial effect

of the compatibilizer on the obtainment of a droplet morphology characterized by small sizes of LDPE phase which is also present with elongated shapes of different sizes.

The spectra reported in Figure 80(b) depict a different scenario for r-PLA and r-LDPE based blends. More specifically, in the non-compatibilized r-PLA/r-LDPE system the intensity of the peak related to the blend constituent is remarkably reduced as compared to the PLA/LDPE blend, indicating a viscous dominant behaviour involving faster relaxation modes of the polymer chains [209]. Besides, the tail appearing at longer relaxation times can be attributed to the relaxation of the droplets constituting the dispersed phase, characterized by a continuous distribution of shapes and interface curvatures [210]. Conversely, the relaxation behaviour of the r-PLA/r-LDPE HLB 12 blend involves the appearance of a broad peak at long relaxation times, associable with the presence of the elongated structures observed through SEM observations, resulting from some coarsening phenomenon, which are not able to fully relax in the investigated time interval.

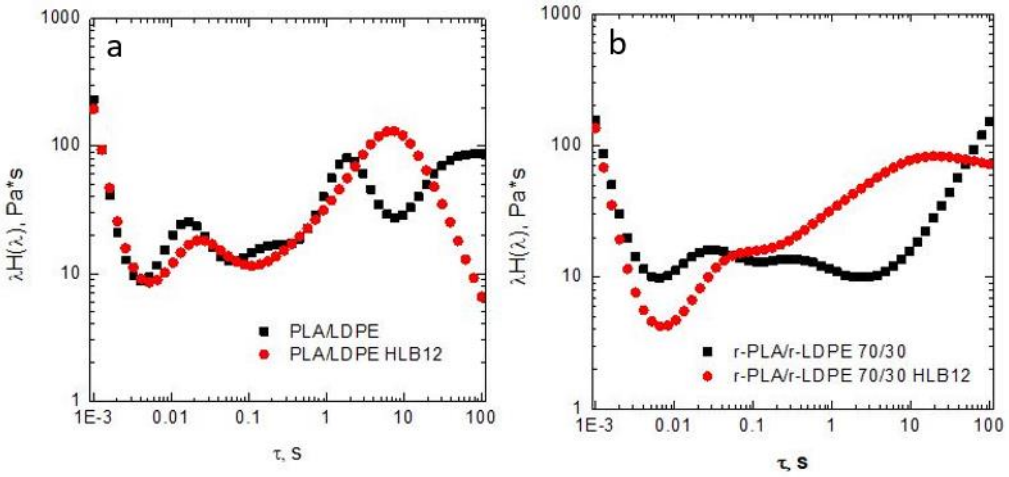

Figure 80. Weighted relaxation spectra for blends based on virgin (a) and re-processed polymers (b). Reprinted with the permission from [189].

5.5 PLA/PHB blends

In this section the results obtained from the characterization of PLA/PHB (70 wt% of PLA and 30 wt% of PHB) blends compatibilized with the two different systems based on non-ionic surfactants will be discussed. In particular, two different systems were used: a liquid mixture of Span 80 and Tween 80 with an HLB index equal 12, selected since it was the most suitable mixture for the model system PLA/LDPE and a solid compatibilizer in form of flakes (Synperonic).

5.5.1 Differential scanning calorimetry analyses

The thermograms of neat polymers are reported in Figure 81; the thermal characteristics of PLA phase are already shown in the previously paragraph 5.4.1. Conversely, as to concern the PHB polymer, in Figure 81 (b) it is possible to notice the presence of glass transition at -3 °C [211], a cold crystallization peak at 53°C and two melting peaks at 108°C and 132°C [212]. According with the literature, the observed double melting peak can be associated with the melting of "as-formed" and the re-crystallized PHB component [213] or with the formation of two different types of lamellae in the PHB phase [214].

Figure 82 reports the thermograms of neat blend and HLB12-containing systems, with weight contents ranging from 0.1 to 5%. The non-compatibilized PLA/PHB blend shows two different T_g values: the first one at -3°C and the second one at 58°C, associable with the glass transition of PHB and PLA polymers, respectively, according to the thermograms of the neat polymers reported in Figure 81. Additionally, an exothermic peak at 110°C and an endothermic peak at 168°C can be observed; it is known from literature [215] that these peaks can be associated with the cold crystallization and the melting of the PLA polymer, respectively. It is worth noting that the PHB present in the blend does not crystalize under the selected process conditions and this thermal treatment.

In compatibilized PLA/PHB blend the presence of HLB12 causes a decrease of the cold crystallization temperature at 100°C compared to the neat blend but, at the same time, it does not modify the T_g values.

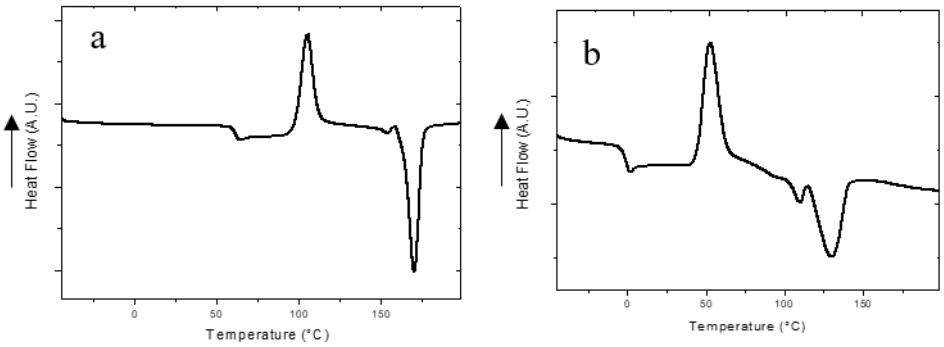

Figure 81. DSC thermograms recorded during second heating scan for neat polymers PLA (a) and PHB (b). Reprinted under CC BY 4.0 license from [190].

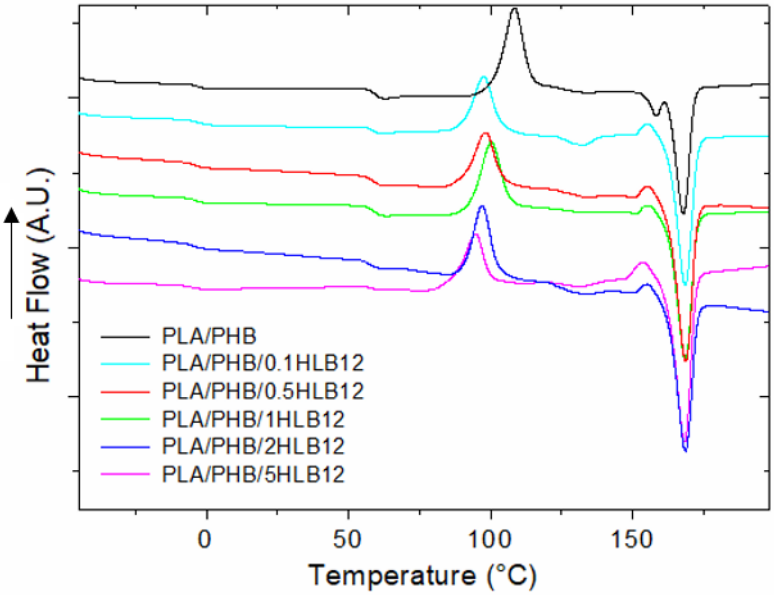

Figure 82. DSC thermograms for non-compatibilized blend and HLB12-containing systems (second heating scan). Reprinted under CC BY 4.0 license from [190].

Table 10 collects the values of ΔH_m, ΔH_{cc}, and crystallinity degree of these formulations. Interestingly, the presence of the HLB12 leads to a remarkable increase of the blend crystallinity degree.

Table 10. Thermal properties of non-compatibilized blend and HLB12-containing systems.

	PLA/PHB	0.1HLB12	0.5HLB12	1HLB12	2HLB12	5HLB12
ΔHm [J/g]	28	48	48	46	50	56
ΔHcc [J/g]	31	23	22	28	25	19
X_c [%]	11	27	29	19	27	40

Figure 83 reports the results of the thermal characterization for the samples containing different amounts of surfactant Syn. Similarly to what already observed for the HLB12-containing blends, the T_g values are not affected by the presence of

Syn, whereas the T_{cc} of compatibilized samples is about 10 °C lower than that of the neat blend. Interestingly, in the Syn-containing system with 5 wt% of compatibilizer, the peak of cold crystallization is not present in the thermogram recorded during the second heating ramp but, the crystallization peak is registered at 93°C [216] during cooling scan as it is possible to see in Figure 83(b).

Table 11 shows the main thermal properties measured during the second heating ramp. Once again, a significant increase of the crystallinity content can be observed as a result of the introduction of compatibilizers mixture.

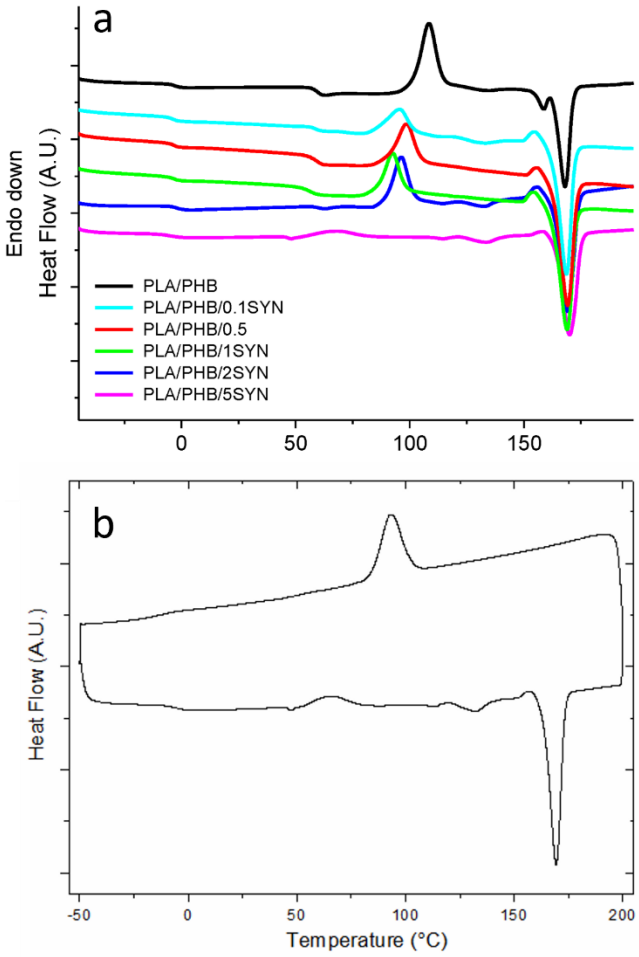

Figure 83. DSC thermograms for Syn-containing systems and non-compatibilized blend (second heating scan) (a) and Syn-containing system with 5 wt% of compatibilizers (second heating and cooling scans) (b). Reprinted under CC BY 4.0 license from [190].

Table 11. Thermal properties of non-compatibilized blend and Syn-containing systems

	PLA/PHB	0.1SYN	0.5SYN	1SYN	2SYN	5SYN
ΔH_m [J/g]	28	49	49	49	50	44
ΔH_{cc} [J/g]	31	15	17	23	22	-
X_c [%]	11	36	34	28	30	44

To sum up, results coming from thermal characterization indicate that the introduction of both additives causes an anticipation of the PLA cold crystallization phenomenon and a progressive increase of the crystallinity content of the blend.

5.5.2 Thermo-mechanical measurements (DMA)

Figure 84(a) and Figure 85(a) report the temperature dependency of the dynamic storage modulus for HLB12-containing and Syn-containing system, respectively, and the non-compatibilized PLA/PHB blend. In the range of temperatures below the PLA glass transition temperature, the compatibilized systems show lower moduli than the neat blend (Figure 84 (a)), apart from the sample containing 1.0 wt.% of HLB12, for which a higher value of E' was recorded; this finding is clearly visible in Figure 84 (b) (black line) which reports the trends of the storage moduli recorded at three different temperatures (40, 70 and 80°C) as a function of the amount of the compatibilizers.

Furthermore, the thermo-mechanical measurements show that the decrease of E' with the increase of temperature involves a consequent remarkable increase of the heat deflection temperature (HDT) which is calculated following the procedure exploited by Takemori [217]. In particular, HDT corresponds to the temperature at which the elastic modulus reaches the value of 800 MPa that is consistent with an applied load of 1.82 MPa. This finding can be better observed looking at the values listed in Table 12. The maximum value of HDT is reached for the blend with 1 wt% of compatibilizers mixture with HLB 12. In fact, the sample PLA/PHB/1HLB12 was selected for further investigations according to the fact that this formulation ensures improved thermo-mechanical properties, either at low and high temperatures.

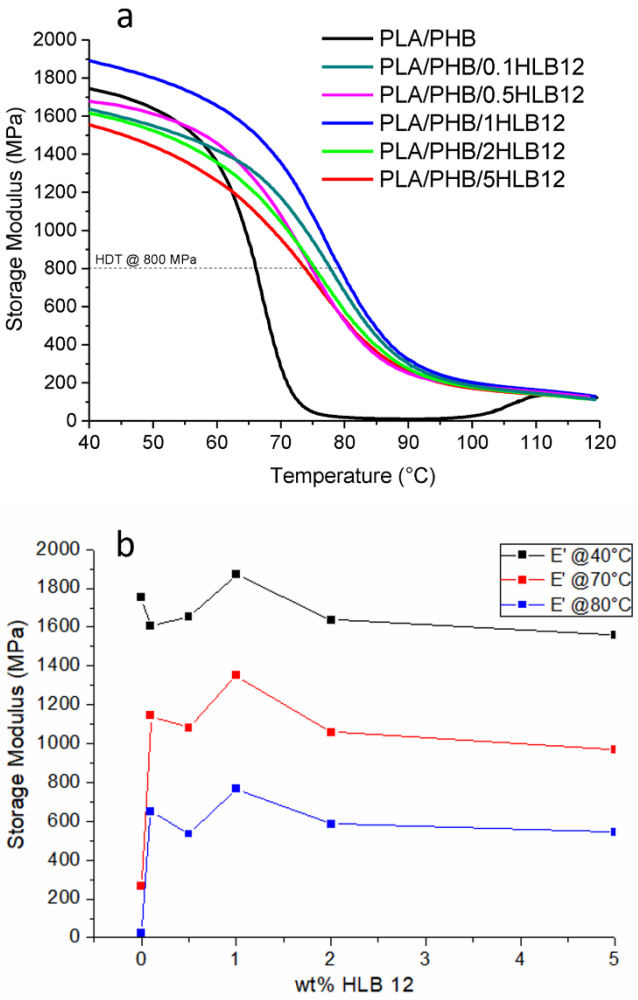

Figure 84. DMA traces for HLB12-containing systems (a) and trend of Storage modulus E' as a function of HLB12 content in the PLA/PHB blends at different temperatures (b). Modified under CC BY 4.0 license from [190].

In Figure 85(a) the DMA curves of Syn-containing systems are reported. The E' value at 40°C in Syn-containing systems is lower as compared to the non-compatibilized system, except for the blend with 0.1 wt% of Syn; this finding is clearly visible in Figure 85(b) (black line). At 70°C and 80°C all compatibilized blends show higher dynamic storage modulus than the non-compatibilized system and among the Syn-containing samples, the blend with 0.1 wt% of exhibits higher E' value as compared to those of the other compatibilized blends at all investigated temperature. Similarly to what was observed for the HLB12-containing samples, the storage modulus of the compatibilized blends shows a less sharp decrease as a function of temperatures due to the occurrence of the PLA glass transition, leading also in this case to a remarkable increase of the HDT values, up to 80°C (Figure 85(a)). It is worth noting that the increase of the HDT values with respect to the non-compatibilized blend is almost unaffected by the Syn amount, as reported in the values listed in Table 12. For this reason, the blend containing the lower amount of Syn was selected for further investigations, since this system allows obtaining

superior mechanical performances, while minimizing the content of the introduced additive.

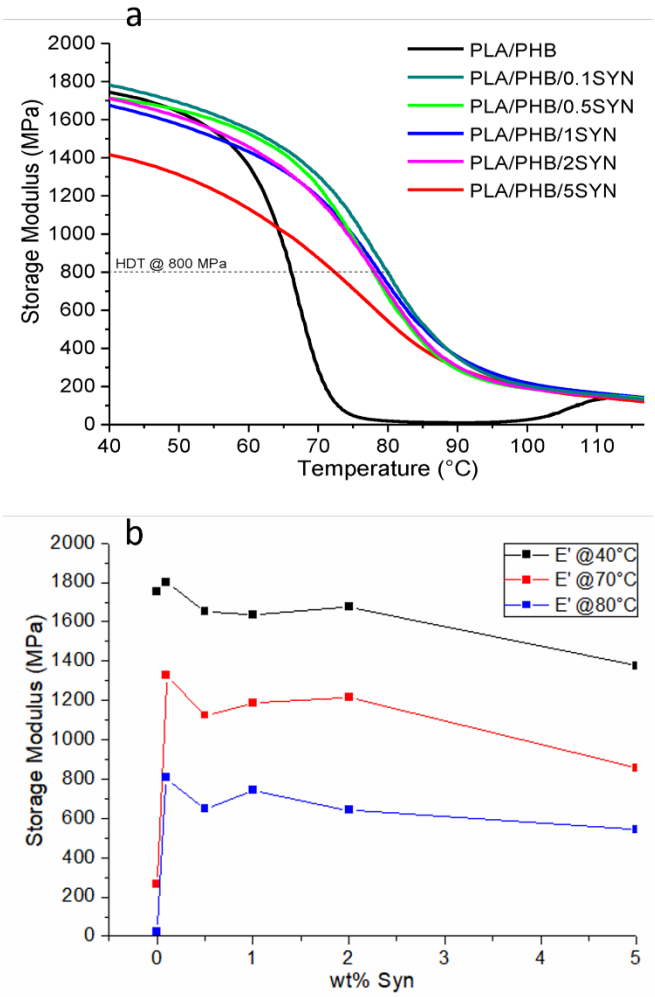

Figure 85. DMA traces for Syn-containing systems (a) and trend of Storage modulus E' as a function of Syn content in the PLA/PHB blends at different temperatures (b). Modified under CC BY 4.0 license from [190].

Table 12. Thermo-mechanical properties of non-compatibilized blend, HLB12- and Syn-containing systems.

Sample	PLA/PHB	0.1HLB12	0.5HLB12	1HLB12	2HLB12	5HLB12
Tandelta [°C]	74	84	82	85	83	83
HDT [°C]	66	78	75	80	75	74
Sample	PLA/PHB	0.1SYN	0.5SYN	1SYN	2SYN	5SYN
Tandelta [°C]	74	86	85	85	84	84
HDT [°C]	66	80	78	79	78	72

Interestingly, as reported in Table 12 both compatibilizers-based systems are characterized by higher temperatures of the corresponding peak of tanδ at all investigated weight contents than the non-compatibilized blend.

The trends of tandδ as a function of the temperature for HLB12- and Syn-containing systems are reported in Figure 86. In both compatibilizers-based systems, the intensity of the tanδ peak decreases, specifically at 0.18-0.23, compared to that of non-compatibilized materials which is set at 1.2. This finding indicates that fewer polymer chains are participating in this transition; thus, the increase in modulus can be attributed to physical interaction between the polymer and compatibilizers [218] [219]. In addition, broader peaks are obtained for Syn- and HLB12-containing systems than the non-compatibilized material indicating the improvement of compatibility between the polymeric phases [106].

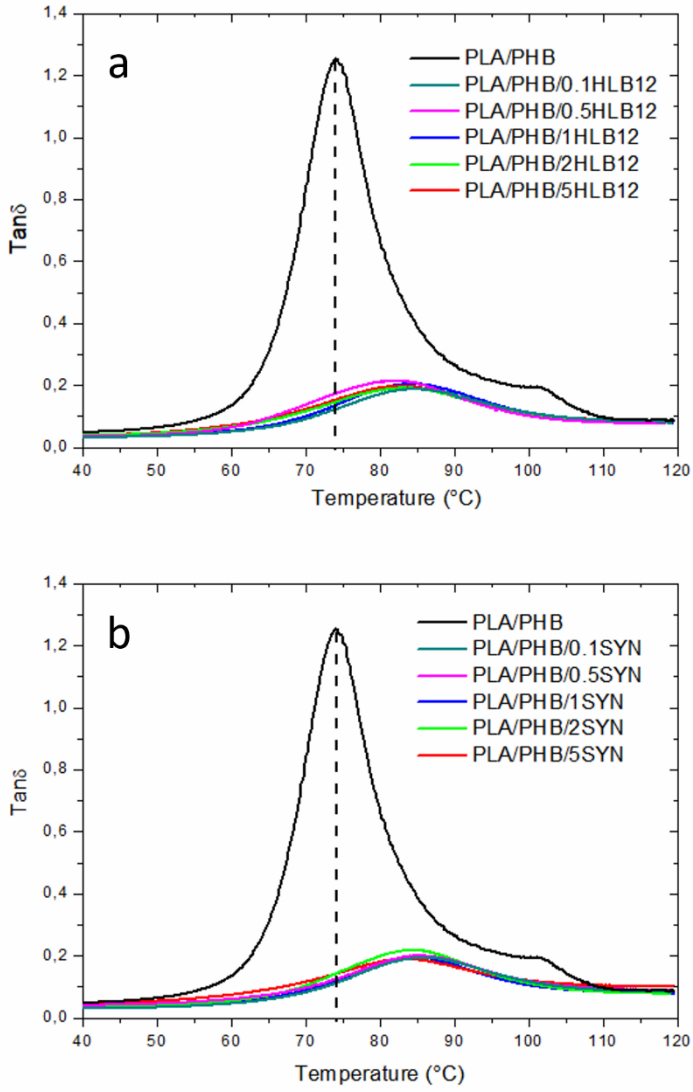

Figure 86. Trends of Tanδ as a function of temperature for Syn- (a) and HLB12-contnaining systems (b) as compared to the non-compatibilized blend.

5.5.3 Rheological measurements and morphological investigations

Figure 87(a) shows the trends of the storage modulus G' as a function of the frequency for the non-compatibilized blend and the PLA/PHB/1HLB12 system.

Significant differences are encountered by comparing the rheological response of the sample containing 1 wt% of HLB12 with that of the non-compatibilized system. In fact, as reported in Figure 87 (a), the presence of the liquid mixture of surfactant causes the disappearance of the aforementioned shoulder in the G' trend; in addition, a decrease of the slope of the modulus curve in the terminal region can be observed.

This finding allows predicting the existence of complex morphologies; thus, the values of the G' slope α were calculated (Equation 39) and the results of the trends of the G' slope as a function of the frequency f or the non-compatibilized PLA/PHB blend and HLB12-containing system are reported in Figure 87(b).

The G' slope in the neat blend decreases with the increase of the frequency as previously reported in the case of PLA/LDPE blend. Differently, the curve of the G' slope of the blend with 1 wt% of HLB12 remains almost constant over the tested frequency range, indicating the presence of particles of dispersed phase with different shapes and dimensions which are able to relax with at different time scales.

Since the structures which formed the PHB phase relax continuously over a long time inducing a continuous spectrum of relaxation times, the G' slope remain unchanged in the investigated frequency region [220].

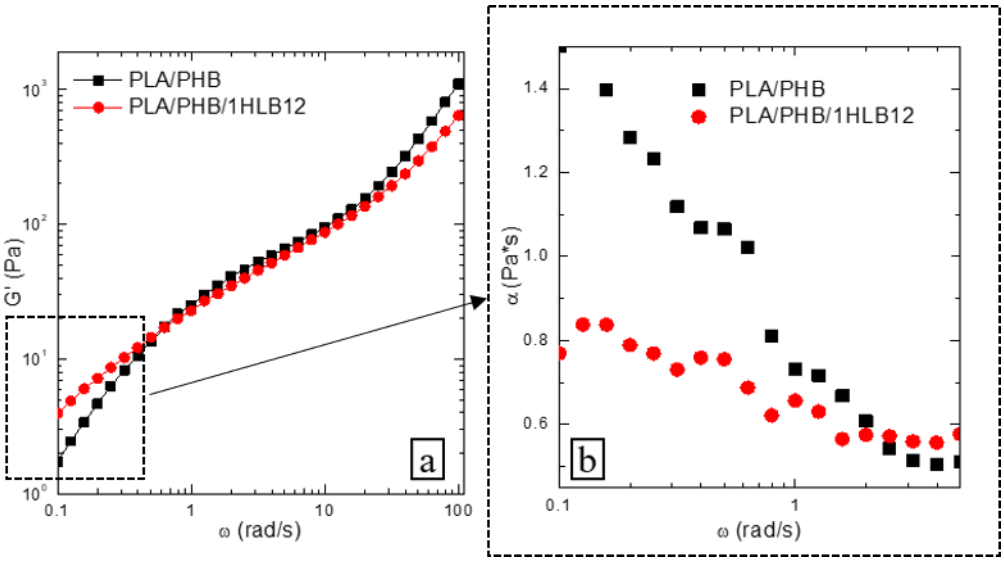

Figure 87. Storage modulus G' (a) and G' slope (b) as a function of the frequency for neat blend and HLB12-containing system (1 wt%). Reprinted under CC BY 4.0 license from [190].

Conversely, the compatibilized blend (with 0.1 wt% of Syn) exhibits a very similar behaviour of PLA/PHB non-compatibilized system in the investigated frequency range but, at the same time, higher values of G' are observed as compared to the non-compatibilized system, as reported in Figure 88.

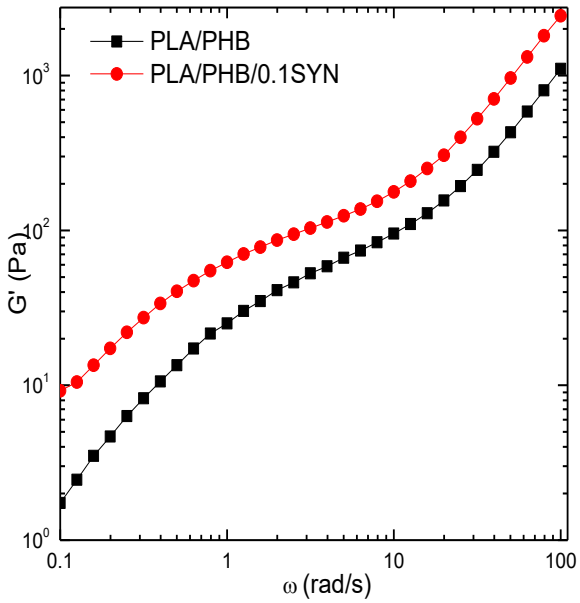

Figure 88. Storage modulus G' as a function of the frequency for neat blend and Syn-containing system (0.1 wt%). Reprinted under CC BY 4.0 license from [190].

Morphological investigations were carried out and are reported in Figure 89. Non-compatibilized PLA/PHB blend shows, as expected, a drop-matrix morphology with roughly spherical PHB particles dispersed in the PLA matrix. During the fracture of the surface most of the PHB particles remained in the structure, while others are pulled out, leaving empty cavities on the surface. As already observed in the micrograph of PLA/LDPE blend model, this finding indicates the lack of interfacial adhesion between the two phases and the immiscibility between PLA and PHB at this explored weight ratio.

As a result of the introduction of 1 wt% of surfactants mixture with HLB12 most relevant morphological changes occur in HLB12-containing system; in fact, as showed in the in the highlighted detail of the micrograph reported in Figure 89(b), the PHB dispersed phase is hardly distinguishable from the matrix and, additionally, it appears in the form of domains with elongated and irregular shapes, as inferred from the study of slope of G' in the rheological measurements.

Conversely, different aspects can be highlighted in Syn-containing system; first, a notable reduction of the amount of pulled-out PHB particles as compared to the neat blend can be observed, as indicated by the reduced number of the empty cavities in the micrograph reported in Figure 89(c). In addition, the surface of the minor phases does not show clear and defined borders, suggesting a certain grade of compatibility and interfacial adhesion between phases in this sample.

Nevertheless, the use of both natural compatibilized systems allows to obtain the increase of the interfacial adhesion between the PLA and PHB phases, resulting in a morphology refinement.

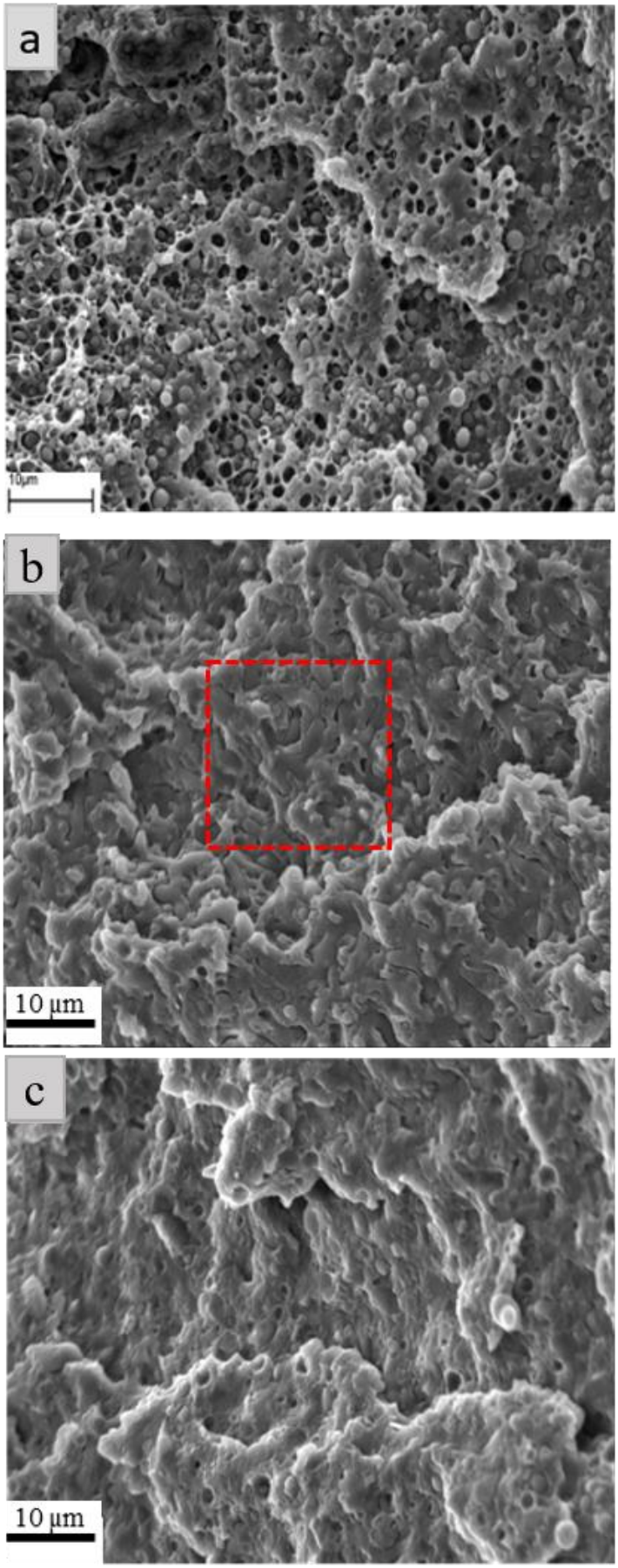

Figure 89. SEM micrographs of PLA/PHB (a), PLA/PHB/1HLB12 (b) and PLA/PHB/0.1SYN (c). Reprinted under CC BY 4.0 license from [190].

Chapter 6

Influence of process parameters in PLA/PHB biopolymer blends

Part of the work described in the Chapter 6 has been previously published in:

''D'Anna A, Arrigo R, Frache A. Rheology, Morphology and Thermal Properties of a PLA/PHB/Clay Blend Nanocomposite: The Influence of Process Parameters. Journal of Polymers and the Environment. 2021.'' [221]

6.1 Introduction

The control of the extrusion process is very complex due to the numerous physical and, possibly, chemical transformations of the materials during the processes. As an example, the mechanical stresses generated during extrusion are a direct function of the rheological properties of the material which in turn depend on the changes in the material microstructure [77]. As extensively discussed in Chapter 2, the development of different morphologies in polymer blends during the process depends on the interfacial tension between the polymers constituting the mixture and the applied stress fields. Thus, the microstructure is closely related to the melt blending process and the conditions under which the process takes place. In particular, several factors influence morphology of the dispersed phase and the final properties of materials such as composition [222] [223] [224], interfacial interactions [225] [226] [227], flow field type and its intensity [225] [228] as well as processing conditions and, thus, screw configuration, time of mixing, screw rotation speed, temperature and flow rate [225].

The main aim of the study reported in this Chapter is the evaluation of the optimization of process parameters on the morphology and properties of a bio-based blends. Although several papers dealing with the formulation and characterization

of biopolymer blends are reported in literature, the study of the influence of process conditions on the development of bio-based polymer blends is still poorly developed. Indeed, in the scientific literature, the role of the processing parameters, especially as far as the influence of the screw profile is concerned, in modifying the microstructure and the final properties of bio-based materials has not been systematically evaluated. In this context, for the full exploitation of materials based on bio-sourced and/or biodegradable polymers also at industrial scale, the evaluation of their processing behaviour and the optimization of the working parameters is of fundamental importance.

The study of the influence of screw profile, flow rate and screw rotation speed on the morphology and properties for PLA/PHB and PLA/PHB/clay blends was reported. Firstly, through thermal and thermo-mechanical analyses and the evaluation of material morphology, a systematic study on PLA/PHB blends with different weight ratios was carried out, aiming at selecting the most suitable composition for the further investigations.

6.2 Preliminary tests: variation of blend composition

In this section, PLA/PHB mixtures with different weight contents of each polymer will be analysed and a co-rotating twin-screw extruder (details in Appendix II) was used to process the mixtures. The barrel temperature was set from 170°C to 190° along the extruder axis and the melt temperature was measured to be 185°C. The screw profile is shown schematically in Figure 90; the working conditions were 400 rpm with an extrusion flow rate of 5 kg/h. The obtained blends are designed as X/Y where X and Y indicate PLA and PHB content (wt%), respectively; the compositions and the codes of the mixtures are listed in Table 13.

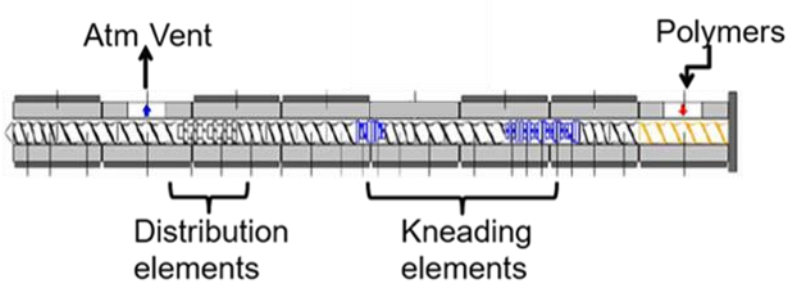

Figure 90. Screw configurations (SP1) used for PLA/PHB X/Y blends.

Table 13. Compositions and codes of PLA/PHB X/Y blends.

Composition	Code
PLA: 55 wt% and PHB: 45 wt%	55/45
PLA: 60 wt% and PHB: 40 wt%	60/40
PLA: 65 wt% and PHB: 35 wt%	65/35
PLA: 70 wt% and PHB: 30 wt%	70/30

Being the aim of the dissertation to study fully biopolymer blends based on PLA polymer, all the studied formulations in this section have been composed by PLA polymer as continuous phase.

Thermal analyses on all formulated PLA/PHB blends are carried out and the thermograms recorded during the second heating scan are shown in Figure 91. The thermal properties of PLA and PHB neat polymers are already reported in Chapter 5, paragraphs 5.4.1 and 5.5.1, respectively.

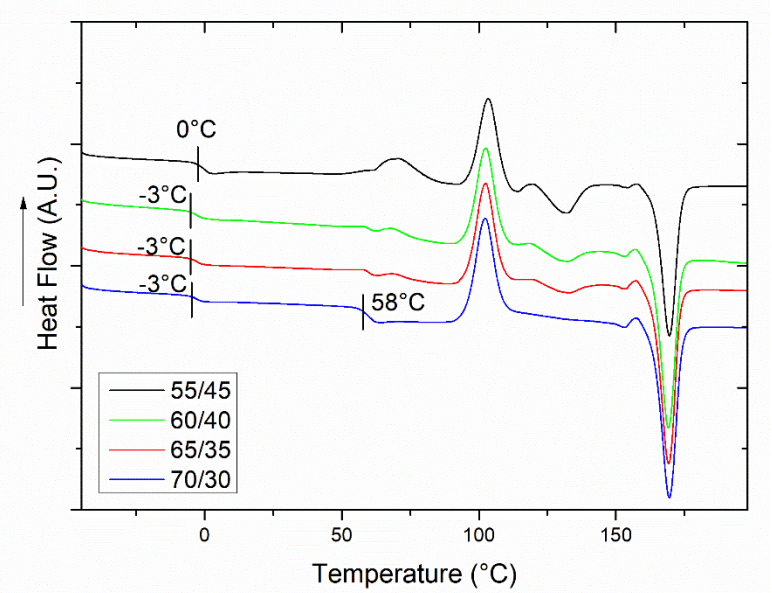

Figure 91. DSC thermograms recorded during second heating scan for all PLA/PHB blends.

In Figure 91, the T_m of PLA and PHB are at 170°C and 132°C, respectively, according to the neat polymers melting. Concerning 70/30 blend no melting peak of PHB are reported, probably due to the low PHB weight content in this formulation; in addition, only in this mixture the glass transition of the PLA phase can be clearly observed at 58°C. In fact, by increasing the PHB content from 30 to 45 wt%, the glass transition of PLA polymer is no longer distinguishable due to the occurrence of the PHB cold-crystallization phenomenon at similar temperature (53°C).

However, in the blends with 30, 35 and 40 wt% content of PHB the T_g of PHB phase remains almost unchanged at -3 °C as compared to the neat polymer, while it increases at 0°C in the blend with the higher amount of PHB phase (45 wt%).

Table 14 shows the crystallinity degrees of PLA and PHB (X_{PLA} and X_{PHB}); and the values of $\Delta H°$, necessary to the calculation of X, for PLA and PHB are reported in Appendix A (A.3.1 Differential scanning calorimetry DSC).

The common behaviour reported in the literature predicts that the PHB phase crystallizes as small spherulites dispersed in the amorphous PLA matrix by acting as nucleating agents for PLA increasing its crystallinity [203]. Conversely, in the results reported in Table 14, a different behaviour was observed, and the crystallinity degree of PLA polymer gradually decreases as the content of PHB

increases from 11% in 70/30 blend to 8% in 55/45 blend. An equivalent behaviour was reported in several literature works using a similar PHB polymer employed in this Chapter. The decrease of crystallinity degree of PLA polymer, as a function of the PHB content, is attributed to the presence of the 3HH unit which causes the reduction of the crystallization rate and decrease of the regularity of the PLA crystals [229] [213].

In addition, the presence of longer side-chains of 3HH comonomers into the short side-chained 3HB in PHBH hinders the molecular mobility and reduces the packing efficiency of the crystallites in PHBH. Therefore, due to the presence of long chains, the PHBH polymer is intrinsically slightly less prone to form crystals compared to the PHB [230].

Conversely, the crystallinity degree of PHB phase results decreased in the systems with highest content of PHB phase, in fact it is 1% in 55/45 blend. This finding also highlights the fact that the glass transition temperature of PHB is higher in 55/45 blend than the other mixtures due to the reduced chain mobility of PHB in this formulation.

Table 14. Crystallinity degree of PLA in PLA/PHB blends

	55/45	60/40	65/35	70/30
X_{PLA} [%]	8	9	10	11
X_{PHB} [%]	1	3	2	-

The results of dynamic thermo-mechanical analyses are shown in Figure 92. Dynamic storage modulus E' increases from 1673 to 2394 MPa as the content of PLA increases. In fact, the highest E' value is recorded in the 70/30 blend with an increase of 30% than that reported in 55/45 mixture.

At temperature lower than the glass transition, the storage modulus decreases as the content of PHB increases in the blends, resulting in a reduction of stiffness [231] [229].

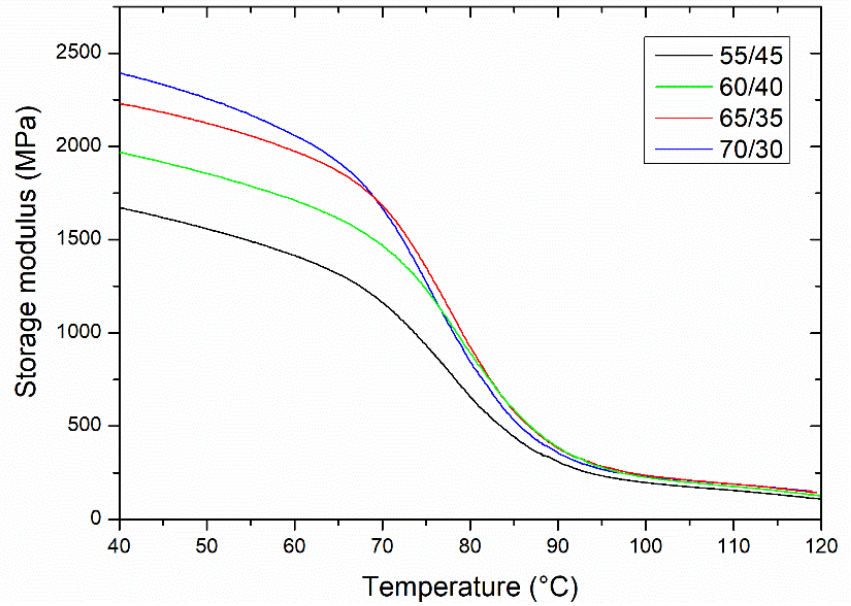

Figure 92. Thermo-mechanical traces for PLA/PHB blends.

Figure 93 reports the SEM micrographs for each formulation. The 70/30 blend shows a droplet-like morphology (Figure 93(a)); by increasing the weight content of the PHB the morphology changes from a discontinuous dispersion of spherical drops to a morphological structure characterized by the coexistence of the two continuous phases of PLA and PHB. This can be seen in Figure 93 (b) (c) and (d) of blends with a higher concentration of PHB polymer where it is difficult to distinguish between the continuous and the dispersed phase.

In order to study the influence of the process parameters, it was decided to focus the study on the 70/30 blend, checking both the final morphology and the properties obtained by changing the variables during the extrusion process, since the blend with 70 wt% of PLA and 30 wt% of PHB exhibits better thermo-mechanical properties than the other systems.

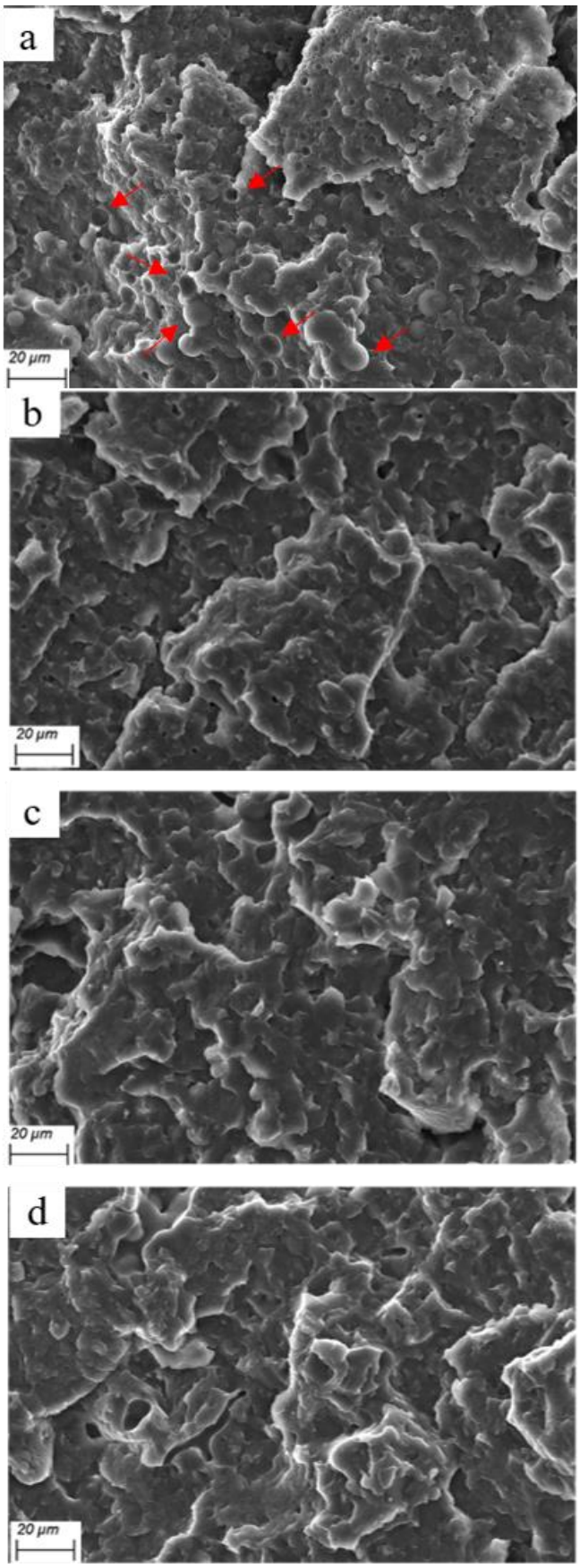

Figure 93. SEM micrographs of PLA/PHB blends: 70/30 (a), 65/35 (b), 60/40 (c) and 55/45 (d).

6.3 Influence of process parameters in PLA/PHB blend with 70 wt% of PLA and 30 wt% of PHB

The configuration of screw, the flow rate and the screw speed are the process parameters that have been varied to evaluate the possible influence of the processing on morphology and properties of PLA/PHB 70/30 blend.

In order to better understand the approach used to vary the process parameters, Figure 94 reports a schematic representation of the experimental trials.

The case studies 1, 2 and 3 which correspond to the influence of the variation of screw profile, flow rate, and screw speed, respectively, are illustrated schematically with the squares and represent the varied process parameters. As an example, in the first case study, the influence of the screw profile variation was analysed by keeping the flow rate (3 kg/h) and the screw speed (400 rpm) constant.

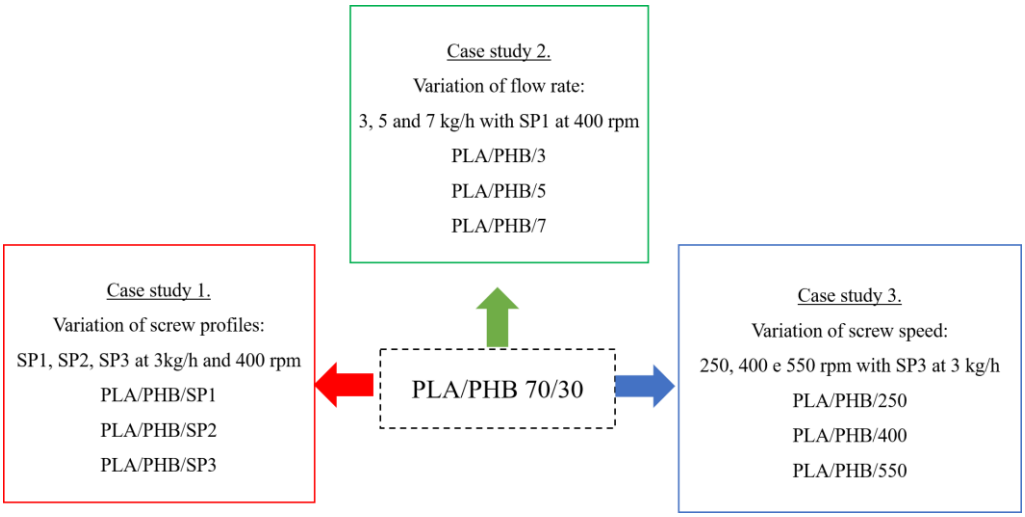

Figure 94. Schematic representation of the different case studies for the development of PLA/PHB 70/30 blends.

6.3.1 Influence of screw profiles

In this section, PLA/PHB 70/30 blends are processed at 3 kg/h and 400 rpm with different screw configurations (Figure 95).

The used twin-screw extruder is constructed of screws with a modular assembly build of individual elements, like conveying, back-conveying, kneading and mixing elements, which are shown in Figure 96, where the temperature profile is also reported. The three screw configurations contain the same kneading blocks for the melting of polymers with constant number and position constants, consisting of five discs of length of 15 mm; the staggering angles are 30°- 60°- 60°- 90°- 90°. The details of the used screw elements are presented in Table 15.

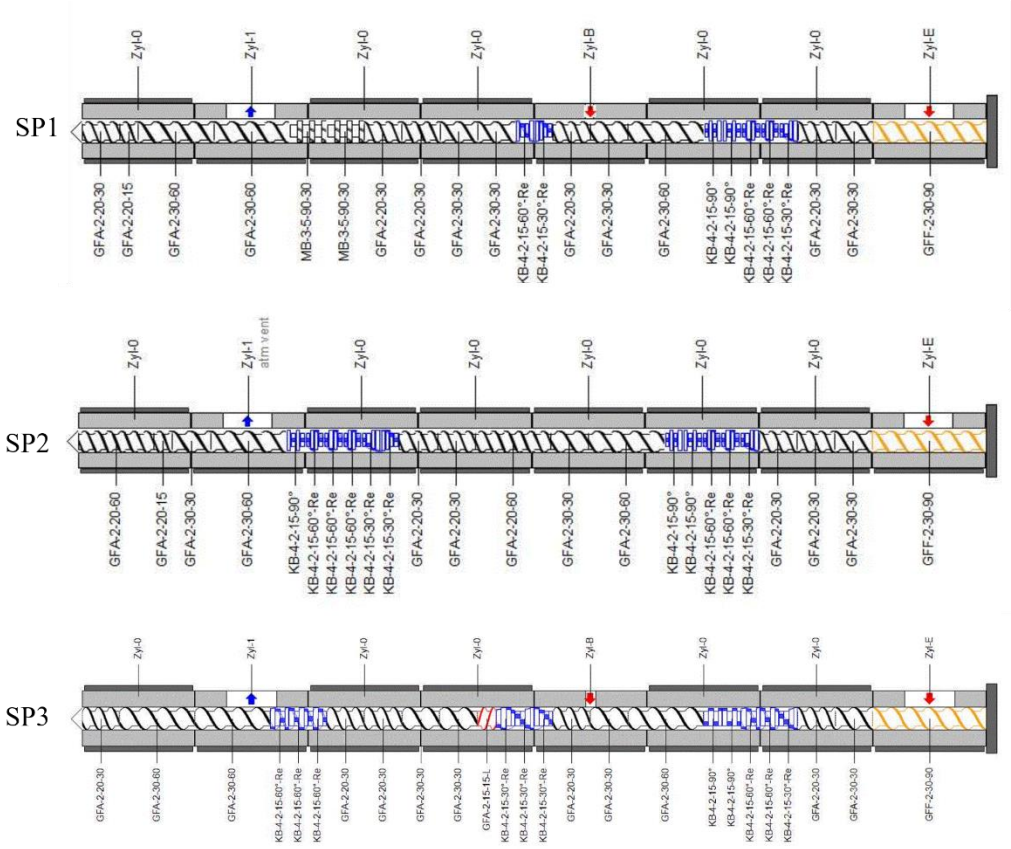

Figure 95. Screw configurations for PLA/PHB process (3 kg/h and 400 rpm).

In particular, the three configurations are summarized as follow:

- *Screw profile 1 (SP1)* is characterized by the presence of a kneading block of two disks with a positive staggering angle of 30° and 60° and two mixing elements; the others are conveying elements used to transport the polymers.
- *Screw profile 2 (SP2)* is characterized by the presence of a kneading block of six elements of which two with a positive staggering angle of 30°, three with an angle of 60° and one, at the end, with an angle of 90°.
- *Screw profile 3 (SP3)* is characterized by the presence of one element of backflow locating among the two kneading blocks constituted by three elements with a positive staggering angle of 30° and 60°.

Figure 96. Screw elements of twin screw-extruder Leistritz: conveying elements (a) kneading elements with staggering angle of 30°, 60° and 90° (b), backflow conveying element (c) and mixing element (d).

Table 15. Specification of extrusion screw elements used for the process of PLA/PHB blend.

	Length [mm]	Pitch [mm]	Type of element: m-mixing k- kneading c-conveying	Number of threads	Staggering angle [°]	Conveying behaviour: L-left handed R-right handed
GFF-2-30-90	90	30	c	2		
GFA-2-30-30	30	30	c	2		
GFA-2-30-60	60	30	c	2		
GFA-2-20-15	15	20	c	2		
GFA-2-20-60	60	20	c	2		
GFA-2-30-30	30	30	c	2		
GFA-2-15-15-L	15	15	c	2		L
KB-4-2-15-30°	15		k	2	30	R
KB-4-2-15-60°	15		k	2	60	R
KB-4-2-15-90°	15		k	2	90	
MB-3-5-90-30	30		m	3		

Thermal analyses were carried out and the results of the second heating scan are reported in Figure 97. Irrespective of the used screw configuration, the T_g value for both PHB and PLA, T_{cc} and T_m of PLA and the crystallinity degree of PLA polymer are unchanged in the blends and the values of the thermal characteristics are before reported in the paragraphs 6.3.1.

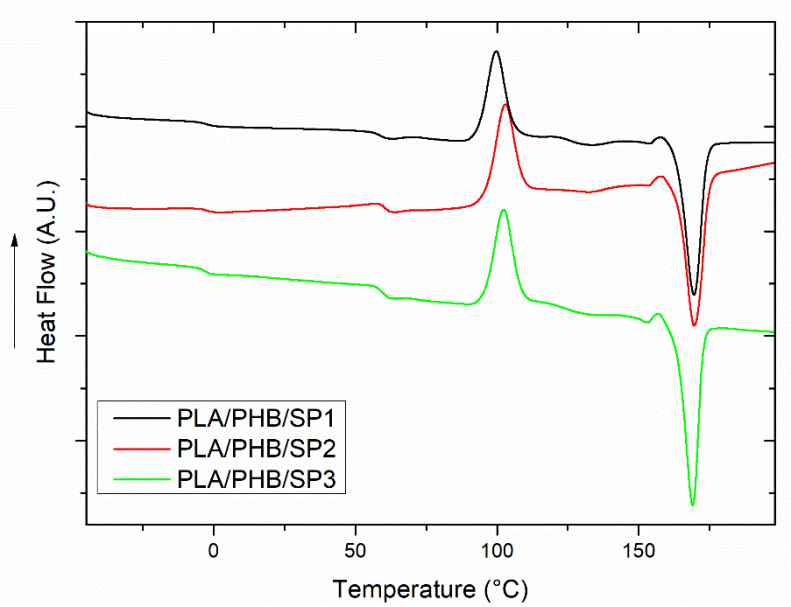

Figure 97. DSC thermograms of PLA/PHB blends processed with different screw profiles recorded during the second heating scan.

Results of rheological measurements are reported in Figure 98; the trends of η* and G' as a function of frequency for the blends are not influenced by the variation of the screw configuration.

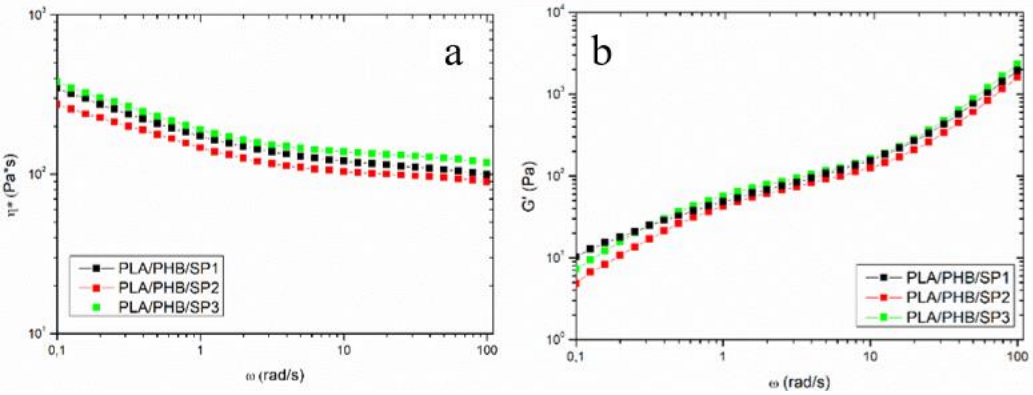

Figure 98. Complex viscosity η* (a) and Storage modulus G' (b) for PLA/PHB blends processed with different screw profiles.

Figure 99 reports the SEM micrographs of the PLA/PHB blends processed with SP1, SP2 and SP3. Although the blends processed with the three screw profiles show a drop-matrix morphology, a close inspection of their microstructure reveals that the blend processed with SP3 shows higher sizes of droplets of disperse phase characterized than those present in the blends obtained with SP1 and SP2.

In order to quantitatively evaluate the differences in the microstructure, ImageJ software was used to calculate the average size d_{av} of the droplets of dispersed phase. In particular, 80 points were included in the calculation of average particles size for each mixture analysed. A schematic representation of the particle dimension calculation is shown in Figure 100 and the corresponding results are reported in Table 16.

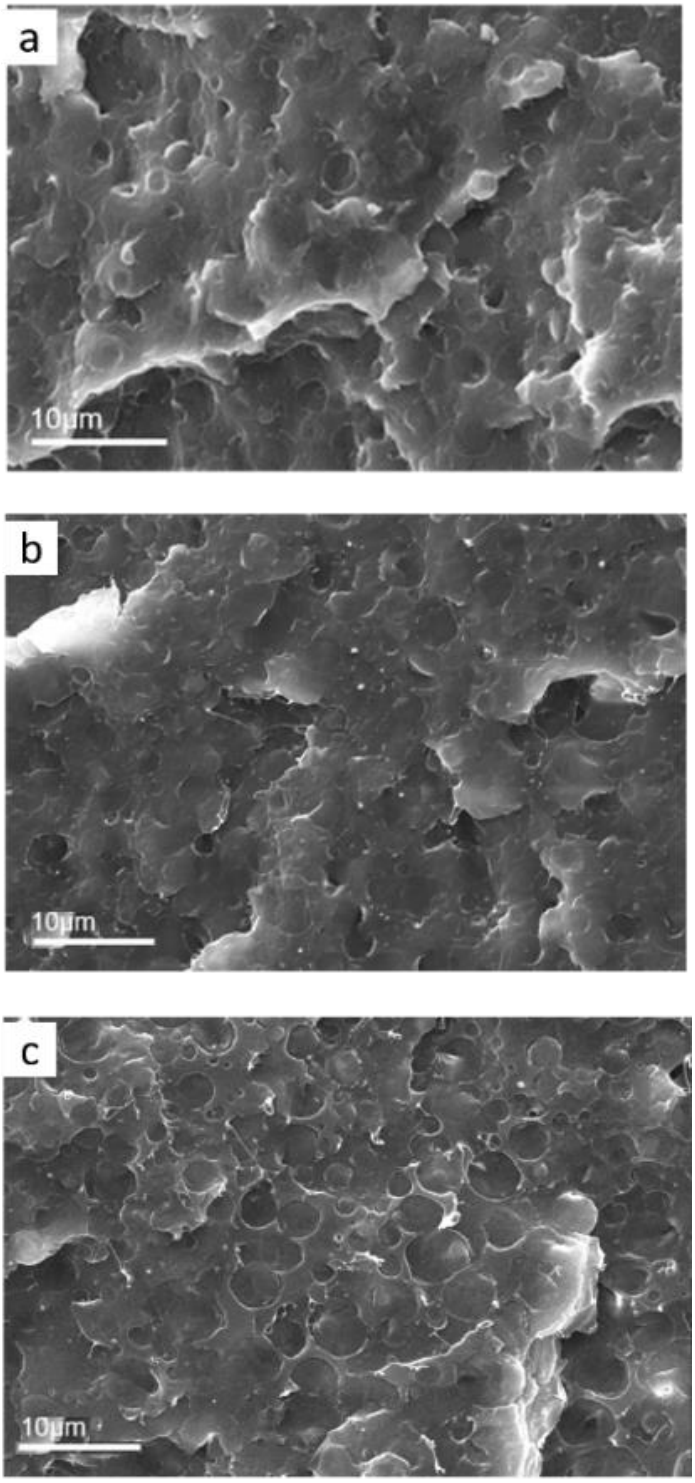

Figure 99. SEM micrographs of PLA/PHB blends processed with different screw profiles: SP1 (a), SP2 (b) and SP3 (c).

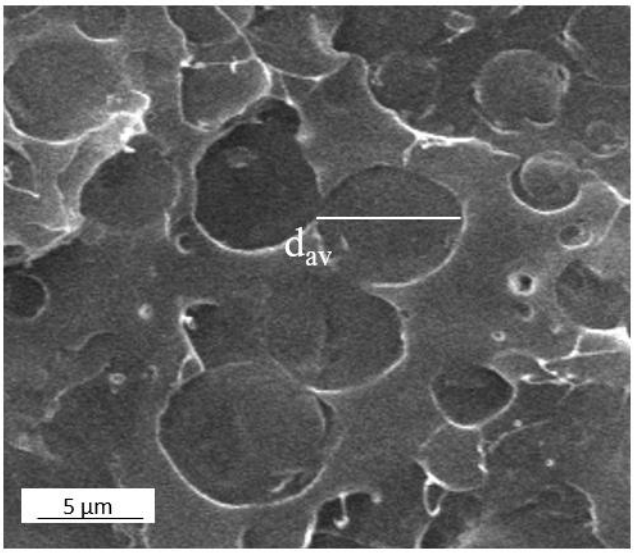

Figure 100. Schematic representation of the calculation of the dimension of dispersed phase particles.

The average particle size of the droplets in the blends processed with SP1 and SP2 is smaller as compared to that of the mixture obtained with SP3. In particular, the dimensions of particles in PLA/PHB/SP1 and PLA/PHB/SP2 blends are 48% lower than those in PLA/PHB/SP3. The changes in the microstructures noticed in these formulations is caused by the specific design of the screw profiles. In particular, the flow conditions established during processing due to the presence of mixing elements (SP1) and a high number of kneading elements (SP2) allow a more efficient mixing of the polymeric phases, resulting in an average decrease in particle sizes of the dispersed phase in blends obtained with SP1 and SP2 of 48% compared to the blend processed with SP3.

Table 16. Results of average particle dimension of PLA/PHB blend calculated using ImageJ software.

	d_{av} [µm]	std. dev.
PLA/PHB/SP1	2.7	0.8
PLA/PHB/SP2	2.6	0.8
PLA/PHB/SP3	5	1.2

PLA/PHB/SP1 and PLA/PHB/SP2 show same values of torque, 26 Nm. Conversely, probably due to the presence of the element of backflow, which induce high shear stresses on the materials during the process, the value of torque is higher in PLA/PHB mixture processed with SP3 (41 Nm) than the others.

6.3.2 Variation of flow rate

The screw configuration used for the process is that already depicted in Figure 95 and the codes of blends processed at 400 rpm with flow rates of 3, 5 and 7 kg/h, are shown in Table 17. During the extrusion process the values of torque are registered and result 26 Nm, 30 Nm and 37 Nm for blends processed at 3, 5 and 7 kg/h, respectively.

Table 17. Code of the PLA/PHB blends processed with screw profile 1 at 400 rpm.

Composition	Code
PLA: 70 wt% and PHB: 30 wt% processed at 3 kg/h	PLA/PHB/3
PLA: 70 wt% and PHB: 30 wt% processed at 5 kg/h	PLA/PHB/5
PLA: 70 wt% and PHB: 30 wt% processed at 7 kg/h	PLA/PHB/7

DSC characterization was carried out and the thermograms recorded during the second heating scan are reported in Figure 101. T_g for both neat polymers remain unchanged in all blends at 58°C and -3°C for PLA and PHB, respectively. In contrast, only PLA/PHB blend processed with flow rate of 3 kg/h exhibits a weak peak at 132°C attributable to the melting of PHB phase [229]. In addition, as shown in Table 18, the value of T_{cc} is lower in the PLA/PHB/3 blend than in the blends processed with 5 and 7 kg/h; this finding is due to an anticipation of the PLA cold crystallization rate enhanced due to the presence of the PHB phase [97] in the mixture processed at 3 kg/h.

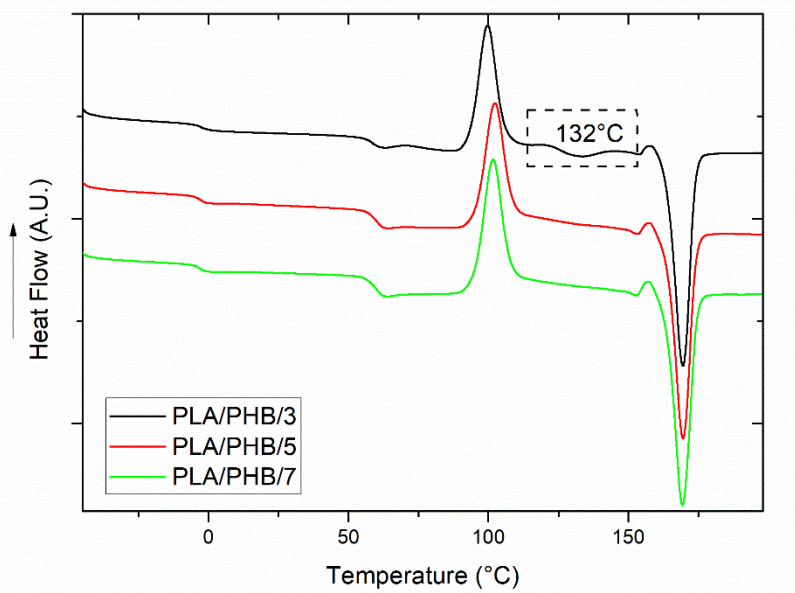

Figure 101. DSC themograms of blends PLA/PHB processed with different flow rates recorded during second heating scan.

In fact, the crystallinity degree of PLA is higher in the PLA/PHB/3 blend with X_{PLA} equal to 13%. This result can be associated to the influence of PHB phase

which acts as a nucleating agent more significantly when processing the blend at a lower flow rate resulting in a greater interaction between the two polymer phases. Probably, when the flow rate increases and the residence time in the extruder decreases by keeping constant the screw speed, the interaction between PLA and PHB is particularly weak [232] [188].

Table 18. Cold-crystallization temperature of PLA and crystallinity degree of blends.

	PLA/PHB/3	PLA/PHB/5	PLA/PHB/7
$T_{cc\ PLA}$ [°C]	100	102	102
X_{PLA} [%]	13	11	10
X_{PHB} [%]	2	-	-

Figure 102 and Figure 103 report the trends of complex viscosity η* and storage modulus G' as a function of frequency.

PLA/PHB/3 blend exhibits higher values of complex viscosity than the blends processed with a flow rate of 5 and 7 kg/h in the whole investigated frequency range. In addition, a different behaviour in the trend of complex viscosity is reported in the blend processed at low flow rate; in particular, a more pronounced non-Newtonian rheological behaviour is observed. The trend is different in the blends obtained with higher flow rate which show a similar behaviour.

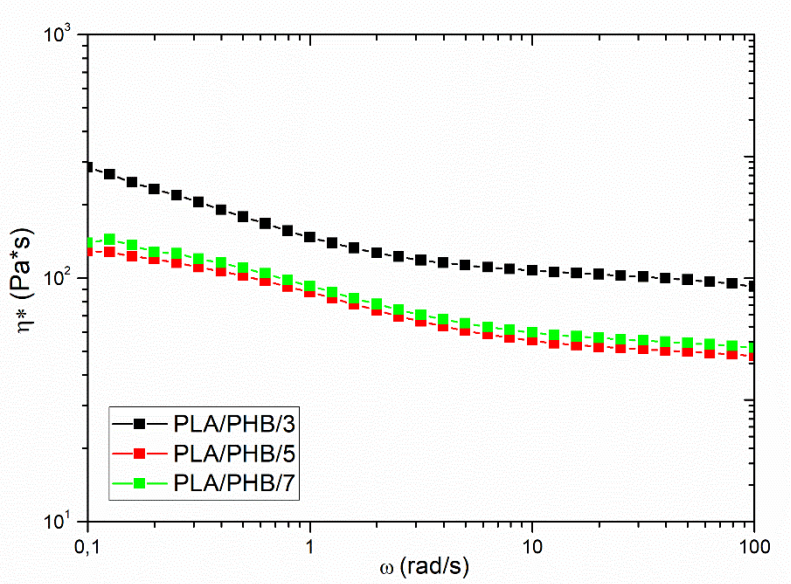

Figure 102. Complex viscosity η* of blends PLA/PHB processed with different flow rates.

The trend of storage modulus G', reported in Figure 103, remains almost unchanged in all the blends studied. However, the PLA/PHB/3 mixture exhibits higher G' values at low frequencies than the others.

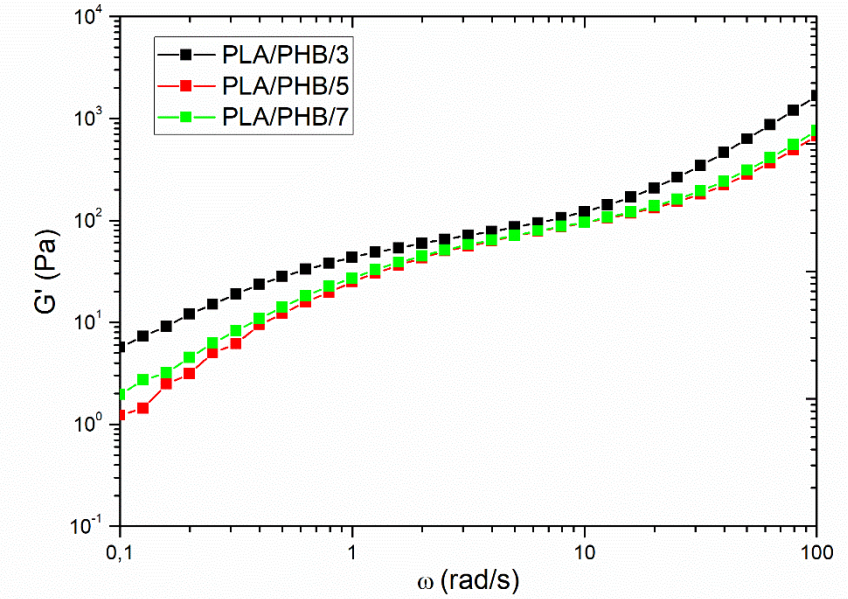

Figure 103. Storage modulus G' of blends PLA/PHB processed with different flow rates.

Since the PLA/PHB blends processed at 5 and 7 kg/h exhibit similar rheological behaviour, the morphological investigation is performed on PLA/PHB/5 and PLA/PHB/3 mixtures in order to compare the systems; the SEM micrographs are reported in Figure 104.

Particularly, both mixtures show a droplet-like morphology; however, in Figure 104(a), the droplets of PLA/PHB/3 blend shows average dimensions lower as compared to the droplets of PLA/PHB/5 blend. The values calculated thought the Image J software are reported in Table 19. Thus, the efficiency of kneading and mixing elements, present in the screw configuration SP1 used to process the blends (Figure 95), is higher by working with a flow rate equal to 3 kg/h than 5 kg/h (or 7 kg/h). In addition, the blend processed at high flow rate shows more empty cavities on the surface indicating weaker interfacial adhesion between polymers constituting the blend as compared to the PLA/PHB/3 blend confirming that the cohesion between PLA and PHB is significantly improved [233].

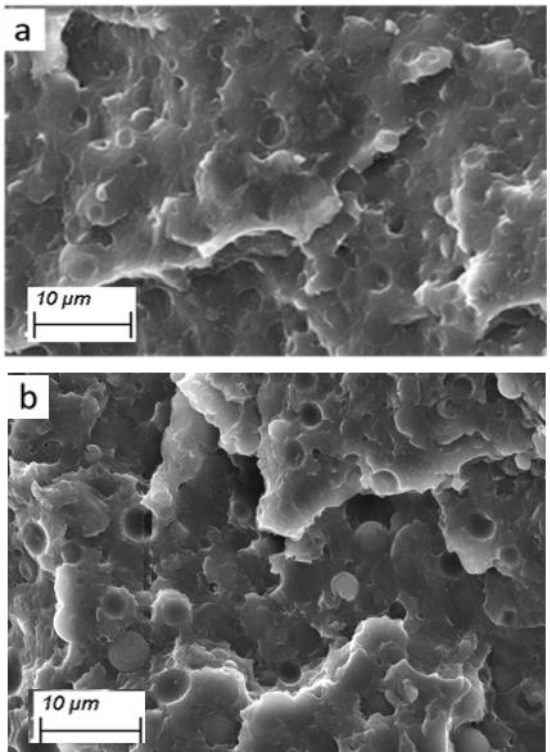

Figure 104. SEM micrographs of PLA/PHB blends processed at 3 kg/h (a) and 5 kg/h (b).

Table 19. Results of average particle dimension of PLA/PHB blend calculated using ImageJ software.

	d_{av} [µm]	std. dev.
PLA/PHB/3	2.7	0.8
PLA/PHB/5	4.5	0.9

Figure 105 shows the trend of dynamic storage modulus E' as a function of temperature for the PLA/PHB blends processed with different flow rates.

The blends processed at high flow rates exhibit higher E' values than the mixture obtained with 3 kg/h. In particular, at 40 °C the value is 2394 MPa and 2281 MPa at 5 kg/h and 7 kg/h, respectively, as compared to 1854 MPa in the blend processed at 3 kg/h. Furthermore, the dynamic storage modulus of PLA/PHB/3 blend shows a dramatic decrease at 60-70°C, due to the occurrence of the PLA glass transition [234] and an increase at about 100-110°C associable to the cold crystallization of PLA [235]. Interestingly, PLA/PHB/5 and PLA/PHB/7 exhibit a less pronounced decrease in modulus, resulting in a significant increase of the E' at high temperature. In fact, at 80°C PLA/PHB/5 blend shows a modulus of 857 MPa as compared to 20 MPa for PLA/PHB/3 mixture.

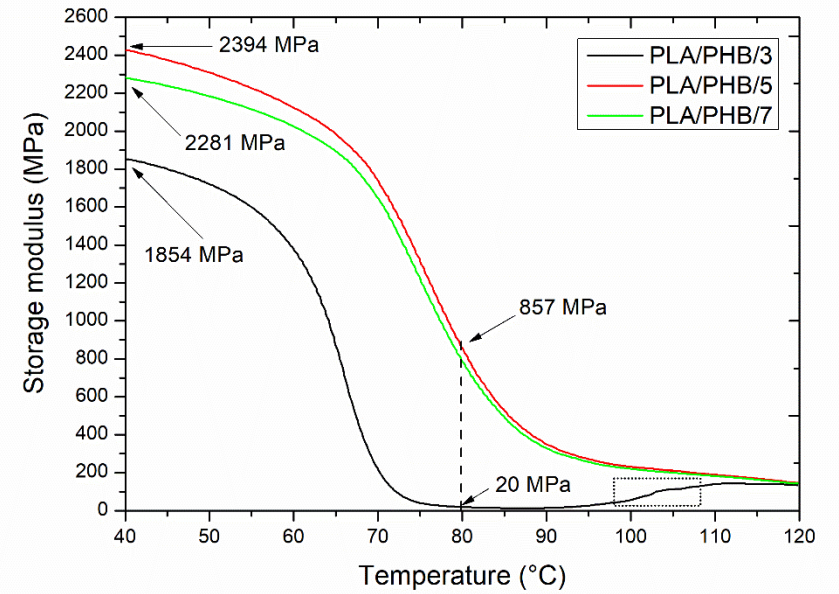

Figure 105. Storage dynamic modulus E' of blends PLA/PHB processed with different flow rates.

6.3.3 Variation of screw speed

In this section, PLA/PHB 70/30 blends are processed at 250, 400 and 550 rpm with screw configuration SP3, previously reported in Figure 95, at 3 kg/h; in Table 20 the codes of the PLA/PHB blends are reported. The values of the torque registered during the extrusion process are: 52 Nm, 40 Nm and 34 Nm for blends processed at 250, 400 and 550 rpm, respectively.

Table 20. Code of the PLA/PHB blends processed with SP3 at different screw speeds (250, 400, 550 rpm).

Composition	Code
PLA: 70 wt% and PHB: 30 wt% processed at 250 rpm	PLA/PHB/250
PLA: 70 wt% and PHB: 30 wt% processed at 400 rpm	PLA/PHB/400
PLA: 70 wt% and PHB: 30 wt% processed at 550 rpm	PLA/PHB/550

In Figure 106 the thermograms recorded during the second heating scan of the blends are reported. From the thermal analyses, regardless of the selected screw speed, T_g for both PLA and PHB and T_{cc} of PLA remain unchanged in all blends. Furthermore, the crystallinity degree X_{PLA} is 17% in the material processed at 250 rpm, whereas X_{PLA} is equal to 13% and 12 % in the blend obtained at 400 rpm and 550 rpm, respectively. In particular, this behaviour is more influent in the blend obtained with low screw speed which corresponds at high residence time process allowing to improve the interaction between the polymer phases.

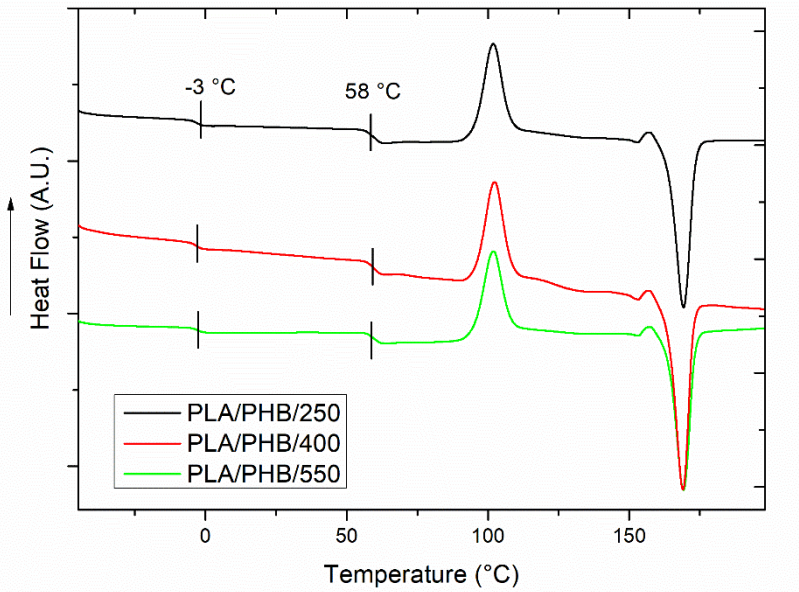

Figure 106. DSC thermograms of PLA/PHB blends processed at different screw speeds (250, 400 and 500 rpm).

The dynamic storage modulus E' recorded during DMA analyses are reported in Figure 107. E' results higher for the blends processed at 550 rpm than for the other ones. In particular, at 40 °C E' is 2113 MPa and 1942 MPa for the blends processed at 550 and 250 rpm, respectively; an intermediate value is found for the

blend obtained at 400 rpm. Nevertheless, the increases of E' is not particularly relevant; in fact, the improvement is of 8% in blend processed at 550 rpm. In addition, at high temperature the dynamic storage modulus is very similar in all mixtures.

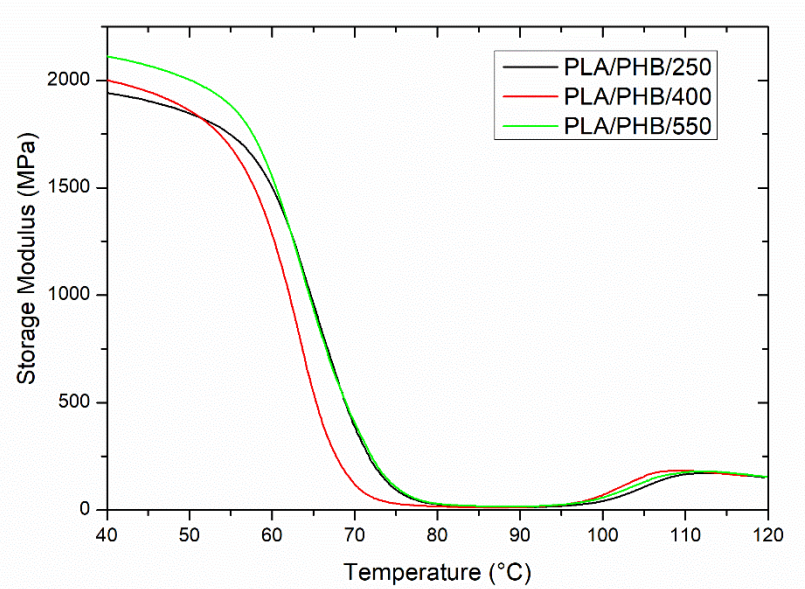

Figure 107. Dynamic storage modulus E' of PLA/PHB blends processed at different screw speeds (250, 400 and 500 rpm).

6.4 Influence of process parameters in PLA/PHB/Clay blend nanocomposite

In this section, the effect of process parameters on the final properties of a PLA/PHB blend (70 wt% of PLA and 30 wt% of PHB) filled with 5wt% of nanoclays was evaluated by concentrating on the combined action of the influence of process condition variations and the presence of the filler possibly acting as a compatibilizer of the immiscible polymer blend. In particular, it has been chosen to vary the screw configuration and the screw speed of the process.

The codes of filled systems are reported in Table 21. Two gravimetric feeders were used during the processing: a principal feeder for the polymers, which is positioned at the beginning of the screw, and a side feeder for the clay, added in the blend at a content of 5 wt%. The filled blends were processed using SP1, SP2 and SP3, whose schematic representations are above reported in Figure 95, at 400 rpm. In addition, maintaining fixed SP3, the screw speed was changed (250, 400 and 550 rpm).

Table 21. Code, composition and registered torque of the studied filled polymer blends.

Code	Process Conditions	Torque [Nm]
PLA/PHB/CL/1/400	Screw profile 1; 400 rpm	30
PLA/PHB/CL/2/400	Screw profile 2; 400 rpm	26
PLA/PHB/CL/3/400	Screw profile 3; 400 rpm	48
PLA/PHB/CL/3/250	Screw profile 3; 250 rpm	35
PLA/PHB/CL/3/550	Screw profile 3; 550 rpm	36

The morphology and the thermal and mechanical properties of the resulting materials, as well as the clay localization were evaluated. Additionally, a detailed study of the rheological response of the blend nanocomposites was performed, aiming at correlating the process parameters and the influence of the filler with the obtained material microstructure.

6.4.1. Thermodynamics of Clay localization

The thermodynamics localization of the filler can be predicted through the determination of the wetting coefficient ω_a, in a thermodynamic equilibrium state. It depends on the interfacial energies γ_{xy} where x or y is polymer A, polymer B or clay according to the Young's equation [161], which is defined as:

Equation 40. $$\omega_a = \frac{\gamma_{clay-polymerB} - \gamma_{clay-polymerA}}{\gamma_{polymerA-polymerB}}$$

If $\omega_a > 1$ the clay will be preferentially dispersed in polymer A, if $\omega_a < -1$ the clay be located in polymer B and for $-1 < \omega_a < 1$ the clay will be located at the interface between the polymers A and B. Since the determination of the interfacial energies between clay and polymers is difficult, these were estimated using surface energies, which consist of dispersive γ^d and polar γ^p components [162]. These two components of surface energy can be used to calculate interface energy using the harmonic-mean equation [163]. The calculation method of these components and the relative equations used to determine the value of wettability have been already presented in the section 4.1.2.4 of Chapter 4.

The total surface energy γ ($\frac{mN}{m}$) at room temperature (25°C) and at processing temperature (190°C), the dispersive γ^d ($\frac{mN}{m}$) and the polar γ^p ($\frac{mN}{m}$) components at 190°C of PLA, PHB and Cloisite 5 have been summarized in Table 22.

Table 22. Surface energy at room temperature and processing temperature for each component. Reprinted under CC BY 4.0 license from [221].

	Room Temperature	Process Temperature			
	γ ($\frac{mN}{m}$)	$-\frac{\partial\gamma}{\partial T}$ ($\frac{mN}{m°C}$)	γ^d ($\frac{mN}{m}$)	γ^p ($\frac{mN}{m}$)	γ ($\frac{mN}{m}$)
PLA	40.6 [236]	0.06 [236]	27.4	3.4	30.8
PHB	46.9 [237]	0.06 [237]	28.18	8.82	37
Cloisite 5	42.54 [238]	0.1 [239]	16.9	6	22.9

Based on the values of the surface tensions, the interfacial tension between pairs of components clay-polymer B, clay-polymer A and polymer A-polymer B, where polymer A is PLA and polymer B is PHB, was calculated according to the harmonic-mean and the geometric-mean equations and the data are shown in Table 23.

Table 23. Interfacial energies calculated from Harmonic-mean equation and Geometric-mean equation. Reprinted under CC BY 4.0 license from [221].

	Harmonic -mean	Geometric-mean
$\gamma_{clay\text{-}PHB}$	3.35	1.70
$\gamma_{clay\text{-}PLA}$	3.10	1.57
$\gamma_{PLA\text{-}PHB}$	2.35	1.23

The values of wettability, calculated through Equation 40, are 0.11 and 0.10; these values suggest that the organoclays are located at the interface between PLA and PHB, based on thermodynamic preference and a schematic representation of the nanoclays localization is reported in Figure 108.

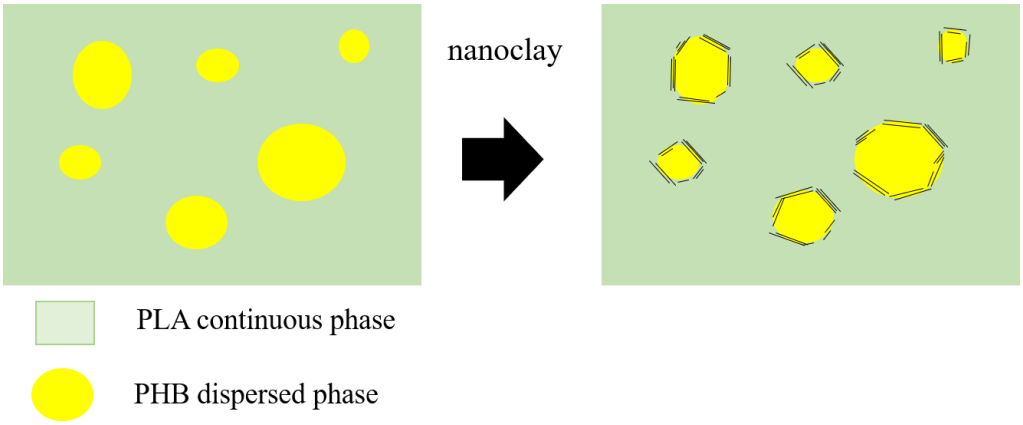

Figure 108. Schematic representation of the localization fillers at the interface between PLA and PHB.

6.4.1 Influence of screw profiles and screw speed

Figure 109 shows the results of thermal analyses of the unfilled blend and the filled blends processed with different screw profiles. In order to compare the results of the thermal characterizations and XRD analyses, the reported thermograms are those recorded during the first heating scan. This choice is related to the fact that a solid sample was used for the XRD analysis and the results obtained in the diffractograms are correlated to the thermal history of the materials recorded in the first heating scan of the DSC analysis.

In the filled blends the values of the T_g of PLA and PHB, the T_{cc} of PLA and T_m of PLA are unchanged compared to the unfilled sample.

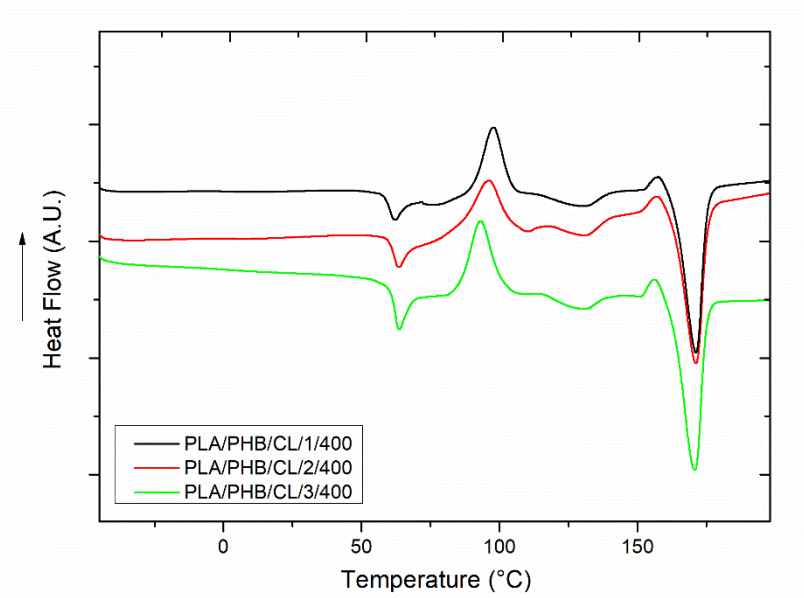

Figure 109. DSC thermograms recorded during the first heating scan for filled blends with different screw profiles. Reprinted under CC BY 4.0 license from [221].

Table 24 reports the main thermal properties, namely cold crystallization enthalpy (ΔH_{cc}), melting enthalpy (ΔH_m) and crystallinity degree (X) measured during the first heating ramp for all the formulations.

Regardless the selected screw profile and screw speed, the introduction of the clay nanoparticles induces a decrease of the crystallinity degree of PHB phase. On the contrary, a different behaviour can be observed regarding the influence of the embedded nanoclays on the crystallinity of PLA; in fact, the nanoparticles cause an increase of the crystalline content due to their well-known nucleating effect, facilitating the crystallization process [240]. However, this effect is more pronounced for blends processed with SP1 and SP3 and specially at high screw speed [241].

Table 24. Thermal properties of PLA, unfilled blend and filled systems with different screw profiles and screw speed. Reprinted under CC BY 4.0 license from [221]

	$\Delta H_{m(PLA)}$[J/g]	$\Delta H_{cc(PLA)}$ [J/g]	X_{PLA} [%]	$\Delta H_{m(PHB)}$[J/g]	X_{PHB} [%]
PLA	46	36	11	-	-
PHB	-	-	-	17	12
PLA/PHB	38	21	18	4	3
PLA/PHB/CL/1/400	36	17	22	5	4
PLA/PHB/CL/2/400	36	18	20	5	4
PLA/PHB/CL/3/400	39	19	23	6	4
PLA/PHB/CL/3/250	29	14	17	5	4
PLA/PHB/CL/3/550	40	19	24	5	4

In order to better study the dispersion of the embedded nanoclays in the systems, XRD analyses were carried out. Figure 110 shows the diffractograms obtained from XRD analysis relative to the neat PLA and PHB polymers and unfilled blend. Regarding the neat PHB, the diffractogram exhibits two peaks at 2θ=13.9° and 16.8° associable with the (020) and (110) of orthorhombic unit cell respectively [242] [243]; conversely, PLA shows an amorphous structure [244].

The diffractogram of the unfilled PLA/PHB polymer blend is similar to that of neat PHB and a peak at about 19° attributable to the PLA phase, appears. This peak is usually present in fully crystallized PLA samples, indicating that the addition of PHB crystal particles significantly improves the crystallinity and the crystallization rate of PLA, according with the results of thermal analyses which suggested an increase in the X_{PLA} in the blend [245].

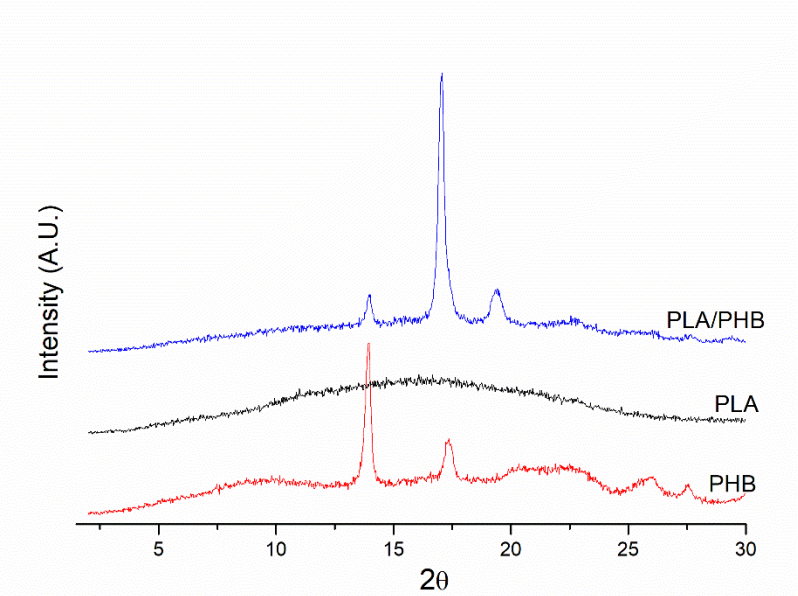

Figure 110. XRD pattern of PLA, PHB and PLA/PHB blend. Reprinted with the permission from [221]. Reprinted under CC BY 4.0 license from [221].

Figure 111(a) reports the diffractogram of filled blends processed with different screw profiles. Interestingly, the ratio between the intensities of the peaks related to PHB is different with respect of neat polymer, indicating a modification of the PHB crystal structure resulting from the interactions between PHB and PLA [245]. The clay particles exhibit a distinct peak at about 2θ=7°, corresponding to a distance between layers calculated by Bragg's law [246] of d_{001}=1.26 nm, and two further peaks at 2θ=19.7° and 22°. Nevertheless, to investigate the interaction of the clay with polymers, it is fundamental the analysis of the first peak. In filled blends obtained with SP1 and SP3 the interlayer distance corresponds to d_{001}=1.77 nm. Differently, in filled blend processed with SP2 a value of d_{001}=1.47 nm was obtained. Among the blend processed with SP3 at different screw speed, as reported in Figure 111 (b), the filled blend obtained with screw speed of 250 rpm exhibits an interlayer distance slightly lower, d_{001}=1.67 nm, as compared to the blends processed at 400 and 550 rpm.

The observed increase of the interlayer distance in filled blends can be associated with the insertion of polymer chains between the clay platelets, leading to the formation of an intercalated structure [247]. The obtained results suggest that SP1 and SP3 allow a good dispersion of the filler by promoting a better intercalation of the polymers in the nanoclay structure, especially at high screw speed.

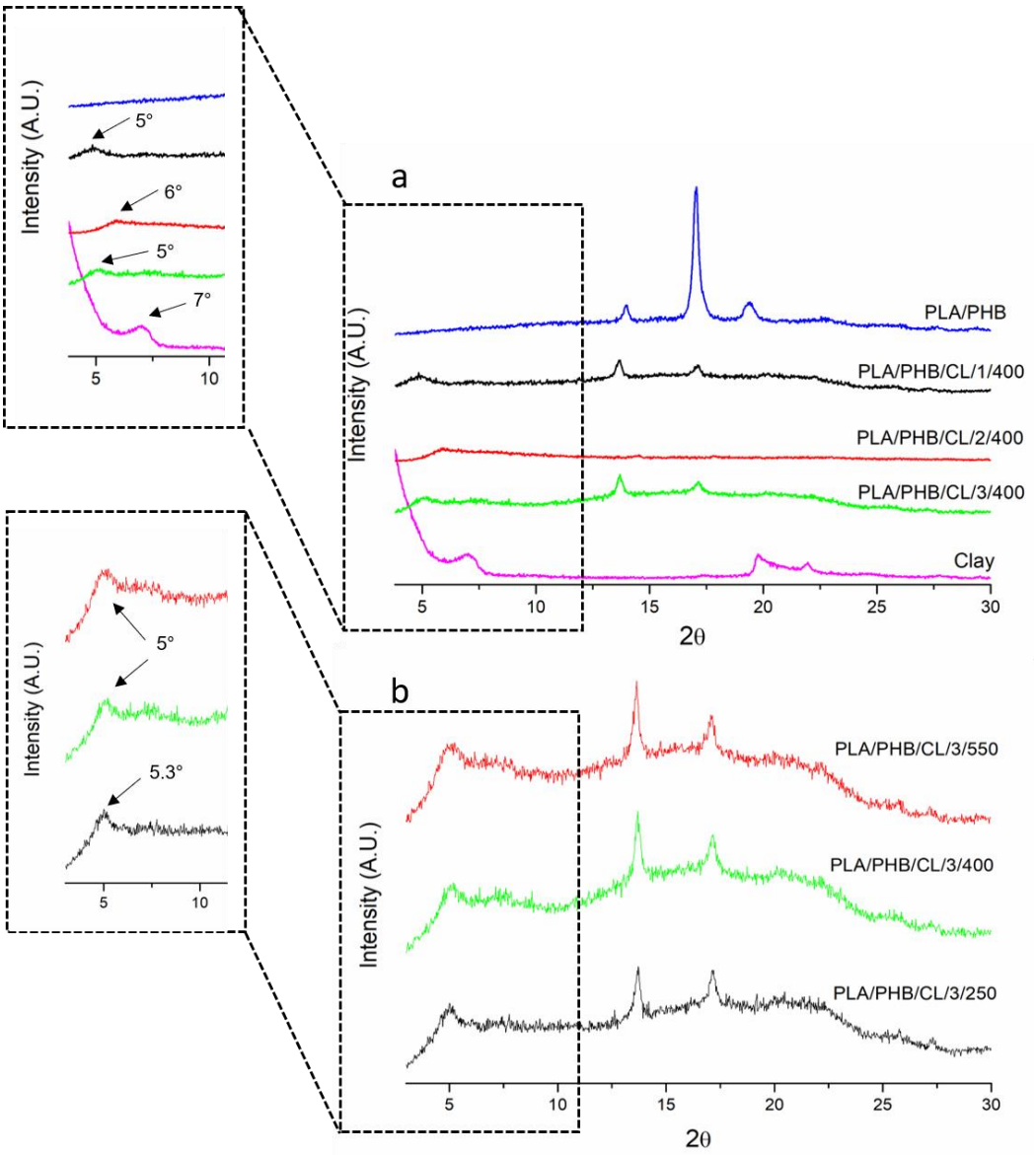

Figure 111. XRD pattern of Clay, PLA/PHB unfilled blend and filled blend processed with SP1, SP2 and SP3 (a) and PLA/PHB filled blends processed with SP3 at different screw speed (b). Reprinted under CC BY 4.0 license from [221].

Concerning the study of the rheological behaviour of the systems, Figure 112 reports the trend of G' as a function of the frequency for unfilled and filled blends. An increase of the G′ modulus can be observed in all filled blends, as compared to the values of the unfilled blend, and this finding is more pronounced in the low frequency region. Filled blends, regardless of the adopted screw configurations, exhibit a remarkable different trend of G′ as a function of the frequency as compared to the unfilled blend and the disappearance of the shoulder at low and intermediate frequencies can be noticed. This different behaviour can be attributed to the

occurrence of strong polymer–filler interactions, promoting an improved blend morphology with respect to the unfilled systems [248]. Looking at the differences between the filled blends processed with the different screw configurations, in the cases of the SP1 and SP3, the rheological responses at low frequencies are different, and a lowering of the slope in the terminal region is observed.

Figure 113 shows the trend of G′ of the formulation obtained using SP3, processed at different screw speeds. At low frequencies the filled blend processed at 250 rpm shows a lower G′ value than those obtained at 400 and 550 rpm; therefore, an increase of screw speed improved the interaction filler-polymers, and consequently an increase of G′ value [249], nevertheless, an invariance in the trend of the storage modulus in the three cases is reported.

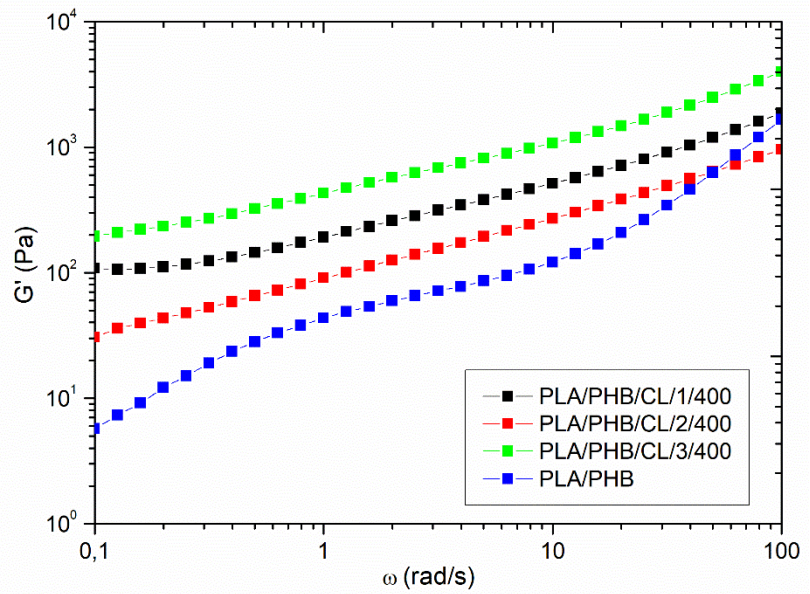

Figure 112. Trend of storage modulus G' of filled blends with different screw profiles and unfilled blend (a) and filled blend processed with SP3 at different screw speeds (b). Reprinted under CC BY 4.0 license from [221].

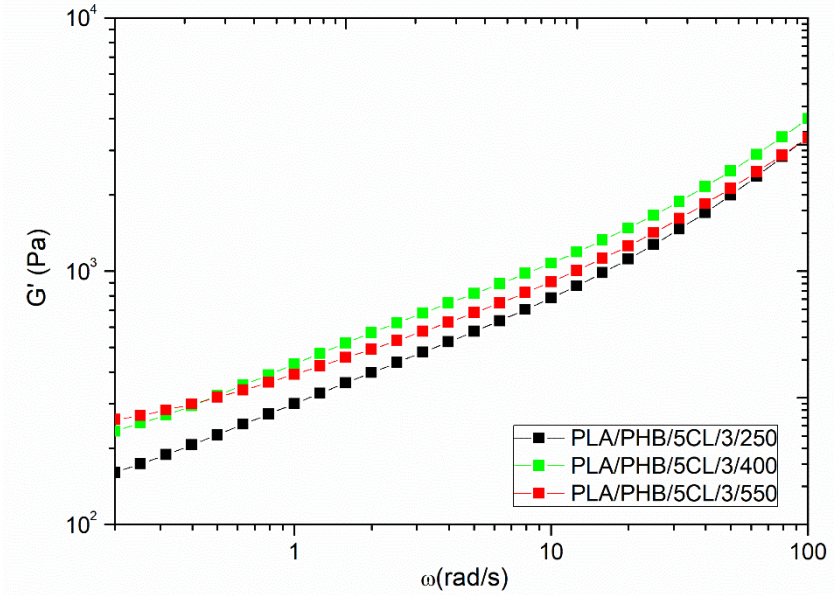

Figure 113. Trend of storage modulus G' of filled blends processed at different screw speed 250, 400 and 550 rpm. Reprinted under CC BY 4.0 license from [221].

To further investigate the low-frequency behaviour of the filled blends obtained with different screw profiles, the slope (α) of the G' trends as a function of frequency was calculated and the data points obtained are reported in Figure 114.

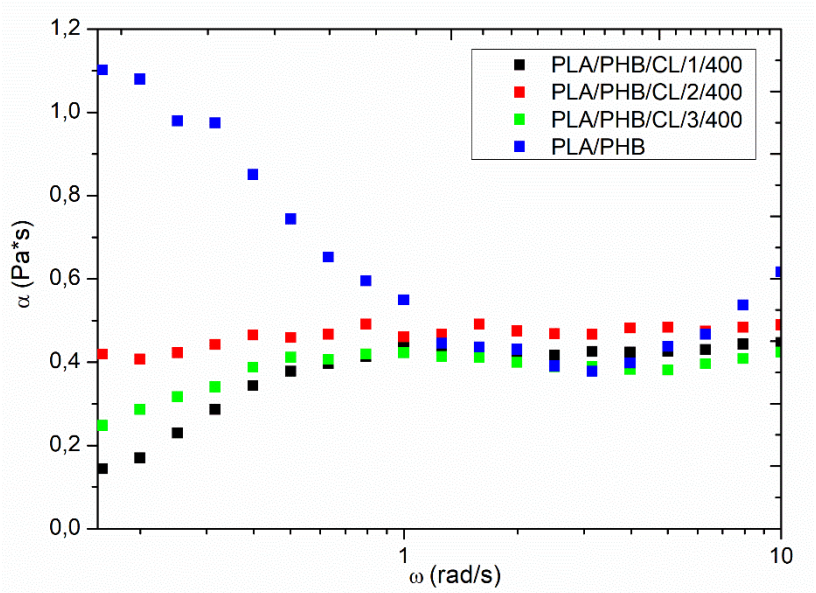

Figure 114. Evolution of slope α as a function of frequency in filled blends obtained with different screw profiles and unfilled blend. Reprinted under CC BY 4.0 license from [221].

The curve of the unfilled blend shows a progressive decrease of the G′ slope with increasing the frequency, reflecting the relaxation of a single dynamic specie related to the droplets constituting the dispersed phase. Differently, the curves of the filled blends exhibit a different response. In particular, at high frequencies the slope of G' have the same trend of the unfilled blend; however, α remains almost

constant up to 1 rad/s of frequency and it decreases for lower frequency ($\omega < 1$ rad/s). This result can be associated to the reduced mobility of the interface due to the presence of the filler [207].

The representation of weighted relaxation spectra ($\lambda H(\lambda)$) of the filled and unfilled blends processed with different screw profiles are plotted in Figure 115 in order to distinguish any changes in the microstructure of a multi-component polymer-based system through the discrimination of the different relaxation process [250].

PLA/PHB blend shows a peak between 1 and 10 s (at about 3 s) attributable to the shape-relaxation of the PHB dispersed droplets [208]. In addition, a rapid decrease of the $H(\lambda)$ function is observed at longer times, indicating the fully relaxation of the PHB droplets in the considered time interval. It is important to note that the peak associated with the relaxation of PLA macromolecules is not present due to their very fast relaxation time ($10^{-3} < t < 10^{-2}$) [251].

As far as the PLA/PHB/CL system processed with screw SP2 is concerned, the relaxation spectrum is very similar to that of the unfilled blend, notwithstanding the shift of the peak related to the shape relaxation of PHB particles towards longer times; this feature can be associated with the slowing down of the relaxation dynamics of the droplets of the dispersed phase, induced by the presence of the embedded clay particles. This result suggests that the screw configuration SP2 is not able to induce remarkable alteration of the material morphology, which remained almost unchanged with respect to that of the unfilled blend. A very different behaviour can be observed for the filled blends obtained with SP1 and SP3. In fact, the peak associated with the relaxation process of the droplets of the dispersed phase is broader as compared to that of the unfilled blend, indicating the presence of various dynamic species relaxing at different times, associable with several populations of PHB particles characterized by different shapes and sizes. In addition, this peak is shifted towards longer times with respect to the unfilled blend, with the formation of a distinct tail at high relaxation times; this finding suggests that the relaxation mechanism of the particles of the dispersed phase is not fully completed in the investigated time range.

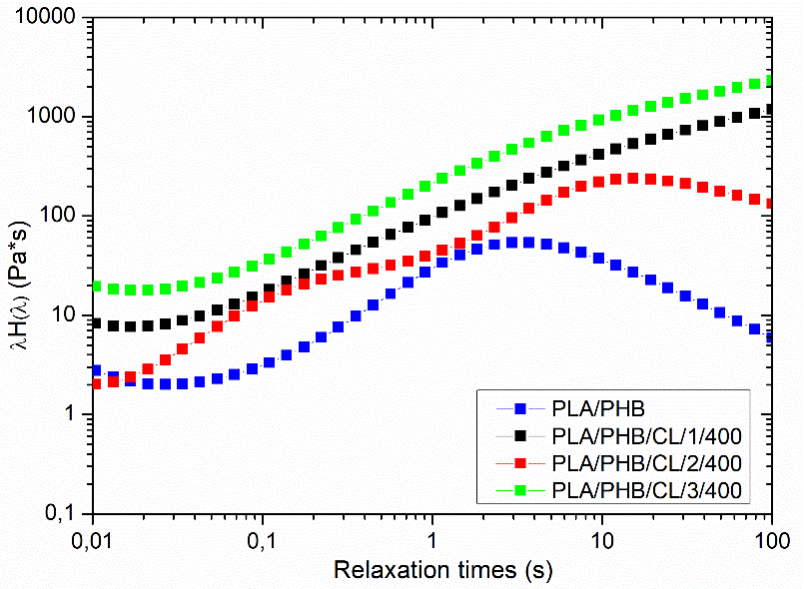

Figure 115. Weighted relaxation spectra for unfilled and filled blends processed with different screw profiles. Reprinted under CC BY 4.0 license from [221].

In fact, looking at the Figure 116(b) and Figure 116(d) which report the micrographs of the filled blends obtained through the different screw profiles it is possible to notice that the filled blend obtained with SP2 shows a droplets configuration: during the fracturing most of the PHB particles remained in the structure, while others were pulled out, leaving empty cavities on the surface. Despite this, a weak improvement of the morphological structure of this filled blend compared to the unfilled one can be observed. Conversely, in the filled blends processed by SP1 and SP3, a clear modification of the microstructure is observable. In particular, no droplet structures are observable at the investigated magnification level. As expected, a refinement of the morphology can be noticed in these formulations due to specific design of the screw profiles that allows a good polymers/clay interaction level with the consequent formation of intercalated structures of polymer chains into the clay, as already discussed in XRD results. This result, which is different from that found in the study of different screw profiles in unfilled blends reported in the paragraph 6.3.1, is a consequence of the coupled effect of the nanoclays presence and the selected screw configuration: the flow conditions established during processing due to the presence of mixing elements in SP1 and backflow in SP3 which induce high shear stresses during the processing, cause the achievement of a good interaction between filler and polymers [251] [232], promoting the obtainment of a refined morphology. This phenomenon does not occur with SP2, probably due to the absence of mixing elements that do not promote optimal miscibility in polymers-filler systems.

Concerning the screw speed variation, (see micrographs reported in Figure 116(d)-(f)) a reduced impact on the modification of the material morphology, as compared to the variation of screw profile, is found.

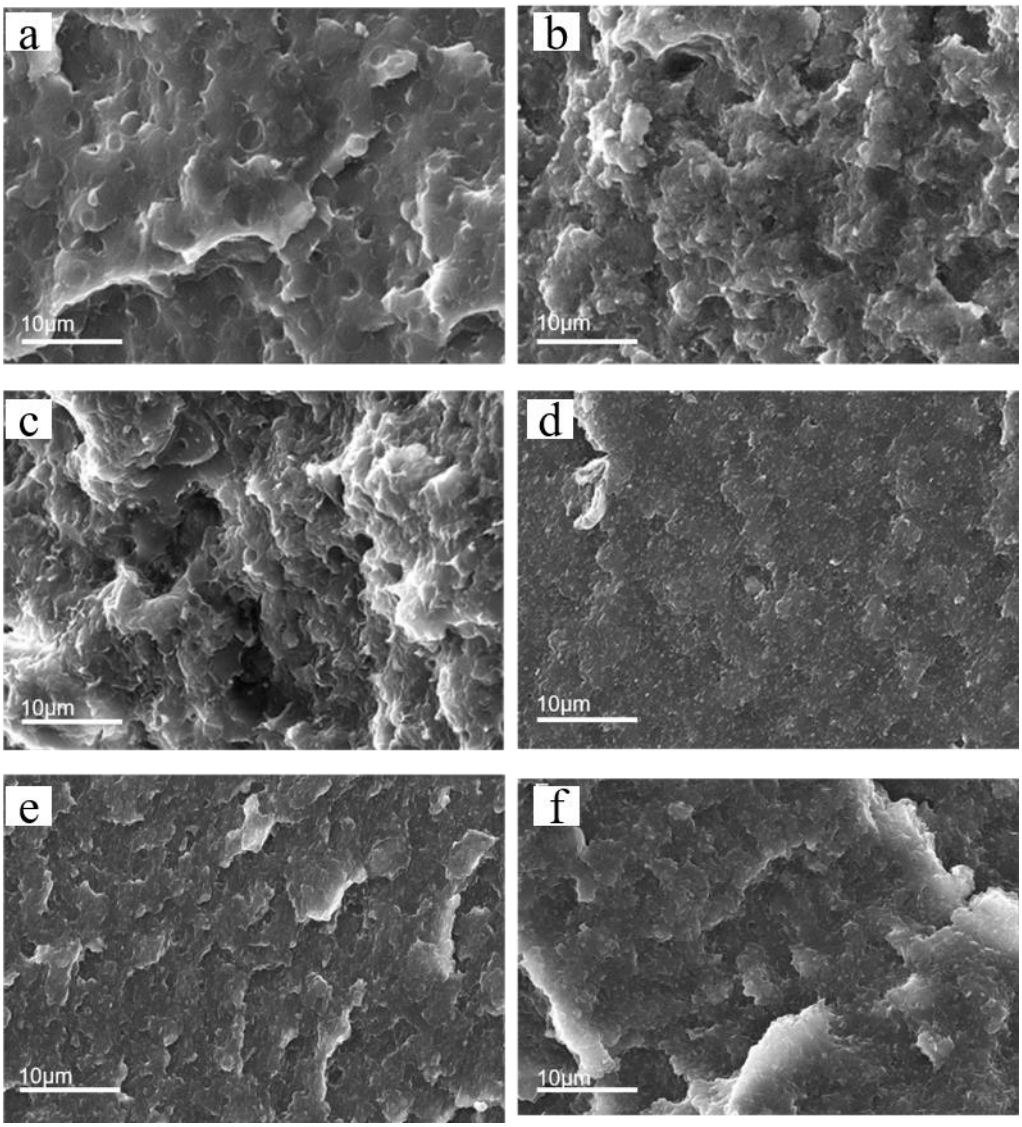

Figure 116. SEM micrographs of: unfilled PLA/PHB blend (a), PLA/PHB/CL/1/400 (b), PLA/PHB/CL/2/400 (c), PLA/PHB/CL/3/400 (d), PLA/PHB/CL/3/250 (e) and PLA/PHB/CL/3/550 (f). Reprinted under CC BY 4.0 license from [221].

Dynamic thermo-mechanical analyses were carried out and Figure 117 reports the curves of E' for unfilled and filled blends. All the filled samples show, as expected, an increase of the modulus value, as compared to their unfilled counterparts, due to the reinforcing effect of the well-dispersed nanoclays [252]. In particular, in the cases of the filled blends obtained with SP1 and SP3, the increase of the modulus at 40 °C is about of 20%, whereas in the filled blends processed using SP2, this improvement is only about 9%. This finding confirms that SP1 and SP3 have a more noticeable effect on the final microstructure of the blends by inducing an enhancement also on the thermo-mechanical properties of the filled blends as compared to SP2.

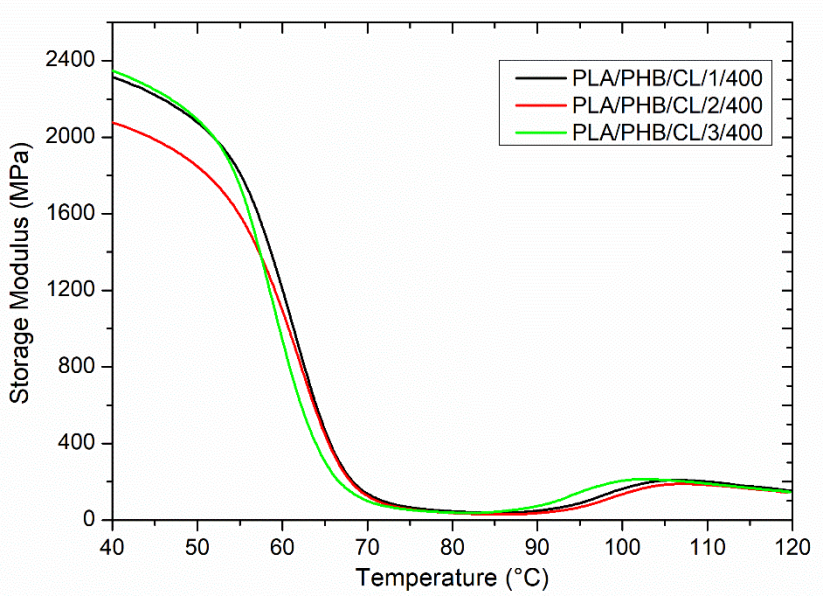

Figure 117. DMA traces for filled blend processed with different screw profiles and unfilled blend. Reprinted under CC BY 4.0 license from [221].

Table 25 shows the values of tan delta and storage modulus at 40 °C of all the filled blend. The values of dynamic storage modulus in the blend processed at high screw speed (400 and 550 rpm) are slightly higher as compared to the blend obtained at 250 rpm.

Table 25. Thermo-mechanical properties of filled blends. Reprinted under CC BY 4.0 license from [221].

	$T_{tan\ delta}$ [°C]	Modulus [MPa] @ *40°C*
PLA/PHB/CL/1/400	73	2310
PLA/PHB/CL/2/400	73	2064
PLA/PHB/CL/3/250	71	2245
PLA/PHB/CL/3/400	72	2326
PLA/PHB/CL/3/550	72	2294

Chapter 7

Development of ternary biopolymer blends

7.1 Introduction

The study and the development of polymer blends based on three different components has raised the attention of both the industrial and the academic world in the last years [253] [254] [255] [256]. The advantages related to the presence of a third polymer phase introduced in an immiscible blend was widely discussed in the Chapter 4 among the methods of non-reactive compatibilization. Most studies on multiphase blends showed that the microstructure can be predicted knowing the interfacial tension between polymers [257] [254] [258] .

A prediction of the phase structure forming in a multi-component system, proposed by Hobbs *et al*. [259] based on the calculation of the spreading coefficient λ_{ABC} in ternary polymer blends composed by A, B and C polymer phases, has been before discussed. Details about the theoretical study of spreading coefficient are previously reported in the Paragraph 4.1.2.3 of Chapter 4.

In this Chapter, immiscible PLA/PBS/PHB ternary polymer blends were studied. The systems were developed using a co-rotating twin screw Thermo Fisher Scientific Process 11 extruder. The selected screw configuration, reported in Figure 118 involves three kneading blocks combined with conveying elements designed for materials transport. Details about the used device and the materials are reported in the Appendices A.2 and A.1.1, respectively.

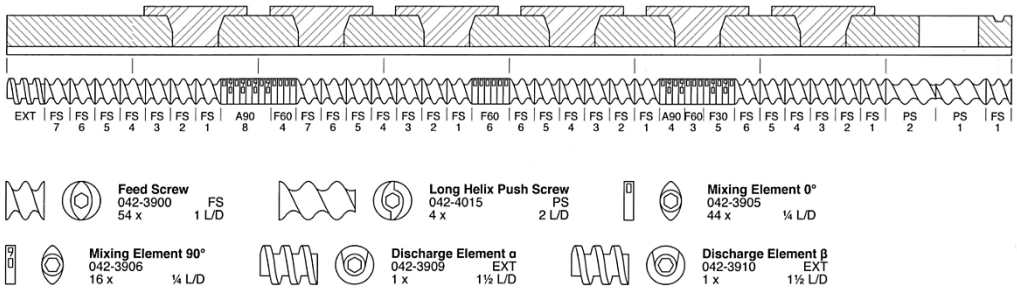

Figure 118. Schematic representation of co-rotating twin-screw extruder.

The main focus of this part of the research was to enhance the mechanical properties of the systems and, particularly, the elongation at break by controlling the morphology. A preliminary study of the interfacial properties of the polymers through contact angle measurements was performed. Thermal analyses, morphological investigations and rheological and mechanical measurements of PLA/PBS/PHB blends based on PLA as matrix have been carried out. To conclude the study, a further type of PHB, and after coded as PHBt, was used in the blends with different weight contents of PLA and PHB polymers by maintaining constant the PBS content at 30 wt%.

7.2 Study of interfacial properties: contact angle analysis and spreading coefficient measurements

The miscibility between pairs of polymers can be predicted by surface free energy calculations using various methods and theories; here, the surface energies of PLA, PBS, PHB and PHBt have been evaluated via contact angle measurements using water and diiodomethane as test liquids.

The value of surface energy and polar and dispersive components of surface energy of the two solvents are listed in Table 26 [260] where γ^p, γ^d and γ are the polar, dispersive and total energy surface components, respectively.

Table 26. Surface tension of water and diiodomethane [260].

	$\gamma^{\mathrm{p}}\ (\frac{mN}{m})$	$\gamma^{\mathrm{d}}(\frac{mN}{m})$	$\gamma\ (\frac{mN}{m})$
water	51	21.8	72.8
diiodomethane	2.3	48.5	50.8

Owens-Wendt-Rabel-Kaelble developed a method [164] [261], named OWRK-method, which is used for the calculation of polar and dispersive components and total energy surface of each polymer through the Equation 41.

Equation 41.

$$\frac{(1+cos\theta)*\gamma_l}{2\sqrt{\gamma_l^d}} = \sqrt{\gamma_s^p} * \sqrt{\frac{\gamma_l^p}{\gamma_l^d}} + \sqrt{\gamma_s^d}$$

where γ_s is the unknown surface tension of the solid and γ_l is the surface tension of liquid represented by water and diiodomethane; θ is the measured contact angle using the two different solvents. Finally, γ^d and γ^p correspond to the dispersive and polar components, respectively.

Table 27 reports the values of measured contact angle values and surface tension, polar and dispersive component, calculated through Equation 1 for PLA, PBS and both PHB samples. The total surface tension γ is equal to the sum of γ^p and γ^d.

Table 27. Contact angle and surface tension of the polymers.

Sample	Contact angle (°)		Surface tension ($\frac{mN}{m}$)		
	Water	Diiodomethane	γ^p	γ^d	γ
PLA	57	45	19.7	27.7	47.3
PBS	69	34	8.9	36.2	45.2
PHB	72	40	8.2	33.8	42.1
PHBt	96.2	57.1	1	29.2	30.3

It is known that lower contact angle with water is characteristics for materials with higher surface wettability and hydrophilicity. From the values reported in Table 2 it is possible to deduce that PLA presents a hydrophilic character, PBS and PHB show intermediate contact angle values, indicating a less pronounced hydrophobic character as compared to the PHBt polymer which is the most hydrophobic polymer.

The highest value of polar component is observed for PLA and the lowest for PHB, particularly PHBt which is characterized by a very low value of polar component: 1($\frac{mN}{m}$). This finding indicates non-polar PHBt surface and the possibility of establishing interaction at interface mainly by dispersive forces.

In order to study the interaction between the polymers constituting the ternary blends which will be analysed in this chapter, the values of interfacial tension of the polymer pairs have been calculated by the Equation of Wu [163] defined as follow:

Equation 42.

$$\gamma_{12} = \gamma_1 + \gamma_2 - 4\left(\frac{\gamma_1^d\gamma_2^d}{\gamma_1^d+\gamma_2^d} + \frac{\gamma_1^p\gamma_2^p}{\gamma_1^p+\gamma_2^p}\right)$$

where γ_{12} is the interfacial tension between materials 1 and 2, γ_1 and γ_2 are the surface tension of the two components. The values of interfacial tension for the polymer pairs are reported in Table 28.

Table 28. Interfacial tension of the polymer pairs in the two different studied systems. In red and grey the polymer pairs with poor and strong interfacial adhesion, respectively.

	Polymer pairs	Interfacial tension ($\frac{mN}{m}$)
1st system	PLA-PBS	5.21
	PLA-PHB	5.34
	PBS-PHB	0.31
2th system	PLA-PBS	5.21
	PLA-PHBt	17
	PBS-PHBt	7.25

It is known that a high value of interfacial tension corresponds to a poor adhesion between the polymeric phases. In the studied systems, the highest value of interfacial tension is obtained for PLA-PHB pairs, regardless the type of used PHB, notwithstanding the significantly higher value achieved for PHBt. This result indicates a poor level of interaction and poor miscibility between PLA and PHB polymers. In PLA/PBS/PHB blends the lowest value of interfacial tension, thus high interfacial adhesion is achieved between PBS and PHB; conversely, in PLA/PBS/PHBt systems good adhesion is found between PLA and PBS phases.

Based on the calculation of interfacial tension data, it is possible to predict the morphology of the ternary systems through the calculation of the spreading coefficient λ. Therefore, using the values reported in Table 3, the calculation of the set of three spreading coefficient for PLA/PBS/PHB and PLA/PBS/PHBt systems has been performed as follow:

- PLA/PBS/PHB blends:

$$\lambda_{PHBH-PLA-PBS} = \gamma_{PBS-PHBH} - \gamma_{PLA-PHBH} - \gamma_{PLA-PBS} = -10.24$$
$$\lambda_{PHBH-PBS-PLA} = \gamma_{PLA-PHBH} - \gamma_{PBS-PHBH} - \gamma_{PLA-PBS} = -0.17$$
$$\lambda_{PLA-PHBH-PBS} = \gamma_{PLA-PBS} - \gamma_{PLA-PHBH} - \gamma_{PBS-PHBH} = -0.44$$

- PLA/PBS/PHBt blends (PLA-based blends):

$$\lambda_{PHBH-PLA-PBS} = \gamma_{PBS-PHBH} - \gamma_{PLA-PHBH} - \gamma_{PLA-PBS} = -14.88$$
$$\lambda_{PHBH-PBS-PLA} = \gamma_{PLA-PHBH} - \gamma_{PBS-PHBH} - \gamma_{PLA-PBS} = 4.47$$
$$\lambda_{PLA-PHBH-PBS} = \gamma_{PLA-PBS} - \gamma_{PLA-PHBH} - \gamma_{PBS-PHBH} = -19$$

- PLA/PBS/PHBt blends (PHBt-based blends):

$$\lambda_{PLA-PHBH-PBS} = \gamma_{PLA-PBS} - \gamma_{PLA-PHBH} - \gamma_{PBS-PHBH} = -19$$
$$\lambda_{PLA-PBS-PHBH} = \gamma_{PLA-PHBH} - \gamma_{PLA-PBS} - \gamma_{PBS-PHBH} = 4.47$$
$$\lambda_{PHBH-PLA-PBS} = \gamma_{PBS-PHBH} - \gamma_{PLA-PHBH} - \gamma_{PLA-PBS} = -14.88$$

In PLA/PBS/PHB blends where PLA is the continuous phase, the three spreading coefficients are negative; this finding can be related to a partial wetting between the dispersed phases PBS and PHB which have demonstrated to have a good compatibility.

Conversely, in PLA/PBS/PHBt systems with PLA and PHB as matrix, the values of spreading coefficients indicate a complete wetting morphology where the liquid drop completely spreads and the dispersed phases are encapsulated within each other.

7.3 PLA/PBS/PHB blends

PLA/PBS/PHB blends at different weight contents of polymers were studied and the explored formulations are reported through the support of a ternary diagram in Figure 119 where A, B and C represent PLA, PBS and PHB phase, respectively. In the systems the PLA polymer was maintained as the matrix, as in the previous experimental studies (Chapter 5 and 6), while PHB and PBS were the dispersed phases. The process parameters used during the processing are reported in Table 29.

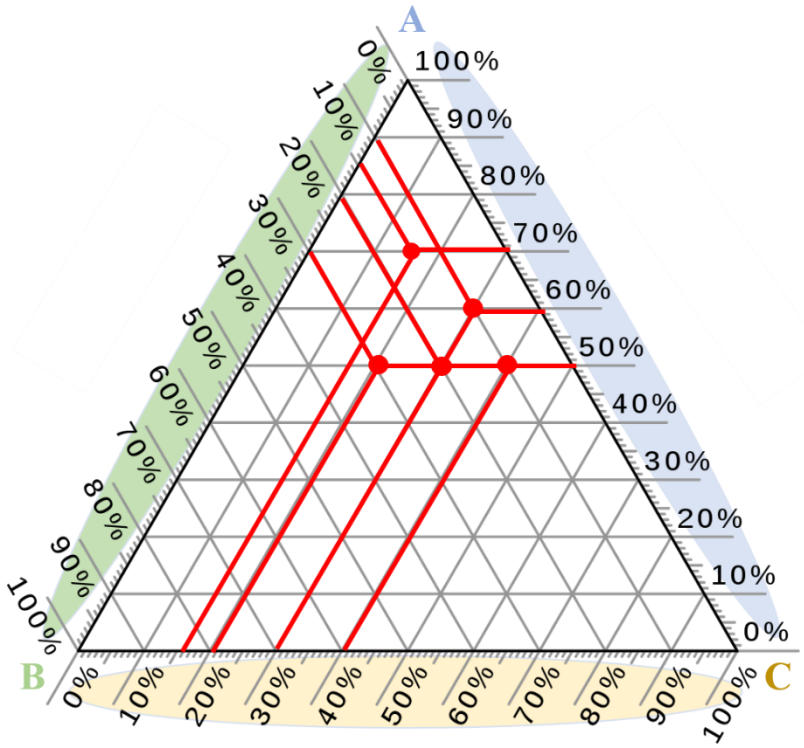

Figure 119. Ternary diagram of the explored PLA/PBS/PHB blends.

Table 29. Extrusion process parameters of PLA/PBS/PHB polymer blends.

	Feed rate [g/h]	Screw speed [rpm]	Melt temperature [°C]	Pressure [bar]	Torque [%]
70/15/15	380	350	170	19	44
60/30/10	340	350	170	27	45
50/20/30	400	350	170	19	40
50/30/20	340	350	170	17	44
50/40/10	450	350	170	22	40

7.3.1 Thermal analyses

Figure 120 reports the thermogram recorded during DSC analyses for PBS polymer. The values of $\Delta H°_{PBS}$, is reported in Appendix A (A.3.1 Differential scanning calorimetry DSC). Concerning the thermal characteristics of PLA and PHB has already been shown and discussed in Chapter 5.

An exothermic peak at 85°C during cooling ramp, associable to the crystallization of the polymers [262] and a bimodal endothermic peak at 104 °C and 114 °C corresponding to melting, in the second heating scan can be observed. The presence of the double peak can be related to the reorganization process of two different types of lamellar crystals and to the presence of two populations of lamellae [263].

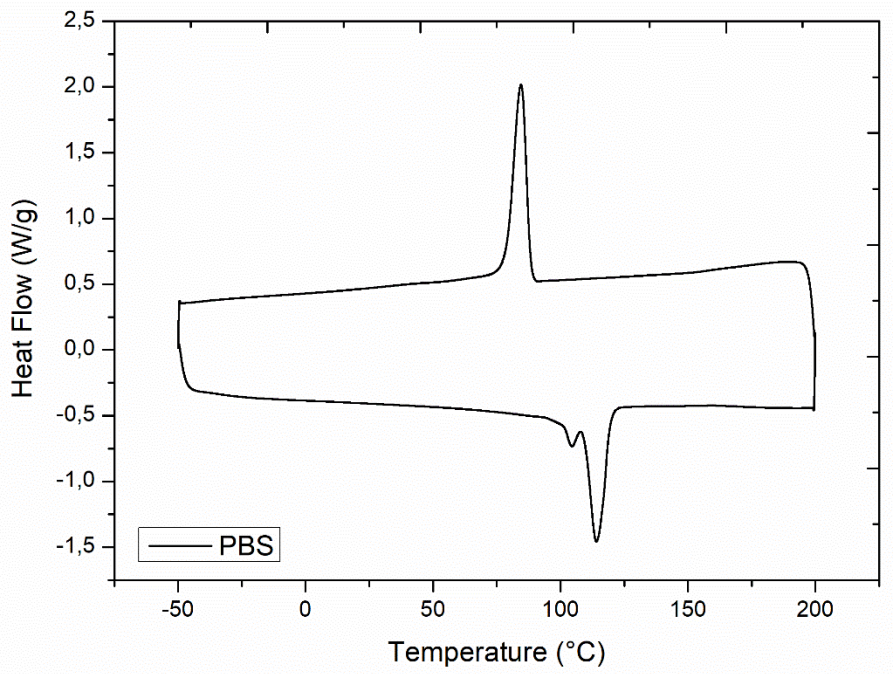

Figure 120. DSC traces recorded during cooling and second heating ramp of PBS polymer.

Figure 121 and Figure 122 report the thermograms for the blends recorded during the cooling and the second heating scan, respectively. Concerning the cooling scan, all the blends show a peak at 80°C, attributable to the crystallization process of the PBS phase. The crystallization temperature is slightly reduced compared to the neat PBS, indicating the decreased crystallization degree of PBS in the presence of PLA and PHB [155].

In Figure 122, the T_g of PLA remains constant at 58 °C. Furthermore, a cold crystallization peak at 98 °C and two different endothermic peaks at 114°C and 169 °C, attributable to the cold crystallization of PLA and melting of PBS and PLA phases, respectively, can be noticed. Furthermore, in the samples with larger amount of PHB (i.e. 20 and 30 wt%) a peak at 132°C, related to the melting of PHB is observable.

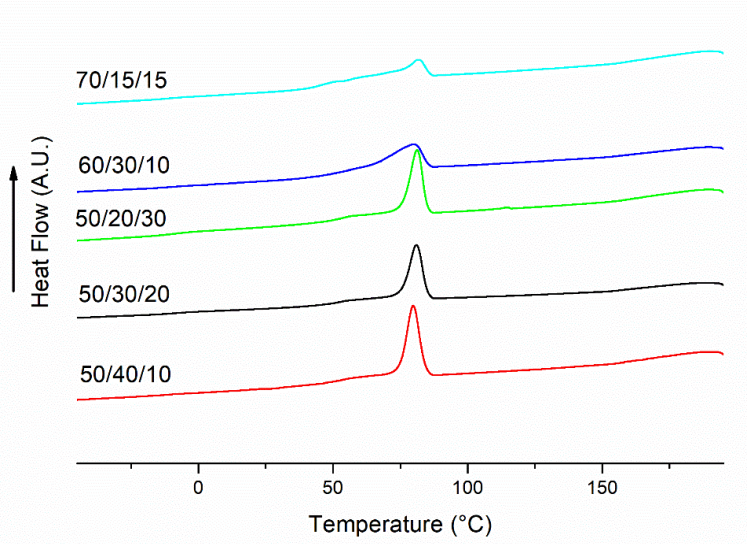

Figure 121. DSC traces recorded during cooling ramp of PLA/PBS/PHB polymer blends.

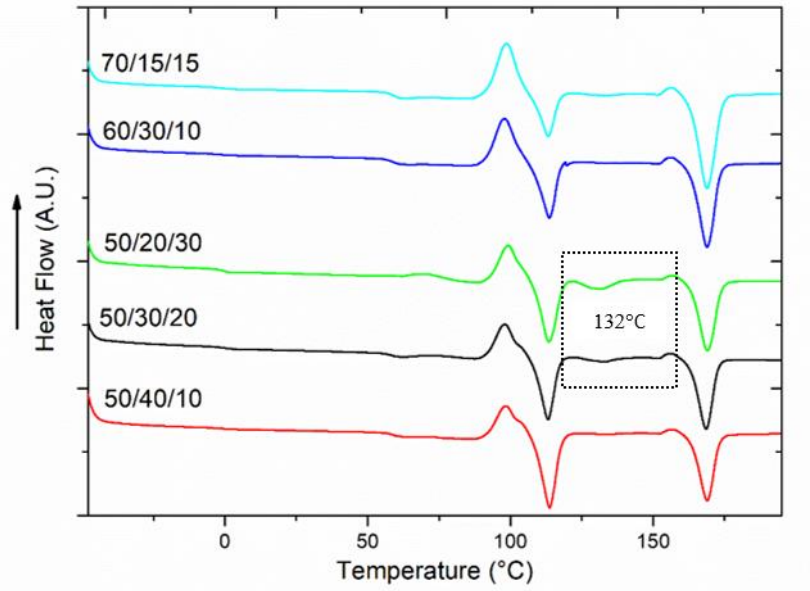

Figure 122. DSC traces recorded during second heating scan of PLA/PBS/PHB polymer blends.

Table 30 reports the value of crystallinity degree of PBS and PLA polymers. In the blends the degree of crystallinity both for PBS and PLA polymers is lower than those of neat polymers. The presence of PBS limited the crystallization of PLA mainly in the case of systems with high content of PBS (30 wt% and 40 wt%); but the crystals growth is more significantly suppressed in PBS due to the presence of PLA phase especially in 70/15/15 blend. Thus, the variation of crystallization degree is strictly connected to the weight content of PLA and PBS in the systems.

Table 30. Thermal properties of PLA and PBS neat polymers and PLA/PBS/PHB blends.

	ΔH_{mPLA} [J/g]	ΔH_{ccPLA}[J/g]	ΔH_{mPBS} [J/g]	X_{PLA} [%]	X_{PBS} [%]
PLA	39	23	-	17	-
PBS	-	-	49	-	44
70/15/15	34	18	11	17	10
60/30/10	30	16	18	15	16
50/20/30	25	11	14	15	12
50/30/20	22	12	16	11	14
50/40/10	22	12	21	11	19

7.3.2 Rheological measurements and morphological investigations

Figure 123 (a) and (b) report the trends of the complex viscosity η* and of the storage modulus G' for neat PLA, PBS and PHB. PBS shows a Newtonian plateau at low frequencies and a shear thinning behaviour at high frequencies. In Figure 123 (b) the G' trend of PBS presents the increase of the modulus with the frequency.

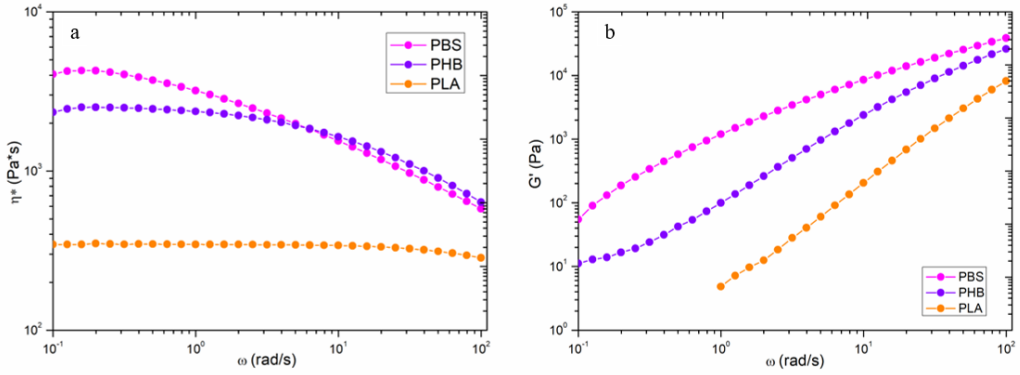

Figure 123. Complex viscosity η* and G' trends of neat polymers PLA, PBS and PHB.

Ternary polymer systems show complex viscosities trend characterized by a well-extended Newtonian behaviour in the whole investigated frequency range, as reported in Figure 124. Furthermore, the values of η* are dependent on the relative content of each polymer in the blend. In fact, 50/40/10 ternary blend exhibits higher value of η* as compared to the other systems, because of the high content of PBS; differently, the 70/15/15 system shows lower values of complex viscosity due to the large content of PLA.

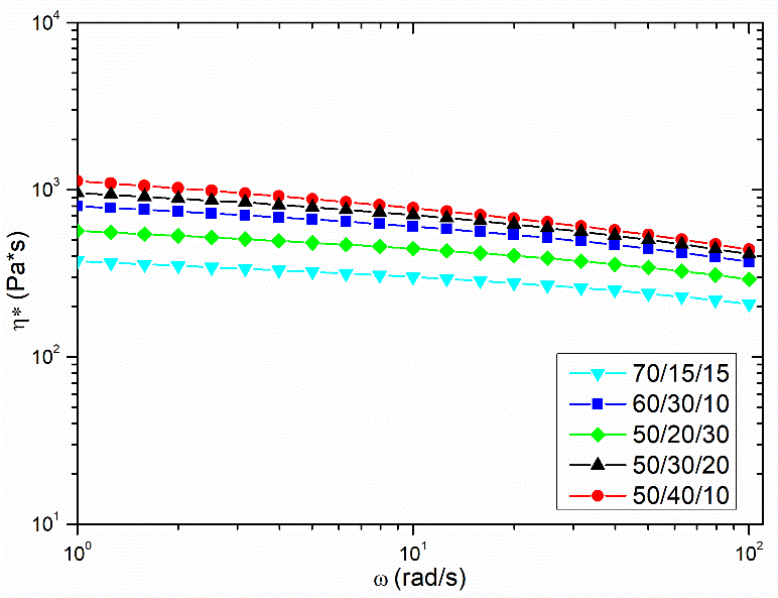

Figure 124. Complex viscosity η* of PLA/PBS/PHB polymer blends.

Similarly to what observed for the η* values, looking at the curves reported in Figure 125, the blends exhibit values of G' intermediate between those of the single components, according to the relative content of PLA, PBS and PHB in the exploited formulations. Ternary systems exhibit the typical rheological response of a miscible blends; in fact, the shoulder in the G' curve, observed up to now in the PLA/PHB immiscible system, is not present. This finding can be related to the presence of PBS phase that enhance the compatibility between the polymers.

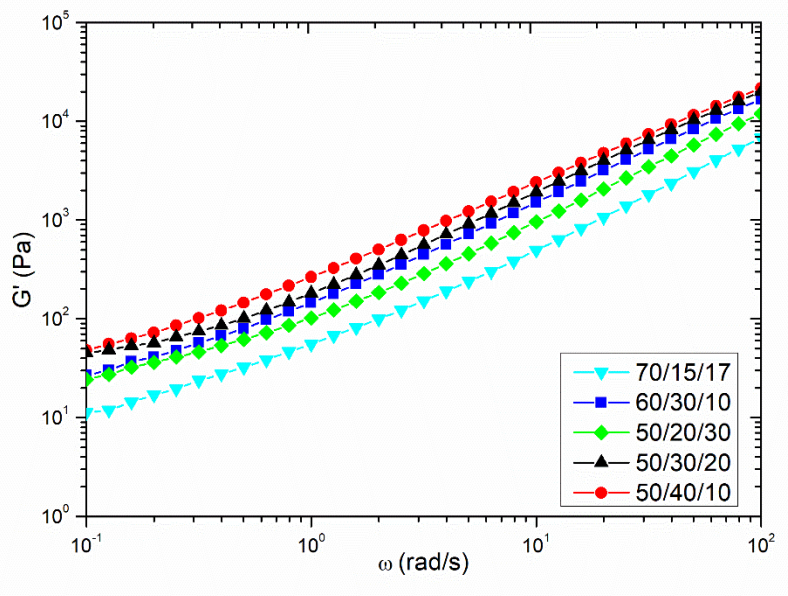

Figure 125. G' trends of PLA/PBS/PHB polymer blends.

Figure 126 reports the micrographs of ternary systems obtained through SEM observations. The ternary blend containing low content of PBS phase, particularly 15 wt% and 20 wt%, reported in Figure 126(a) and Figure 126 (c) are characterized by a droplet morphology. Conversely, as the content of PBS phase increases at 30 wt%, the morphology is no droplet-like and become more homogeneous (Figure 126(b) and Figure 126(d)) indicating a better compatibility between the phases. A further increases of weight content of PBS in 50/40/10 allow to obtain a microstructure of the system is entirely different: in fact, a certain degree of structural order can be noticed.

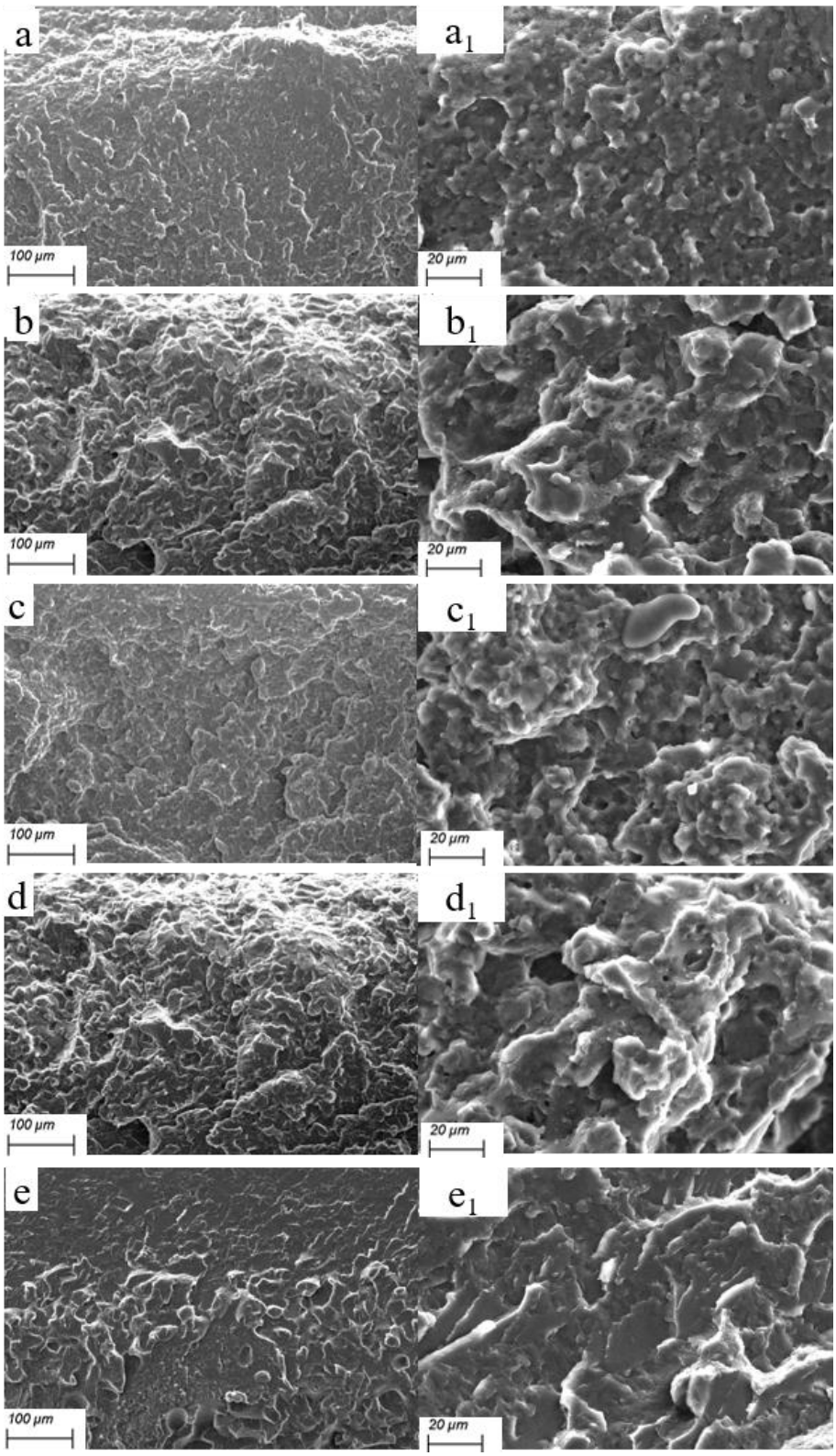

Figure 126. SEM micrographs of PLA/PBS/PHB polymer blends at different magnification: 70/15/15 (a) and (a_1), 60/30/10 (b) and (b_1), 50/20/30 (c) and (c_1), 50/30/20 (d) and (d_1) and 50/40/10 (e) and (e_1).

7.3.3 Mechanical properties: tensile and impact tests

Figure 127 shows the representative strain-stress curves of PLA, PBS and PHB. PLA is a quite brittle material with a very low elongation at break of 4.8%, a tensile modulus of 3600 MPa and a tensile strength of 63 MPa. The elongation at break of neat PHB is similar to that of PLA (8%), the tensile modulus is 1700 MPa and the tensile strength of 52 MPa. On contrary, neat PBS exhibits a tensile modulus and a tensile strength of 700 MPa and 33 MPa, respectively; the elongation at break is 244%, denoting a more ductile behaviour. Similar results of the mechanical properties of the neat polymers can be observed in th e work of Garcia-Campo et al., Zhang et al. and Mizuno et al. [264] [156] [265]. The main mechanical properties of the neat polymers are reported in Table 31.

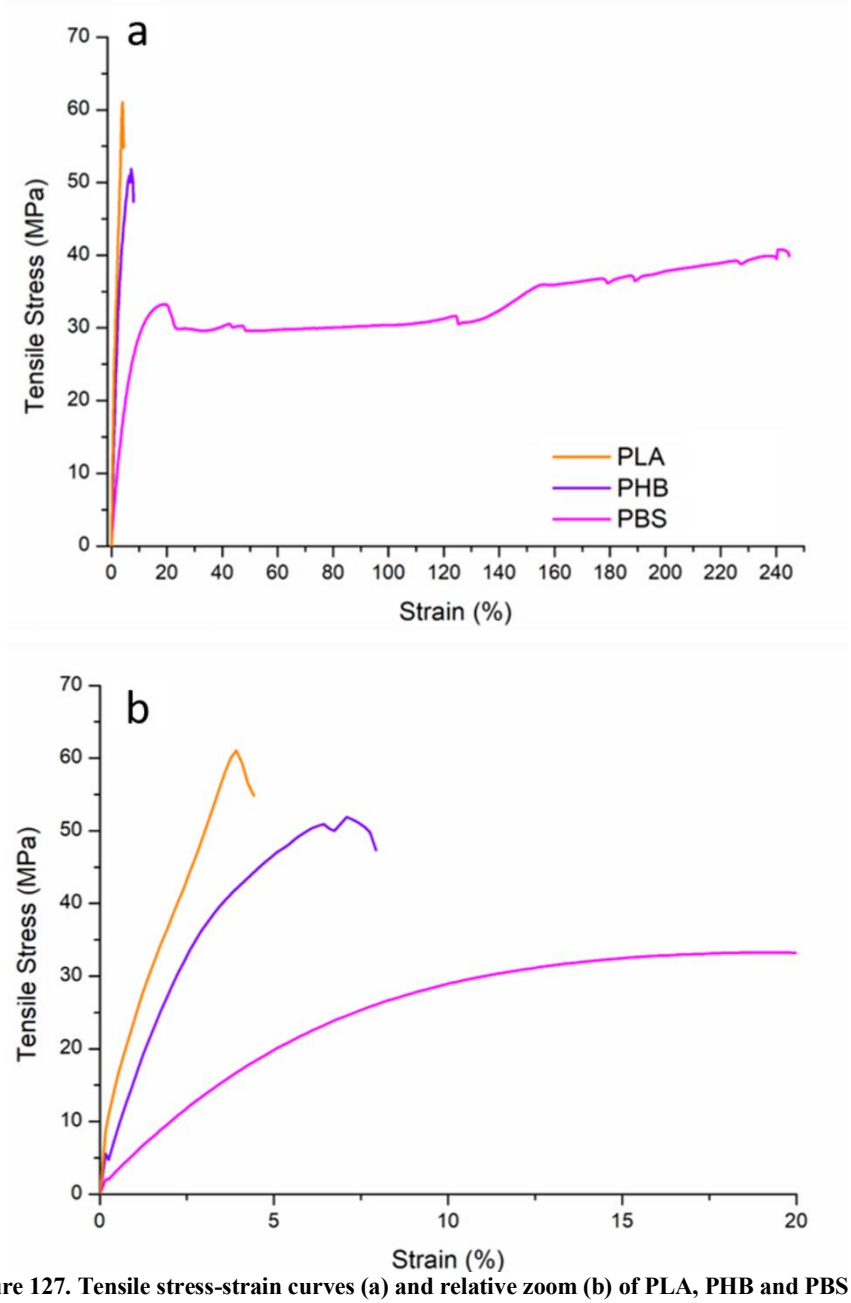

Figure 127. Tensile stress-strain curves (a) and relative zoom (b) of PLA, PHB and PBS polymers.

Table 31. Mechanical properties of neat polymers PLA, PBS and PHB.

	Tensile modulus (MPa)	Elongation at break (%)	Tensile strength (MPa)
PLA	3600 ± 48	4.8 ± 0.6	63 ± 3
PBS	700 ± 57	244 ± 3	33 ± 1
PHB	1700 ± 43	8 ± 1.6	52 ± 2

The results of the tensile tests of the ternary blends are reported in Table 32 and the stress-strain curves are depicted in Figure 128.

The values of the mechanical properties are significantly influenced by the content of PBS in the blends.

Particularly, tensile modulus and tensile strength decreases as the PBS content increases; additionally, the value of the modulus is also influenced by the relative content of PLA and PHB; in fact, the modulus results higher in blends with higher amount of PLA compared to the other systems [156].

Table 32. Mechanical properties of PLA/PBS/PHB polymer blends.

	Tensile modulus (MPa)	Elongation at break (%)	Tensile strength (MPa)	Impact strength (kJ/m)
70/15/15	4300 ± 828	24 ± 6	44 ± 1	16 ± 1.5
60/30/10	3270 ± 427	245 ± 8	44 ± 0.6	18 ± 1 .3
50/20/30	3100 ± 443	40 ± 3	36 ± 3	24 ± 6.7
50/30/20	3200 ± 116	205 ±42	42 ± 1.4	31 ± 4.7
50/40/10	2100 ± 775	297 ± 4.7	41 ± 0.7	-

It is notable in Figure 128 that all the ternary blends underwent distinct yielding indicating a transition from brittle to ductile fracture. Similar results have been obtained by Zhang *et al*. in ternary systems with PLA, PHB and PBS phases [156].

In fact, the elongation at break results higher in all ternary systems than those of the PLA and PHB brittle polymers. However, in the systems with low content of soft PBS phase this enhancement is less noticeable. As the content of PBS phase increases at 30 wt% the materials are more ductile. Particularly the 60/30/10 system exhibits an elongation at break of 245% by maintaining high values of tensile modulus and tensile strength. This finding means that in order to obtain a highly ductile material, at least 30 wt% of PBS phase must be present in the formulation.

In Table 32 the results obtained from impact tests are also reported. Looking at the values of the impact strength it is possible to confirm that the 70/15/15 and 60/30/10 systems exhibit a low interfacial adhesion between the polymers: in fact, for these materials the values of impact strength are similar to that of neat PLA (17 J/m) [156]. Conversely, in the systems with high amount of PBS, the value increases; in particular it results 31 J/m in 50/30/20 system. Thus, an increase in the content of PBS results in a gradual increase in the toughness of the blends. The impact strength value for the 50/40/10 system is not recorded due to the non-breakage of the specimen, confirming the improved adhesion between the polymer constituent the blend. In addition, it is well-known that toughness implies energy absorption and it can be achieved through the addition of a more ductile phase as

PBS. In fact, in the systems with the same content of PLA phase, the PBS is more effective than the PHB when used as impact modifier of the blends.

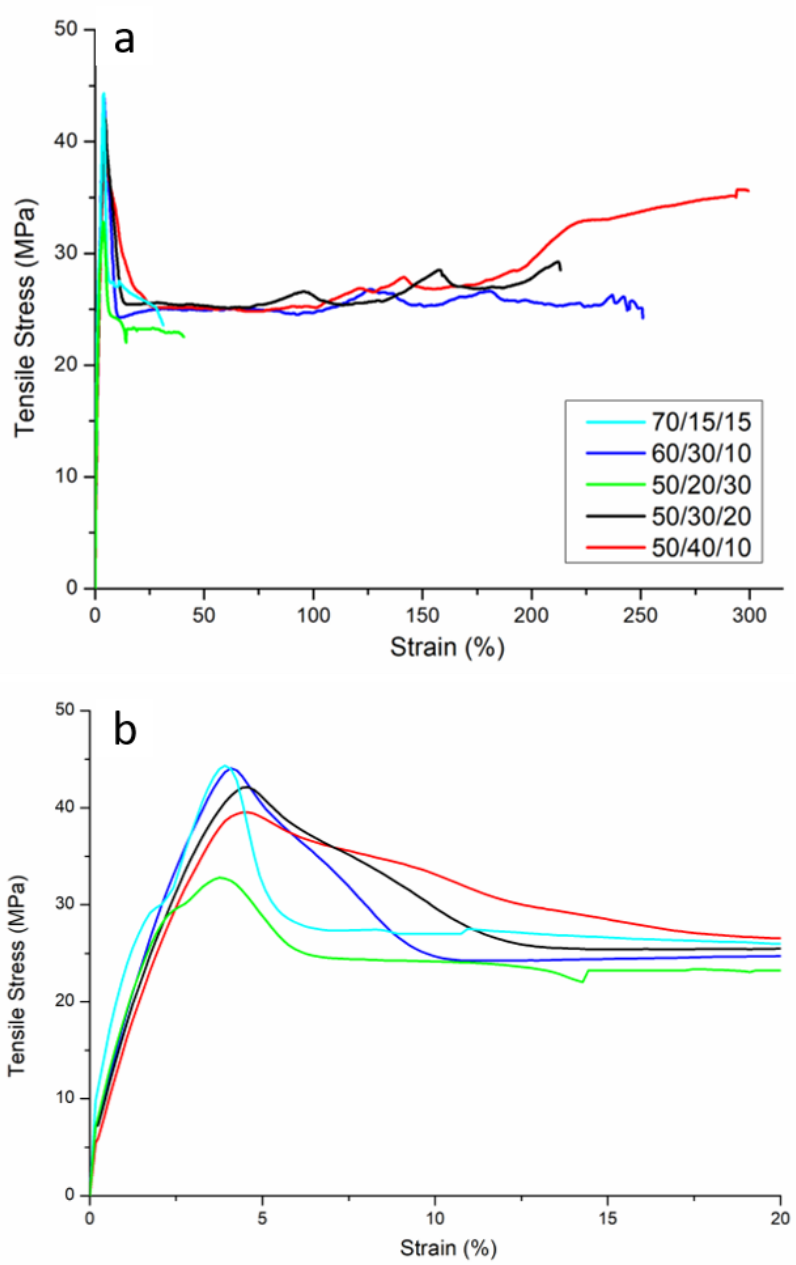

Figure 128. Tensile stress-strain curves (a) and relative zoom (b) of PLA/PBS/PHB polymer blends.

7.4 PLA/PBS/PHBt blends

In this second section part of the research a different PHBt polymer, whose details are reported in the Appendices A.1, was used and a preliminary characterization of this polymer was carried out. Figure 129(a) shows the microstructure of PHBt where a presence of platelets can be observed. To further investigate the possible content of a filler in the PHBt, not declared by the supplier, the sample was subjected to energy dispersive X-ray analysis (EDX). The resulting spectrum is shown in Figure 129(b) and confirmed the presence of Si and Mg, contained in talc ($Mg_3Si_4O_{10}(OH)_2$), which is frequently used in biopolymers as a nucleating agent.

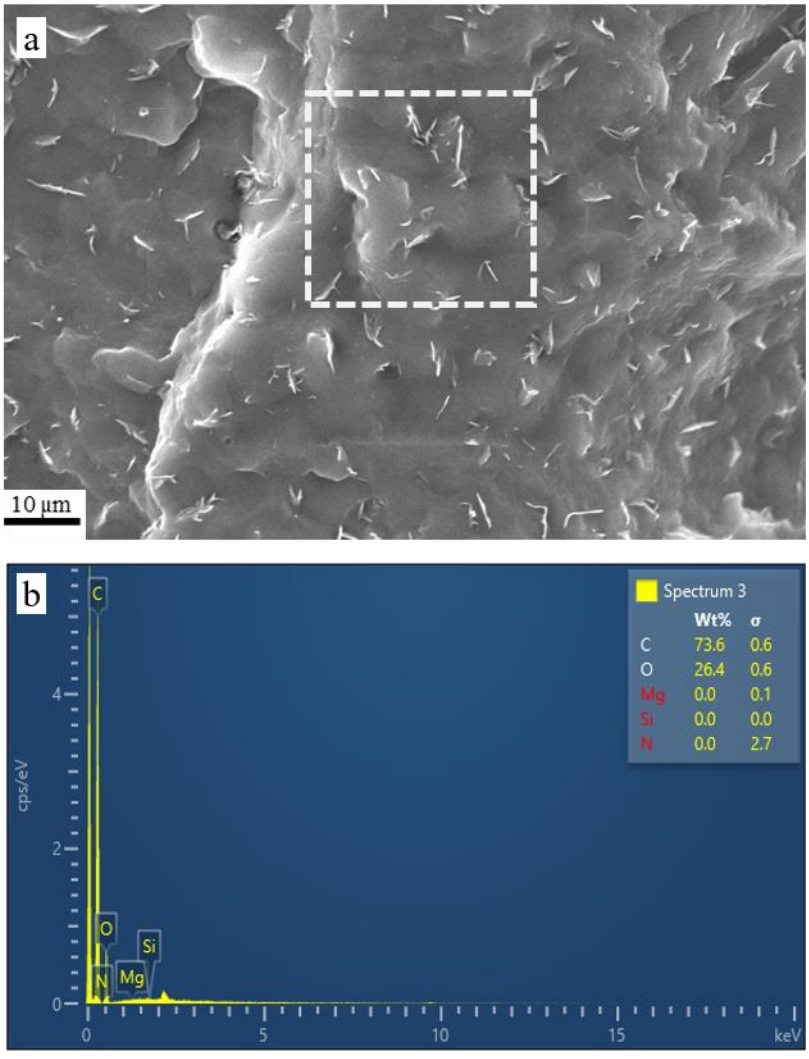

Figure 129. SEM micrograph and results of EDX analysis of PHBt polymer.

Furthermore, TGA characterization was also performed and the result is reported in Figure 130. No residue can be observed at 700°C probably due to the low weight content very of talc.

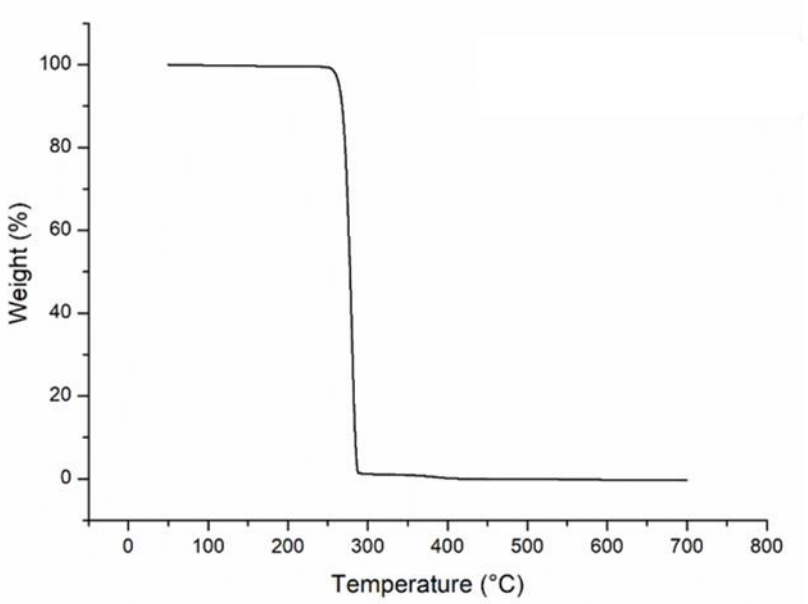

Figure 130. Result of TGA analysis of PHBt polymer.

From the trend of the complex viscosity as a function of frequency reported in Figure 131, it can be observed that PHBt exhibits a yield stress behaviour at low frequencies. This finding is typically observed in filled polymers [266], and it can be related to the limitation of the macromolecules relaxation due to the restriction of chain mobility resulting from the establishment of strong filler-filler and polymer-filler interactions [267].

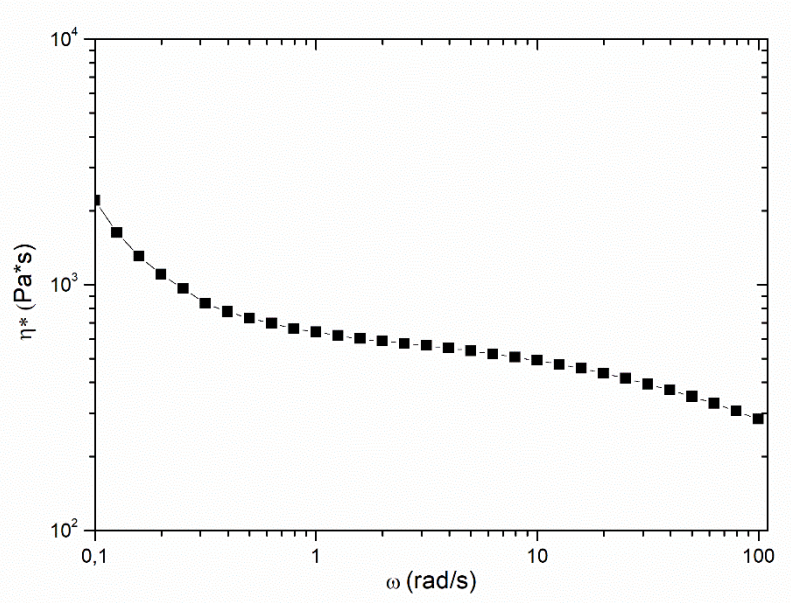

Figure 131. Complex viscosity η* trend of PHBt polymer.

PLA/PBS/PHBt blends with different weight contents of PLA and PHBt were formulated maintaining constant the amount of PBS at 30 wt%.

The process parameters used during the extrusion processes are reported in Table 33.

Table 33. Extrusion process parameters for the development of PLA/PBS/PHBt polymer blends.

	Feed rate [g/h]	Screw speed [rpm]	Melt temperature [°C]	Pressure [bar]	Torque [%]
50/30/20	380	250	155	19	44
40/30/30	700	250	156	27	45
35/30/35	630	250	157	19	40
30/30/40	680	230	153	17	44
20/30/50	740	300	161	22	40

7.4.1 Thermal analyses

Figure 132 reports the thermograms recorded during cooling and second heating of PHBt polymer. The PHBt exhibits a crystallization temperature T_c detectable during cooling scan at 62°C; during the second heating scan a T_g and a melting at 3°C and 148°C, respectively, are recorded.

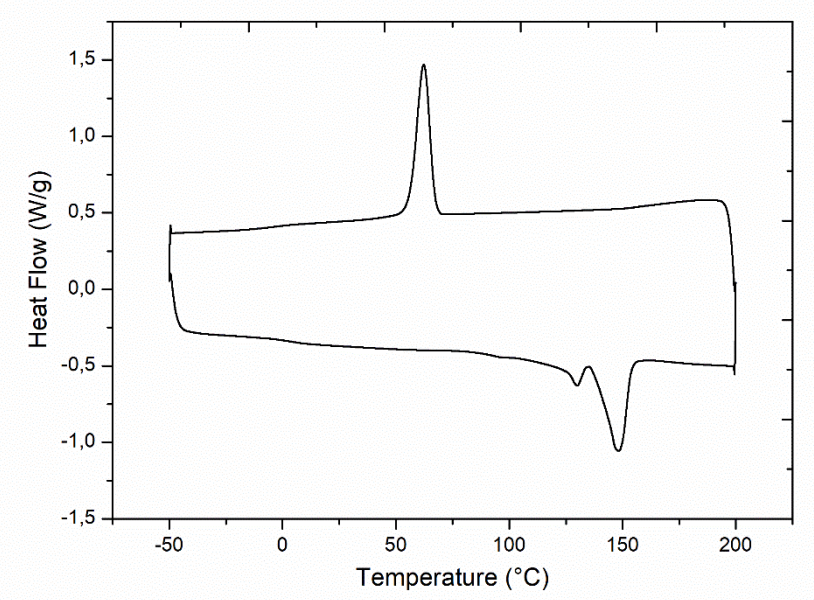

Figure 132. DSC traces recorded during cooling and second heating ramp of PHBt.

Figure 133 reports the cooling thermograms of PLA/PBS/PHBt blends. It is possible to notice that as the content of PHBt increases, the crystallization peak of PBS shifts towards lower temperatures until merging with the crystallization peak of PHBt, thus indicating that crystallization of PBS can be restricted by the presence

of PHBt [268]. Conversely, the higher the PLA content, the more the crystallization peaks of PHBt shift to higher temperature compared to neat PHBt, indicating that PLA and PBS might restrict PHBt crystallization. Additionally, it is known from literature that the decrease of the crystallization rate could be caused by the dilution effect between phases which reduces the amount of chain segments toward the growing crystals [156].

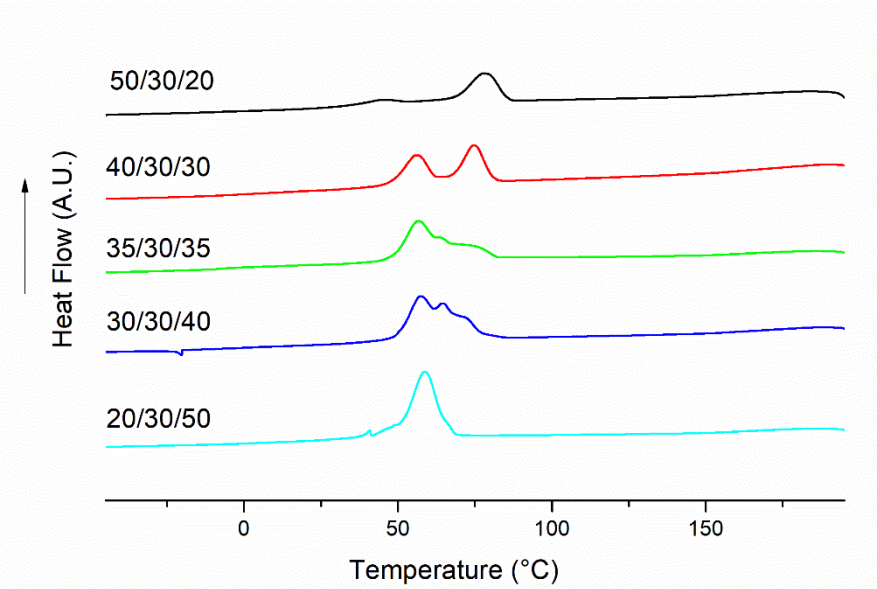

Figure 133. DSC traces recorded during cooling ramp of PLA/PBS/PHBt polymer blends.

In Figure 134 the thermal properties of the ternary systems recorded during the second heating scan are reported. The PLA glass transition remains constant at about 58 °C in all ternary blends. The glass transition of PBS, as previously discussed, is not detectable in the thermograms of neat polymer; but, at the same time, also the T_g of PHB polymer is not visible in the thermogram. This finding can be attributable to an improved compatibility between the phases of the systems [269].

All ternary blends show endothermic peaks at 168, 148 and 113 °C corresponding to the melting of PLA, PHB and PBS respectively. PLA cold crystallization temperature in the blends slightly shifts towards lower temperatures compared to neat PLA, indicating that PHB and PBS promote cold crystallization phenomena of PLA [270]. The reason of the observed increase of cold crystallization can be attributed to the fact that, showing limited miscibility with PLA, PHB and PBS amorphous phases could activate the chain mobility of PLA. If the locally activated chain mobility is sufficient, cold crystallization will be improved as a consequence of dynamic chain alignment. Secondly, the surface of PHB and PBS phases might act as nucleating center thus enhancing crystallization of PLA [263] [156].

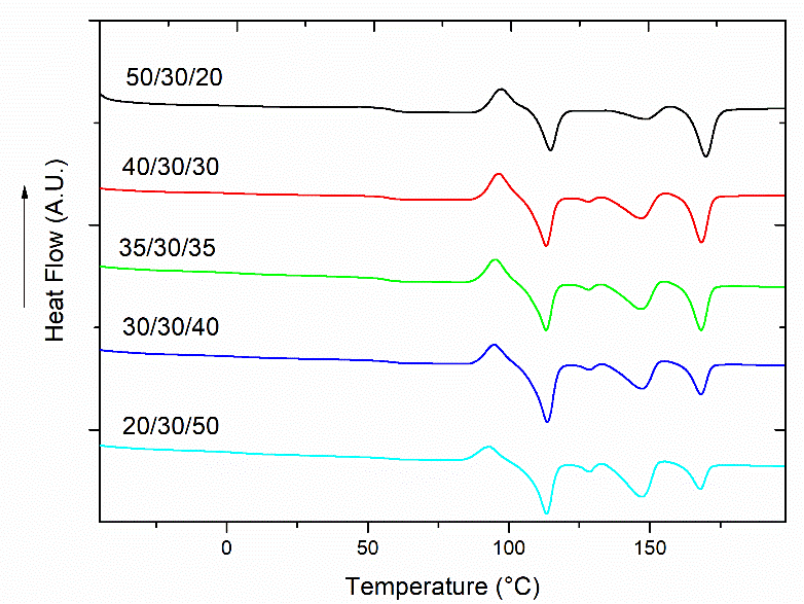

Figure 134. DSC traces recorded during second heating ramp of PLA/PBS/PHBt polymer blends.

7.4.2 Rheological measurements and morphological investigations

Figure 135 reports the trends of the complex viscosity of the ternary systems. Taking into account the previously considerations on rheological behaviour of filled PHB neat polymer, all blends exhibit yield stress behaviour at low frequencies. This finding is more pronounced in the systems with higher PHBt content due to the presence of talc platelets well dispersed in the matrix.

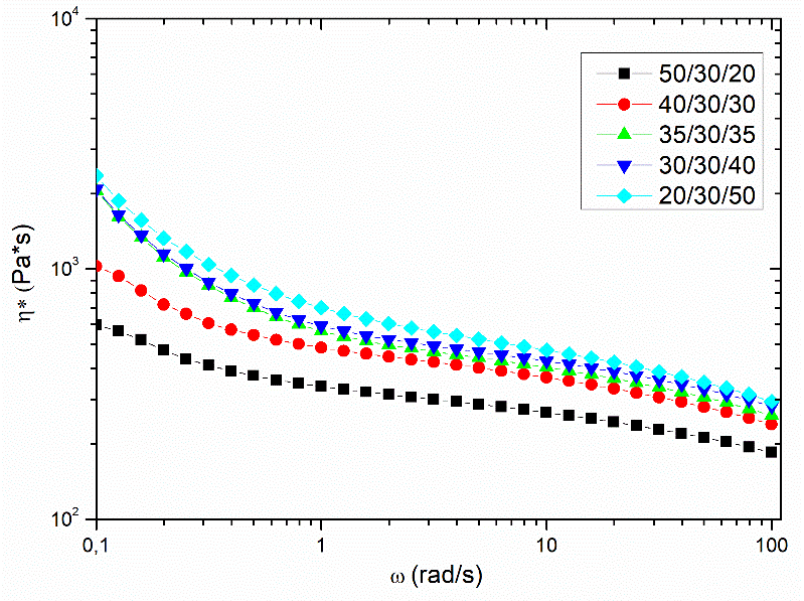

Figure 135. Complex viscosity η* of PLA/PBS/PHBt polymer blends.

Figure 136 shows the trend of the storage modulus G' of ternary blends; the curves do not exhibit the typical shoulder of immiscible blends, suggesting an improvement in compatibility between the polymers. In the high frequency region,

the values of G' of the blends are intermediate to those of neat polymers, indicating that the short-range dynamics of the polymer macromolecules are not affected by the presence of the interface between the phases. Differently, at low and intermediate frequencies the storage moduli of the blends show higher values as compared to the neat polymers. The presence of interfaces between the phases and the occurrence of shape relaxation phenomenon of the dispersed phases subjected to an oscillatory shear stress, result in an increase of G' compared to neat polymers. This behaviour is more noticeable at low frequencies where the curves reflect the response of large portion of macromolecules relaxing at long times [30]. Furthermore, the blends containing a high amount of PHBt exhibit higher G' values in the whole investigated frequency region, due to the presence of talc in the polymer.

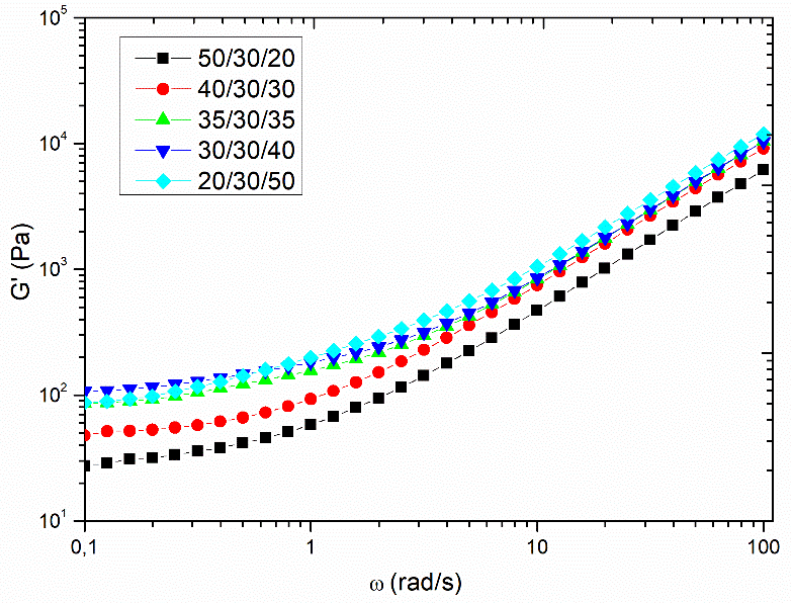

Figure 136. G' trend of PLA/PBS/PHBt ternary polymer blends.

SEM observations on ternary systems have been carried out and the micrographs are reported in Figure 137. In order to have a more defined view of the microstructure of ternary systems, the samples were treated with acetic acid before the observations [271]. All the blends show a roughly droplet-like morphology with minor dispersed phases particles and dark holes left by them during the fracturing. Nevertheless, the surface of the minor phases does not show clear and defined borders and seems quite rough, suggesting a certain grade of compatibility and interfacial adhesion between phases in all ternary blends. Among the PLA- and PHBt-based systems, in the blends with PLA as continuous phase (Figure 137(a) and (b)), the dispersed phase composed of PBS and PHBt exhibits larger dimension as compared to the blends based on PHBt whit PLA and PBS as discontinuous phases. These findings can be explained considering the value of interfacial tensions, before reported in the Paragraph 7.1. In fact, the interfacial tension value between PBS and PHBt polymers results 7.25 ($\frac{mN}{m}$), whereas between PLA-PBS is

5.20 ($\frac{mN}{m}$). It is well-known that at higher interfacial tensions correspond lower interfacial adhesions between the phases. Therefore, based on the performed interfacial tension calculations, the interfacial adhesion improves in the blends based on PHB polymer with dispersed PLA and PBS phases allow to obtain dispersed particles with lower dimensions as compared to the PLA-based systems. Similar results have been found blends characterized by a core-shell morphology, as those reported in the systems of this paragraph. The authors reports the obtainment of different morphology in PHB/PLA/PBS blends according to the matrix phase, whether PLA or PHB [156]. Concerning the blend 35/30/35 with the same content of PLA and PHBt phases, it is characterized by intermediate sizes of the dispersed phases with respect to the ternary PLA- and PHBt-based blends.

In order to quantitatively evaluate the differences in the microstructure, ImageJ software is used to calculate the average size d_{av} of the droplets of dispersed phase; the corresponding results are reported in Table 34: the calculated average size of the dispersed phase decreases as the content of PHBt increases.

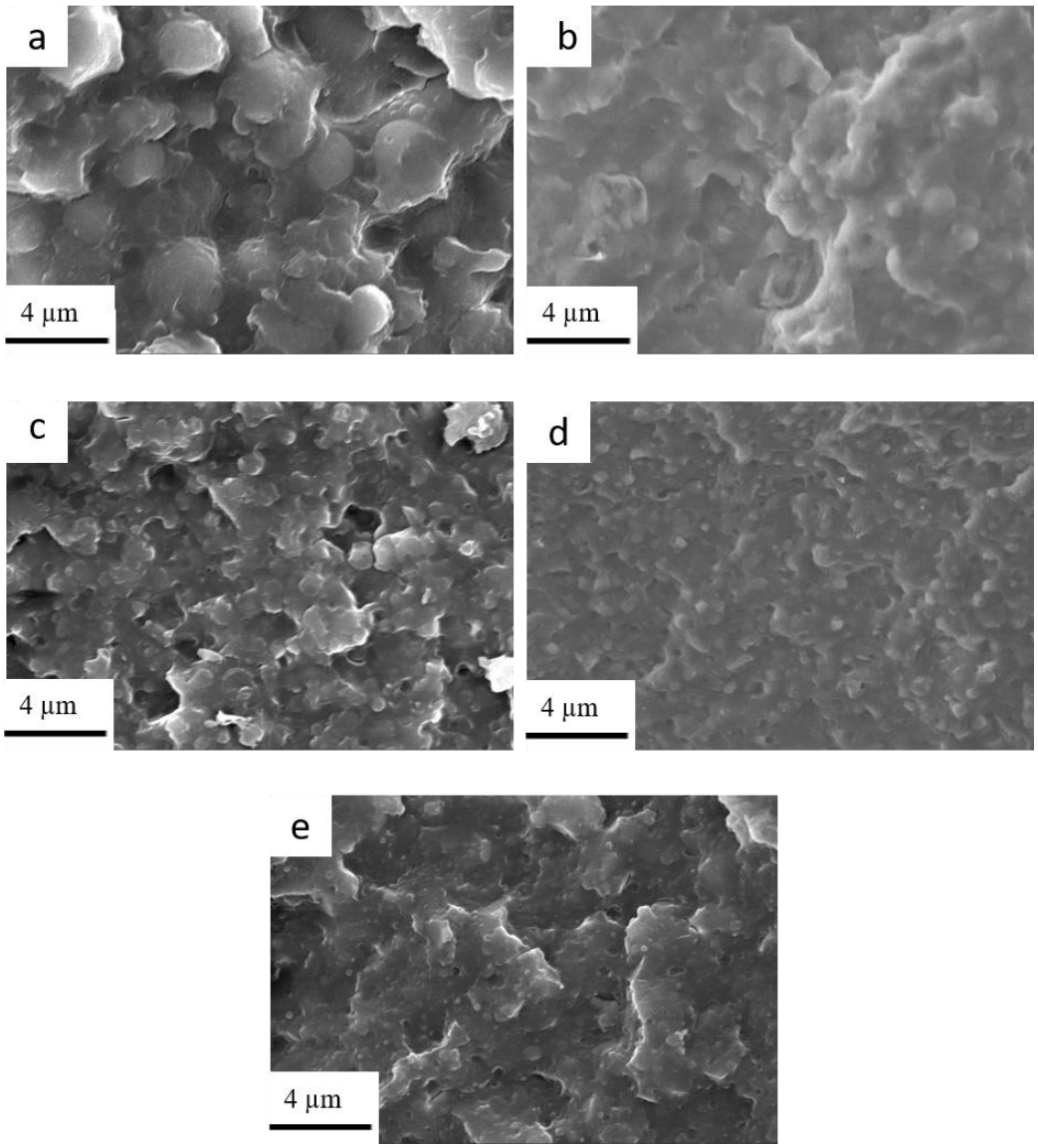

Figure 137. SEM micrographs of PLA/PBS/PHBt polymer blends: 50/30/20 (a), 40/30/30 (b), 35/30/35 (c), 30/30/40 (d) and 20/30/50 (e).

Table 34. Results of average particle dimension of PLA/PBS/PHBt blends calculated using ImageJ software.

	d_{av} [μm]	std. dev.
50/30/20	2.65	0.6
40/30/30	0.88	0.1
35/30/35	0.62	0.02
30/30/40	0.42	0.04
20/30/50	0.17	0.03

7.4.3 Mechanical properties: tensile tests

Figure 138 shows the stress-strain curve of PHBt polymer and the main mechanical properties are reported in Table 35. PHBt shows a higher tensile modulus and a lower elongation at break (2%) as compared to the PHB used in the first part of experimental trials. These results are consistent with the presence of the mineral filler in the PHBt polymer.

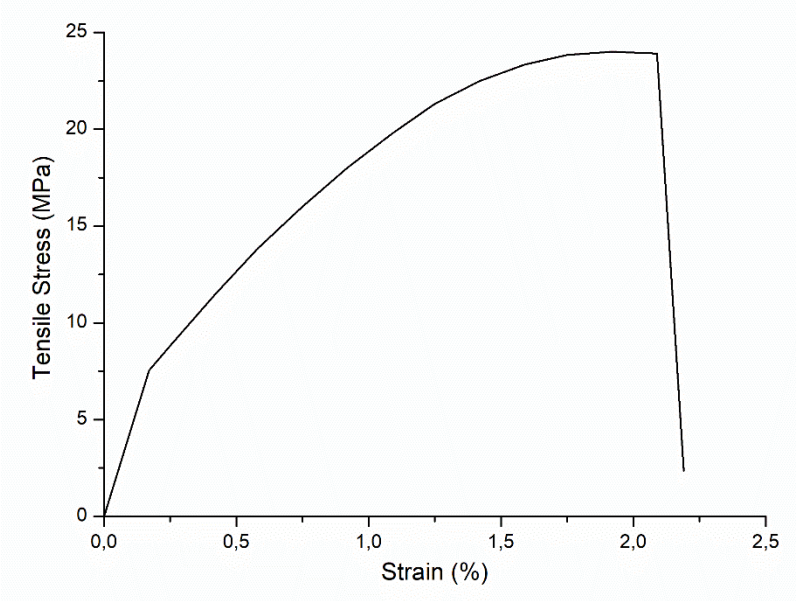

Figure 138. Tensile stress-strain curve of PHBt polymer.

Table 35. Mechanical properties of PHBt polymer.

	Tensile modulus (MPa)	Elongation at break (%)	Yield stress (MPa)
PHBt	1900 ± 30	2 ± 1	24 ± 1

The results of tensile tests on the blends are reported in Figure 139 and the values of the main mechanical properties are summarized in Table 36.

The modulus is lower in ternary systems compared to both PLA and PHBt; it varies from 1670 MPa to 1841 MPa: in particular, the lowest modulus is achieved for 20/30/50 blend (1341 MPa).

All ternary systems show improved ductility as compared to neat PLA and neat PHBt, with values of elongation at break above 7% and up to 157%. In addition, all samples underwent yielding and their fracture behaviour is ductile due to the presence of the soft PBS phase, as opposed to PLA and PHBt which exhibit brittle fracture.

However, strictly in the PLA-matrix blends the enhancement is consistent; especially with blend 50/30/20 and 40/30/30, showing elongation at break of 157 and 46% respectively. On the other hand, as the content of PHBt increases the systems exhibit less ductile behaviour by showing an elongation at break of only 7% in 20/30/50 blend. These results can be related to the presence of the filler in PHBt, which contributes to making the material more brittle at the equal amount of PBS flexible phase.

The tensile strength results higher in the blends with 50 wt% and 40wt% of PLA as compared to those based on PHBt polymer, consistently with the yield stress values of neat PLA and PHBt which are 63 MPa and 24 MPa, respectively. In addition, at the same content of PBS phase.

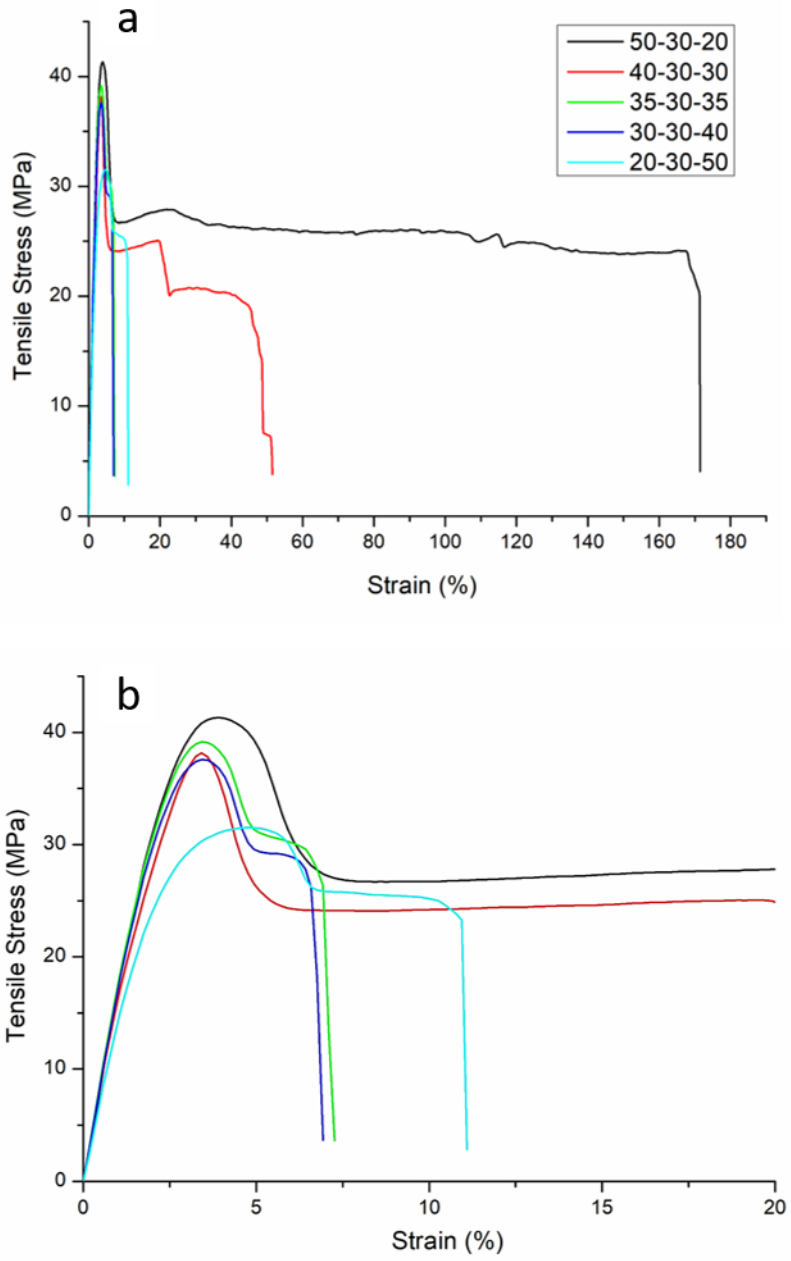

Figure 139. Tensile stress-strain curves (a) and relative zoom (b) of PLA/PBS/PHBt polymer blends.

Table 36. Mechanical properties of PLA/PBS/PHBt polymer blends.

	Tensile modulus (MPa)	Elongation at break (%)	Tensile strength (MPa)
50/30/20	1841 ± 452	157 ± 42	43 ± 1
40/30/30	1763 ± 38	46 ± 13	42 ± 3
35/30/35	1744 ± 16	12 ± 1	37 ± 3
30/30/40	1670 ± 39	8 ± 1	37 ± 1
20/30/50	1341 ± 29	7 ± 1	31 ± 1

Concluding remarks

The increased interest over the last 20 years on biopolymers due to their properties comparable to those of fossil fuel-based polymers has enabled the development of new sustainable materials to cope the decrease of the fossil resources and the increase of the costs for their extraction. Biopolymers represent a sustainable alternative for a wide variety of applications, ranging from industrial to biomedical fields. However, this growing demand of new eco-friendly sources and materials has encouraged the development of bio-based systems with tailored properties and one way to achieve this is by the formulation of bio-based blends. The well-considered choice of the appropriate compatibility strategy of biopolymer blends is of crucial relevance from both a process and an economic point of view, especially from an industrial perspective: the introduction of a compatibilizer into the mixture must be straightforward and cost-effective.

The PhD thesis was focused on the development of new materials based on biopolymer blends with the main aim to overcome the problem of the immiscibility accountable for their poor properties restricting the application fields of these materials.

Different compatibilization strategies have been exploited, such as the use of natural surfactants and the influence of a third polymeric phase on the final properties of immiscible polymer systems.

For example, as reported in Chapter 5, both in Syn- and HLB- containing systems, solid and liquid compatibilizer respectively, a significant improvement of the heat distortion temperature has been found. This finding, which broadens the field of application of these materials, has been attributed to the physical interaction between the polymers and compatibilizers. However, the use of the solid surfactant Syn presents the advantage, over the liquid non-ionic surfactant, of introducing a solid additive in the blend formulation, representing an easier and much more industrially viable processing route.

In Chapter 7 the use of a third ductile PBS phase in the immiscible mixtures allowed to increase the elongation at break of the materials in both PLA/PHB and PLA/PHBt blends compared to the brittle PLA and PHB biopolymers. In fact, ternary blends with ductile behaviour (up to 297% of elongation at break) were obtained. In addition, changes in the final microstructures, strictly connected to the lowered interfacial adhesion between the polymers constituting the dispersed phase, were found.

Of relevant importance in this thesis project was also the study of the influence of process parameters during melt compounding. As has been widely discussed in Chapter 4, the variation of process conditions cannot be considered as a "standard" method of compatibilization. However, the development of different morphologies in polymer blends during the process depends on the interfacial tension between the polymers constituting the mixture and the applied stress fields. Since the study of the influence of process conditions on the development of bio-based polymer blends is still poorly developed in the literature, in Chapter 6 of this thesis, the process parameters of bio-based blends were investigated.

Particularly, it was decided to study different configurations of screw profile, flow rate and screw speed in the development of PLA/PHB blends. Among the screw configurations evaluated the presence two kneading blocks provided to obtain better material properties. In addition, the blend processed at 3 kg/h showed, in the morphological investigation, a low average size (2.7 μm) of the particles of the dispersed phase indicating higher interfacial adhesion between polymers constituting the blend.

Further, the effect of the presence of a nanoclay on the final properties was evaluated. In this context, it was essential to consider the coupled effect of the nanoclays presence and the selected screw configuration in the process of filled blend: the flow conditions, established during the processing, due to the presence of mixing and backflow elements, caused the achievement of a good interaction between filler and polymers.

To conclude, all these results indicated that the use of selected natural surfactants (Chapter 5), the evaluation of processing behaviour related to the presence of nanoclays in the system (Chapter 6) and the addition of a ductile polymer phase in the blends (Chapter 7) are potentially strategies to obtain a fully bio-based system with advanced properties.

Focusing on the term ‘’fully bio-based’’, it can be argued that these results are particularly innovative in view of the impending necessity to implement an alternative economic model to the linear one still used in many Countries. In fact, the development and the academic research on materials with potentially low environmental impact is an excellent starting point to achieve the goal of a global circular economy expressed in the European Parliament in 2021. The plan foresees the adoption of a zero-carbon, ecologically sustainable, toxic-free and fully circular economy by 2050.

Appendix A

A.1 Materials

A.1.1 Polymers

PLA was supplied in pellets by IngeoTM Natural Natureworks (Minnetonka, MN, USA) under the trade name PLA 3251D. In Table 37 the typical properties of PLA are reported.

Table 37. Physical and mechanical properties of PLA Ingeo 3251D.

	PLA 3251D	ASTM Method
Density [g/cc]	1.24	D792
Relative Viscosity	2.5	-
Melt flow Index [g/10 min] (210°C, 2.16kg)	80	D1238
Glass Transition Temperature [°C]	55-60	D3418
Crystalline Melt Temperature [ºC]	155-170	D3418
Clarity	Transparent	
Tensile Yield Strength [MPa]	62	D638
Tensile Elongation [%]	3.5	D638
Notched Izod Impact [J/m]	17	D256
Heat Distortion Temperate [°C]	55	E2092

PHB was manufactured by Aonilex, KANEKA Biopolymer (Osaka, Japan) under the trade name PHBX151A and commercialized in pellet form. Aonilex is produced by microorganisms in a specific fermentation condition using plant oils as the carbon source. This biopolymer shows excellent biodegradability under aerobic and anaerobic conditions. Table 38 reports its typical properties.

Table 38. Physical and mechanical properties of PHB X151A.

	PHB X151A	ASTM Method
Density [g/cc]	1.19	D792
Melt flow Index [g/10 min] (165°C, 5kg)	3	D1238
Glass Transition Temperature [°C]	0	DSC
Crystalline Melt Temperature [ºC]	126	DSC
Tensile Strength [MPa]	26	D527
Tensile Modulus [MPa]	950	D527
Charpy impact strength [kJ/m^2]	3	D179

LDPE was supplied in pellets by Repsol (Madrid, Spain) under trade name ALCUDIA® PE022; its main properties are reported in Table 39.

Table 39. Physical and mechanical properties of LDPE PE022.

	LDPE	ASTM Method
Density [g/cc]	0.915	D792
Melt flow Index [g/10 min] (190°C, 2.16kg)	70	D1238
Melting point [°C]	105	DSC
Tensile strength at break [MPa]	9	D527
Elongation at break [%]	120	D527

PHBt was supplied by Maip under the trade name IamNature B6A13 and commercialized in pellet form. Table 40 reports its typical properties.

Table 40. Physical and mechanical properties of PHBt B6A13.

	PHBt B6A13	ASTM Method
Density [g/cc]	1.20	D792
Melt flow Index [g/10 min] (165°C, 5kg)	7	D1238
Glass Transition Temperature [°C]	2	DSC
Crystalline Melt Temperature [ºC]	145	DSC
Heat Distortion Temperate [°C] (0.45/1.8 MPa)	110/-	ISO75
Izod notched impact [kJ/m^2]	2.5	ISO180-1A
Elongation at break [%]	5	D527

PBS was supplied in pellet form by Natureplast under the name PBE003. Table 41 reports its typical properties.

Table 41. Physical and mechanical properties of PBS PBE003.

	PBS PBE003	ASTM Method
Density [g/cc]	1.26	D1183
Melt flow Index [g/10 min] (190°C, 2.16kg)	5	D1133
Heat Distortion Temperature [°C] (HDT-B)	90	75-2
Elongation at break [%]	330	D527
Tensile Modulus [MPa]	720	D527
Charpy impact strength [kJ/m^2]	No break	D179

PLA, PHB, PHBt and PBS polymers were dried for 4 hours at 80°C in an industrial drier (Piovan HR50 model) before the melt mixing.

A.1.2 Compatibilizers

Span TM 80-LQ-(RB) is a sorbitan ester, and Tween TM 80-LQ-(CQ) is an ethoxylated sorbitan ester. Both additives are bio-based non-ionic liquid surfactants commercialized by CRODA.

Synperonic (Syn) is a polyalkylene oxide block copolymer in the form of flakes (at 25 °C). It is a polymeric emulsion stabilizer commercialized by CRODA under the trade name Synperonic PE_F87.

A.1.3 Filler

Cloisite 5 bentonite organo-modified with bis(hydrogenated tallow alkyl)dimethyl salt (CL) was supplied by BYK Additives & Instruments, ALTANA in powder form. The typical properties are reported in Table 42. The filler was dried over the night at 120°C in the oven before the melt mixing.

Table 42. Physical properties of Cloisite 5.

	Properties
Moisture [%]	< 3
Typical dry particle size [µm] (d_{50})	< 40
Color	Off White
Packed bulk density [g/l]	480
Density [g/cm^3]	1.77
X-ray results [nm]	d_{001}= 3.27

A.2 Instruments

DSM Explorer is a mini twin-screw extruder used for the development of binary blends (Chapter 5). The processing conditions in PLA/LDPE systems were: T = 190°C, screw speed= 50 rpm (during addition of pellets), 100 rpm (during mixing), 70 rpm (output), mixing time = 2 min at 100 rpm. Conversely, the PLA/PHB blends were obtained using: T = 180 °C, screw speed = 100 rpm (for all the phases) and mixing time = 3 min. Both of systems are prepared under protective Nitrogen atmosphere.

Leistrizt ZSE is a co-rotating twin-screw extruder used for the development of PLA/PHB blends and PLA/PHB/CL nanocomposites (Chapter 6). The extruder exhibits the following characteristics: diameter Φ=18 mm and L/D ratio=40. The barrel temperature was set from 170 to 190 °C, as reported in the Chapter 6, along the extruder axis and the melt temperature was measured to be 185 °C. The polymer pellets, cold-mixed at specific weight content, were fed into the extruder by a pellet gravimetric feeder.

During the extrusions of PLA/PHB/CL blends a further powder gravimetric side feeder was used for the clay.

Thermoscientific Process 11 is a co-rotating twin-screw extruder used for the development of ternary PLA/PBS/PHB and PLA/PBS/PHBt blends (Chapter 7). The extruder is characterized by diameter Φ = 11mm and L/D ratio = 40. The used

screw profile is a standard type with three mixing sections. The screw configuration and the extrusion process parameters are reported in Chapter 7.

Collins Teach Line 200 T is a compression moulding machine used for the development of samples designed for rheological, thermo-mechanical and XRD measurements. The conditions for each sample were: pressure= 100 bar T= 190°C for 3 min.

Babyplast 6/10P Cronoplast is an injection moulding machine used for the preparation of dog-bone specimens for the mechanical tests (ternary blend reported in Chapter 7). The temperature was maintained at 180°C and the process conditions were optimized and are reported in Table 43.

Table 43. Process conditions of the injection moulding machine used in the preparation of do-bone specimens.

Parameter	Ternary blends
3 Zone temperatures [°C]	180/180/180
Mould temperature [°C]	18
Shot size [mm]	10
Cooling time [s]	10
1st Injection pressure [bar]	90
1st Pressure time [s]	10
2nd Injection pressure [bar]	80
2nd Pressure time [s]	20
Decompression [mm]	1

A.3 Characterization techniques

The specimens used for thermomechanical measurements (DMA), X-ray diffraction analysis (XRD) and rheological characterizations were obtained by compression moulding, using a Collin P 200 T press (operating at 190°C under a pressure of 100 bar).

A.3.1 Differential scanning calorimetry (DSC)

DSC measurements were carried on weighted samples of about 8 mg placed in sealed aluminum pans using a Q20 TA Instrument (New Castle, DE, USA). All the experiments were performed under dry N_2 gas (20 ml min^{-1}). The samples were subjected to the following cycle: a heating ramp from -50 to 200°C, a cooling ramp from 200 to -50 °C, and a second heating ramp from -50 to 200°C. All the heating/cooling ramps were performed at a scanning rate of 10 °C/min. The glass transition temperature (T_g), crystallization temperature (T_c), cold crystallization temperature (T_{cc}), melting temperature (T_m) and melting and cold crystallization enthalpy (ΔH_m and ΔH_{cc}) were determined from the second heating scan. The crystallinity percentage X in all investigated systems was evaluated as [30]:

Equation 43. $$X = \frac{\Delta H}{\Delta H_{m0}} * 100$$

where: $\Delta H = \Delta H_m - \Delta H_{cc}$ and ΔH_{m0} is the melting enthalpy of a 100% crystalline PLA (93.0 J/g [31]), PHB (146.0 J/g [32]), PBS (116.0 J/g [32]).

A.3.2 Thermo-mechanical measurements (DMA)

DMA measurements were performed using Q800 TA Instrument (New Castle, USA) with tension film clamp. Samples 6 mm width x 26 mm height x 1 mm thickness were used. The temperature was varied in the range from 30 to 120°C, applying a heating rate of 3°C/min. The test conditions were: 1 Hz of frequency in strain-controlled mode with 15 m of amplitude, static loading of 125% of dynamic loading and 0.01 N of preload. For each formulation, the test was repeated three times and the mean was calculated and reported. The experimental error as standard deviation for all the tests was less than 5%.

The HDT (1.82 MPa) was measured as the temperature at which the modulus achieves 800 MPa.

A.3.3 Rheological measurements

Rheological measurements were performed using an ARES TA Instrument (New Castle, USA) rheometer in parallel plate geometry (plate diameter=25 mm), under nitrogen atmosphere to avoid polymer oxidative degradation. Complex viscosity, elastic and loss moduli were measured performing frequency scans from 0,1 to 100 rad/s at 190°C or 170°C. The strain was fixed to be in the polymer linear viscoelastic regime. The typical gap between the plates imposed during the tests was 1 mm. Prior to the measurements, the samples were vacuum dried at 80°C for 4 hours.

A.3.4 X-ray diffraction analysis (XRD)

X-ray diffraction-analyses (XRD) were performed on compression moulded specimens, using PANalytical X'PERT PRO with Cu–Kα-ray source (1.540562Å) and a scanning rate of 0.026 °min^{-1}. The data were collected over the range 2-30° 2θ; fixed anti-scatter and divergence slits of 1/16° and 1/32° were used together with a beam mask of 10 mm.

A.3.5 Mechanical tests

Mechanical properties were determined on dog bones samples using an Instron 5966 machine according to the ASTM method D638 under ambient temperature with two different cross-head speed of 1 mm/min and 10 mm/min (applied by the strain value equal to 0.25%). The dimensions of specimen were 30 mm in length, 4 mm in width and a thickness of 2 mm. For each formulation five samples were examined and all samples were conditioned per 72h at 23°C and a relative humidity of 50% in a climate-controlled chamber Binder BFK240, until reaching constant weight. All mechanical tests were performed at room temperature.

The tests provided the Young's modulus values (E), elongation at break (Ɛ), and maximum and yield tensile strength (σ_{max} and σ_y) of the ternary blends.

A.3.6 Impact tests

The impact strength was obtained by the Charpy tests with 2 J of impact energy have been carried out, at impact speed equal to 2.9 m/s at room temperature, following UNI EN ISO 179-1/1Eu and the tests were performed on fine samples for each ternary blend.

A.3.7 Thermogravimetric analysis (TGA)

Discovery TA Instruments (New Castle, DE, USA) was used for thermogravimetric analyses (TGA) on non-ionic surfactants Tween80, Span80, the mixture with HLB12 and Syn (Chapter 5) in air from 50 to 300°C with a heating rate of 10°C/min. The sample (ca. 10 mg) was placed in open alumina pan and fluxed with nitrogen (gas flow: 35 ml/min).

The test was performed also on PHBt polymer both in nitrogen and air from 50 to 800°C with a heating rate of 10°C/min. The sample (ca. 10 mg) was placed in open alumina pan and fluxed with nitrogen or air (gas flow: 35 ml/min). The mass final residue at 700°C was evaluated.

A.3.8 Morphological investigations

The morphology of the blends reported in Chapter 5 and Chapter 6 was observed using a LEO-1450VP Scanning Electron Microscope SEM (beam voltage: 20 kV). Conversely, the morphological investigation of the materials reported in Chapter 7 was observed using an EVO15 Scanning Electron Microscope SEM from Zeiss (beam voltage: 20 kV).

All the observations were performed on the cross-section of the samples, obtained through fracturing in liquid nitrogen. Before the tests, the fracture surface was coated with a thin gold layer.

Concerning the investigation on PHBt polymer, elemental analysis was carried out by EDX (Energy dispersive X-rat spectroscopy) using an X-ray probe (Oxford Ultim Max, model 40, High Wycombe, UK).

References

1. Filiciotto, L. and G. Rothenberg, *Biodegradable Plastics: Standards, Policies, and Impacts.* ChemSusChem, 2020. **14**(1): p. 56-72.
2. Nesic, A., et al., *Bio-based packaging materials*, in *Biobased products and industries*. 2020, Elsevier. p. 279-309.
3. Paper, H. 2016; Available from: https://www.heritagepaper.net/the-difference-between-biodegradable-and-compostable-packaging-materials/.
4. Mtibe, A., et al., *Synthetic Biopolymers and Their Composites: Advantages and Limitations-An Overview.* Macromol Rapid Commun, 2021: p. e2100130.
5. European Bioplastics e.V., M. 2019; Available from: https://www.european-bioplastics.org/market/
6. Flaris, V. and G. Singh, *Recent developments in biopolymers.* Journal of Vinyl and Additive Technology, 2009. **15**(1): p. 1-11.
7. Sustainable Biopolymers: A BCC Research Outlooks, W., MA, BCC Publishing, 2019.
8. Kai, D., et al., *Engineering poly (lactide)–lignin nanofibers with antioxidant activity for biomedical application.* ACS Sustainable Chemistry & Engineering, 2016. **4**(10): p. 5268-5276.
9. Metanomski, W., *Compendium of macromolecular nomenclature*. 1991: Blackwell Scientific Publications.
10. Pracella, M., *Blends and Alloys.* 2017: p. 155-184.
11. Visakh, P.M., G. Markovic, and D. Pasquini, *Recent Developments in Polymer Macro, Micro and Nano Blends : Preparation and Characterisation*. 2016, Cambridge, UNITED KINGDOM: Elsevier Science & Technology.
12. Flory, P.J., *Thermodynamics of high polymer solutions.* The Journal of chemical physics, 1941. **9**(8): p. 660-660.
13. Flory, P.J., *Thermodynamics of high polymer solutions.* The Journal of chemical physics, 1942. **10**(1): p. 51-61.
14. Huggins, M.L., *Solutions of long chain compounds.* The Journal of chemical physics, 1941. **9**(5): p. 440-440.
15. Huggins, M.L., *Some properties of solutions of long-chain compounds.* The Journal of Physical Chemistry, 1942. **46**(1): p. 151-158.
16. Utracki, L.A. and C.A. Wilkie, *Polymer blends handbook*. Vol. 1. 2002: Kluwer academic publishers Dordrecht.
17. Coleman, M.M., P.C. Painter, and J.F. Graf, *Specific interactions and the miscibility of polymer blends*. 1995: CRC Press.
18. Patterson, D., *Polymer compatibility with and without a solvent.* Polymer Engineering & Science, 1982. **22**(2): p. 64-73.
19. Manias, E. and L.A. Utracki, *Thermodynamics of polymer blends.* Polymer blends handbook, 2014: p. 171-289.
20. Bates, F.S., *Polymer-polymer phase behavior.* Science, 1991. **251**(4996): p. 898-905.

21. Favis, B.D. and J. Willis, *Phase size/composition dependence in immiscible blends: Experimental and theoretical considerations.* Journal of Polymer Science Part B: Polymer Physics, 1990. **28**(12): p. 2259-2269.
22. Haward, R. and C. Bucknall, *The provision of toughness in one and two phase polymers*, in *Macromolecular Chemistry–11*. 1977, Elsevier. p. 227-238.
23. Coran, A. and R. Patel, *Rubber-thermoplastic compositions. Part VIII. Nitrile rubber polyolefin blends with technological compatibilization.* Rubber Chemistry and Technology, 1983. **56**(5): p. 1045-1060.
24. Lyngaae-Jørgensen, J. and L. Utracki. *Dual phase continuity in polymer blends*. in *Makromolekulare Chemie. Macromolecular Symposia*. 1991. Wiley Online Library.
25. Good, R.J. and L. Girifalco, *A theory for estimation of surface and interfacial energies. III. Estimation of surface energies of solids from contact angle data.* The Journal of Physical Chemistry, 1960. **64**(5): p. 561-565.
26. Wu, S., *Polymer interfacial and adhesion*. 1982, Marcel Dekker Inc., New York.
27. Grace, H.P., *Dispersion phenomena in high viscosity immiscible fluid systems and application of static mixers as dispersion devices in such systems.* Chemical Engineering Communications, 1982. **14**(3-6): p. 225-277.
28. Taylor, G.I., *The viscosity of a fluid containing small drops of another fluid.* Proceedings of the Royal Society of London. Series A, Containing Papers of a Mathematical and Physical Character, 1932. **138**(834): p. 41-48.
29. Barai, N. and N. Mandal, *Breakup modes of fluid drops in confined shear flows.* Physics of Fluids, 2016. **28**(7): p. 073302.
30. Fortelný, I. *Coalescence in polymer blends: solved and open problems*. in *Macromolecular Symposia*. 2000. Wiley Online Library.
31. Sundararaj, U. and C. Macosko, *Drop breakup and coalescence in polymer blends: the effects of concentration and compatibilization.* Macromolecules, 1995. **28**(8): p. 2647-2657.
32. Grosso, M. and P.L. Maffettone, *Fourier Transform Rheology: A New Tool to Characterize Material Properties.* Fourier Transforms: New Analytical Approaches and FTIR Strategies, 2011: p. 285.
33. Pötschke, P. and D. Paul, *Formation of co-continuous structures in melt-mixed immiscible polymer blends.* Journal of Macromolecular Science, Part C: Polymer Reviews, 2003. **43**(1): p. 87-141.
34. Jordhamo, G., J. Manson, and L. Sperling, *Phase continuity and inversion in polymer blends and simultaneous interpenetrating networks.* Polymer Engineering & Science, 1986. **26**(8): p. 517-524.
35. Paul, D. and J. Barlow, *Polymer blends.* Journal of Macromolecular Science—Reviews in Macromolecular Chemistry, 1980. **18**(1): p. 109-168.
36. Avgeropoulos, G., et al., *Heterogeneous blends of polymers. Rheology and morphology.* Rubber chemistry and technology, 1976. **49**(1): p. 93-104.
37. Landel, R.F. and L.E. Nielsen, *Mechanical properties of polymers and composites*. 1993: CRC press.
38. Ablazova, T., et al., *The rheological properties of molten mixtures of polyoxymethylene and copolyamide: Their fibrillation and microstructure.* Journal of Applied Polymer Science, 1975. **19**(7): p. 1781-1798.

39. Morris, B., *6-Polymer Blending for Packaging Applications.* The Science and Technology of Flexible Packaging. Oxford: William Andrew Publishing, 2017: p. 149-77.
40. Utracki, L., *On the viscosity-concentration dependence of immiscible polymer blends.* Journal of Rheology, 1991. **35**(8): p. 1615-1637.
41. Taylor, G.I., *The formation of emulsions in definable fields of flow.* Proceedings of the Royal Society of London. Series A, containing papers of a mathematical and physical character, 1934. **146**(858): p. 501-523.
42. Choi, S.J. and W. Schowalter, *Rheological properties of nondilute suspensions of deformable particles.* The Physics of Fluids, 1975. **18**(4): p. 420-427.
43. Janssen, J. and H. Meijer, *Droplet breakup mechanisms: Stepwise equilibrium versus transient dispersion.* Journal of Rheology, 1993. **37**(4): p. 597-608.
44. Elmendrop, J., *A Study on Polymer Blending Microrheologie*. 1986, Dissertation Techn. Hogesch. Delft.
45. Cardinaels, R. and P. Moldenaers, *Viscoelastic relaxation and morphology of blends of rubbery polymers.* Encyclopedia of Polymeric Nanomaterials, 2014.
46. Palierne, J., *Rheologica Acta Rheol Acta 30: 497 (1991).* Rheologica Acta, 1991. **30**(497).
47. Honerkamp, J. and J. Weese, *A nonlinear regularization method for the calculation of relaxation spectra.* Rheologica acta, 1993. **32**(1): p. 65-73.
48. Vinckier, I., P. Moldenaers, and J. Mewis, *Relationship between rheology and morphology of model blends in steady shear flow.* Journal of Rheology, 1996. **40**(4): p. 613-631.
49. Bátori, V., et al., *Anaerobic degradation of bioplastics: A review.* Waste management, 2018. **80**: p. 406-413.
50. Saeidlou, S., et al., *Poly(lactic acid) crystallization.* Progress in Polymer Science, 2012. **37**(12): p. 1657-1677.
51. Armentano, I., et al., *Processing and characterization of plasticized PLA/PHB blends for biodegradable multiphase systems.* 2015.
52. Hamad, K., et al., *Polylactic acid blends: The future of green, light and tough.* Progress in Polymer Science, 2018. **85**: p. 83-127.
53. Hu, Y., et al., *Newly developed techniques on polycondensation, ring-opening polymerization and polymer modification: Focus on poly (lactic acid).* Materials, 2016. **9**(3): p. 133.
54. Scaffaro, R., et al., *Polysaccharide nanocrystals as fillers for PLA based nanocomposites.* Cellulose, 2017. **24**(2): p. 447-478.
55. Lee, S.Y., *Bacterial polyhydroxyalkanoates.* Biotechnology and bioengineering, 1996. **49**(1): p. 1-14.
56. Avella, M., E. Martuscelli, and M. Raimo, *Review Properties of blends and composites based on poly (3-hydroxy) butyrate (PHB) and poly (3-hydroxybutyrate-hydroxyvalerate)(PHBV) copolymers.* Journal of materials science, 2000. **35**(3): p. 523-545.
57. Jiang, L. and J. Zhang, *Biodegradable polymers and polymer blends.* Handbook of Biopolymers and Biodegradable Plastics: Properties, Processing and Applications, 2012: p. 109-128.
58. Fujimaki, T., *Processability and properties of aliphatic polyesters,'BIONOLLE', synthesized by polycondensation reaction.* Polymer degradation and stability, 1998. **59**(1-3): p. 209-214.

59. Peelman, N., et al., *Use of biobased materials for modified atmosphere packaging of short and medium shelf-life food products.* Innovative Food Science & Emerging Technologies, 2014. **26**: p. 319-329.
60. Cinelli, P., et al., *Whey protein layer applied on biodegradable packaging film to improve barrier properties while maintaining biodegradability.* Polymer Degradation and Stability, 2014. **108**: p. 151-157.
61. Mochane, M.J., et al., *The effect of filler localization on the properties of biopolymer blends, recent advances: A review.* Polymer Composites, 2020. **41**(7): p. 2958-2979.
62. Wootthikanokkhan, J., et al., *Crystallization and thermomechanical properties of PLA composites: Effects of additive types and heat treatment.* Journal of Applied Polymer Science, 2013. **129**(1): p. 215-223.
63. Bhatia, A., et al., *Effect of clay on thermal, mechanical and gas barrier properties of biodegradable poly (lactic acid)/poly (butylene succinate)(PLA/PBS) nanocomposites.* International Polymer Processing, 2010. **25**(1): p. 5-14.
64. Domínguez-Robles, J., et al., *Antioxidant PLA composites containing lignin for 3D printing applications: A potential material for healthcare applications.* Pharmaceutics, 2019. **11**(4): p. 165.
65. Mtibe, A., et al., *Synthetic Biopolymers and Their Composites: Advantages and Limitations—An Overview.* Macromolecular Rapid Communications, 2021: p. 2100130.
66. Cooper, C.J., et al., *Hybrid Green Bionanocomposites of Bio-based Poly (butylene succinate) Reinforced with Pyrolyzed Perennial Grass Microparticles and Graphene Nanoplatelets.* ACS omega, 2019. **4**(24): p. 20476-20485.
67. Mistretta, M.C., et al., *Film Blowing of Biodegradable Polymer Nanocomposites for Agricultural Applications.* Macromolecular Materials and Engineering. **n/a**(n/a): p. 2100177.
68. La Mantia, F.P., et al., *Biodegradable Polymers for the Production of Nets for Agricultural Product Packaging.* Materials, 2021. **14**(2): p. 323.
69. Rapisarda, M., et al., *Photo-oxidative and soil burial degradation of irrigation tubes based on biodegradable polymer blends.* Polymers, 2019. **11**(9): p. 1489.
70. Nakatsuka, T., *Polylactic acid-coated cable.* Fujikura Tech. Rev, 2011. **40**: p. 39-45.
71. Barillari, F. and F. Chini, *Biopolymers - Sustainability for the Automotive Value-added Chain.* ATZ worldwide, 2020. **122**(11): p. 36-39.
72. Elkamel, A., et al. *Modeling the mechanical properties of biopolymers for automotive applications*. in *2015 International Conference on Industrial Engineering and Operations Management (IEOM)*. 2015.
73. Paul, D.R., *Control of phase structure in polymer blends*, in *Functional polymers*. 1989, Springer. p. 1-18.
74. Peesan, M., R. Rujiravanit, and P. Supaphol, *Electrospinning of hexanoyl chitosan/polylactide blends.* Journal of Biomaterials Science, Polymer Edition, 2006. **17**(5): p. 547-565.
75. Han, C.D., K.Y. Lee, and N.C. Wheeler, *Plasticating single-screw extrusion of amorphous polymers: Development of a mathematical model and comparison with experiment.* Polymer Engineering & Science, 1996. **36**(10): p. 1360-1376.

76. Zhang, L., C. Xiong, and X. Deng, *Miscibility, crystallization and morphology of poly (β-hydroxybutyrate)/poly (d, l-lactide) blends.* Polymer, 1996. **37**(2): p. 235-241.
77. Emin, M. and H. Schuchmann, *A mechanistic approach to analyze extrusion processing of biopolymers by numerical, rheological, and optical methods.* Trends in Food Science & Technology, 2017. **60**: p. 88-95.
78. Emin, M. and H. Schuchmann, *Droplet breakup and coalescence in a twin-screw extrusion processing of starch based matrix.* Journal of Food Engineering, 2013. **116**(1): p. 118-129.
79. Habeych, E., A.J. van der Goot, and R. Boom, *In situ compatibilization of starch–zein blends under shear flow.* Chemical Engineering Science, 2009. **64**(15): p. 3516-3524.
80. Della Valle, G., et al., *Relations between rheological properties of molten starches and their expansion behaviour in extrusion.* Journal of Food Engineering, 1997. **31**(3): p. 277-295.
81. Emin, M.A. and H.P. Schuchmann, *Analysis of the dispersive mixing efficiency in a twin-screw extrusion processing of starch based matrix.* Journal of Food Engineering, 2013. **115**(1): p. 132-143.
82. van Lengerich, B., *Influence of Extrusion Processing on In-Line Rheological Behavior, Structure, and Function of Wheat Starch*, in *Dough Rheology and Baked Product Texture*, H. Faridi and J.M. Faubion, Editors. 1990, Springer US: Boston, MA. p. 421-471.
83. Utracki, L.A., et al., *Compounding Polymer Blends*, in *Polymer Blends Handbook*, L.A. Utracki and C.A. Wilkie, Editors. 2014, Springer Netherlands: Dordrecht. p. 919-1028.
84. Imre, B., K. Renner, and B. Pukánszky, *Interactions, structure and properties in poly (lactic acid)/thermoplastic polymer blends.* Express Polymer Letters, 2014. **8**(1): p. 2-14.
85. Gui, Z.-y., et al., *Morphology and melt rheology of biodegradable poly (lactic acid)/poly (butylene succinate adipate) blends: effect of blend compositions.* Iranian Polymer Journal, 2012. **21**(2): p. 81-89.
86. Nofar, M., et al., *Interfacial and rheological properties of PLA/PBAT and PLA/PBSA blends and their morphological stability under shear flow.* Journal of Rheology, 2015. **59**(2): p. 317-333.
87. Wu, D., et al., *Interfacial properties, viscoelasticity, and thermal behaviors of poly (butylene succinate)/polylactide blend.* Industrial & engineering chemistry research, 2012. **51**(5): p. 2290-2298.
88. Yokohara, T. and M. Yamaguchi, *Structure and properties for biomass-based polyester blends of PLA and PBS.* European Polymer Journal, 2008. **44**(3): p. 677-685.
89. Xu, L.Q. and H.X. Huang, *Relaxation behavior of poly (lactic acid)/poly (butylene succinate) blend and a new method for calculating its interfacial tension.* Journal of Applied Polymer Science, 2012. **125**(S2): p. E272-E277.
90. Bhatia, A., et al., *Compatibility of biodegradable poly (lactic acid)(PLA) and poly (butylene succinate)(PBS) blends for packaging application.* Korea-Australia rheology journal, 2007. **19**(3): p. 125-131.
91. Ojijo, V., S. Sinha Ray, and R. Sadiku, *Role of specific interfacial area in controlling properties of immiscible blends of biodegradable polylactide and poly [(butylene succinate)-co-adipate].* ACS applied materials & interfaces, 2012. **4**(12): p. 6690-6701.

92. Guan, Q., R. Rizvi, and H.E. Naguib, *A study of the physical and mechanical properties of biobased polylactic acid/polyhydroxybutyrate-co-valerate blend and foams.* Journal of Biobased Materials and Bioenergy, 2013. **7**(5): p. 600-608.
93. Gerard, T. and T. Budtova, *Morphology and molten-state rheology of polylactide and polyhydroxyalkanoate blends.* European polymer journal, 2012. **48**(6): p. 1110-1117.
94. Groeninckx, G., M. Vanneste, and V. Everaert, *Crystallization, Morphological Structure, and Melting of Polymer Blends*, in *Polymer Blends Handbook*, L.A. Utracki, Editor. 2003, Springer Netherlands: Dordrecht. p. 203-294.
95. Park, J.W. and S.S. Im, *Morphological changes during heating in poly (l-lactic acid)/poly (butylene succinate) blend systems as studied by synchrotron X-ray scattering.* Journal of Polymer Science Part B: Polymer Physics, 2002. **40**(17): p. 1931-1939.
96. Park, J.W. and S.S. Im, *Phase behavior and morphology in blends of poly (L-lactic acid) and poly (butylene succinate).* Journal of applied polymer science, 2002. **86**(3): p. 647-655.
97. Wang, R., et al., *Toughening modification of PLLA/PBS blends via in situ compatibilization.* Polymer Engineering & Science, 2009. **49**(1): p. 26-33.
98. Deng, Y. and N.L. Thomas, *Blending poly (butylene succinate) with poly (lactic acid): Ductility and phase inversion effects.* European Polymer Journal, 2015. **71**: p. 534-546.
99. Bartczak, Z., et al., *Tough blends of poly (lactide) and amorphous poly ([R, S]-3-hydroxy butyrate)–morphology and properties.* European Polymer Journal, 2013. **49**(11): p. 3630-3641.
100. Musioł, M., et al., *(Bio) degradable polymers as a potential material for food packaging: studies on the (bio) degradation process of PLA/(R, S)-PHB rigid foils under industrial composting conditions.* European Food Research and Technology, 2016. **242**(6): p. 815-823.
101. Zembouai, I., et al., *Poly (3-hydroxybutyrate-co-3-hydroxyvalerate)/polylactide blends: thermal stability, flammability and thermo-mechanical behavior.* Journal of Polymers and the Environment, 2014. **22**(1): p. 131-139.
102. Liu, Q., et al., *Blends of polylactide and poly (3-hydroxybutyrate-co-3-hydroxyvalerate) with low content of hydroxyvalerate unit: Morphology, structure, and property.* Journal of Applied Polymer Science, 2015. **132**(42).
103. Lee, S.-M. and J.-W. Lee, *Characterization and processing of biodegradable polymer blends of poly (lactic acid) with poly (butylene succinate adipate).* Korea-Australia Rheology Journal, 2005. **17**(2): p. 71-77.
104. Pivsa-Art, W., et al., *Compression molding and melt-spinning of the blends of poly (lactic acid) and poly (butylene succinate-co-adipate).* Journal of Applied Polymer Science, 2015. **132**(16).
105. Nofar, M., et al., *Mechanical and bead foaming behavior of PLA-PBAT and PLA-PBSA blends with different morphologies.* European Polymer Journal, 2017. **90**: p. 231-244.
106. Hassan, E., et al., *Dynamic mechanical properties and thermal stability of poly (lactic acid) and poly (butylene succinate) blends composites.* Journal of fiber Bioengineering and Informatics, 2013. **6**(1): p. 85-94.

107. Abdelwahab, M.A., et al., *Thermal, mechanical and morphological characterization of plasticized PLA–PHB blends.* Polymer Degradation and Stability, 2012. **97**(9): p. 1822-1828.
108. Arrieta, M.P., et al., *On the Use of PLA-PHB Blends for Sustainable Food Packaging Applications.* Materials, 2017. **10**(9): p. 1008.
109. Koning, C., et al., *Strategies for compatibilization of polymer blends.* Progress in Polymer Science, 1998. **23**(4): p. 707-757.
110. Zeng, J.-B., K.-A. Li, and A.-K. Du, *Compatibilization strategies in poly(lactic acid)-based blends.* RSC Advances, 2015. **5**(41): p. 32546-32565.
111. Muthuraj, R., M. Misra, and A.K. Mohanty, *Biodegradable compatibilized polymer blends for packaging applications: A literature review.* Journal of Applied Polymer Science, 2018. **135**(24): p. 45726.
112. Hassouna, F., et al., *New approach on the development of plasticized polylactide (PLA): Grafting of poly (ethylene glycol)(PEG) via reactive extrusion.* European Polymer Journal, 2011. **47**(11): p. 2134-2144.
113. Avella, M., et al., *Preparation and characterisation of compatibilised polycaprolactone/starch composites.* Polymer, 2000. **41**(10): p. 3875-3881.
114. Wu, C.-S., *Physical properties and biodegradability of maleated-polycaprolactone/starch composite.* Polymer degradation and stability, 2003. **80**(1): p. 127-134.
115. Liao, H.-T. and C.-S. Wu, *Performance of an acrylic-acid-grafted poly (3-hydroxybutyric acid)/starch bio-blend: characterization and physical properties.* Designed monomers and polymers, 2007. **10**(1): p. 1-18.
116. Huneault, M.A. and H. Li, *Morphology and properties of compatibilized polylactide/thermoplastic starch blends.* Polymer, 2007. **48**(1): p. 270-280.
117. Li, H. and M.A. Huneault, *Effect of chain extension on the properties of PLA/TPS blends.* Journal of Applied Polymer Science, 2011. **122**(1): p. 134-141.
118. Gardella, L., M. Calabrese, and O. Monticelli, *PLA maleation: an easy and effective method to modify the properties of PLA/PCL immiscible blends.* Colloid and Polymer Science, 2014. **292**(9): p. 2391-2398.
119. Xanthos, M. and S.S. Dagli, *Compatibilization of polymer blends by reactive processing.* Polymer Engineering & Science, 1991. **31**(13): p. 929-935.
120. Najafi, N., et al., *Control of thermal degradation of polylactide (PLA)-clay nanocomposites using chain extenders.* Polymer Degradation and Stability, 2012. **97**(4): p. 554-565.
121. Ojijo, V., S. Sinha Ray, and R. Sadiku, *Toughening of Biodegradable Polylactide/Poly(butylene succinate-co-adipate) Blends via in Situ Reactive Compatibilization.* ACS Applied Materials & Interfaces, 2013. **5**(10): p. 4266-4276.
122. Harada, M., et al., *Reactive compatibilization of biodegradable poly(lactic acid)/poly(ε-caprolactone) blends with reactive processing agents.* Polymer Engineering & Science, 2008. **48**(7): p. 1359-1368.
123. Ojijo, V. and S.S. Ray, *Super toughened biodegradable polylactide blends with non-linear copolymer interfacial architecture obtained via facile in-situ reactive compatibilization.* Polymer, 2015. **80**: p. 1-17.
124. Dong, W., et al., *Effect of partial crosslinking on morphology and properties of the poly(β-hydroxybutyrate)/poly(d,l-lactic acid) blends.* Polymer Degradation and Stability, 2013. **98**(9): p. 1549-1555.

125. Yang, X., A. Finne-Wistrand, and M. Hakkarainen, *Improved dispersion of grafted starch granules leads to lower water resistance for starch-g-PLA/PLA composites.* Composites Science and Technology, 2013. **86**: p. 149-156.
126. Na, Y.-H., et al., *Compatibilization Effect of Poly(ε-caprolactone)-b-poly(ethylene glycol) Block Copolymers and Phase Morphology Analysis in Immiscible Poly(lactide)/Poly(ε-caprolactone) Blends.* Biomacromolecules, 2002. **3**(6): p. 1179-1186.
127. Zhang, B., et al., *High Melt Strength and High Toughness PLLA/PBS Blends by Copolymerization and in Situ Reactive Compatibilization.* Industrial & Engineering Chemistry Research, 2017. **56**(1): p. 52-62.
128. Supthanyakul, R., N. Kaabbuathong, and S. Chirachanchai, *Random poly(butylene succinate-co-lactic acid) as a multi-functional additive for miscibility, toughness, and clarity of PLA/PBS blends.* Polymer, 2016. **105**: p. 1-9.
129. Sun, Z., et al., *Synergistic effect of PLA–PBAT–PLA tri-block copolymers with two molecular weights as compatibilizers on the mechanical and rheological properties of PLA/PBAT blends.* RSC Advances, 2015. **5**(90): p. 73842-73849.
130. Chen, L., et al., *Poly(l-lactide)/starch blends compatibilized with poly(l-lactide)-g-starch copolymer.* Carbohydrate Polymers, 2006. **65**(1): p. 75-80.
131. Tsuji, H., et al., *Part 7. Effects of poly(L-lactide-co-ϵ-caprolactone) on morphology, structure, crystallization, and physical properties of blends of poly(L-lactide) and poly(ϵ-caprolactone).* Polymer International, 2003. **52**(2): p. 269-275.
132. Choi, N.-S., et al., *Morphology and hydrolysis of PCL/PLLA blends compatibilized with P(LLA-co-ϵCL) or P(LLA-b-ϵCL).* Journal of Applied Polymer Science, 2002. **86**(8): p. 1892-1898.
133. Macosko, C.W., et al., *Compatibilizers for Melt Blending: Premade Block Copolymers.* Macromolecules, 1996. **29**(17): p. 5590-5598.
134. Ryan, A.J., *Designer polymer blends.* Nature Materials, 2002. **1**(1): p. 8-10.
135. Merianos, J., *Surface-active agents.* Disinfection, sterilization, and preservation, 2001.
136. Benvegnu, T., D. Plusquellec, and L. Lemiègre, *Surfactants from renewable sources: synthesis and applications*, in *Monomers, polymers and composites from renewable resources*. 2008, Elsevier. p. 153-178.
137. Thanatuksorn, P., et al., *Improvement of the oral bioavailability of coenzyme Q10 by emulsification with fats and emulsifiers used in the food industry.* LWT-Food Science and Technology, 2009. **42**(1): p. 385-390.
138. Lu, L. and L. Zhu, *Reducing plant uptake of PAHs by cationic surfactant-enhanced soil retention.* Environmental pollution, 2009. **157**(6): p. 1794-1799.
139. Corradini, E., et al., *Preparation and characterization of thermoplastic starch/zein blends.* Materials Research, 2007. **10**: p. 227-231.
140. Habeych, E., et al., *Starch–zein blends formed by shear flow.* Chemical Engineering Science, 2008. **63**(21): p. 5229-5238.
141. Huang, H., T. Chang, and J. Jane, *Mechanical and physical properties of protein-starch based plastics produced by extrusion and injection molding.* Journal of the American Oil Chemists' Society, 1999. **76**(9): p. 1101-1108.

142. Yokesahachart, C. and R. Yoksan, *Effect of amphiphilic molecules on characteristics and tensile properties of thermoplastic starch and its blends with poly(lactic acid).* Carbohydrate Polymers, 2011. **83**(1): p. 22-31.
143. Lahor, A., M. Nithitanakul, and B.P. Grady, *Blends of low-density polyethylene with nylon compatibilized with a sodium-neutralized carboxylate ionomer.* European Polymer Journal, 2004. **40**(11): p. 2409-2420.
144. Lim, J.S., I. Noda, and S.S. Im, *Effects of metal ion-carbonyl interaction on miscibility and crystallization kinetic of poly(3-hydroxybutyrate-co-3-hydroxyhexanoate)/lightly ionized PBS.* European Polymer Journal, 2008. **44**(5): p. 1428-1440.
145. Han, S.-I., S.S. Im, and D.K. Kim, *Dynamic mechanical and melt rheological properties of sulfonated poly(butylene succinate) ionomers.* Polymer, 2003. **44**(23): p. 7165-7173.
146. Zhu, W., et al., *Study of polyurethane/sulfonated dimethyl fumarate complex.* Journal of applied polymer science, 2002. **84**(1): p. 67-74.
147. Ishida, K., et al., *Novel Poly (butylene succinate)-Based Ionomers with Sulfonated Succinate Units: Synthesis, Morphology, and the Unique Nucleation Effect on Crystallization.* Macromolecular Chemistry and Physics, 2005. **206**(10): p. 1028-1034.
148. Park, S.B., et al., *Plasticizer effect of novel PBS ionomer in PLA/PBS ionomer blends.* Macromolecular Research, 2010. **18**(5): p. 463-471.
149. Harkins, W.D., *A general thermodynamic theory of the spreading of liquids to form duplex films and of liquids or solids to form monolayers.* The Journal of Chemical Physics, 1941. **9**(7): p. 552-568.
150. Harkins, W.D. and A. Feldman, *Films. The spreading of liquids and the spreading coefficient.* Journal of the American Chemical Society, 1922. **44**(12): p. 2665-2685.
151. Torza, S. and S. Mason, *Three-phase interactions in shear and electrical fields.* Journal of colloid and interface science, 1970. **33**(1): p. 67-83.
152. Virgilio, N., C. Marc-Aurèle, and B.D. Favis, *Novel Self-Assembling Close-Packed Droplet Array at the Interface in Ternary Polymer Blends.* Macromolecules, 2009. **42**(9): p. 3405-3416.
153. Bulatović, V.O., et al., *Biodegradable Polymer Blends Based on Thermoplastic Starch.* Journal of Polymers and the Environment, 2020. **29**(2): p. 492-508.
154. Fenni, S.E., et al., *Nucleation modalities in poly(lactide), poly(butylene succinate), and poly(ε-caprolactone) ternary blends with partial wetting morphology.* Polymer Crystallization, 2020. **3**(6).
155. Hedrick, M.M., et al., *Morphology and performance relationship studies on biodegradable ternary blends of poly (3-hydroxybutyrate-co-3-hydroxyvalerate), polylactic acid, and polypropylene carbonate.* RSC Advances, 2020. **10**(73): p. 44624-44632.
156. Zhang, K., A.K. Mohanty, and M. Misra, *Fully biodegradable and biorenewable ternary blends from polylactide, poly (3-hydroxybutyrate-co-hydroxyvalerate) and poly (butylene succinate) with balanced properties.* ACS applied materials & interfaces, 2012. **4**(6): p. 3091-3101.
157. Nofar, M., R. Salehiyan, and S.S. Ray, *Influence of nanoparticles and their selective localization on the structure and properties of polylactide-based blend nanocomposites.* Composites Part B: Engineering, 2021. **215**: p. 108845.

158. de Luna, M.S. and G. Filippone, *Effects of nanoparticles on the morphology of immiscible polymer blends–challenges and opportunities.* European Polymer Journal, 2016. **79**: p. 198-218.
159. Salehiyan, R. and S.S. Ray, *Processing of polymer blends, emphasizing: melt compounding; influence of nanoparticles on blend morphology and rheology; reactive processing in ternary systems; morphology–property relationships; performance and application challenges; and opportunities and future trends*, in *Processing of polymer-based nanocomposites*. 2018, Springer. p. 167-197.
160. Filippone, G., et al., *The role of organoclay in promoting co-continuous morphology in high-density poly(ethylene)/poly(amide) 6 blends.* Polymer, 2008. **49**(5): p. 1312-1322.
161. Young, T., *III. An essay on the cohesion of fluids.* Philosophical transactions of the royal society of London, 1805(95): p. 65-87.
162. Fowkes, F.M., *Attractive forces at interfaces.* Industrial & Engineering Chemistry, 1964. **56**(12): p. 40-52.
163. Wu, S., *Polar and nonpolar interactions in adhesion.* The Journal of Adhesion, 1973. **5**(1): p. 39-55.
164. Owens, D.K. and R. Wendt, *Estimation of the surface free energy of polymers.* Journal of applied polymer science, 1969. **13**(8): p. 1741-1747.
165. Dharaiya, D. and S.C. Jana, *Thermal decomposition of alkyl ammonium ions and its effects on surface polarity of organically treated nanoclay.* Polymer, 2005. **46**(23): p. 10139-10147.
166. Wang, X.-f., et al., *Super toughened immiscible poly (L-lactide)/poly (ethylene vinyl acetate)(PLLA/EVA) blend achieved by in situ cross-linking reaction and carbon nanotubes.* Composites Part A: Applied Science and Manufacturing, 2016. **91**: p. 105-116.
167. Bai, L., et al., *Kinetic control of graphene localization in co-continuous polymer blends via melt compounding.* Langmuir, 2018. **34**(3): p. 1073-1083.
168. Chen, J., et al., *Effect of organoclay on morphology and electrical conductivity of PC/PVDF/CNT blend composites.* Composites Science and Technology, 2014. **94**: p. 30-38.
169. Liu, C.-m., et al., *Selective localization of organic montmorillonite in poly (l-lactide)/poly (ethylene vinyl acetate) blends and the resultant properties.* Composites Part B: Engineering, 2017. **123**: p. 1-9.
170. Huang, J., et al., *Control of carbon nanotubes at the interface of a co-continuous immiscible polymer blend to fabricate conductive composites with ultralow percolation thresholds.* Carbon, 2014. **73**: p. 267-274.
171. Fenouillot, F., P. Cassagnau, and J.-C. Majesté, *Uneven distribution of nanoparticles in immiscible fluids: Morphology development in polymer blends.* Polymer, 2009. **50**(6): p. 1333-1350.
172. Taguet, A., P. Cassagnau, and J.-M. Lopez-Cuesta, *Structuration, selective dispersion and compatibilizing effect of (nano) fillers in polymer blends.* Progress in Polymer Science, 2014. **39**(8): p. 1526-1563.
173. Shahlari, M. and S. Lee, *Mechanical and morphological properties of poly (butylene adipate-co-terephthalate) and poly (lactic acid) blended with organically modified silicate layers.* Polymer Engineering & Science, 2012. **52**(7): p. 1420-1428.
174. Zembouai, I., et al., *Combined effects of Sepiolite and Cloisite 30B on morphology and properties of poly (3-hydroxybutyrate-co-3-*

hydroxyvalerate)/polylactide blends. Polymer degradation and stability, 2018. **153**: p. 47-52.
175. Chen, G.-X., et al., *Compatibilization-like effect of reactive organoclay on the poly (l-lactide)/poly (butylene succinate) blends.* Polymer, 2005. **46**(25): p. 11829-11836.
176. Hoidy, W.H., E.A.J. Al-Mulla, and K.W. Al-Janabi, *Mechanical and thermal properties of PLLA/PCL modified clay nanocomposites.* Journal of Polymers and the Environment, 2010. **18**(4): p. 608-616.
177. Risse, S., et al., *Microstructure, rheological behavior, and properties of poly (lactic acid)/poly (butylene succinate)/organoclay nanocomposites.* Journal of Applied Polymer Science, 2014. **131**(12).
178. Utracki, L. and Z. Shi, *Development of polymer blend morphology during compounding in a twin-screw extruder. Part I: Droplet dispersion and coalescence—a review.* Polymer Engineering & Science, 1992. **32**(24): p. 1824-1833.
179. Huneault, M., Z. Shi, and L. Utracki, *Development of polymer blend morphology during compounding in a twin-screw extruder. Part IV: A new computational model with coalescence.* Polymer Engineering & Science, 1995. **35**(1): p. 115-127.
180. Lee, J.K. and C.D. Han, *Evolution of polymer blend morphology during compounding in a twin-screw extruder.* Polymer, 2000. **41**(5): p. 1799-1815.
181. Alsteens, B., V. Legat, and T. Avalosse, *Parametric study of the mixing efficiency in a kneading block section of a twin-screw extruder.* International Polymer Processing, 2004. **19**(3): p. 207-217.
182. Erdmenger, R., *Zur Entwicklung von Schneckenverdampfern.* Chemie Ingenieur Technik, 1962. **34**(11): p. 751-754.
183. Booy, M., *Isothermal flow of viscous liquids in corotating twin screw devices.* Polymer Engineering & Science, 1980. **20**(18): p. 1220-1228.
184. Sastrohartono, T., et al., *Numerical and experimental studies of the flow in the nip region of a partially intermeshing co-rotating twin-screw extruder.* Polymer Engineering & Science, 1990. **30**(21): p. 1382-1398.
185. Bigio, D. and W. Stry, *Measures of mixing in laminar flow.* Polymer Engineering & Science, 1990. **30**(3): p. 153-161.
186. Todd, D.B., *Plastics compounding: equipment and processing*. 1998: Hanser Publishers.
187. Ambrósio, J.D., et al., *Influence of the process parameters of an intermeshing co-rotating twin screw extruder on the morphology and notched Izod impact strength of PBT/ABS/MGE blends.* Polymer Engineering & Science, 2010. **50**(12): p. 2382-2391.
188. Hu, G.-H., Y.-J. Sun, and M. Lambla, *Effects of processing parameters on the in situ compatibilization of polypropylene and poly(butylene terephthalate) blends by one-step reactive extrusion.* Journal of Applied Polymer Science, 1996. **61**(6): p. 1039-1047.
189. Casamento, F., et al., *Rheological behavior and morphology of poly (lactic acid)/low-density polyethylene blends based on virgin and recycled polymers: Compatibilization with natural surfactants.* Journal of Applied Polymer Science, 2021. **138**(25): p. 50590.
190. D'Anna, A., R. Arrigo, and A. Frache, *PLA/PHB Blends: Biocompatibilizer Effects.* Polymers (Basel), 2019. **11**(9).

191. Lucassen-Reynders, E. and K. Kuijpers, *The role of interfacial properties in emulsification.* Colloids and Surfaces, 1992. **65**(2-3): p. 175-184.
192. Janssen, J., A. Boon, and W. Agterof, *Influence of dynamic interfacial properties on droplet breakup in simple shear flow.* AIChE journal, 1994. **40**(12): p. 1929-1939.
193. Briscoe, B., C. Lawrence, and W. Mietus, *A review of immiscible fluid mixing.* Advances in Colloid and Interface Science, 1999. **81**(1): p. 1-17.
194. Shamsuri, A.A., et al., *Nylon-6/liquid natural rubber blends prepared via emulsion dispersion.* Journal of Polymer Research, 2009. **16**(4): p. 381-387.
195. Sudari, A., et al., *Exploration on compatibilizing effect of nonionic, anionic, and cationic surfactants on mechanical, morphological, and chemical properties of high-density polyethylene/low-density polyethylene/cellulose biocomposites.* Journal of Thermoplastic Composite Materials, 2017. **30**(6): p. 855-884.
196. De, S., et al., *A review on natural surfactants.* RSC Advances, 2015. **5**(81): p. 65757-65767.
197. Shamsuri, A.A., et al., *Influence of Surface Treatment on Tensile Properties of Low-Density Polyethylene/Cellulose Woven Biocomposites: A Preliminary Study.* Polymers, 2014. **6**(9): p. 2345-2356.
198. ICI Americas, I., *The HLB system: A Time-Saving Guide to Emulsifier Selection*. 1984, ICI Americas, Inc: Wilmington
199. Huang, Y., et al., *A new strategy to improve viscoelasticity, crystallization and mechanical properties of polylactide.* Polymer Testing, 2021. **97**: p. 107160.
200. Hemsri, S., et al. *Low density polyethylene/poly (butylene adipate-co-terephthalate) films: Effect of a compatibilizer on morphology and properties*. in *IOP Conference Series: Materials Science and Engineering*. 2020. IOP Publishing.
201. Arrigo, R., M. Bartoli, and G. Malucelli, *Poly(lactic Acid)-Biochar Biocomposites: Effect of Processing and Filler Content on Rheological, Thermal, and Mechanical Properties.* Polymers (Basel), 2020. **12**(4).
202. Xue, L., J. Zhang, and Y. Han, *Phase separation induced ordered patterns in thin polymer blend films.* Progress in polymer science, 2012. **37**(4): p. 564-594.
203. Abdelwahab, M.A., et al. , *"Thermal, mechanical and morphological characterization of plasticized PLA–PHB blends.* Polymer degradation and stability 2012. **97**(9): p. 1822-1828.
204. George, K., et al., *Dynamic mechanical analysis of binary and ternary polymer blends based on nylon copolymer/EPDM rubber and EPM grafted maleic anhydride compatibilizer.* 2007.
205. Soroudi, A., and Ignacy Jakubowicz., *Recycling of bioplastics, their blends and biocomposites: A review.* European Polymer Journal, 2013. **49**(10): p. 2839-2858.
206. Anastasiadis, S.H., I. Gancarz, and J.T. Koberstein, *Interfacial tension of immiscible polymer blends: temperature and molecular weight dependence.* Macromolecules, 1988. **21**(10): p. 2980-2987.
207. Filippone, G., G. Romeo, and D. Acierno, *Role of Interface Rheology in Altering the Onset of Co-Continuity in Nanoparticle-Filled Polymer Blends.* Macromolecular Materials and Engineering, 2011. **296**(7): p. 658-665.

208. Lacroix, C., Michel Aressy, and Pierre J. Carreau., *Linear viscoelastic behavior of molten polymer blends: a comparative study of the Palierne and Lee and Park models.* Rheologica Acta, 1997. **36**(4): p. 416-428.
209. Ahmadzadeh, Y., Amir Babaei, and Alireza Goudarzi, *Assessment of localization and degradation of ZnO nano-particles in the PLA/PCL biocompatible blend through a comprehensive rheological characterization.* Polymer Degradation and Stability, 2018. **158**: p. 136-147.
210. López-Barrón, C.R., and Christopher W. Macosko. , *Rheological and morphological study of cocontinuous polymer blends during coarsening.* Journal of Rheology, 2012. **56**(6): p. 1315-1334.
211. Bucci, D., L. Tavares, and I. Sell, . Polymer testing, 2007. **26**(7): p. 908-915.
212. Di Lorenzo, M.L., M. Gazzano, and M.C. Righetti, *The Role of the Rigid Amorphous Fraction on Cold Crystallization of Poly(3-hydroxybutyrate).* Macromolecules, 2012. **45**(14): p. 5684-5691.
213. Furukawa, T., et al., *Comparison of miscibility and structure of poly (3-hydroxybutyrate-co-3-hydroxyhexanoate)/poly (l-lactic acid) blends with those of poly (3-hydroxybutyrate)/poly (l-lactic acid) blends studied by wide angle X-ray diffraction, differential scanning calorimetry, and FTIR microspectroscopy.* Polymer, 2007. **48**(6): p. 1749-1755.
214. Sato, H., et al., *Infrared Spectroscopy and X-Ray Diffraction Studies on the Structure and Thermal Behavior of Biodegradable Polyhydroxyalkanoates.* Macromolecular Symposia, 2005. **220**(1): p. 123-138.
215. Battegazzore, D., S. Bocchini, and A. Frache, *Crystallization kinetics of poly (lactic acid)-talc composites.* Express Polym Lett, 2011. **5**(10): p. 849-858.
216. Botana, A., et al., *Effect of modified montmorillonite on biodegradable PHB nanocomposites.* Applied Clay Science, 2010. **47**(3-4): p. 263-270.
217. Takemori, M.T., *Towards an understanding of the heat distortion temperature of thermoplastics.* Polymer Engineering & Science, 1979. **19**(15): p. 1104-1109.
218. Bondeson, D., P. Syre, and K.O. Niska, *All cellulose nanocomposites produced by extrusion.* Journal of Biobased Materials and Bioenergy, 2007. **1**(3): p. 367-371.
219. Gong, X., et al., *Surfactant-Assisted Processing of Carbon Nanotube/Polymer Composites.* Chemistry of Materials, 2000. **12**(4): p. 1049-1052.
220. Filippone, G., P.A. Netti, and D. Acierno, *Microstructural evolutions of LDPE/PA6 blends by rheological and rheo-optical analyses: Influence of flow and compatibilizer on break-up and coalescence processes.* Polymer, 2007. **48**(2): p. 564-573.
221. D'Anna, A., R. Arrigo, and A. Frache, *Rheology, Morphology and Thermal Properties of a PLA/PHB/Clay Blend Nanocomposite: The Influence of Process Parameters.* Journal of Polymers and the Environment, 2021. 30(1), 102-113.
222. Favis, B. and J. Chalifoux, *Influence of composition on the morphology of polypropylene/polycarbonate blends.* Polymer, 1988. **29**(10): p. 1761-1767.
223. Favis, B.D., *The effect of processing parameters on the morphology of an immiscible binary blend.* Journal of applied polymer science, 1990. **39**(2): p. 285-300.

224. Elmendorp, J.J., *A study on polymer blending microrheology.* Polymer Engineering & Science, 1986. **26**(6): p. 418-426.
225. Min, K., J.L. White, and J.F. Fellers, *Development of phase morphology in incompatible polymer blends during mixing and its variation in extrusion.* Polymer Engineering & Science, 1984. **24**(17): p. 1327-1336.
226. Willis, J., B. Favis, and J. Lunt, *Reactive processing of polystyrene-co-maleic anhydride/elastomer blends: Processing-morphology-property relationships.* Polymer Engineering & Science, 1990. **30**(17): p. 1073-1084.
227. Wu, S., *Formation of dispersed phase in incompatible polymer blends: Interfacial and rheological effects.* Polymer Engineering & Science, 1987. **27**(5): p. 335-343.
228. Bai Chin, H. and C. Dae Han, *Studies on droplet deformation and breakup. I. Droplet deformation in extensional flow.* Journal of Rheology, 1979. **23**(5): p. 557-590.
229. Lim, J.S., et al., *Effect of composition ratio on the thermal and physical properties of semicrystalline PLA/PHB-HHx composites.* Materials Science and Engineering: C, 2013. **33**(4): p. 2131-2137.
230. Cheng, M.-L., et al., *Structure, mechanical properties and degradation behaviors of the electrospun fibrous blends of PHBHHx/PDLLA.* Polymer, 2011. **52**(6): p. 1391-1401.
231. Ishida, H. and D.J. Allen, *Mechanical characterization of copolymers based on benzoxazine and epoxy.* Polymer, 1996. **37**(20): p. 4487-4495.
232. Villmow, T., B. Kretzschmar, and P. Pötschke, *Influence of screw configuration, residence time, and specific mechanical energy in twin-screw extrusion of polycaprolactone/multi-walled carbon nanotube composites.* Composites Science and Technology, 2010. **70**(14): p. 2045-2055.
233. Walha, F., et al., *Rheological, morphological and mechanical studies of sustainably sourced polymer blends based on poly (lactic acid) and polyamide 11.* Polymers, 2016. **8**(3): p. 61.
234. Bai, Z. and Q. Dou, *Rheology, morphology, crystallization behaviors, mechanical and thermal properties of poly (lactic acid)/polypropylene/maleic anhydride-grafted polypropylene blends.* Journal of Polymers and the Environment, 2018. **26**(3): p. 959-969.
235. Vladoiu, R., et al., *Thermionic Vacuum Arc—A versatile technology for thin film deposition and its applications.* Coatings, 2020. **10**(3): p. 211.
236. Mirzadeh, A., et al., *Reactive extrusion effects on rheological and mechanical properties of poly (lactic acid)/poly [(butylene succinate)-co-adipate]/epoxy chain extender blends and clay nanocomposites.* Journal of Applied Polymer Science, 2015. **132**(48).
237. Zubairi, S.I., A. Bismarck, and A. Mantalaris, *The effect of surface heterogeneity on wettability of porous three dimensional (3-D) scaffolds of poly (3-hydroxybutyric acid)(PHB) and poly (3-hydroxybutyric-co-3-hydroxyvaleric acid)(PHBV).* Jurnal Teknologi, 2015. **75**(1).
238. Gomari, S., et al., *Organoclay localization in polyamide 6/ethylene-butene copolymer grafted maleic anhydride blends: the effect of different types of organoclay.* Journal of Polymer Research, 2012. **19**(1): p. 1-11.
239. Lewin, M., A. Mey-Marom, and R. Frank, *Surface free energies of polymeric materials, additives and minerals.* Polymers for advanced technologies, 2005. **16**(6): p. 429-441.

240. Das, K., et al., *Crystalline morphology of PLA/clay nanocomposite films and its correlation with other properties.* Journal of applied polymer science, 2010. **118**(1): p. 143-151.
241. Vergnes, B., *Influence of Processing Conditions on the Preparation of Clay-Based Nanocomposites by Twin-Screw Extrusion.* International Polymer Processing, 2019. **34**(5): p. 482-501.
242. Silverajah, V., et al., *Mechanical, thermal and morphological properties of poly (lactic acid)/epoxidized palm olein blend.* Molecules, 2012. **17**(10): p. 11729-11747.
243. Hurrell, B. and R. Cameron, *A wide-angle X-ray scattering study of the ageing of poly (hydroxybutyrate).* Journal of Materials Science, 1998. **33**(7): p. 1709-1713.
244. Sun, X., et al., *A study on the crystallization behavior of poly (β-hydroxybutyrate) thin films on Si wafers.* Polymer, 2011. **52**(17): p. 3865-3870.
245. Zhang, M. and N.L. Thomas, *Blending polylactic acid with polyhydroxybutyrate: the effect on thermal, mechanical, and biodegradation properties.* Advances in Polymer Technology, 2011. **30**(2): p. 67-79.
246. Elton, L. and D.F. Jackson, *X-ray diffraction and the bragg law.* American Journal of Physics, 1966. **34**(11): p. 1036-1038.
247. Abbasi, F., A. Tavakoli, and M.K. Razavi Aghjeh, *Rheology, morphology, and mechanical properties of reactive compatibilized polypropylene/polystyrene blends via Friedel–Crafts alkylation reaction in the presence of clay.* Journal of Vinyl and Additive Technology, 2018. **24**(1): p. 18-26.
248. Remili, C., et al., *The effects of reprocessing cycles on the structure and properties of polystyrene/Cloisite15A nanocomposites.* Polymer Degradation and Stability, 2011. **96**(8): p. 1489-1496.
249. Dil, E.J. and B.D. Favis, *Localization of micro-and nano-silica particles in heterophase poly (lactic acid)/poly (butylene adipate-co-terephthalate) blends.* Polymer, 2015. **76**: p. 295-306.
250. Arrigo, R., et al., *Effect of SiO2 Particles on the Relaxation Dynamics of Epoxidized Natural Rubber (ENR) in the Melt State by Time-Resolved Mechanical Spectroscopy.* Polymers (Basel), 2021. **13**(2).
251. Potente, H. and M. Bastian, *Polymer Blends in Co-Rotating Twin-Screw Extruders.* International Polymer Processing, 2001. **16**(1): p. 14-30.
252. Dean, K., et al., *Gelatinized starch/biodegradable polyester blends: Processing, morphology, and properties.* Journal of applied polymer science, 2007. **103**(2): p. 802-811.
253. Reignier, J. and B.D. Favis, *Control of the subinclusion microstructure in HDPE/PS/PMMA ternary blends.* Macromolecules, 2000. **33**(19): p. 6998-7008.
254. Valera, T.S., A.T. Morita, and N.R. Demarquette, *Study of morphologies of PMMA/PP/PS ternary blends.* Macromolecules, 2006. **39**(7): p. 2663-2675.
255. Shokoohi, S. and A. Arefazar, *A review on ternary immiscible polymer blends: morphology and effective parameters.* Polymers for Advanced Technologies, 2009. **20**(5): p. 433-447.
256. Zhang, Y., et al., *Bio-based polyamide-assisted supertoughening of polylactide through hardening of the EGMA elastomeric domains of much low amount.* Applied Surface Science, 2021. **556**.

257. Urashita, S. and T. Kawakatsu, *Morphologies of multiphase polymer blend systems.* Progress of Theoretical Physics Supplement, 2000. **138**: p. 412-413.
258. Virgilio, N., et al., *In situ measure of interfacial tensions in ternary and quaternary immiscible polymer blends demonstrating partial wetting.* Macromolecules, 2009. **42**(19): p. 7518-7529.
259. Hobbs, S., M. Dekkers, and V. Watkins, *Effect of interfacial forces on polymer blend morphologies.* Polymer, 1988. **29**(9): p. 1598-1602.
260. Jańczuk, B. and T. Białłopiotrowicz, *Surface free-energy components of liquids and low energy solids and contact angles.* Journal of Colloid and Interface Science, 1989. **127**(1): p. 189-204.
261. Kaelble, D., *Dispersion-polar surface tension properties of organic solids.* The Journal of Adhesion, 1970. **2**(2): p. 66-81.
262. Yang, Y. and Z. Qiu, *Crystallization kinetics and morphology of biodegradable poly (butylene succinate-co-ethylene succinate) copolyesters: effects of comonomer composition and crystallization temperature.* CrystEngComm, 2011. **13**(7): p. 2408-2417.
263. Fenni, S., et al., *Correlating the morphology of poly (L-lactide)/poly (butylene succinate)/graphene oxide blends nanocomposites with their crystallization behavior.* Express Polymer Letters, 2018. **12**(1).
264. García-Campo, M.J., et al., *Manufacturing and characterization of toughened poly (lactic acid)(PLA) formulations by ternary blends with biopolyesters.* Polymers, 2018. **10**(1): p. 3.
265. Mizuno, S., et al., *Biodegradability, reprocessability, and mechanical properties of polybutylene succinate (PBS) photografted by hydrophilic or hydrophobic membranes.* Polymer degradation and stability, 2015. **117**: p. 58-65.
266. Boutaleb, S., et al., *Micromechanics-based modelling of stiffness and yield stress for silica/polymer nanocomposites.* International Journal of Solids and Structures, 2009. **46**(7-8): p. 1716-1726.
267. Zare, Y., V. Mišković-Stanković, and K.Y. Rhee, *The complex viscosity of polymer carbon nanotubes nanocomposites as a function of networks properties.* Carbon Letters, 2019. **29**(5): p. 535-545.
268. Qiu, Z., T. Ikehara, and T. Nishi, *Miscibility and crystallization behaviour of biodegradable blends of two aliphatic polyesters. Poly (3-hydroxybutyrate-co-hydroxyvalerate) and poly (butylene succinate) blends.* Polymer, 2003. **44**(24): p. 7519-7527.
269. Zetsche, A., et al., *Dielectric study on the miscibility of binary polymer blends.* Polymer, 1990. **31**(10): p. 1883-1887.
270. Zhang, H., et al., *Toughening of polylactide by melt blending with methyl methacrylate–butadiene–styrene copolymer.* Journal of Applied Polymer Science, 2012. **125**(S2): p. E550-E561.
271. Ravati, S., et al., *High performance materials based on a self-assembled multiple-percolated ternary blend.* AIChE Journal, 2014. **60**(8): p. 3005-3012.